DANMARKS OG GRØNLANDS GEOLOGISKE UNDERSØGELSE RAPPORT 2010/111

Evaluation and modelling of geophysical data from Inglefield Land with emphasis on the Minturn magnetic anomaly

Report prepared for NunaMinerals A/S

T. M. Rasmussen

GEOLOGICAL SURVEY OF DENMARK AND GREENLAND
MINISTRY OF CLIMATE AND ENERGY

GEUS

DANMARKS OG GRØNLANDS GEOLOGISKE UNDERSØGELSE RAPPORT 2010/111

Evaluation and modelling of geophysical data from Inglefield Land with emphasis on the Minturn magnetic anomaly

Report prepared for NunaMinerals A/S

T. M. Rasmussen

Released 01.10.2013

GEOLOGICAL SURVEY OF DENMARK AND GREENLAND
MINISTRY OF CLIMATE END ENERGY

GEUS

Contents

1. Summary and conclusions

Geophysical data from Inglefield Land with emphasis on the Minturn magnetic anomaly are evaluated with respect to possible occurrences of iron oxides. The geophysical data are magnetic data from three airborne surveys and gravity data from an airborne survey performed in 2010. Electromagnetic data are included in a discussion on possible iron oxide copper gold mineralisations.

Modelling of the Minturn anomaly is performed on magnetic data from selected profiles and subsets of data. A modelling based on typical susceptibility values for magnetite indicates that the magnetite occurrences mainly are found in thin (6 m or less) sheets. Models based on disseminated magnetite or coarser aggregates are possible and would increase the volume of the mineralised zone. The total amount of iron oxide is, however, not increased for such a model. A volume estimate of magnetite associated with a triangular shaped anomaly is about 0.0045 km^3 provided that the anomaly is solely due to a 100 % content of magnetite with a typical susceptibility value of 10 SI. An interpretation with haematite causing the gravity response at the location of the triangular shaped magnetic anomaly cannot be excluded. This would increase the volume of iron oxide by more than one order of magnitude.

Gravity responses from models derived from the magnetic data and based on typical density values for magnetite are too small to be detected by the airborne gravity survey.

A clear correlation between measured gravity and magnetic response maxima is not present. Instead, peaks in the magnetic response show good correlation at both the western and eastern part of the survey area with the location of density boundaries obtained from application of a terracing technique to the gravity data. A model in which upper crustal blocks with small density contrasts accounts for the observed gravity field and where magnetite located mainly at block boundaries, produces the observed magnetic response is favoured.

The magnetic data is not able to discriminate between a model with magnetite concentrated in thin sheets or disseminated within more wide zones.

Target areas have been defined for IOCG occurrences. In total 14 areas are outlined. An evaluation of the target areas done by including geochemical data is suggested in order to prioritise the targets and for an expansion of the number of target areas.

2. Introduction

A pronounced elongated magnetic anomaly was mapped in Inglefield Land from the government funded airborne electromagnetic and magnetic survey referred to as AEM Greenland 1994 (Stemp & Thorning, 1995). The anomaly cross the Minturn River (Figure 1) in an orthogonal east-west orientation and has a peak value adjacent to this river. The anomaly is therefore referred as the Minturn anomaly. The anomaly has a coherent extent of about 90 km. The AEM Greenland 1994 survey collected time-domain electromagnetic data using the GEOTEM system developed by Geoterrex-Dighem Ltd. using a fixed-wing aircraft as survey platform. In addition, magnetic data were recorded. An airborne magnetic survey using a helicopter as survey platform was done in 2008 by SkyTEM APS on behalf of NunaMinerals A/S. In 2010 a combined airborne gravity and magnetic survey was flown by Sander Geophysical Ltd (SGL) on behalf of NunaMinerals A/S. Line paths for the SkyTEM 2008 survey and SGL 2010 survey are shown in Figure 1 This report contains an evaluation of the data from the airborne surveys. Data from a ground magnetic profile collected by GEUS in 1999 is also included. The focus for this report is the interpretation of the Minturn anomaly with the purpose of providing an estimate of the geometry of the mineralisation. The report also includes a discussion of possible target areas for iron oxide copper gold mineralisations (IOCG).

Geological field work around the Minturn anomaly has indicated that magnetite is likely to be the cause of the Minturn anomaly. Floats consisting of 90% magnetite have been reported in the area by Appel et al. (1995) and two up to 1 m thick massive magnetite bands was found outcropping by NunaMinerals A/S during field work in August 2010 (Brown, personal communication). The location with outcropping magnetite bands is in the vicinity of GEUS same 425340 with longitude 68.59999 and latitude 78.51200.The magnetite is magmatic in origin and associated with basic and ultrabasic rocks. Martitization to massive haematite was reported by Appel et al. (1995) for one boulder. In general magnetite has a magnetic susceptibility several orders of magnitude higher than haematite whereas the densities are in the same order of magnitude. The susceptibility of haematite is in the same range as common rock types such as gneiss, and magnetic data are therefore not indicative by themselves in a search for haematite. The high densities for both magnetite and haematite make gravity data suitable in a search for these mineralisations. Magnetite and haematite mineralisations are often without any associated electrical conductivity anomalies.

The great variability among known IOCG deposits imposes some difficulties in establishing a well-defined strategy for target definition based on geophysical data. Discussions on geophysical characteristics of IOCG's can be found in Smith (2002), Corriveau (2007), Sandrin and Elming (2006), Sandrin et al. (2007). The feature quoted to be most indicative is the association of IOCG occurrences with high Bouguer gravity anomalies. For some of the cases with a coincidence of gravity high, similar gravity anomalies are often encountered in the vicinity, but without any mapped association with an IOCG occurrence. A co-location of a magnetic high is quoted for some occurrences whereas in others the IOCG occurrences are correlated with magnetic lows. In the case of the Olympic Dam occurrence, a coincidence of a gravity high (13 mGal) and a magnetic high is observed but the source for the magnetic high is likely to be a structure below the actual mineral occurrence (Smith, 2002). Sandrin et al. (2007) interpret linear magnetic lows associated with the IOCG occurrences in the Kiruna area to be caused by alteration of magnetite to haematite in fracture and fault zones. The area around Kiruna investigated by Sandrin et al. (2007) has some simi-

larities to the geological setting in Inglefield Land; the conclusions from their investigation are listed below:

1. Fe-oxide and base metal sulphides deposits occur in proximity of major faults and crustal deformation zones.
2. The crustal deformations are located at the edges of granitic/syenitic intrusions.
3. The host rocks of the mineral deposits are mostly supracrustal rocks (volcanic or in few cases sedimentary).
4. The deposits are related to gravity highs, which are expressions of high density volcanics that surround low density massive granitic/syenitic plutons.
5. The deposits are related with major crustal deformation zones expressed as linear patterns of low magnetic field intensity and high gradients of the gravity field.
6. IOCG deposits are located in areas with high K/Th ratio, which may be interpreted as an expression of potassic alteration.

A common feature for IOCG occurrences is that they occur in areas referred to as “magnetic active”, i.e. areas with abundant high to moderate magnetic anomalies, even though that the actual occurrence may be linked to a magnetic low. Some IOCG occurrences have an associated electrical conductivity anomaly.

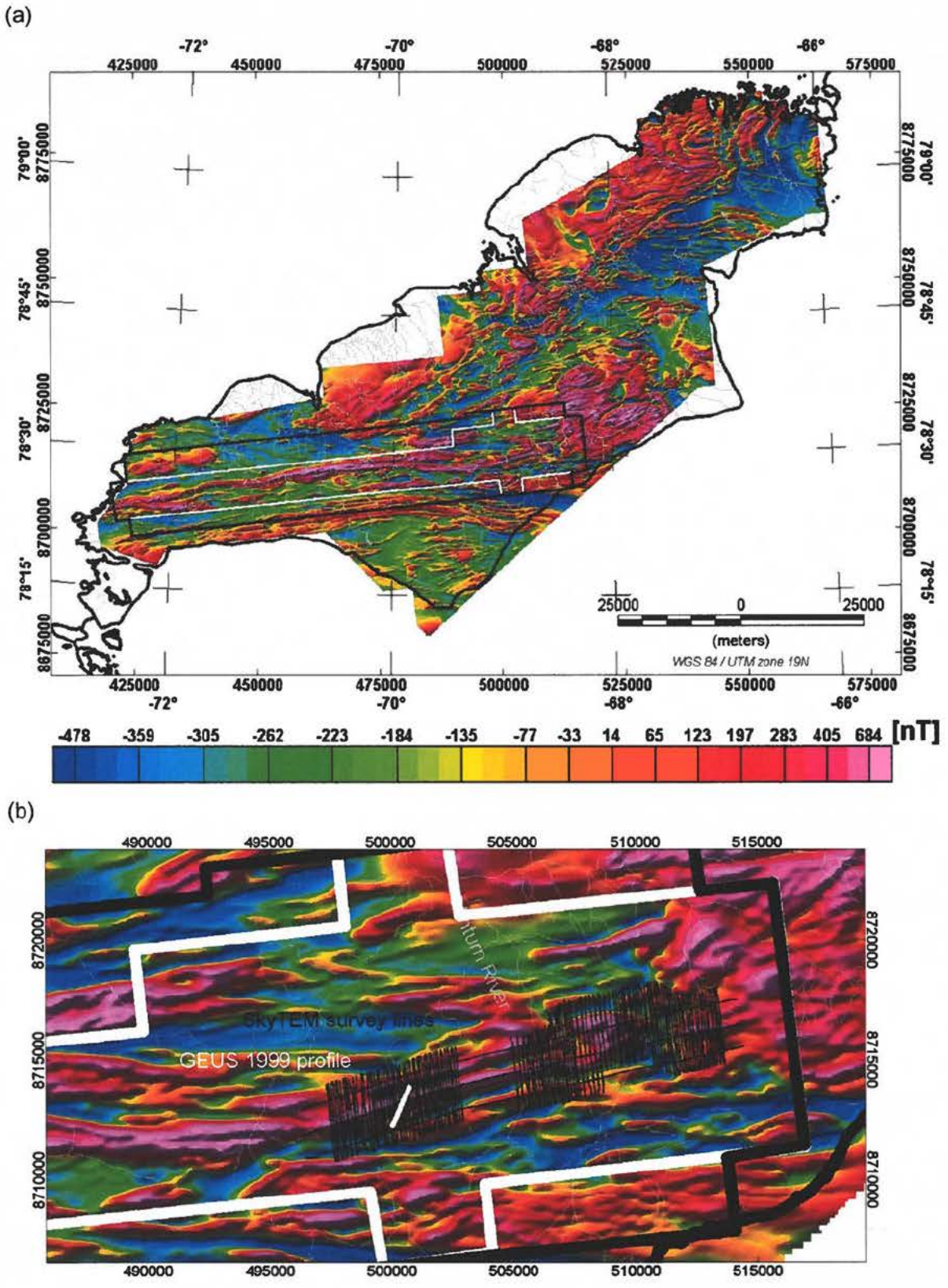

Figure 1. *(a) Areal coverage of the AEM Greenland 1994 survey shown by the image of the total magnetic field anomaly and areal coverage of the SGL 2010 survey shown by outline of two grid types produced from this survey (polygons in black and grey colour respectively). (b) Area coverage of the SkyTEM 2008 survey shown by line path in black colour and coverage of the GEUS 1999 profile shown by the white line.*

3. Measured geophysical field characteristics

This chapter includes a description of survey parameters and geophysical data characteristics for the various surveys in Inglefield Land. Products provided by the geophysical contractors are listed and discussed in relation to utilisation of the data for the interpretation. Table 1 contains survey parameters for all airborne surveys. Survey altitude is a key parameter with respect to the possibility of separating responses from adjacent structures and this is exemplified in a section below in a comparison with responses along coincident lines from the surveys.

Table 1. *Survey parameters. Altitude refers to magnetic sensor position. In the case of the AEM Greenland 1994 survey, the EM sensor is positioned approximately 10 meter above the magnetic sensor. For the combined gravimetric and magnetic survey by SGL the gravity sensor and magnetic sensors are located approximately at the same distance above ground.*

Name	Line spacing	Mean altitude	Min. altitude	Max. altitude	Line km
AEM Greenland 1994	400 m	85 m	51 m	534 m	17338 km
GEUS 1999	NA	2 m	2 m	2	1.8 km
SkyTEM 2008	100 m	49 m	25 m	119	489 km
SGL 2010	100 & 50 m	121 m	57 m	508 m	13980 km

3.1 Magnetic data

3.1.1 AEM Greenland 1994

The AEM Greenland 1994 survey provides an excellent data set for the identification of lineaments on both a regional and a more local scale. Figure 2 displays some of the major linear features that can be observed from a simple visual inspection of the data. The lines in black colour mark lineaments with low magnetic field intensities or locations where structures seem to be cut by fault or shear zones. The survey area can be classified or divided into a number of regional domains based on the field characteristics. Some of the domain boundaries show good correlation to the mapped geological units. The correlation is discussed in some detail in a separate section.

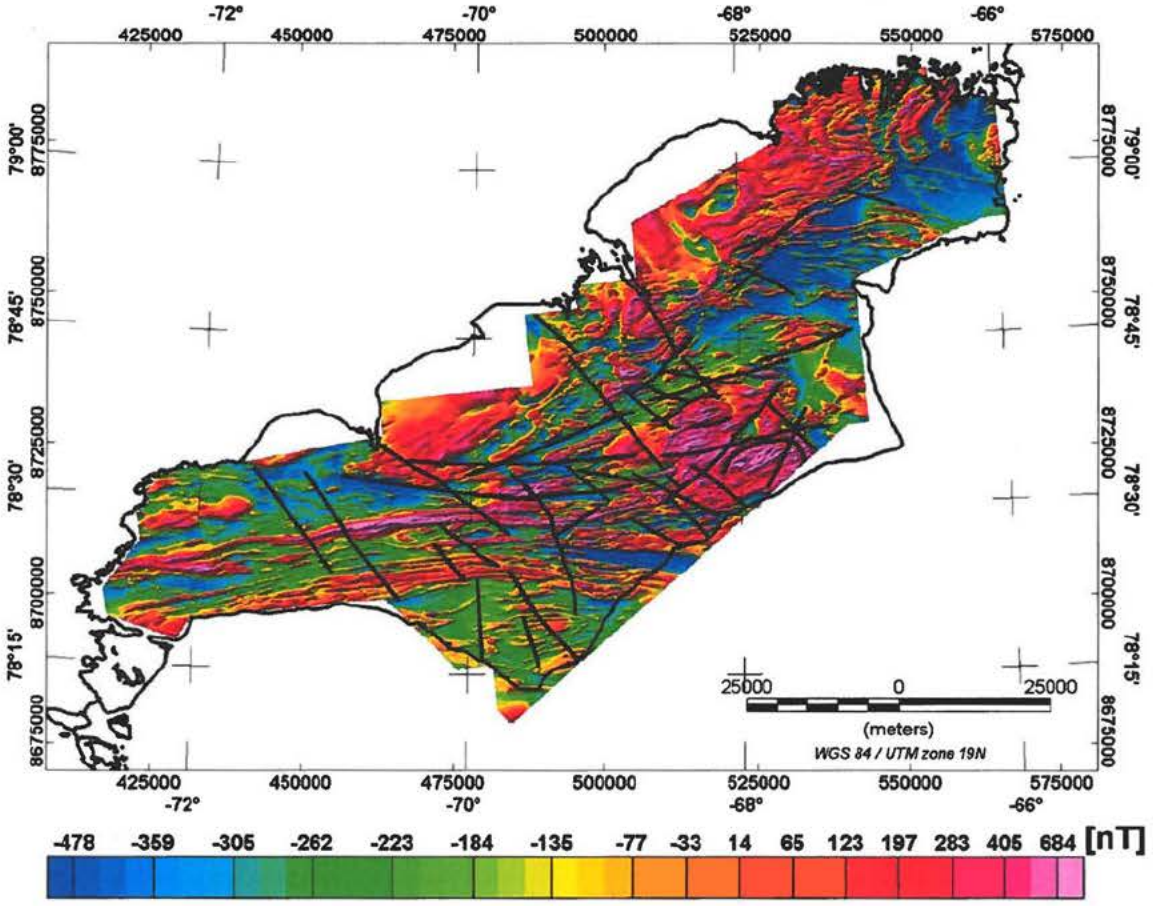

Figure 2. *Image of magnetic total field anomalies with the major lineament marked by lines in black colour.*

3.1.2 GEUS 1999

Magnetic data were obtained along a 1.8 km profile crossing the Minturn anomaly close to the location with maximum magnetic response for the AEM Greenland 1994 data. Data were collected with a sampling distance of about 10 m by using a Geometrics G856 magnetometer.

3.1.3 SkyTEM 2008

This survey is focussed on the part of the Minturn anomaly with maximum magnetic response. Due to the lower survey altitude and more dense line spacing than used for the AEM Greenland 1994, the Minturn anomaly is mapped with better resolution, facilitating better quantitative modelling and target definition. Note however that the non-uniqueness with respect to modelling of potential field data is not removed by the denser sampling.

3.1.4 SGL 2010

The survey by SGL included measurements of both horizontal and vertical gradients of the magnetic field. Sensor set-up is illustrated in Figure 3. These gradient quantities can also be calculated from the measured total field data (AEM Greenland 1994 and SkyTEM), but access to good measured data is clearly advantageous. The gradient data provides a good image of local structures as can be seen in Figure 4 which shows a comparison between vertical gradient data from the tree airborne systems. In terms of resolution of anomalies, the inclusion of measured gradients makes the SGL data comparable to the helicopter-borne survey, which was flown closer to the ground. The data clearly show deformation patterns and allow easy identification of folds and a number of shear and fracture zones.

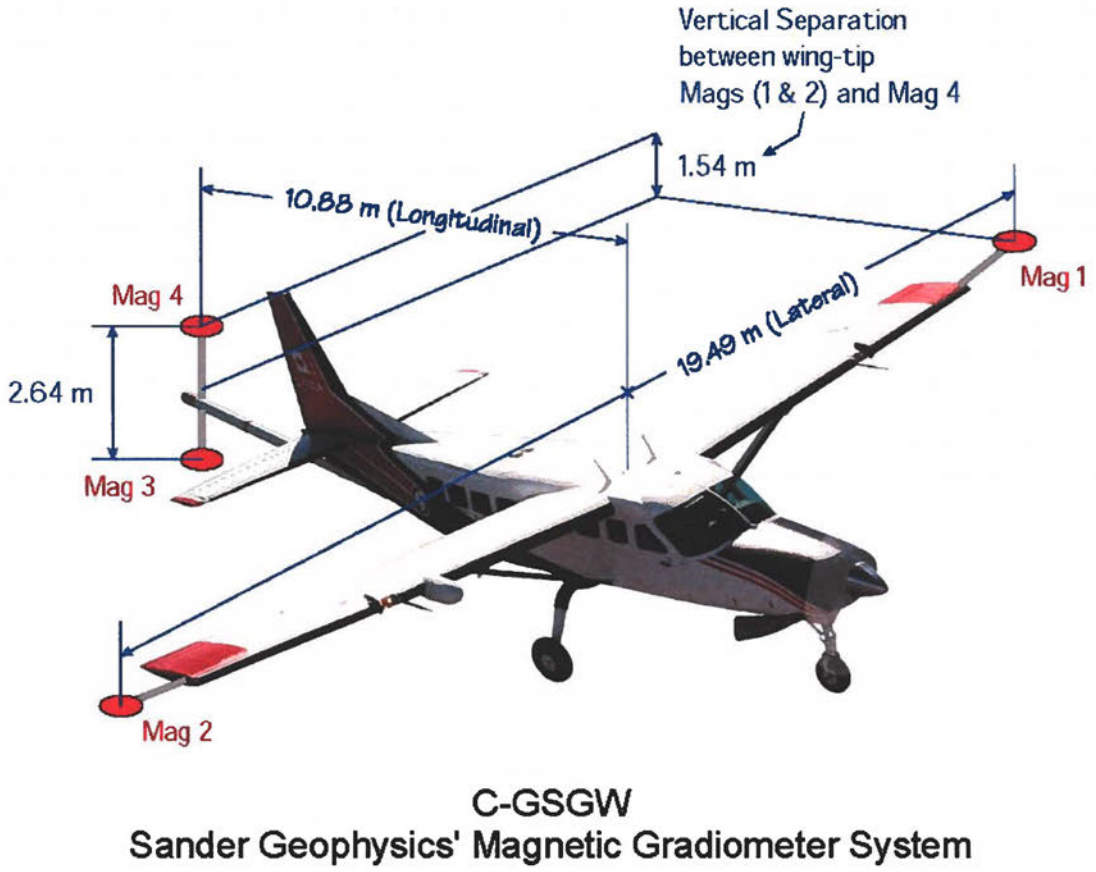

Figure 3. *Magnetic sensor set-up for the SGL 2010 survey.*

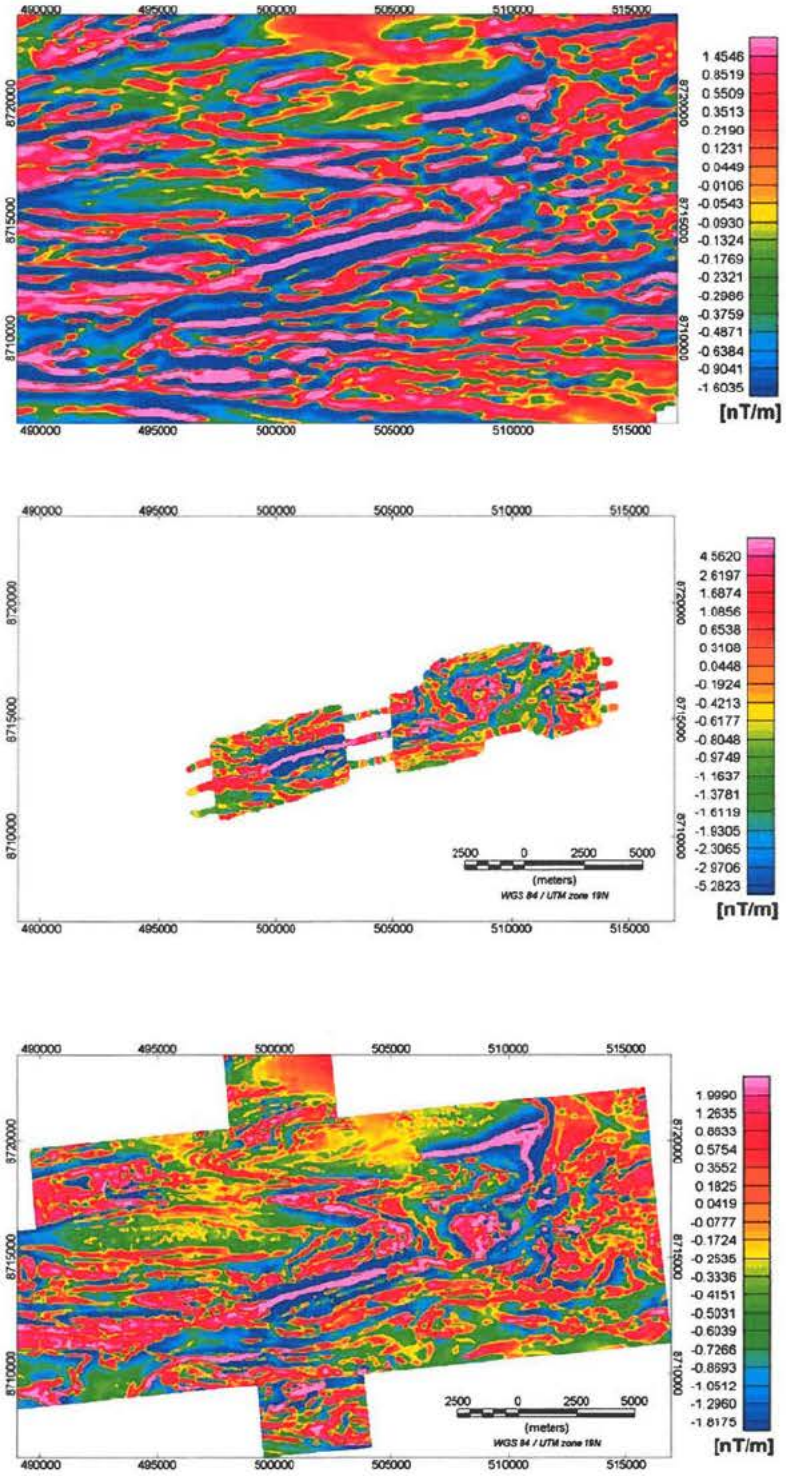

Figure 4. *Vertical derivative of magnetic field. The upper panel and middle panels show calculated values for the AEM Greenland 1994 and SkyTEM 2008 surveys respectively, the lower panel shows measured vertical gradient from the SGL 2010 survey.*

3.1.5 Comparison of magnetic data along the 1999 GEUS profile

This section includes a comparison of line data obtained along adjacent lines for the tree airborne surveys and the ground survey. Figure 5 shows position of survey lines (straight line) and the corresponding data plotted as profile data using the line path as abscissa. The difference in field strength is attributed to sensor ground clearance. The GEUS 1999 ground profile data indicate that the source for the anomaly must have a width smaller than 200 m. As explained later, the actual width is likely to be much smaller.

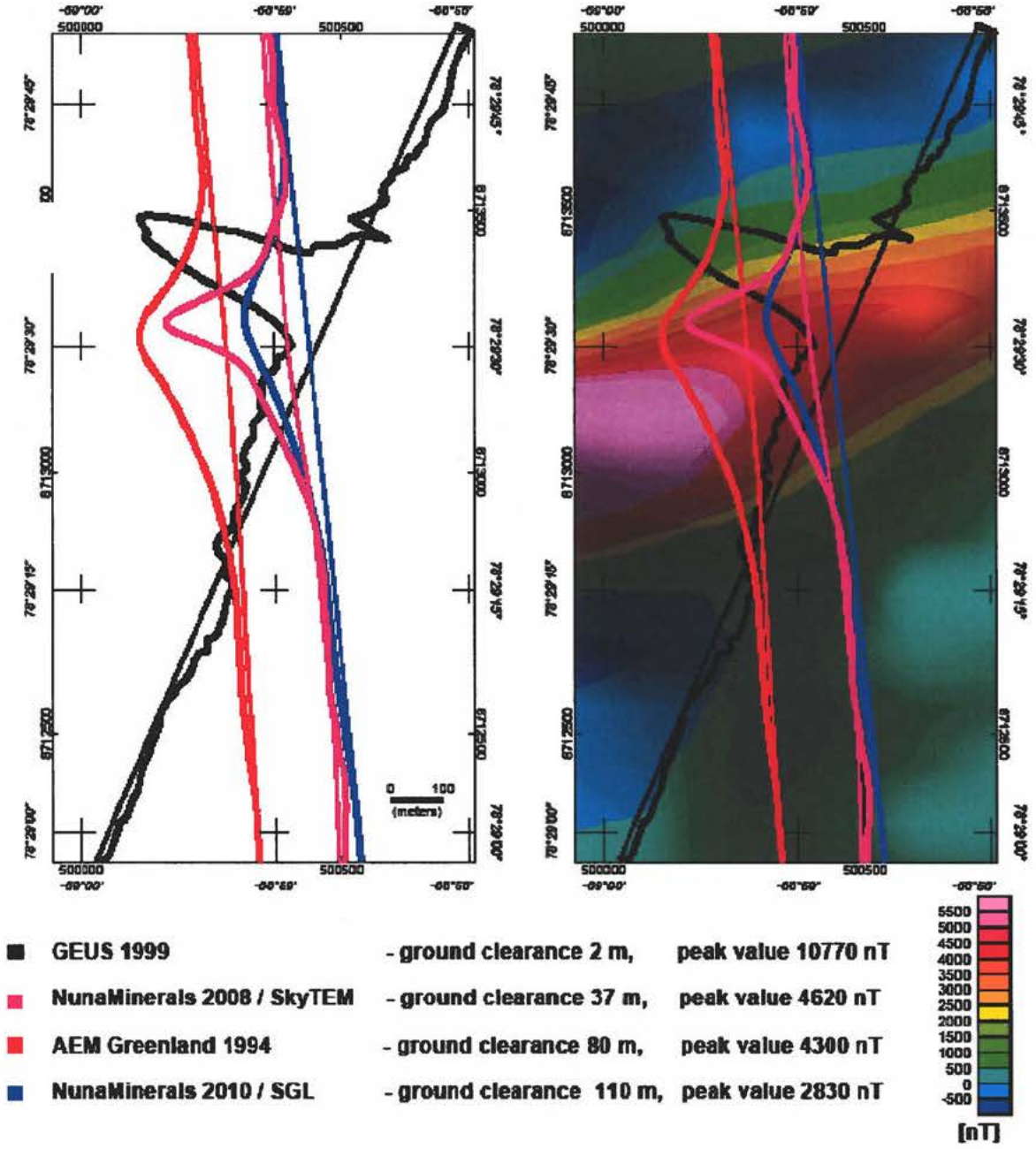

Figure 5. *Magnetic total field data from the four surveys.*

3.2 Gravity data

Airborne gravity data differs very much from standard ground gravity data, because the measured raw gravity accelerations include the accelerations (data noise) of the aircraft. An important part of the data processing of airborne gravity data is the application of a low-pass filter, which is used to separate noise from the earth gravity response. The cut-off wavelength must be chosen in such a manner that artefacts are minimised in the final processed data. The low-pass filter acts as a spatial averaging of the measured raw data, whereby random noise is eliminated. The longer cut-off wavelength the more noise is removed. However, the wavelength should not be too long in order still to retain data with geological information. SGL provided data with a half-wavelength cut-off of 1000 m and 1500 m. This imply that the final processed data are fully represented by samples every 1000 m or 1500 m. Gravity response features smaller than the cut-off wavelength is not included in the final data. Note however that the gravity response in general is smooth (the gravity response from a structure with vertical discontinuities is smooth!) and this imply that structures smaller than the sampling distance is reflected in the final processed data. The processed data might however be more smooth that the true responses, when viewed along profiles or as images. A separate section is included, which exemplify this important feature of airborne gravity data by showing responses from some simple structures before and after low-pass filtering. The remaining noise level after filtering is in the order of 0.5 mGal.

The usual processing applied to gravity data are also performed to the airborne data; i.e. free-air corrections, Bouguer plate corrections and terrain corrections. The terrain corrected Bouguer gravity data (BTC) are the data of interest for the interpretation. Both the Bouguer correction and terrain correction require a selection of a density to represent average upper crustal properties. SGL provided calculations based on densities of 2.40 g/cm^3, 2.67 g/cm^3 and 3.00 g/cm^3. Figure 6 shows four different versions of the BTC-data. The data in upper panel is based on a 1000 m half-wavelength cut-off and density of 2.67 g/cm^3. The data in the other tree panels are all based on a 1500 m half-wavelength cut-off. The densities for these are 2.40 g/cm^3, 2.67 g/cm^3 and 3.00 g/cm^3. The same colour scale is used for the data and this might not be fully optimum for the data based on the density of 3.00 g/cm^3. Apart from some differences in the amount of short wavelength content and data range, no major differences exist. The important features to search for in relation to mineralisations are local peaks in the gravity field. A common procedure to emphasize responses from local structures is to remove a regional trend from the data or to calculate the vertical gradient. Figures 7 and 8 show the detrended and vertical gradient data, respectively.

The most prominent features in the gravity data is the gravity high situated in the northwestern corner of the survey area. Other local peaks exist in the central part and a more coherent high with local peaks exist in the eastern part of the survey area. The amplitudes are in the order of 5 mGal above the background level.

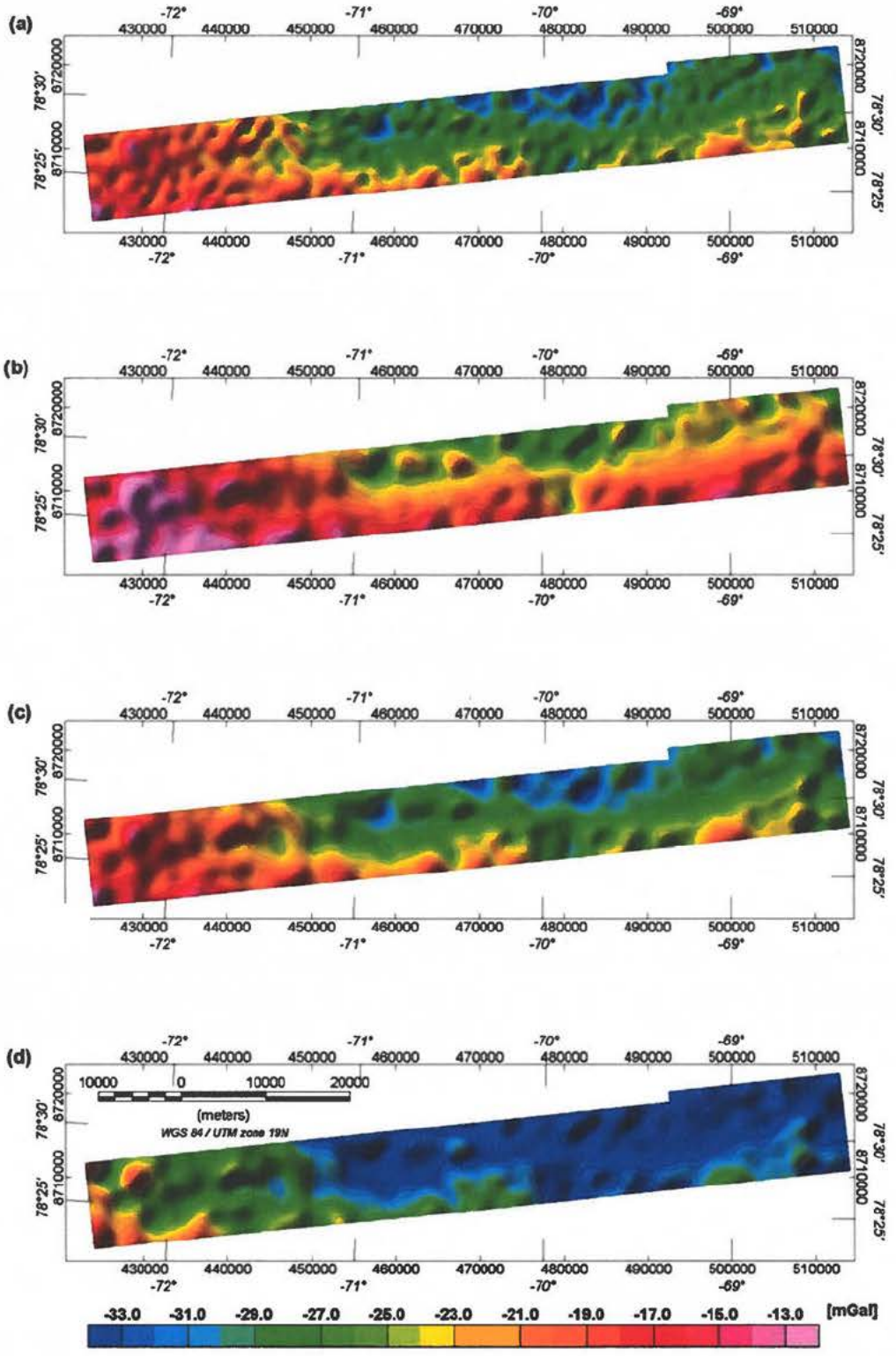

Figure 6. *Display of terrain corrected Bouguer gravity data for various types of data processing: (a) 1000 m half-wavelength filter and 2.67 g/cm^3 density for Bouguer correction; (b) 1500 m half-wavelength filter and 2.40 g/cm^3 density for Bouguer correction; (c) 1500 m half-wavelength filter and 2.67 g/cm^3 density for Bouguer correction and (d) 1500 m half-wavelength filter and 3.00 g/cm^3 density for Bouguer correction.*

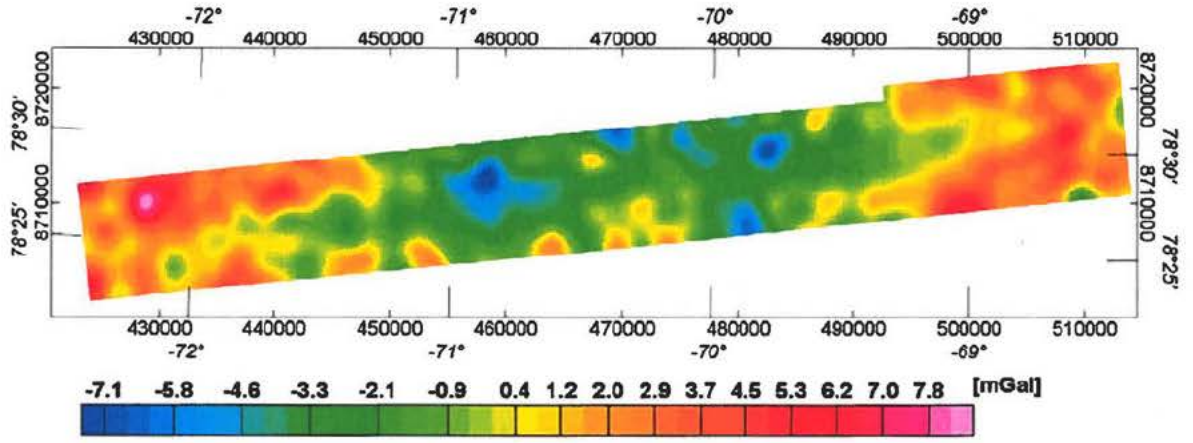

Figure 7. *Detrended terrain corrected Bouguer gravity field. Half-wavelength cut-off filter of 1500 m.*

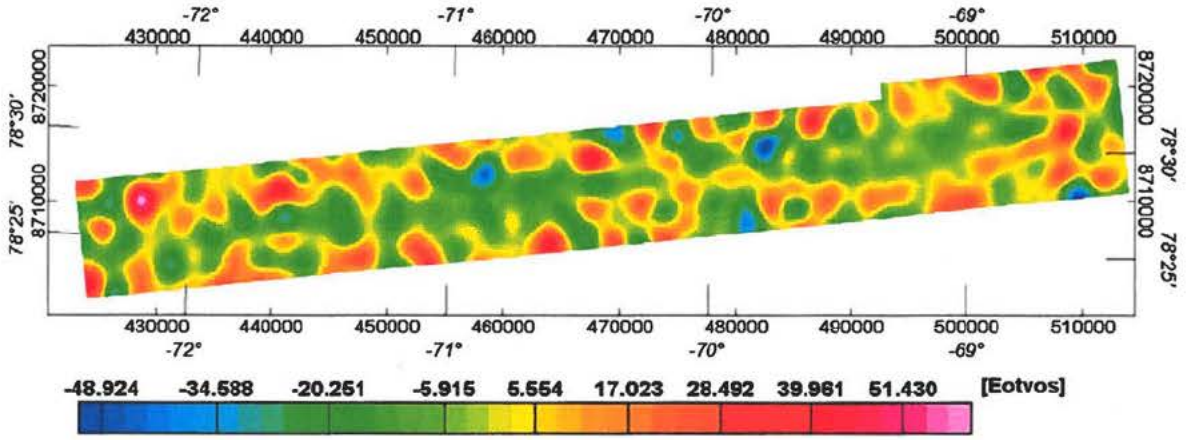

Figure 8. *Vertical gradient of Bouguer gravity field in units of Eotvos=0.1 mGal/m. Half-wavelength cut-off filter of 1500 m.*

3.3 Electromagnetic GEOTEM data

The electromagnetic data from the AEM Greenland 1994 survey are available as the line data for each of the time-gates recorded during surveying and as grids of selected parameters after processing. The results in this report are based on the grids and they include the conductance, amplitude of X-component channel 2 and finally the decay constant. The amplitude of the X-component channel 2 is a measured quantity, whereas both the conductance and decay constants are calculated after processing. The decay constant is a measure of the attenuation of the electromagnetic signal after turn-off of the electromagnetic source. If good conductors are present, the decay constant (units of micro seconds) will be long compared to cases with a resistive ground.

Grids of apparent X-component channel 2, apparent conductivity and decay constant tau are shown in Figures 9-11. Elongated conductors are characteristic for the area of the Minturn magnetic anomaly. Note however that some of these are not coincident with the magnetic anomalies.

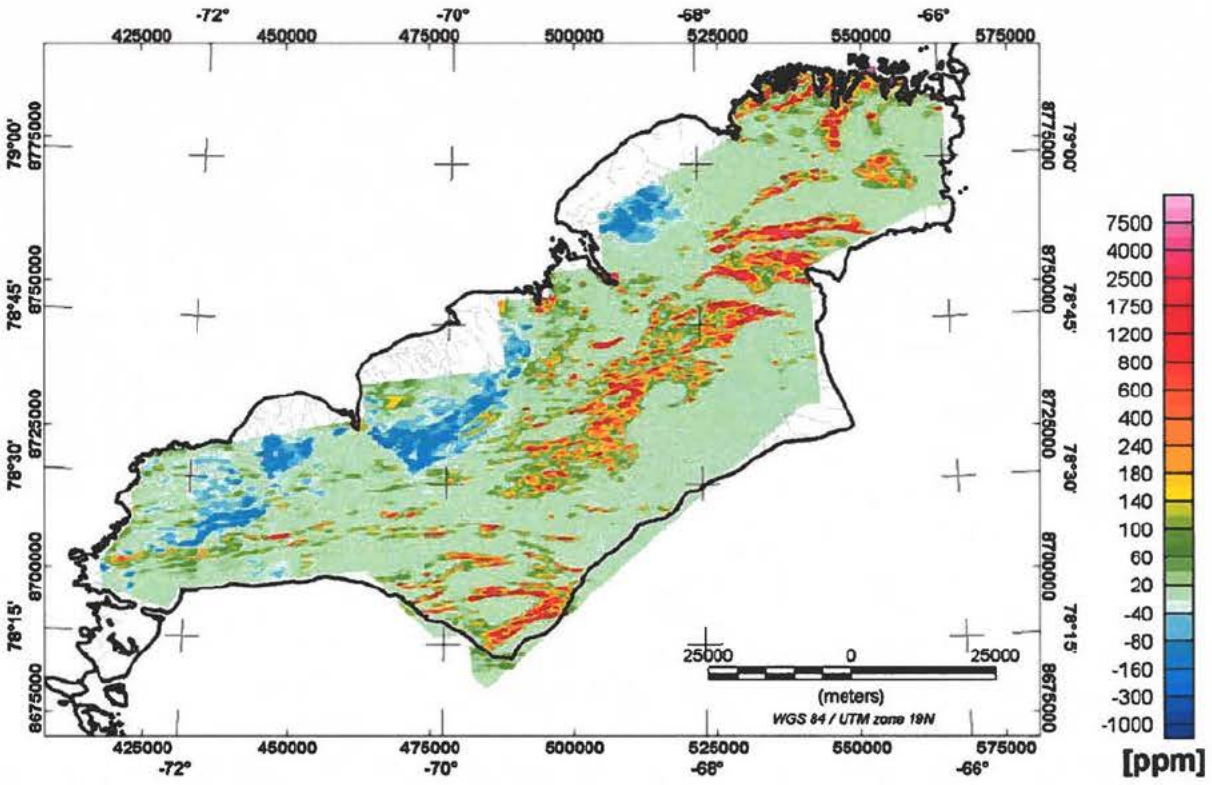

Figure 9. *Amplitude of GEOTEM X-component channel 2. Units are in ppm of the primary source field.*

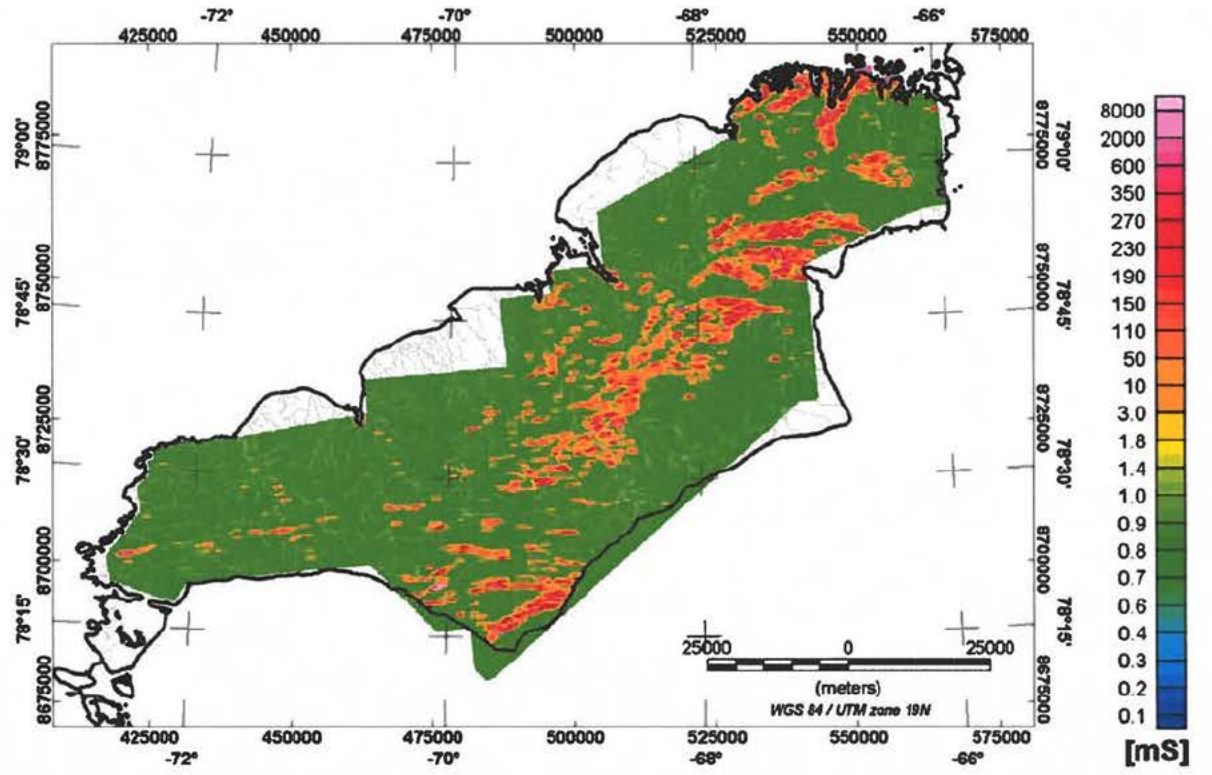

Figure 10. *Calculated conductance from the GEOTEM data. Units in mSiemens.*

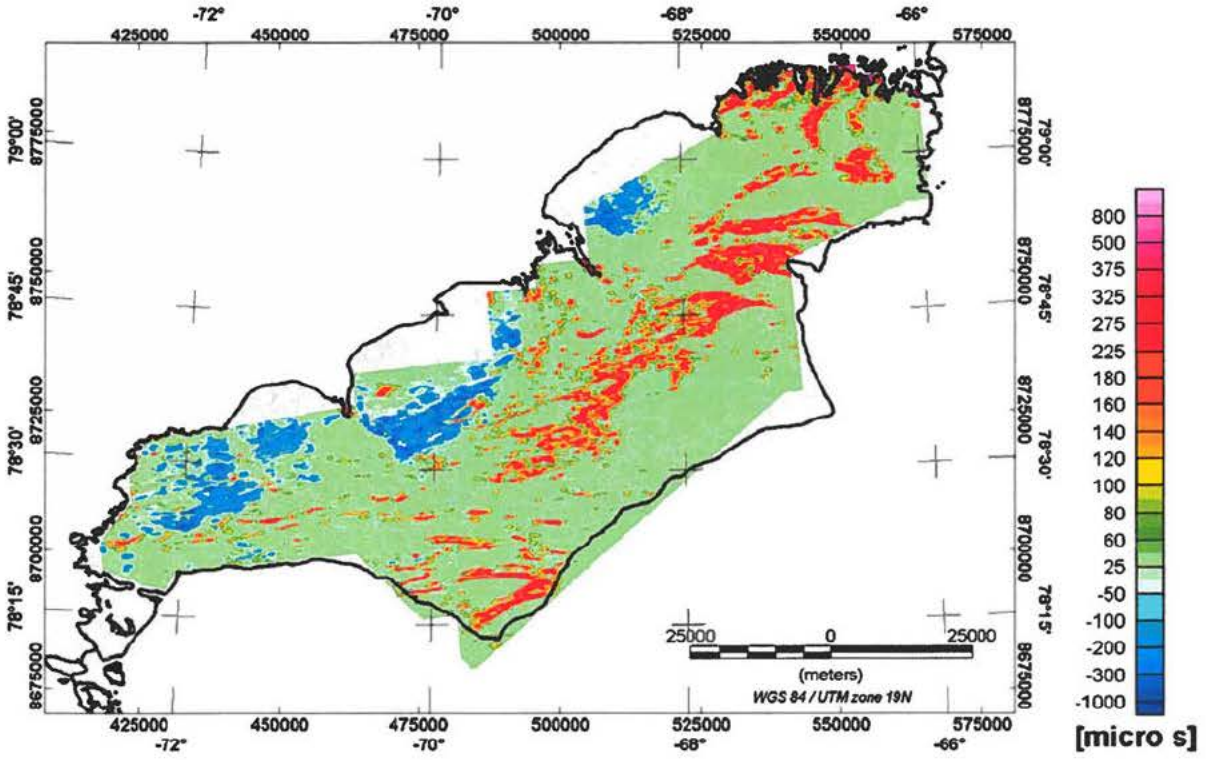

Figure 11. *Calculated decay constant tau from the GEOTEM data. Units in micro seconds.*

3.4 Petrophysical data

Appel et al. (1995) provided magnetic and density information based on laboratory measurement on rocks samples from the Minturn area. Magnetic susceptibility of 8 SI and10.2 SI are given which is close to the average values quoted in the literature of 6 SI (Telford el. Al., 1990). Densities for the samples vary from 4.295 to 4.75 g/cm^3.

Magnetic susceptibility measurements were made in-situ by NunaMinerals A/S in Spetember 2010 along profiles crossing the Minturn magnetic anomaly. The results are displayed in Figure 12 where average values for each particular site (10 samples) are plotted with the vertical gradient of the magnetic field as background image. A total of 2527 measurements were performed. Mininum and maximum are -0.01*10^{-3} SI and 854*10^{-3} SI. Mean and standard deviation are 30.*10^{-3} SI and 45. *10^{-3} SI. The location with maximum values is reported to be an exposure with a 1-2 m wide black rock. Some positive correlation can be noted in Figure 12 between measured susceptibility and measured vertical magnetic gradient. The correlation is however weak as can be seen in Figure 13. A similar type of investigation with respect to correlation between measured susceptibility and the first vertical gradient of the Bouguer gravity field shows no correlation.

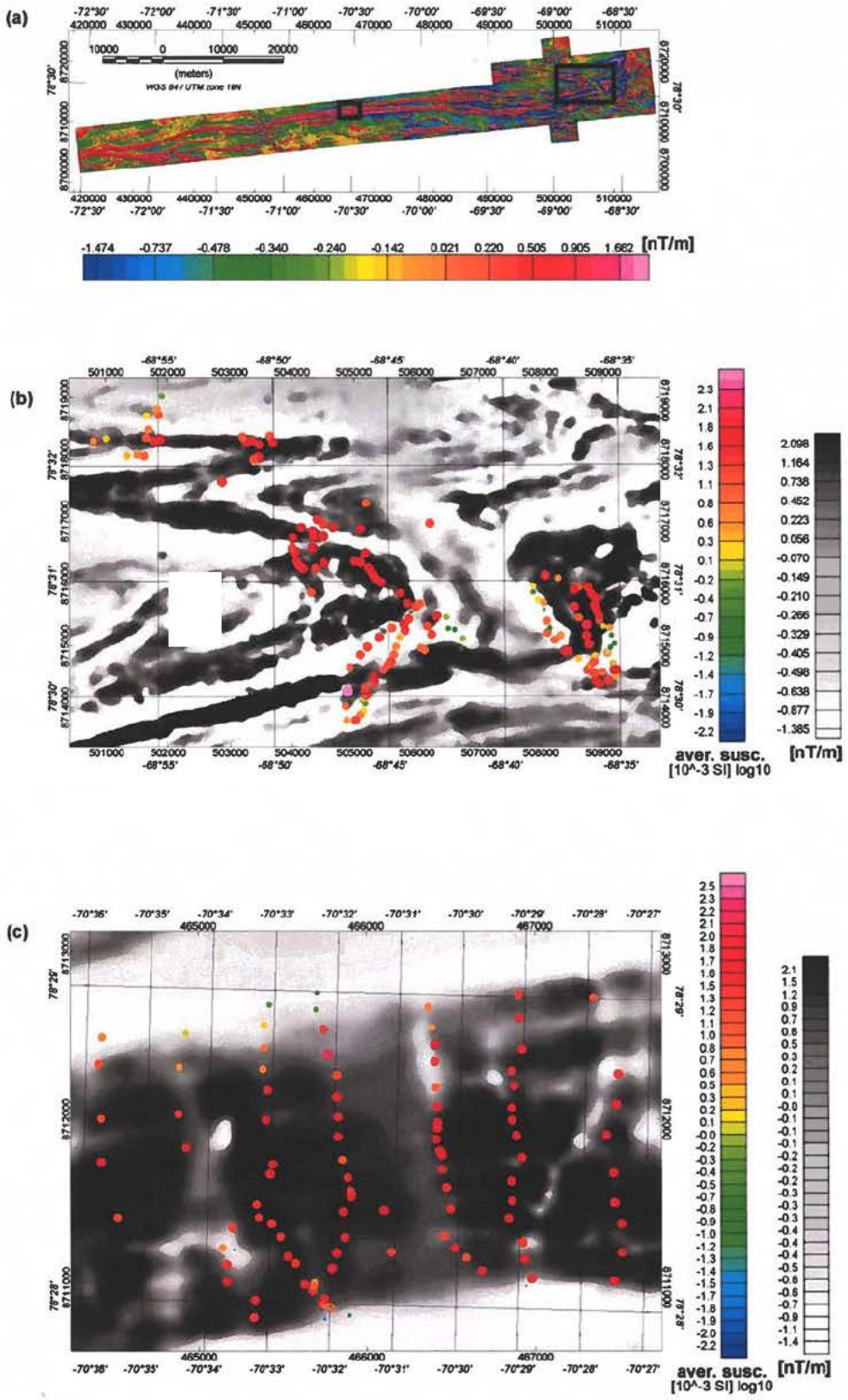

Figure 12. *Magnetic susceptibility measurements by NunaMinerals A/S September 2010. (a) Image of vertical magnetic gradient from the SGL 2010 survey with black rectangles showing areas displayed in (b) and (c). The magnetic susceptibility data are log_{10} of the data in units of 10^{-3} SI. The symbol size is proportional to the data value after subtraction of a base level of -4; i.e. a data value of 10^{-7} SI corresponds to zero symbol size. The data value can also be read from the colour scales.*

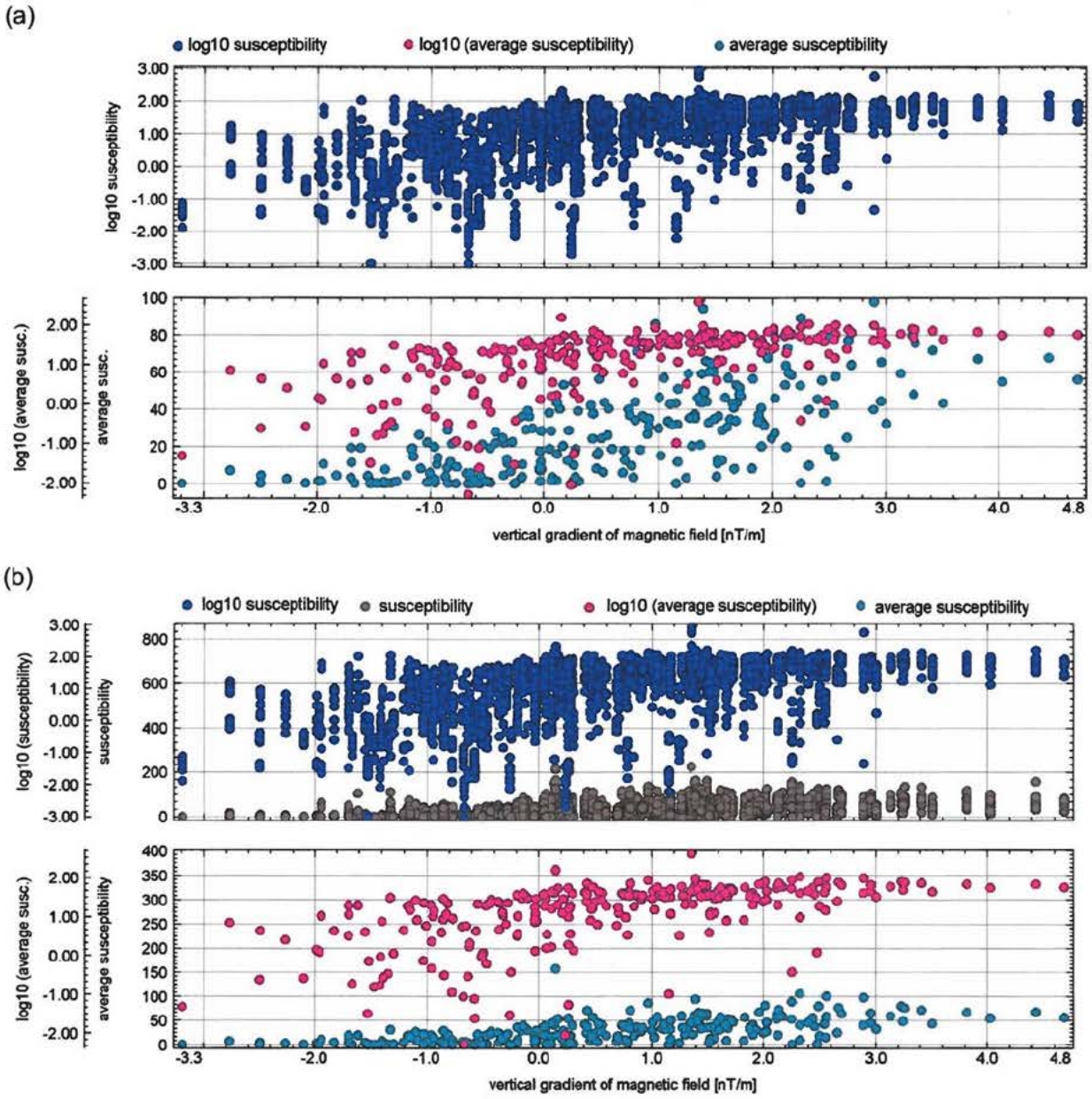

Figure 13. *Measured susceptibility versus the vertical gradient of the magnetic field. The difference between panels (a) and (b) is the data range used for the ordinate. All susceptibility values are in units of 10^{-3} SI apart for the use of logarithm for some of the plots.*

4. Data correlation

This chapter includes a description of correlation between the various geophysical data types available from Inglefield Land. Furthermore, the geophysical data are discussed in relation to the geological map of the area with emphasis on possible correlation/coincidence of major geophysical anomalies with mapped geological units. The correlation is done visually based on detailed map sections of the various data and by the use of a three-dimensional or perspective plot, in which one data type is used to represent a relief, onto which another data type is draped. Each map is marked with coordinate system (X,Y,Z), where X refers to north direction, Y east direction and Z is vertical.

The gravity data used are the Bouguer and terr[illegible] er removal of a first order data trend (1500 m half-wavelength data). The[illegible] chosen to represent the regional gravity variation and is supposed to be[illegible] ron ore occurrences. The purpose of subtracting the first order data tren[illegible] anomalies. The Bouguer data used are based on the 2.67 g/cm^3 densit[illegible] it change of result is obtained by using the other densities of 2.40 g/cm^3 or 3.00 g/cm^3. vertical gradient of the Bouguer data (based on the 1000 m half-wavelength filter and 2.67 g/cm^3 density value) is also used for the analysis.

The reliefs onto which the data are draped are always based on a linear data presentation. A scaling factor is applied to each relief in order to enable visualisation of certain data features. This is a somewhat subjective approach and other choices might be useful for the correlation analysis. Figure 14 shows the colour scales used for the draped geophysical data.

It is important to keep in mind that the original geological map has a scale 1:500 000 and boundaries of the geological units are therefore not necessarily well resolved. Significant quaternary cover in the area also impacts negatively on the possibility of performing a correlation analysis. A colour legend for the maps with geological units is shown in Figure 15. For details about units and stratigraphy, reference is made to Dawes (2004).

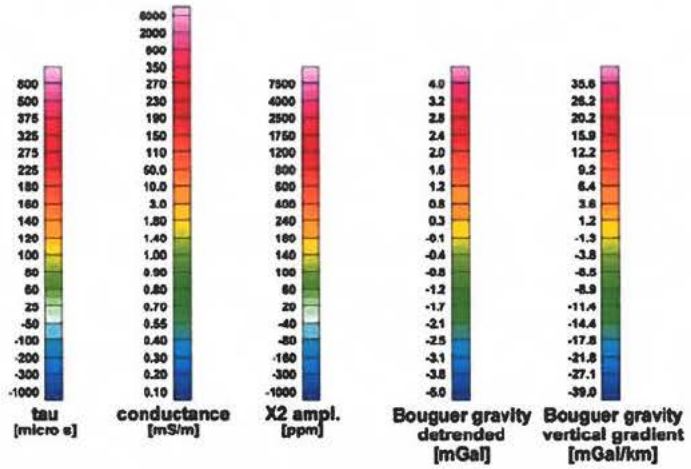

Figure 14. *Colour legends used for the display of geophysical data. From left to right are decay constant tau for the AEM Greenland 1994 data followed by conductance and amplitude of X-component channel. Bouguer gravity data are shown after detrending and after calculation of the vertical gradient.*

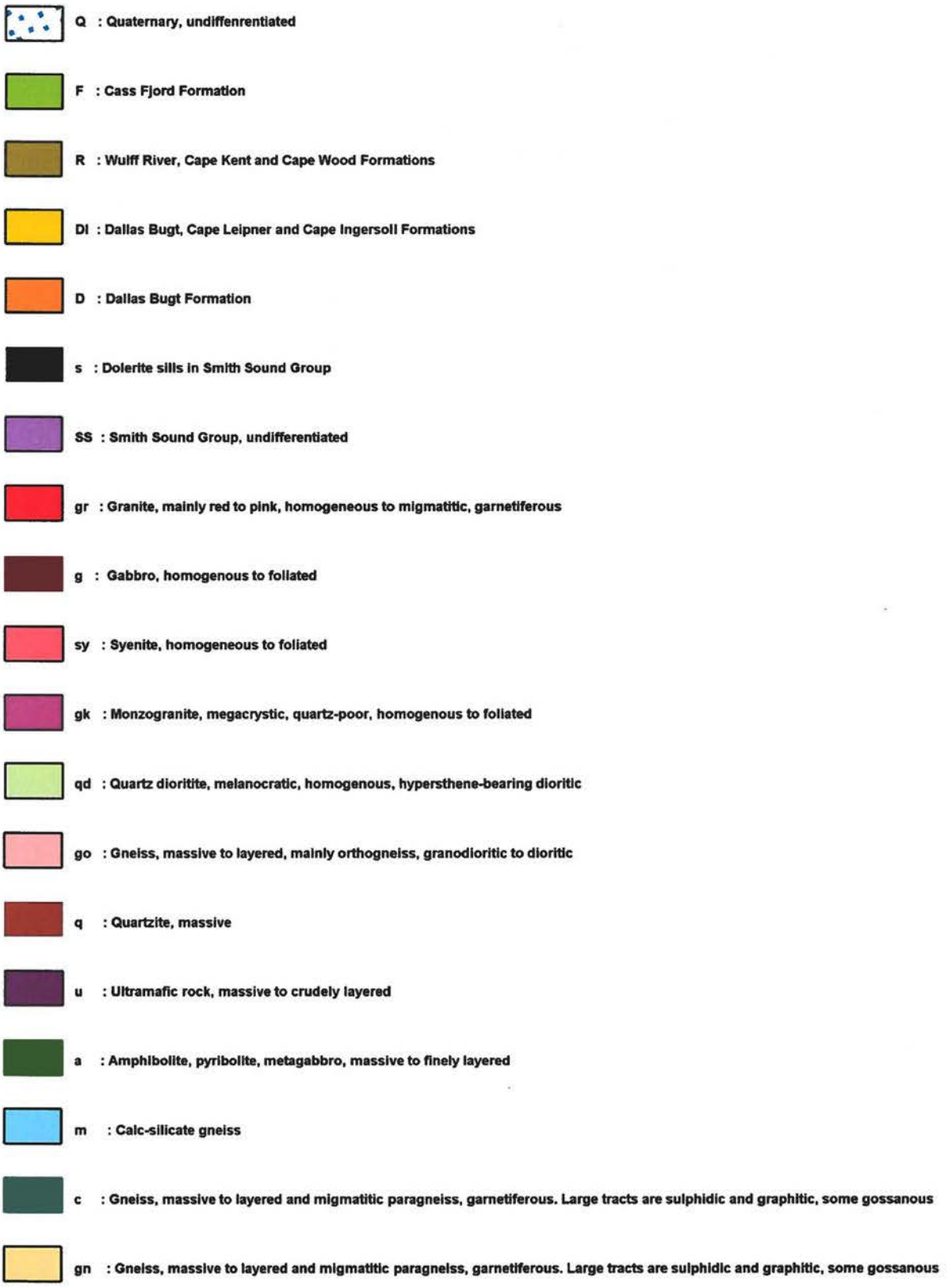

Figure 15. *Legend for the geological maps included. Descriptions of rock units can be found in Dawes (2004).*

4.1 Magnetic data and geological map

Figures 16-19 show information from an area encompassing the location with maximum magnetic response and the Minturn River. The geological map (Figure 16) is redrawn from Dawes (2004) and an image of the total magnetic field from the AEM Greenland 1994 survey is shown in Figure 17. The corresponding magnetic tilt angle is shown in Figure 18, and the analytic signal based on the 2008 Skytem APS data is shown in Figure 19. Measured susceptibility values from the 2010 fieldwork by NunaMinerals A/S are plotted on the geological map. Figures 16 and 17 have a display of the 1:500 000 geological map draped onto a relief based on total magnetic field intensity data from the SGL 2010 airborne survey. Figures 18 and 19 have a display of the 1:500 000 geological map draped onto a relief of the magnetic data from the AEM Greenland 1994 survey.

As mentioned above, some uncertainties may exist with respect to the accuracy of the mapped geological boundaries. This appears to be the case for the 5 km elongated occurrence of syenite (sy) (labelled A in Figures 16 and 17). At the location marked B a much better correlation is seen between mapped units of syenite and the observed magnetic field variations. Note, however, that the co-location of syenite and the magnetic high at B is not necessarily an indication that the syenite is causing the high magnetic values. Another location with a good correlation is at the location marked C where orthogneiss (go) is seen to be associated with high magnetic field values and where marble is associated with low values of the magnetic field. At the location marked D the interpretation is somewhat difficult and the utilisation of tilt angle data (Figure 18) or analytic signal (Figure 19) does not provide a unique answer with respect to which unit is linked to the high magnetic field values at this particular site. The association of high magnetic field intensity and syenite occurrences is very pronounced further east from location D where large areas (about 400 km^2) are mapped as syenite. This area is characterised by average magnetic field intensity values around 800 nT.

The maps in Figures 20 to 23 show that othogneisses are associated with intermediate values of the magnetic field. The elongated magnetic anomaly in focus for the SGL 2010 survey is found to cross both the Smith Sound Group (SS) and the paragneisses (gn) without any disruption at the boundary between the two geological units.

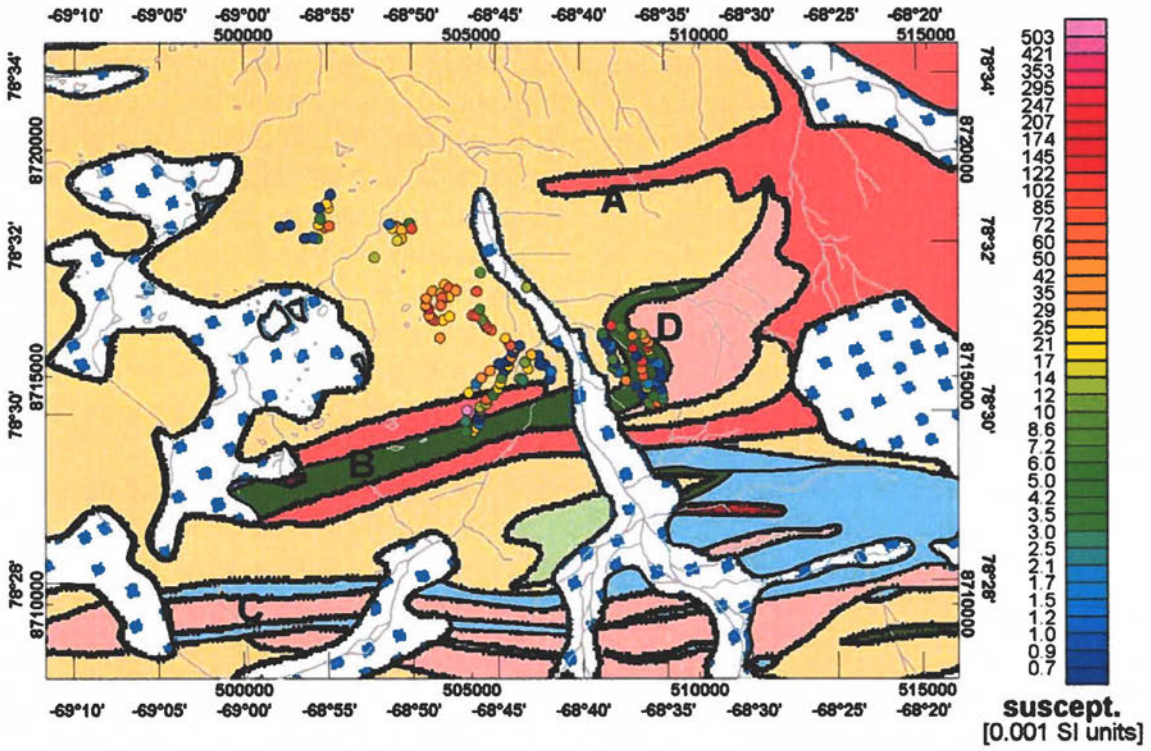

Figure 16. *Geological map around the location with maximum magnetic field anomaly (redrawn from Dawes, 2004). Locations marked A-D are referred explicitly in the text. Measured susceptibility values from fieldwork by NunaMinerals A/S September 2010 are plotted as colour filled circles.*

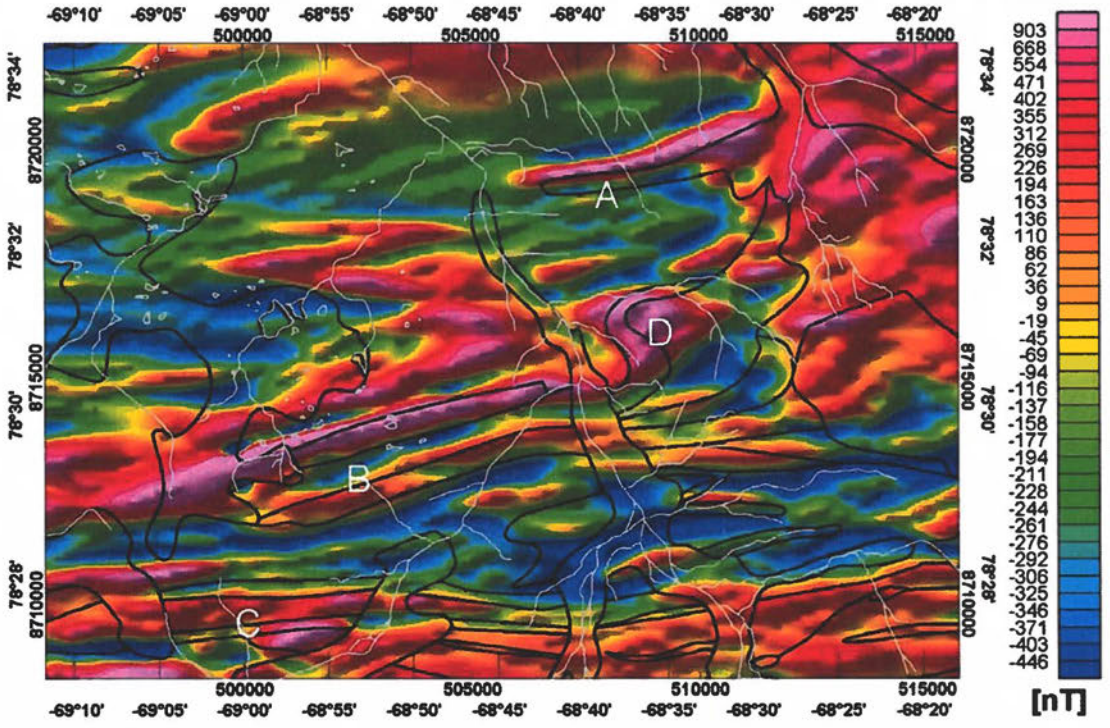

Figure 17. *Total magnetic field anomaly from the AEM Greenland 1994 survey around the location with maximum magnetic field anomaly. The map section is similar to the geological map in Figure 16. Locations marked A-D are referred explicitly in the text.*

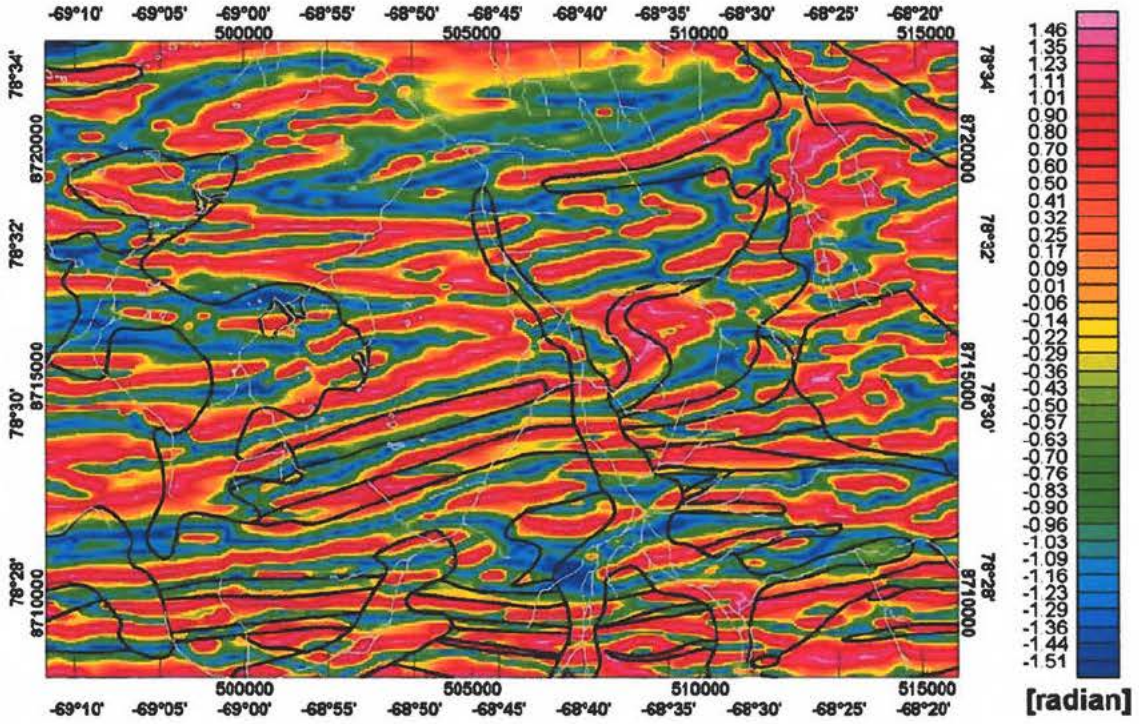

Figure 18. *Tilt angle of total magnetic field anomaly from the AEM Greenland 1994 survey around the location with maximum magnetic field anomaly. The map section is similar to the geological map in Figure 16.*

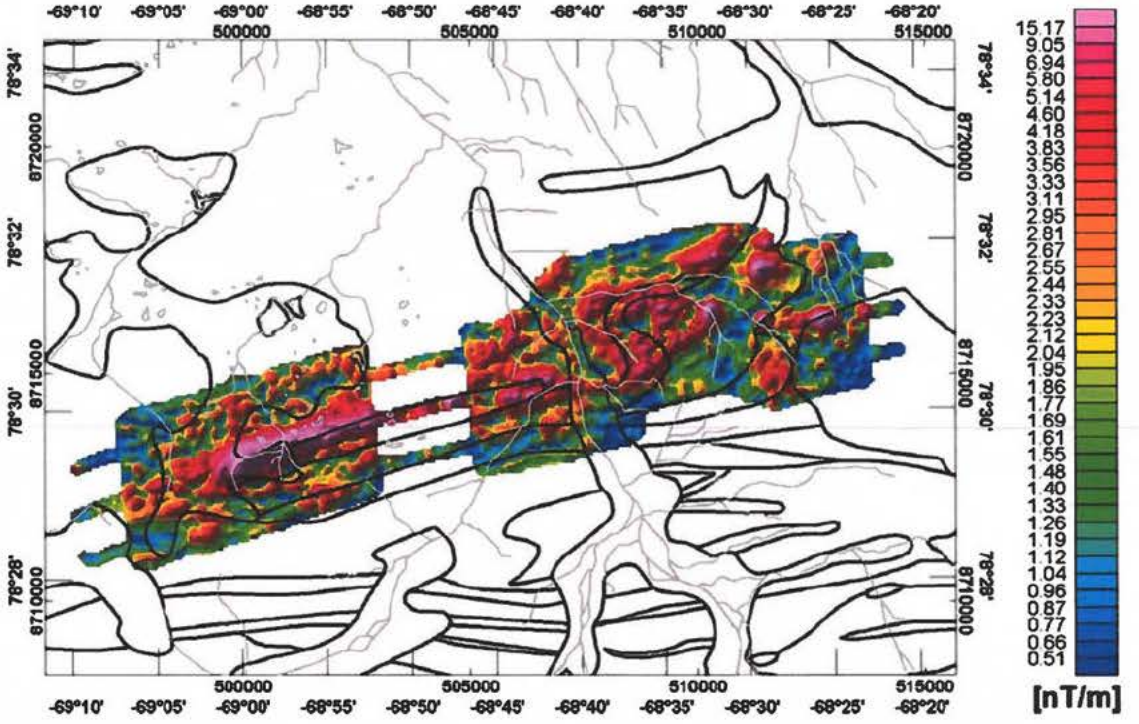

Figure 19. *Total magnetic field anomaly from the AEM Greenland 1994 survey around the location with maximum magnetic field anomaly. The map section is similar to the geological map in Figure 16..*

Figure 20. *Geological map draped on total magnetic field anomaly data from the SGL 2010 survey. View from southeast. With the exception for the Smith Sound Group, black lines represent boundaries between rock units.*

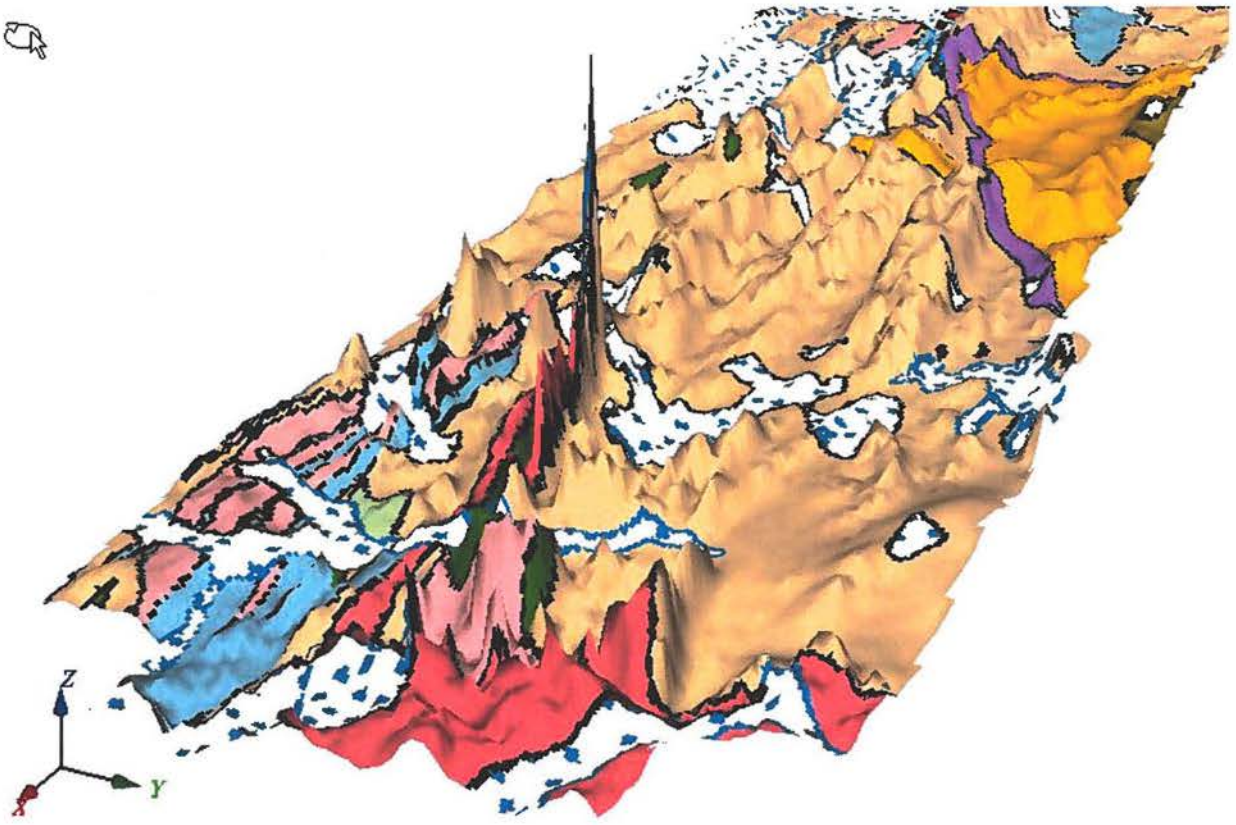

Figure 21. *Geological map draped onto the relief of the total magnetic field anomaly from the SGL 2010 survey. Eastern part of survey. View from east-northeast. With the exception for the Smith Sound Group, black lines represent boundaries between rock units.*

Figure 22. *Geological map draped onto the relief of the total magnetic field anomaly from the AEM Greenland 1994 surve. View from northeast. With the exception for the Smith Sound Group, black lines represent boundaries between rock units.*

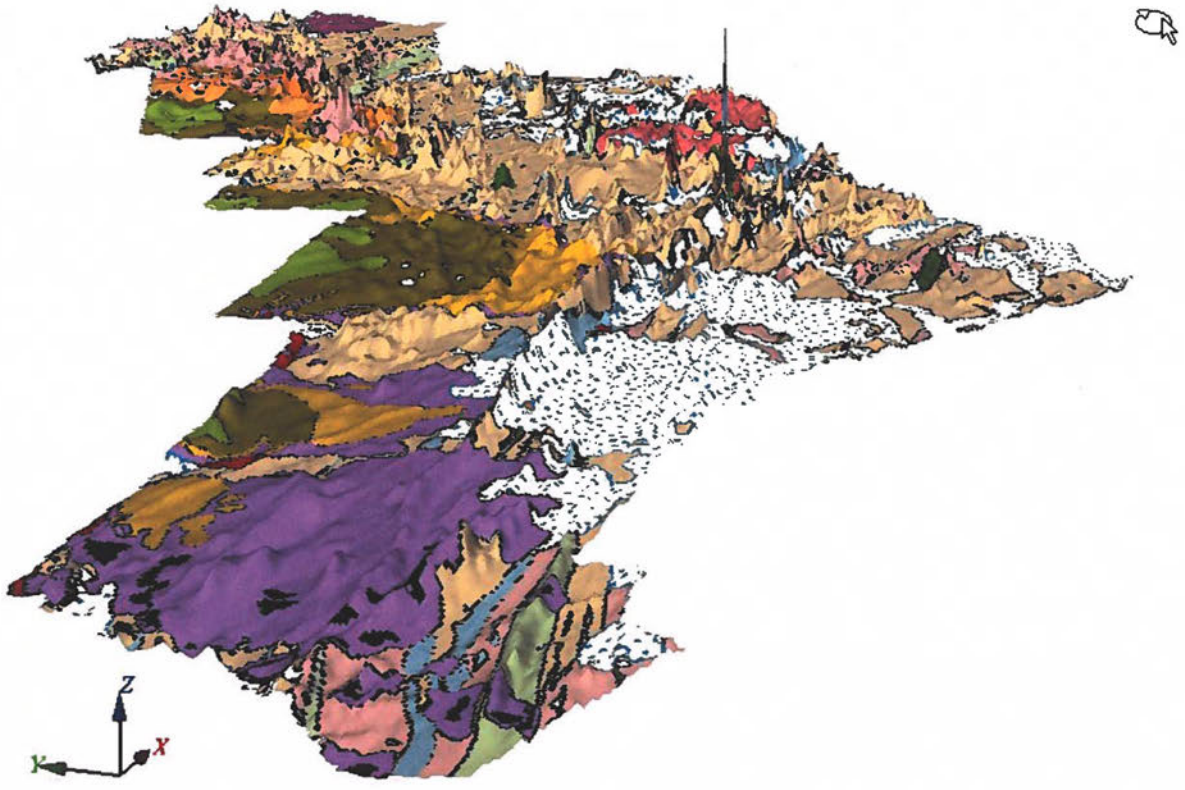

Figure 23. *Geological map draped onto the relief of the total magnetic field anomaly from the AEM Greenland 1994 survey. View from west-southwest. With the exception for the Smith Sound Group, black lines represent boundaries between rock units.*

4.2 Magnetic data and electromagnetic data

Figures 24 to 29 show various representations of the GEOTEM data draped onto the relief of the magnetic field anomaly data from the AEM Greenland 1994 survey. The data presentations used are GEOTEM X-component channel 2, conductance and decay constant tau. For all three types of presentations of the electromagnetic data, high values imply the presence of a conductor. The colour scales used are shown in Figure 14. The X-component channel 2 might pick up small scale conductors that are not necessarily pronounced in the apparent conductivity data presentation. The apparent conductivity will tend to show conductors of larger size. High values of the decay constant might be an indication of deep conductors or conductors of large size.

Good conductors in association with high magnetic field anomalies would in general be obvious targets for ground follow-up in a search for mineralisations. IOCG's are not expected to be highly conductive (Smith, 2002; Corriveau, 2007) due to the general sulphide deficiency. Moderate conductivity is however expected to occur in areas with breccia core and in relation to large volumes of disseminated mineralisation. In order to evaluate the correlation and for the search of outliers, which might be of interest in relation to mineralisations, maps are produced with emphasis on peak values for the magnetic response and electromagnetic data. The following maps are produced (Figures 30 and 31):

- Locations with maximum vertical gradient of magnetic field and values of decay constant tau
- Locations with maximum decay constant and values of vertical gradient of magnetic field
- Locations with minimum vertical gradient of magnetic field and values of decay constant tau

The correlation between electromagnetic and magnetic data is primarily linked to larger domains with similar response characteristics, whereas the correlation between peak values is weak. Some interesting outliers or anomalies can however be picked from these maps. These anomalies are included in a separate section on target identification.

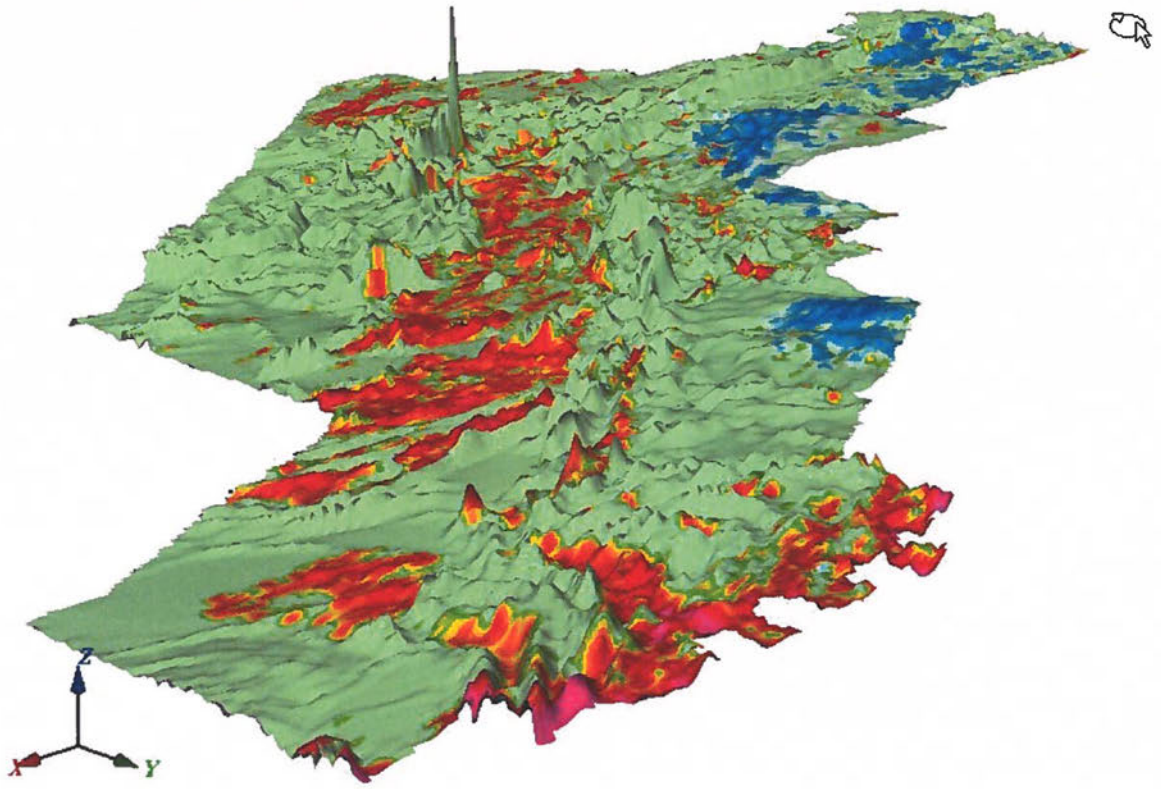

Figure 24. *GEOTEM decay constant tau draped onto the relief of the total magnetic field anomaly from the AEM Greenland 1994 survey. View from northwest. The colour legend is shown in Figure 14.*

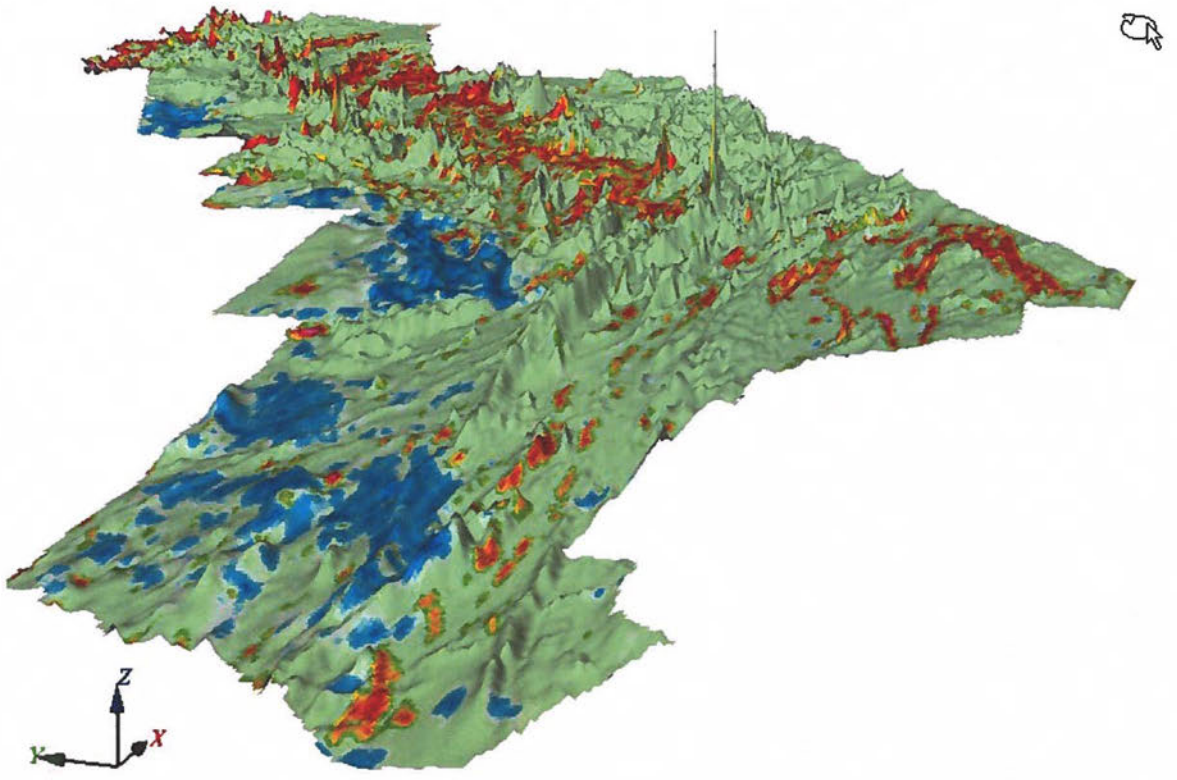

Figure 25. *GEOTEM decay constant tau draped onto the relief of the total magnetic field anomaly from the AEM Greenland 1994 survey. View from west-southwest. The colour legend is shown in Figure 14.*

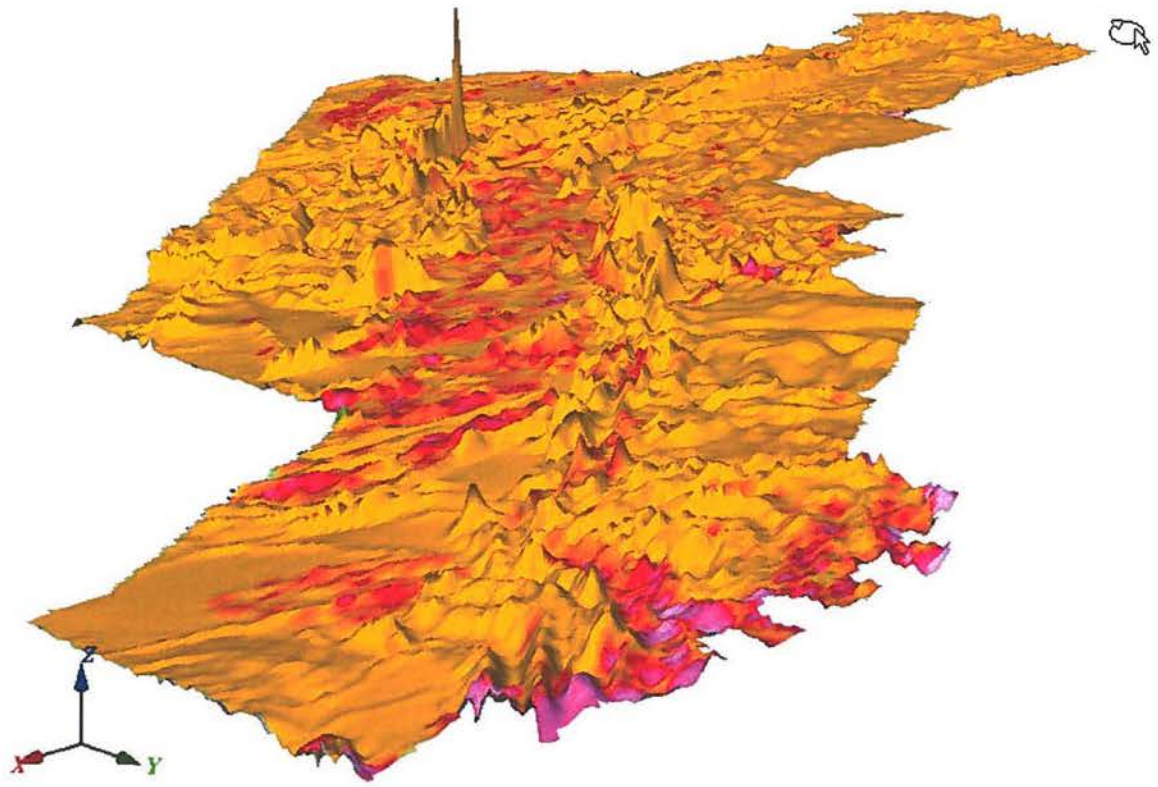

Figure 26. *GEOTEM apparent conductivity draped onto the relief of the total magnetic field anomaly from the AEM Greenland 1994 survey. View from northwest. The colour legend is shown in Figure 14.*

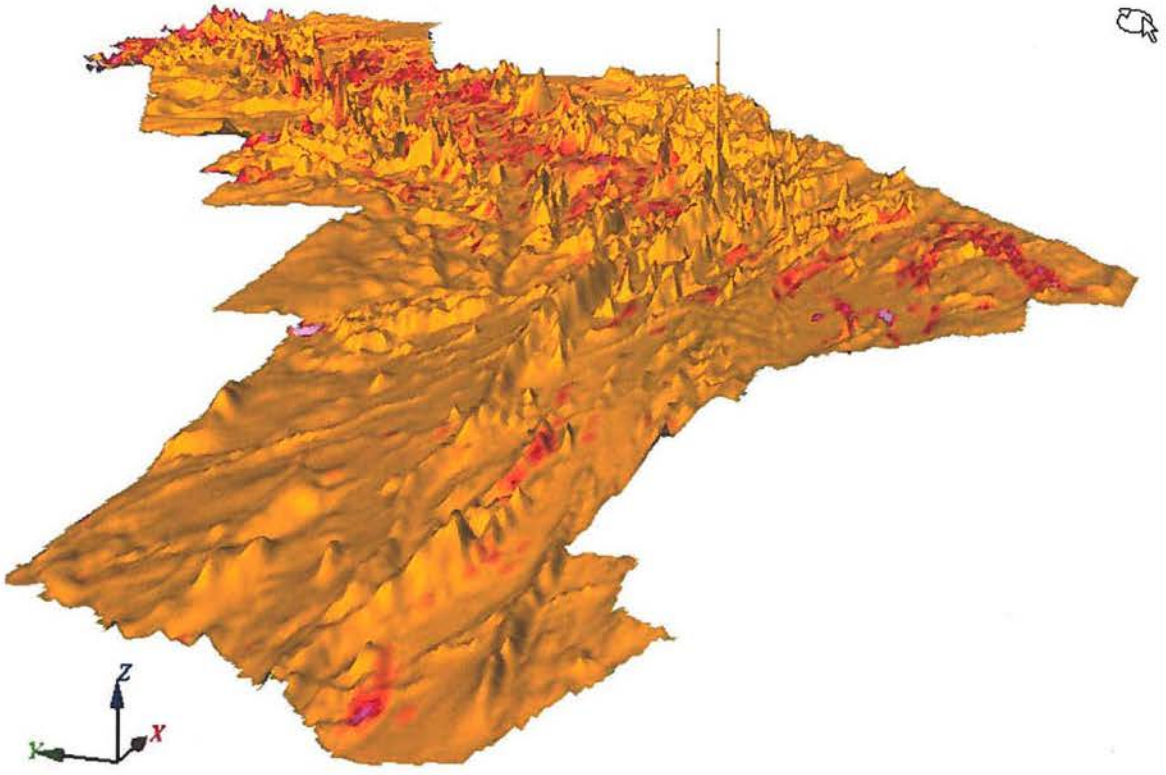

Figure 27. *GEOTEM apparent conductivity draped onto the relief of the total magnetic field anomaly from the AEM Greenland 1994 survey. View from west-southwest. The colour legend is shown in Figure 14.*

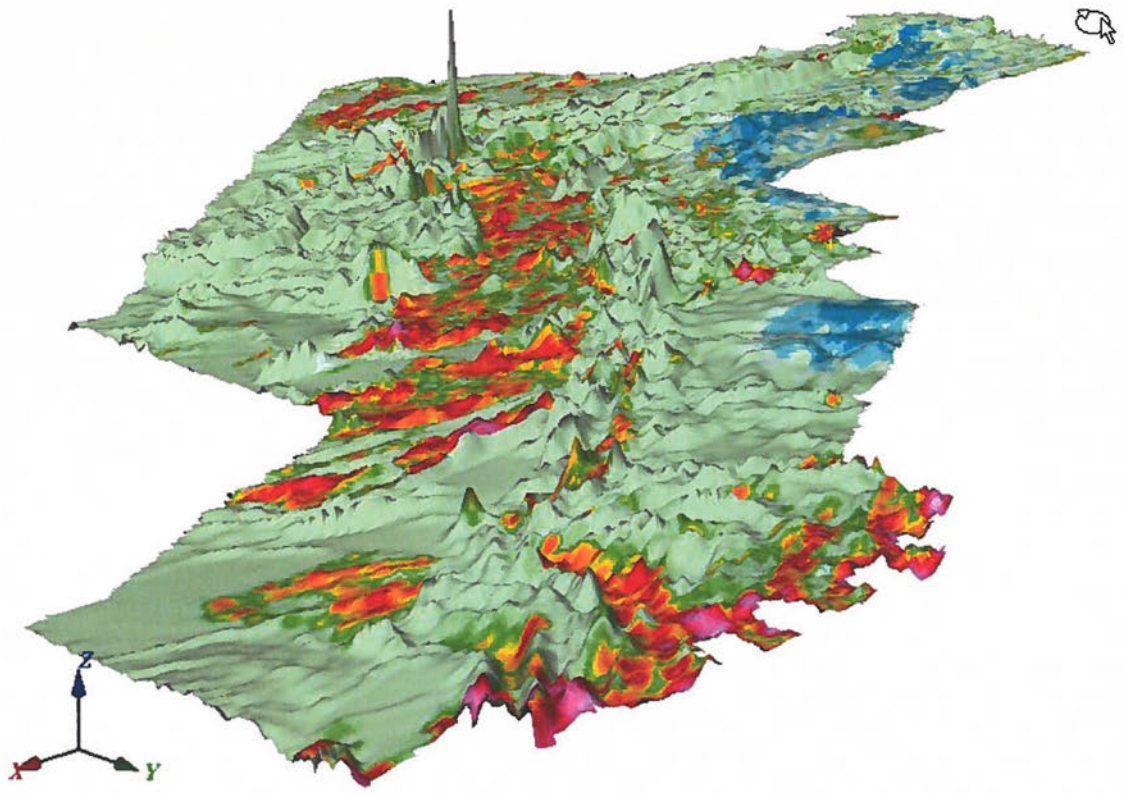

Figure 28. *GEOTEM X-component channel 2 draped onto the relief of the total magnetic field anomaly from the AEM Greenland 1994 survey. View from northwest. The colour legend is shown in Figure 14.*

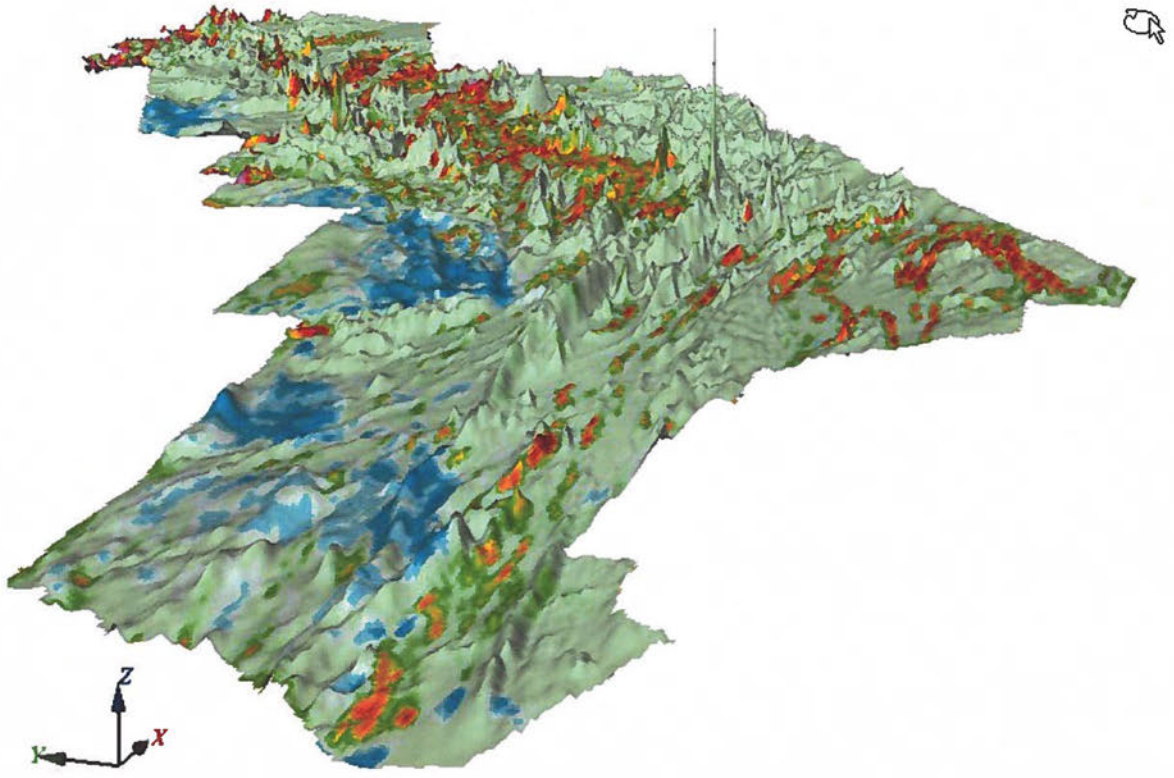

Figure 29. *GEOTEM X-component channel 2 draped onto the relief of the total magnetic field anomaly from the AEM Greenland 1994 survey. View from west-southwest. The colour legend is shown in Figure 14.*

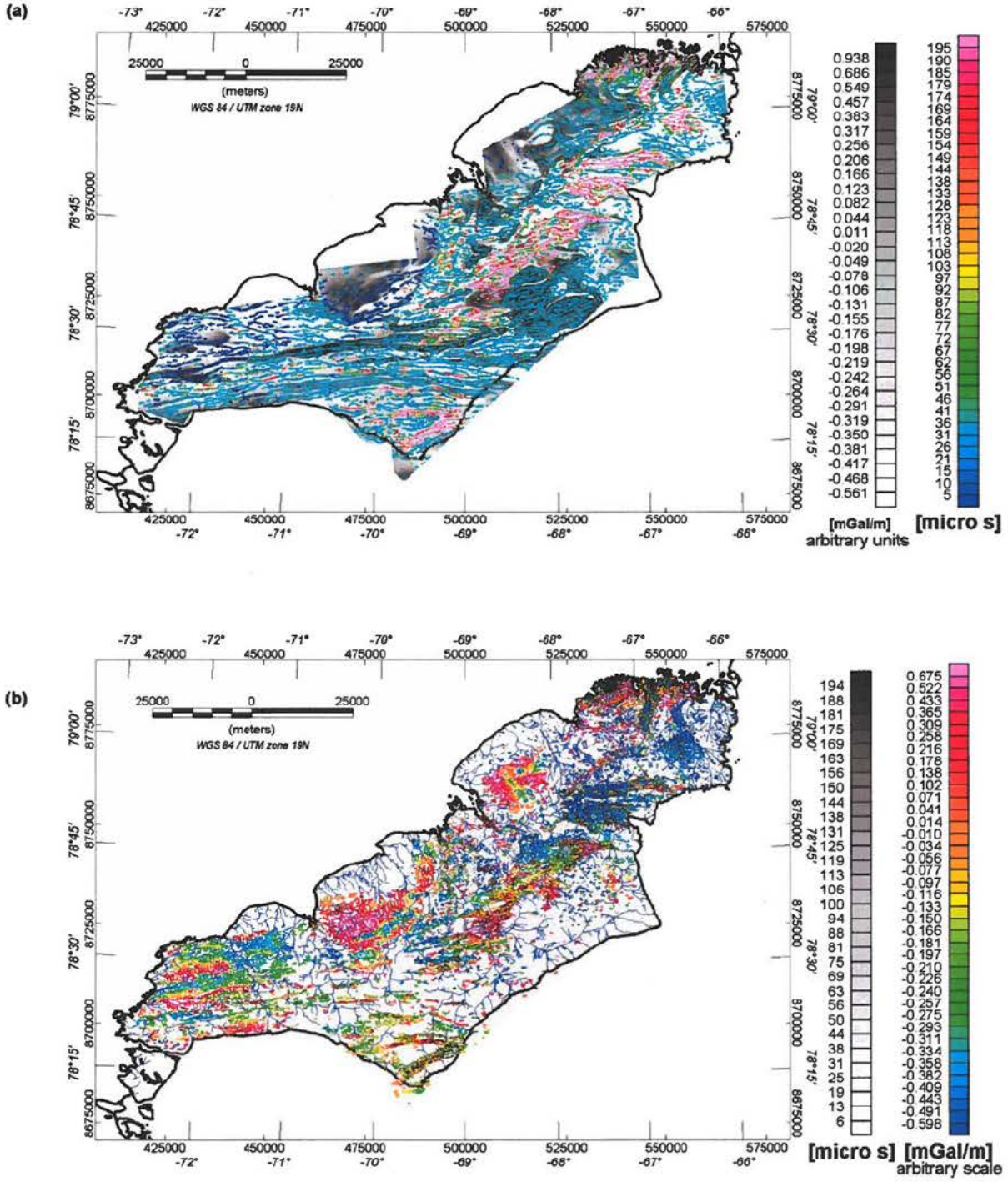

Figure 30. *(a) Colour filled circles show values of the GEOTEM decay constant superimposed on a grey scale image (arbitrary scale in unit of mGal/m) of the vertical gradient of the pseudo gravity field. The symbol location corresponds to the location where the vertical gradient of the pseudo gravity has local maxima, (b) Colour filled circles show values of the vertical gradient of the pseudo gravity superimposed on a grey scale image of the GEOTEM decay constant. The symbol location corresponds to the location where the GEOTEM decay constant has local maxima.*

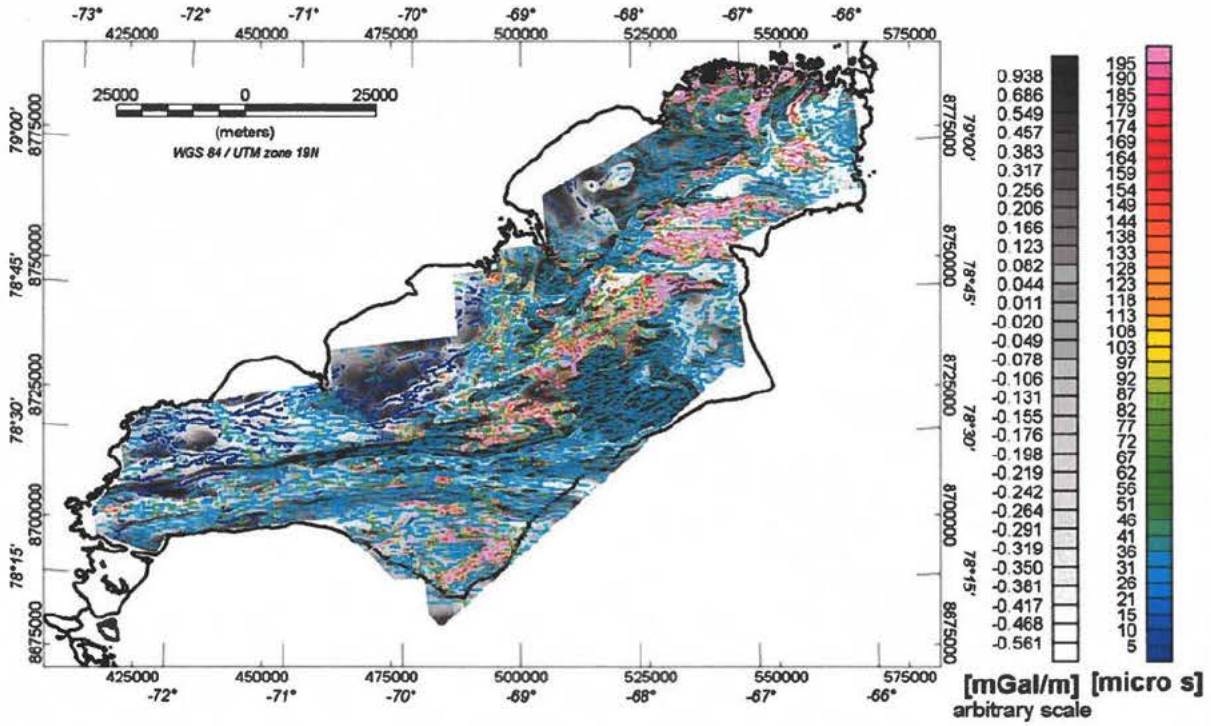

Figure 31. *Colour filled circles show values of the GEOTEM decay constant superimposed on a grey scale image (arbitrary scale in unit of mGal/m) of the vertical gradient of the pseudo gravity field. The symbol location corresponds to the location where the vertical gradient of the pseudo gravity has local minima.*

4.3 Magnetic data and gravimetric data

Figure 32 shows the detrended Bouguer gravity anomaly superimposed on the total magnetic field intensity from the entire area covered by SGL 2010 survey. It is evident that no systematic correlation exists between high magnetic field anomalies and high Bouguer gravity values. At some locations with high gravity the magnetic field is high, whereas at other location the magnetic field is low. An area where high Bouguer gravity is associated with high magnetic field values occur in the area close to the Minturn River and the location with maximum magnetic field strength has a high Bouguer gravity anomaly.

The lack of correlation between the gravity field and magnetic field is visualised in Figure 35, which show values of the vertical gradient of the Bouguer gravity field at locations, where the vertical gradient of the pseudo gravity has maximum values. The pseudo gravity field is a transformation of the magnetic field, which would be identical to the gravity field provided that all rock densities are related to the magnetic susceptibilities by a constant scaling factor. The reason for using the vertical gradient is to emphasize short wavelength features. The scatter plots in Figure 33 demonstrate clearly that no systematic correlation exists. Note that the location with high magnetic field strength marked D in Figures 16 and 17 has high values for both the vertical gradient of the pseudo gravity field and the vertical gradient of the Bouguer field.

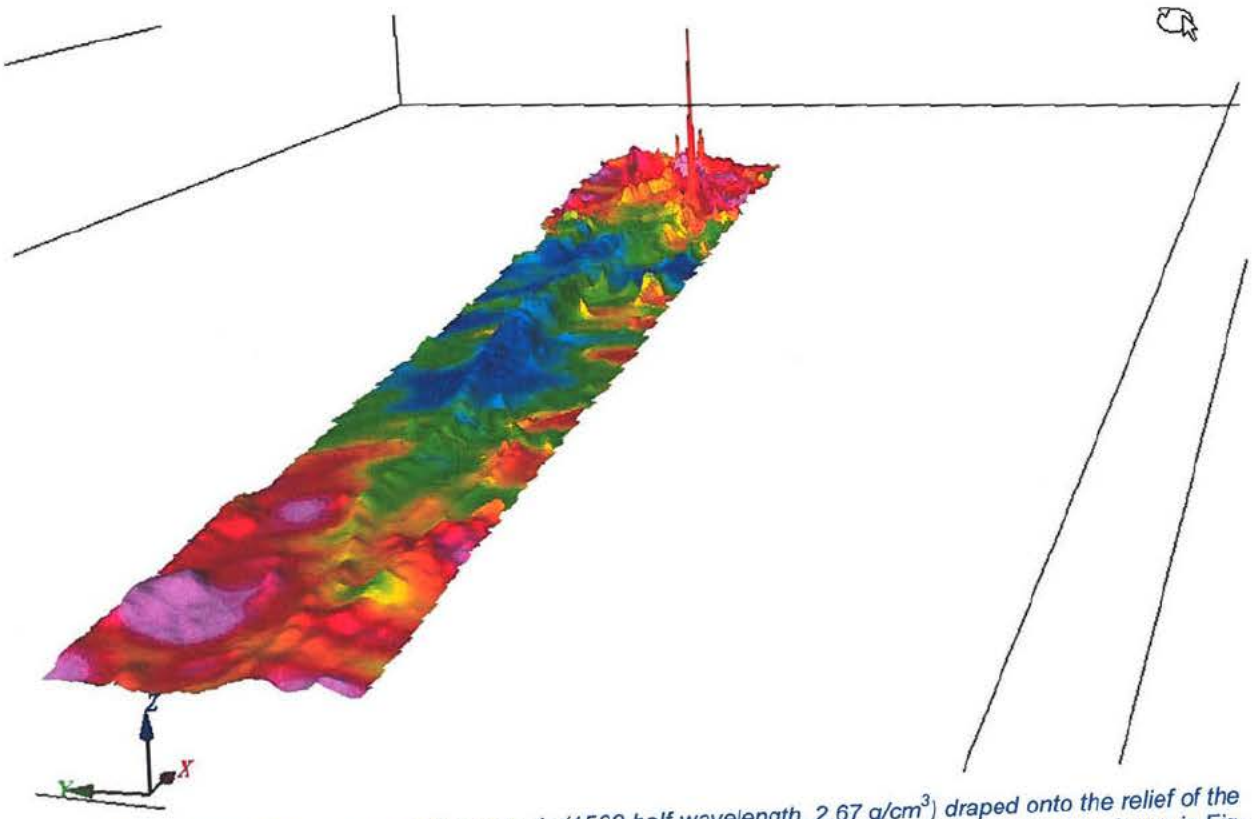

Figure 32. *Detrended Bouguer gravity anomaly (1500 half-wavelength, 2.67 g/cm^3) draped onto the relief of the total magnetic field anomaly from the 2010 survey. View from west-southwest. The colour legend is shown in Figure 14.*

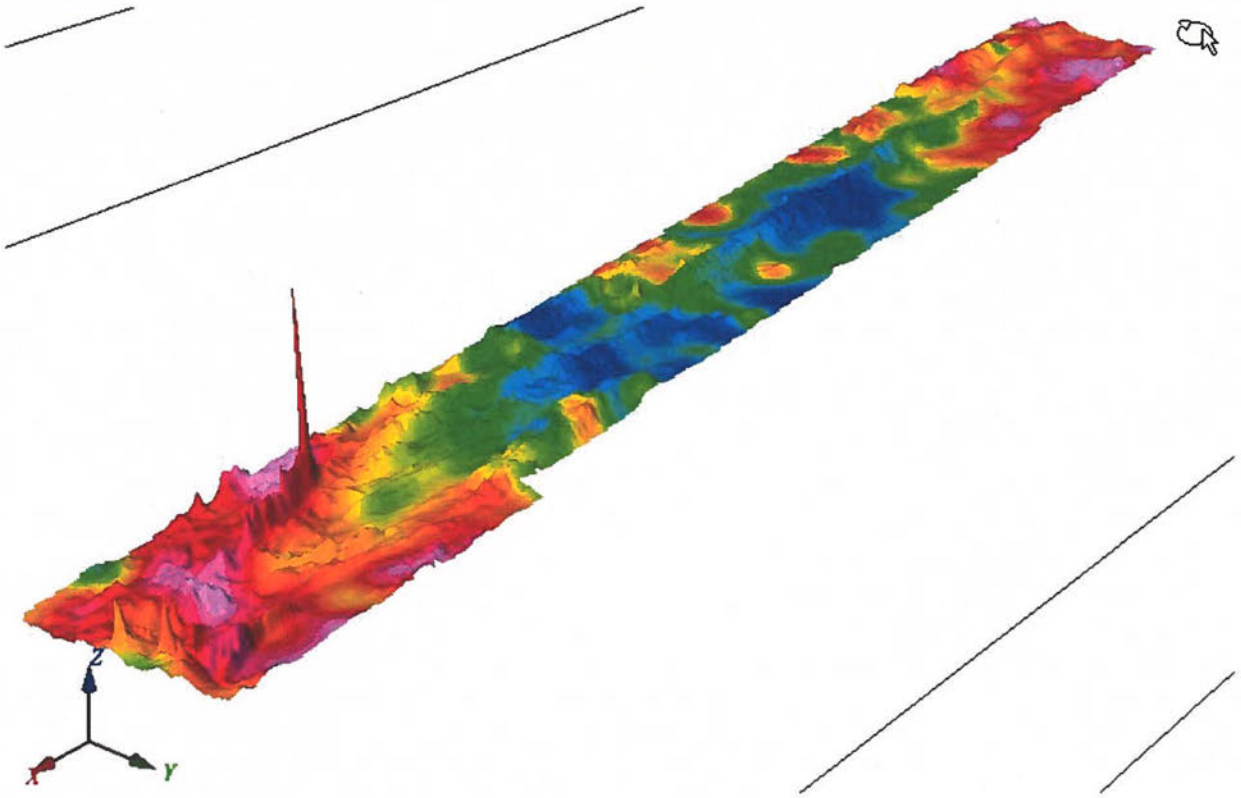

Figure 33. *Detrended Bouguer gravity anomaly (1500 half-wavelength, 2.67 g/cm^3) draped onto the relief of the total magnetic field anomaly from the 2010 survey. View from northeast. The colour legend is shown in Figure 14.*

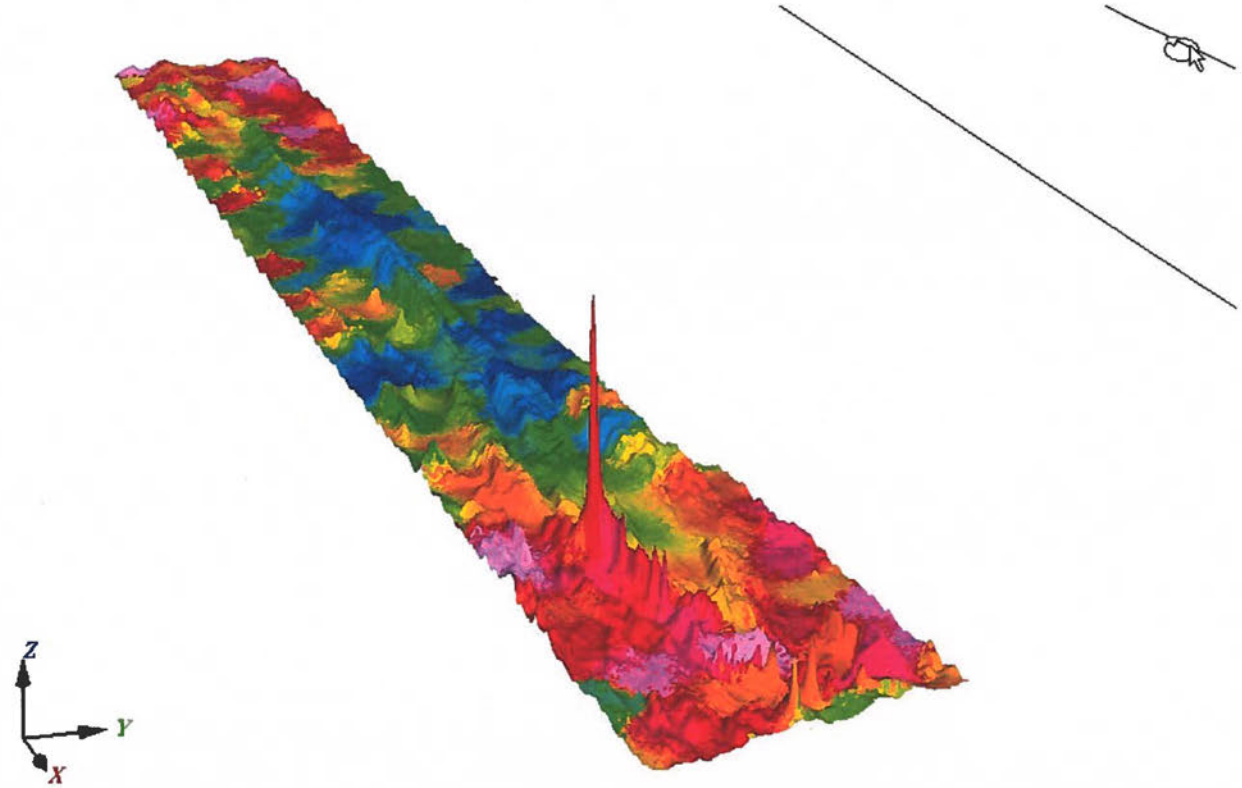

Figure 34. *Detrended Bouguer gravity anomaly (1500 half-wavelength, 2.67 g/cm^3) draped onto the relief of the total magnetic field anomaly from the 2010 survey. View from east-southeast. The colour legend is shown in Figure 14.*

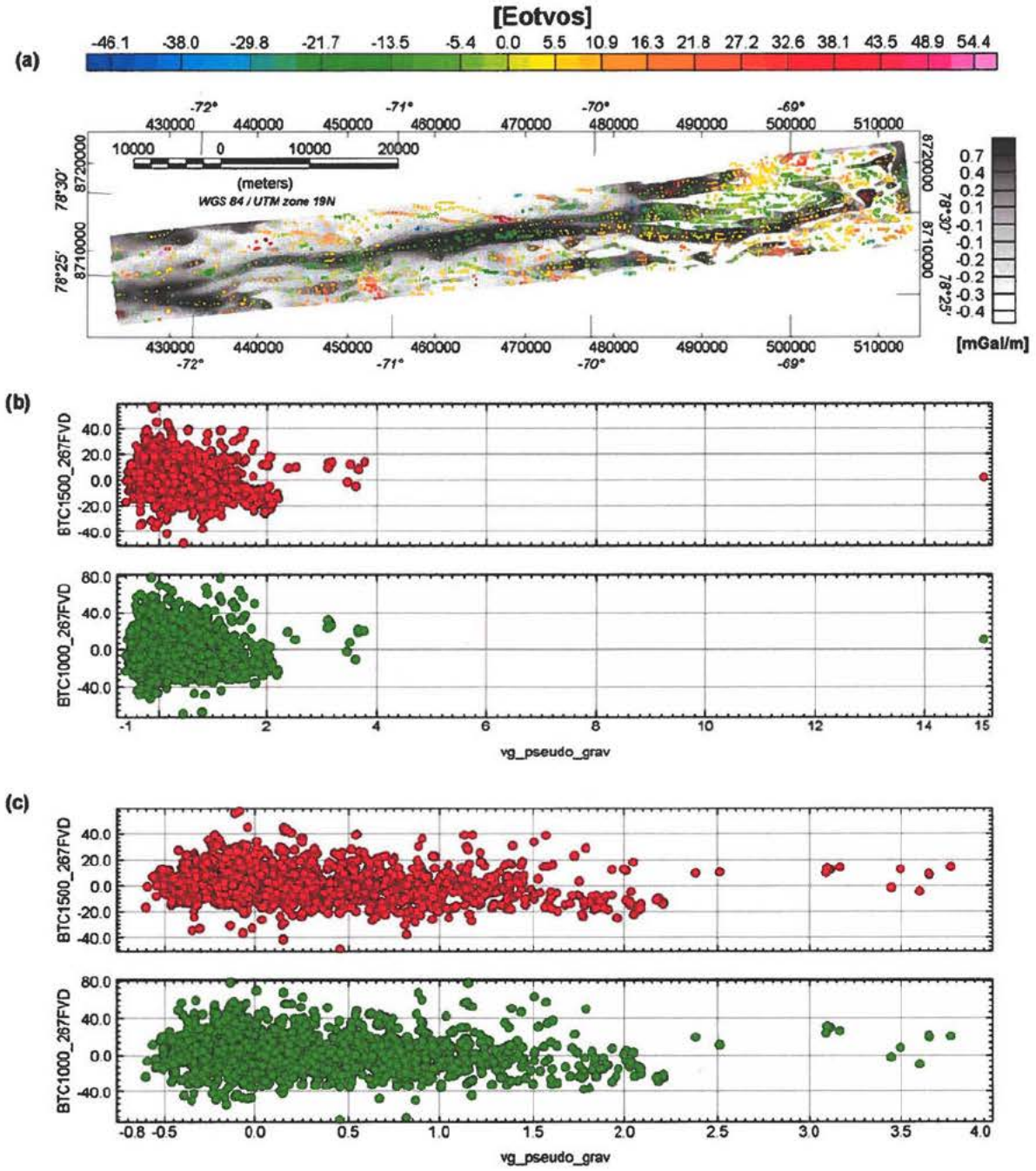

Figure 35. *(a) Colour filled circles show values of the vertical derivative of the Bouguer gravity field (1500 m half wavelength, 2.67 g/cm3) superimposed on a grey scale image (arbitrary scale in units of mGal/m) of the vertical gradient of the pseudo gravity field. The symbol location corresponds to the location where the vertical gradient of the pseudo gravity has local maxima, (b) Vertical derivative of Bouguer gravity field in units of Eotvos as function of corresponding value of vertical gradient of pseudo gravity field at maxima locations. Red circles are for the 1500 m half-wavelength and green for the 1000 m half-wavelength. (c) Similar as in (b) but with abscissa truncated at 4 mGal/m (arbitrary units).*

4.4 Gravimetric data and geological map

Figures 36 and 37 show the geological map (Dawes, 2004) draped onto the detrended Bouguer gravity field. Figures 38 and 39 show the geological map draped onto the vertical gradient of the Bouguer gravity anomaly. There is no systematic correlation between mapped units and the gravity data. Most likely the reason for the lack of correlation is partly the low-pass filtering that is applied to the raw gravity data in order to separate geological responses from noise. Another reason that most geological units are inhomogeneous. Yet another reason that the gravity data reflect subsurface structures that are not evident on the geological map.

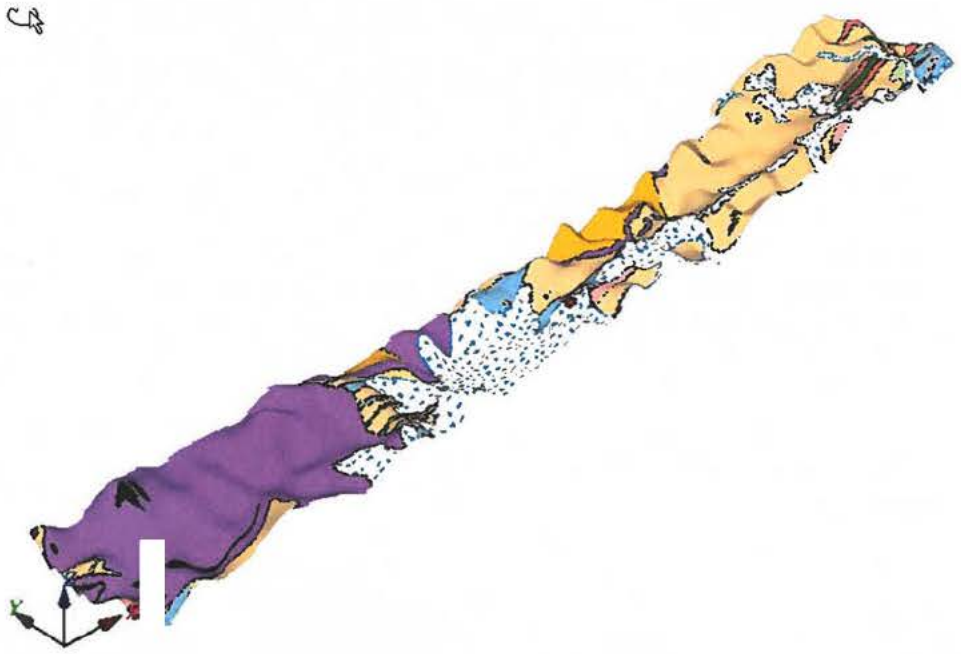

Figure 36. *Geological map draped on Bouguer anomaly (1500 m half-wavelength, 2.67 g/cm^3) from the 2010 survey. View from southwest. With the exception for the Smith Sound Group, black lines represent boundaries between rock units. The legend is shown in Figure 15.*

Figure 37. *Geological map draped on Bouguer anomaly (1500 m half-wavelength, 2.67 g/cm^3) from eastern part of the 2010 survey. View from northeast. With the exception for the Smith Sound Group, black lines represent boundaries between rock units. The legend is shown in Figure 15.*

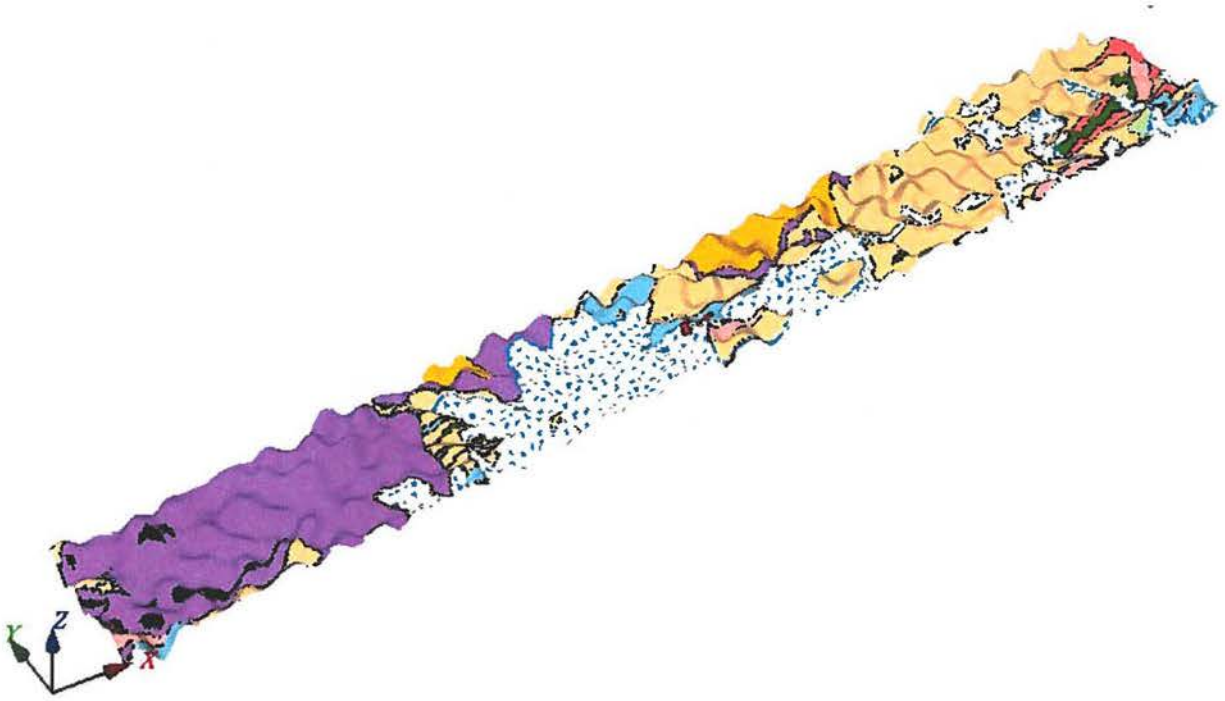

Figure 38. *Geological map draped on vertical gradient of the Bouguer anomaly (1000 m half-wavelength, 2.67 g/cm^3) from the 2010 survey. View from southwest. With the exception for the Smith Sound Group, black lines represent boundaries between rock units. The legend is shown in Figure 15.*

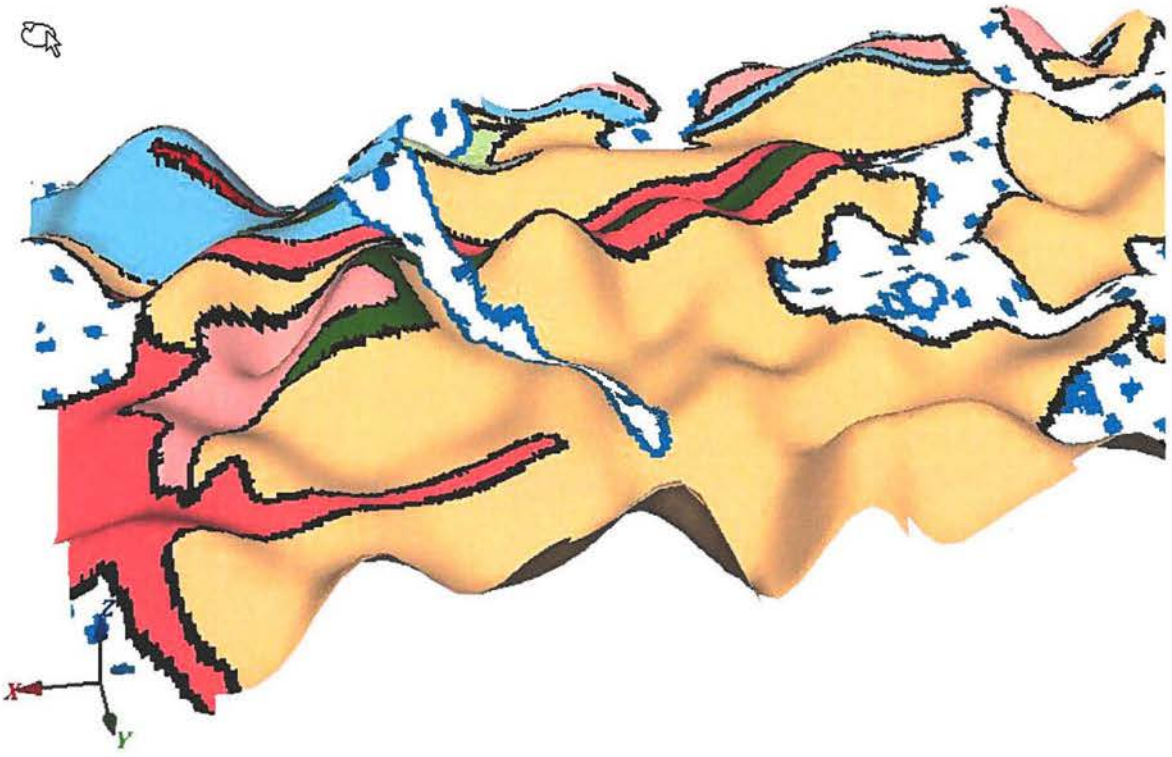

Figure 39. *Geological map draped on vertical gradient of the Bouguer anomaly (1000 m half-wavelength, 2.67 g/cm^3) from eastern part of the 2010 survey. View from northeast. With the exception for the Smith Sound Group, black lines represent boundaries between rock units. The legend is shown in Figure 15.*

4.5 Electromagnetic data and geological map

Figures 40 to 43 show the geological map draped onto various presentations of the GEOTEM data; i.e. GEOTEM X-component channel 2, conductance and decay constant tau. A general observation is that the area covered in the SGL 2010 survey is not associated with high conductivity when compared to the surrounding area.

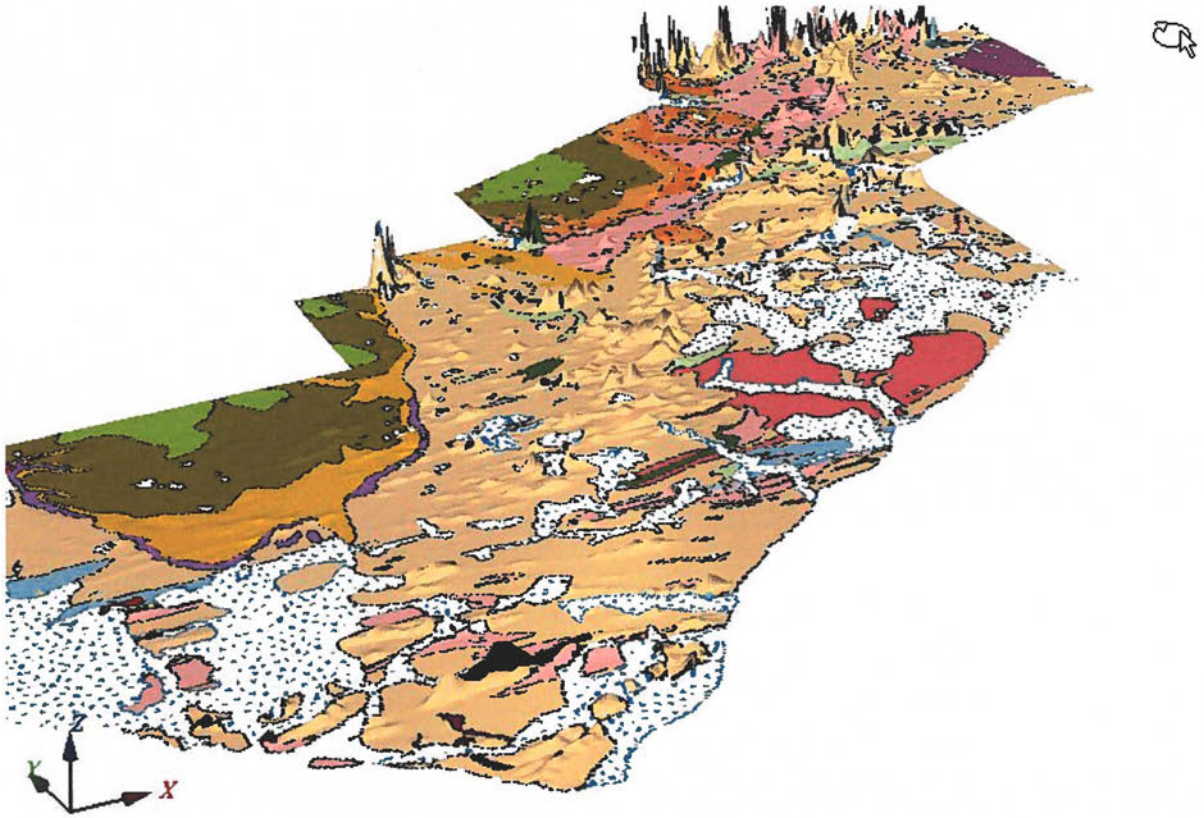

Figure 40. *Geological map draped onto the relief of the X-component channel 2 from the AEM Greenland 1994 survey. View from southwest. With the exception for the Smith Sound Group, black lines represent boundaries between rock units. The legend is shown in Figure 15.*

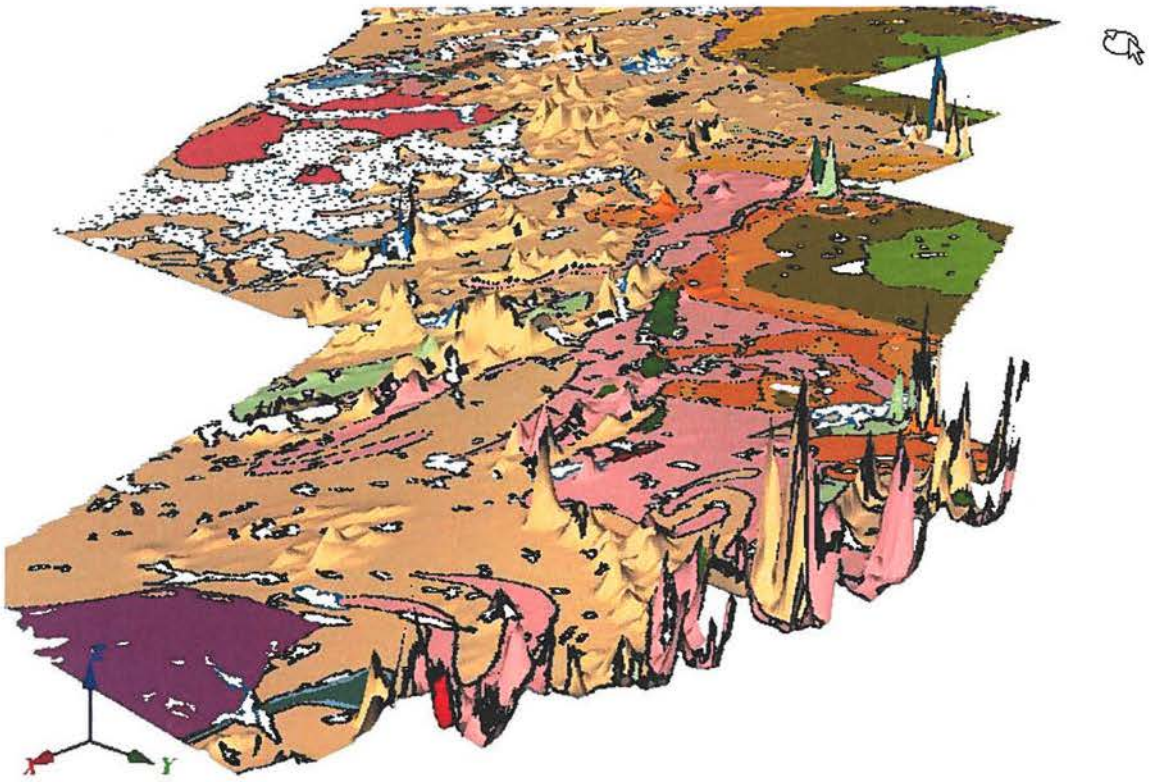

Figure 41. *Geological map draped onto the relief of the X-component channel 2 from the AEM Greenland 1994 survey. View from northeast. With the exception for the Smith Sound Group, black lines represent boundaries between rock units. The legend is shown in Figure 15.*

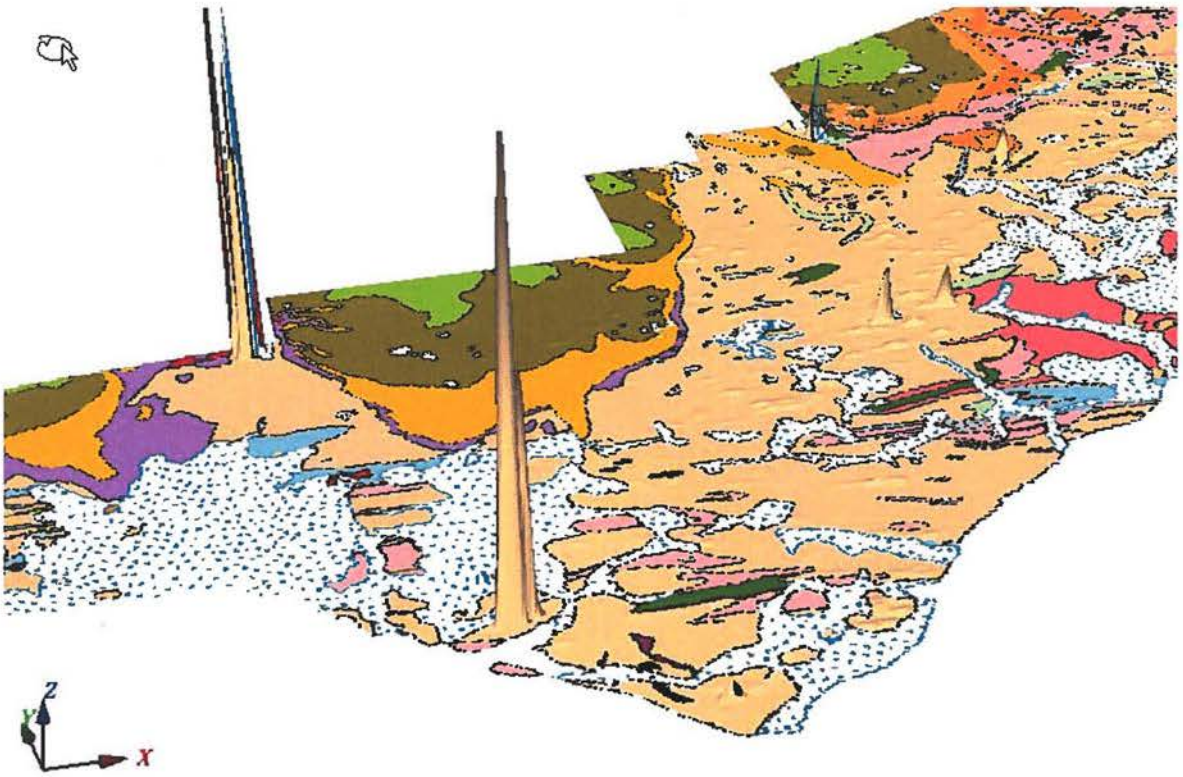

Figure 42. *Geological map draped onto the relief of the conductance from the AEM Greenland 1994 survey. View from south-southwest. With the exception for the Smith Sound Group, black lines represent boundaries between rock units. The legend is shown in Figure 15.*

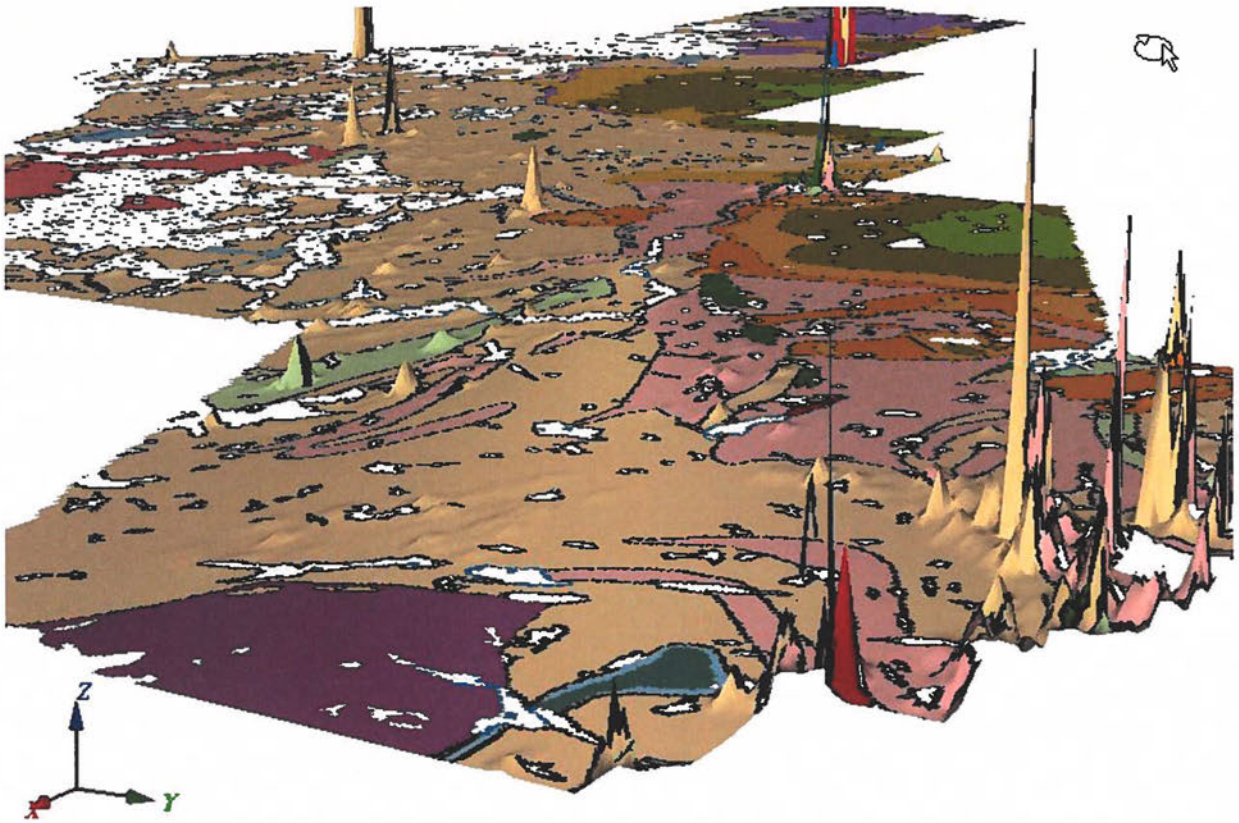

Figure 43. *Geological map draped onto the relief of the conductance from the AEM Greenland 1994 survey. View from northeast. With the exception for the Smith Sound Group, black lines represent boundaries between rock units. The legend is shown in Figure 15.*

4.6 Electromagnetic data and gravimetric data

Figures 44 and 45 show the vertical gradient of the Bouguer anomaly draped onto apparent conductivity derived from the GEOTEM data. In section 4.5 it was noted that the conductivity within the area covered by the SGL 2010 survey are weak compared to the surrounding area. The data presentations in Figures 44 and 45 are based on different scaling factors for the plotting of the relief which imply that also weak conductors are visible. The conductors seem to follow a trend along a line from the northeastern corner to the southwestern corner. The vertical gradient appears to be slightly smaller north of the trend line in the central part of the survey area compared to the area towards south.

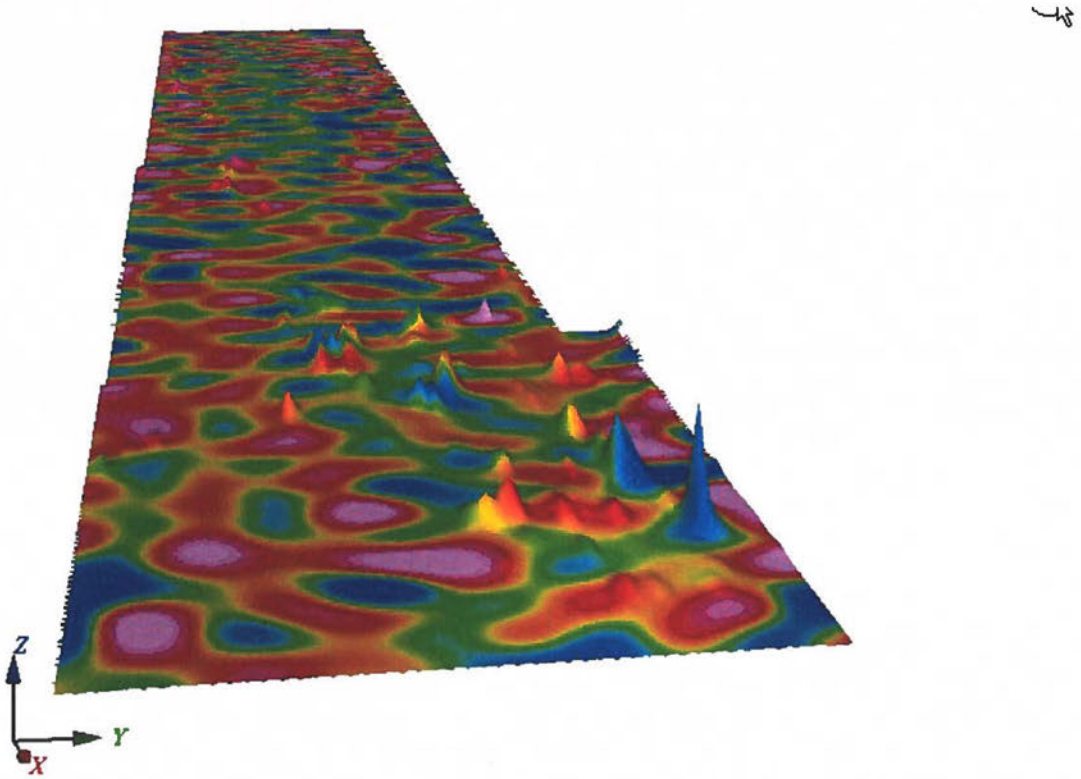

Figure 44. *Vertical gradient of Bouguer anomaly (1000 m half wavelength, 2.67 g/cm^3) draped onto the relief of the apparent conductivity anomaly from the AEM Greenland 1994 survey. View from east. The colour legend is shown in Figure 14.*

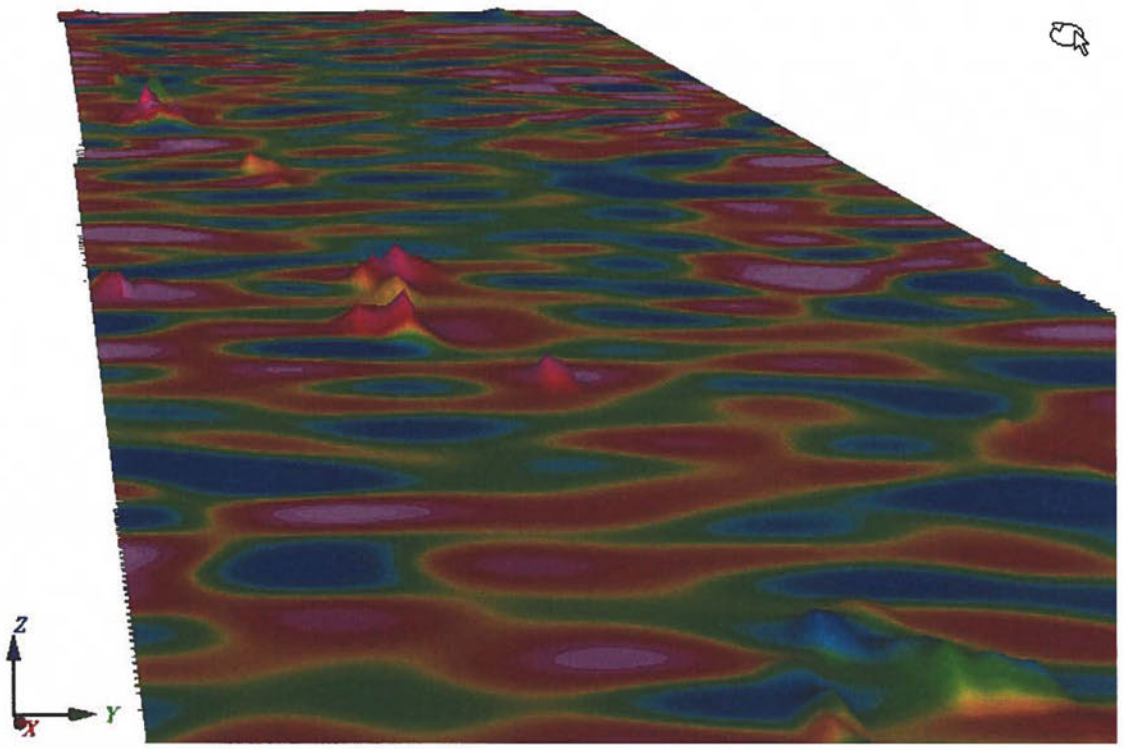

Figure 45. *Vertical gradient of Bouguer anomaly (1000 m half wavelength, 2.67 g/cm^3) draped onto the relief of the apparent conductivity anomaly from the AEM Greenland 1994 survey. View from east over western half of the 2010 survey. The colour legend is shown in Figure 14.*

5. Geophysical field characteristics from some simple models

In the section above, the measured geophysical data from the surveys in Inglefield Land were described and particular features of significance for the interpretation were described and discussed. In this section, synthetic geophysical responses from some simple structures are presented and some statements are given in relation to the observations made for the actual measured data. The conclusions presented in this section serve as guidelines for a detailed modelling of the actual data, which are presented in a later section.

The examples with synthetic responses presented in this section also illustrate the significance of some of the key parameters for the surveying and data processing such as altitude, line orientations and low-pass filtering of the gravity data. Note that responses calculated for a particular height and a particular depth only depends on distance between altitude and depth. Thus, the models responses for various combinations of altitude and depth are identical as long as this distance is the same.

5.1 Example 1 – three dykes with variable width

Magnetic and gravimetric responses are calculated from 3 vertical dykes extending from the surface to a depth of 500 m. The responses are calculated at distances 75m, 175m, 275m, 275m, 375m 475m and 575m above ground. The widths of the dykes used are 5m, 50m and 200m respectively. The density contrast to the background density is +2 g/cm^3 and the susceptibility contrast is 10 SI; i.e. approximately equal to typical average value values for magnetite. The inducing field is 56000 nT and with an inclination of 86 degree and a declination of -66 degree. The values are chosen to correspond to the inducing field in Inglefield Land. Responses for all dykes are shown in Figure 46 and for each dyke separately in Figures 47. Furthermore, low-pass filtered gravimetric responses are included in Figure 48 for the case of a 5 m dyke. We note the following:

- The decay of peak amplitude with survey altitude is clearly depicted and emphasizes the importance of including survey altitude in the data evaluation.
- The low-pass filtering applied to the gravimetric field data are mainly of significance when survey altitude is low in an evaluation based on peak amplitudes.
- The gravimetric response for the dyke having a thickness of 5 m is not detectable with the airborne system.
- The gravimetric response for the dyke having a thickness of 50 m is close to the limit of what is detectable; i.e. 1 mGal
- The gravimetric response for the dyke having a thickness of 200 m is similar in amplitude to those recorded in the survey, but the corresponding magnetic responses for the dyke model are in this case significantly larger (an order of magnitude) than those observed in the survey.

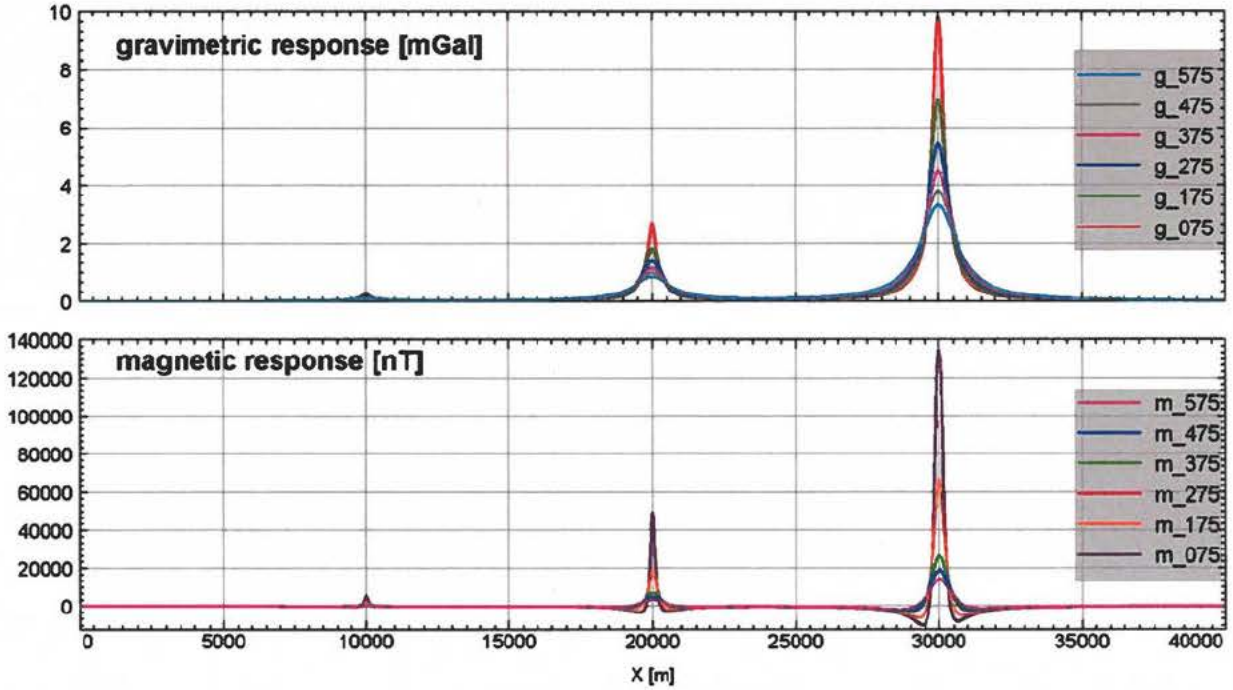

Figure 46. *Gravimetric and magnetic responses at six different altitudes from three dykes.*

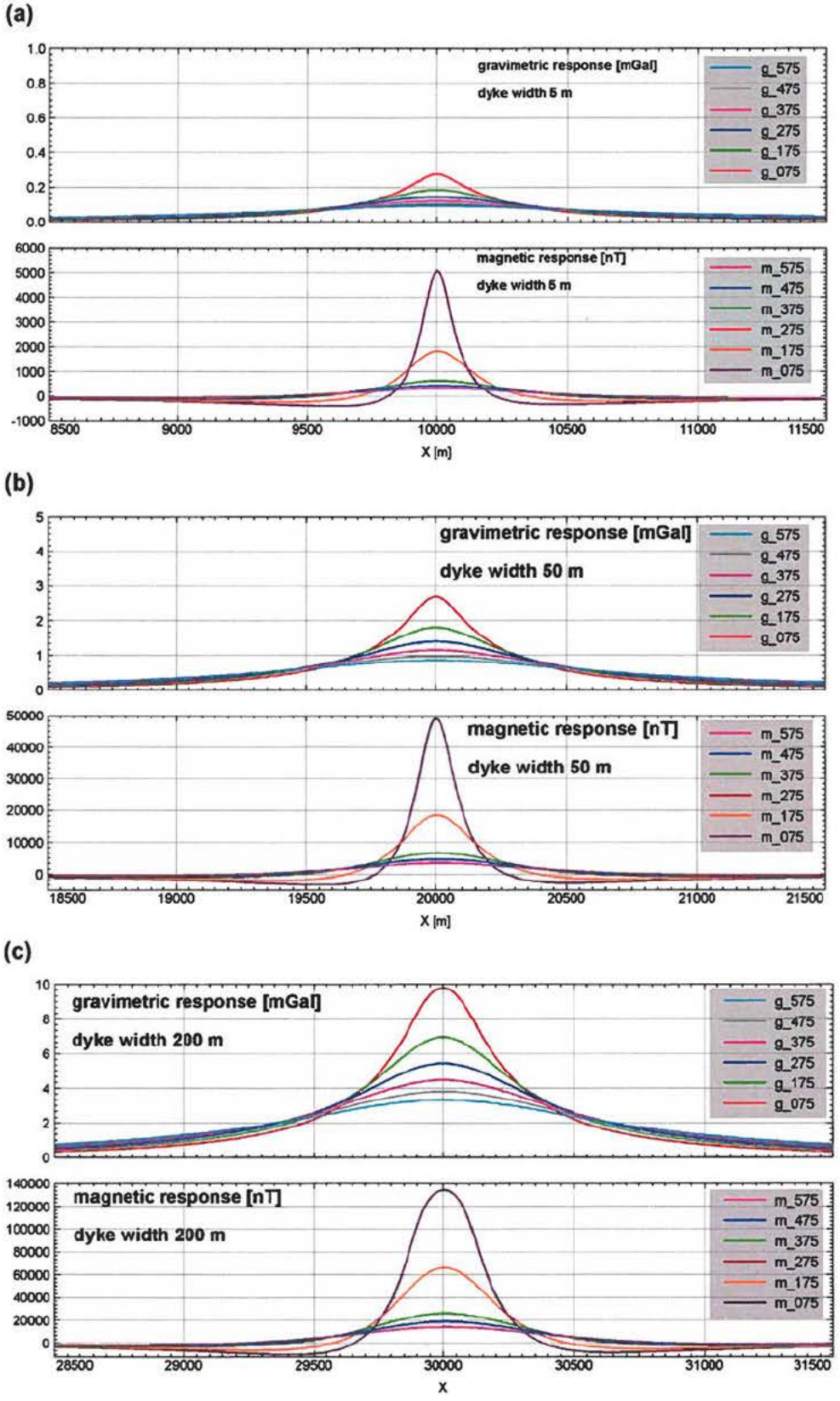

Figure 47. *Gravimetric and magnetic responses at six different altitudes a dyke with width of (a) 5 m, (b) 50m and (c) 200 m.*

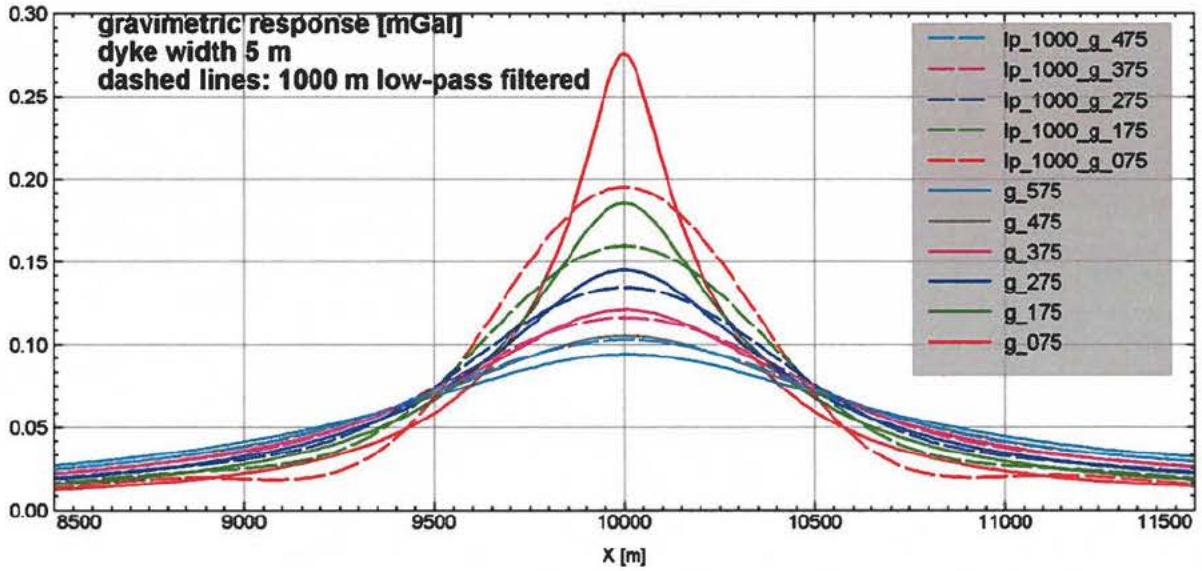

Figure 48. *Gravimetric responses at six different altitudes from a dyke with width of 5 m. Solid lines represent unfiltered data and dashed lines are the responses after low-pass filtering using a 1000 m half-wavelength cut-off.*

5.2 Example 2 – densely spaced dykes

Magnetic responses are calculated for 5 vertical dykes extending from 5 m below surface to 505 m. The responses are compared to the response of a single dyke. The responses are calculated at ground level and at distances 75m, 175m, 275m, 275m, 375m 475m and 575m above ground. The width of the dykes used is 1 m and two cases are presented. In the first case, the horizontal separation between the dykes is 1 m (Figure 49) and in the second case the horizontal separation between dykes is 50 m (Figure 50). The susceptibility contrast is 10 SI, i.e. approximately equal to typical average value values for magnetite. The inducing field is 56000 nT.

We note the following:

- The response at ground level for the 5 dykes with 1 m separation has a single maximum and the response does not allow an immediate identification of the presence of 5 dykes instead of 1. Basically the response is almost identical to the sum of 5 responses from a single 1 m dyke (Figure 49a)
- The responses for the 5 dykes with 50 m separation for altitudes at or above 75 m have a single local maximum and the responses do not allow an immediate identification of the presence of 5 dykes instead of 1 (Figure 50c). At ground level the presence of 5 separated dykes is evident immediately. (Figure 50a).
- The peak response of the 5 dykes is of the same order of magnitude as observed from the various magnetic surveys in the Inglefield Land/Minturn area.

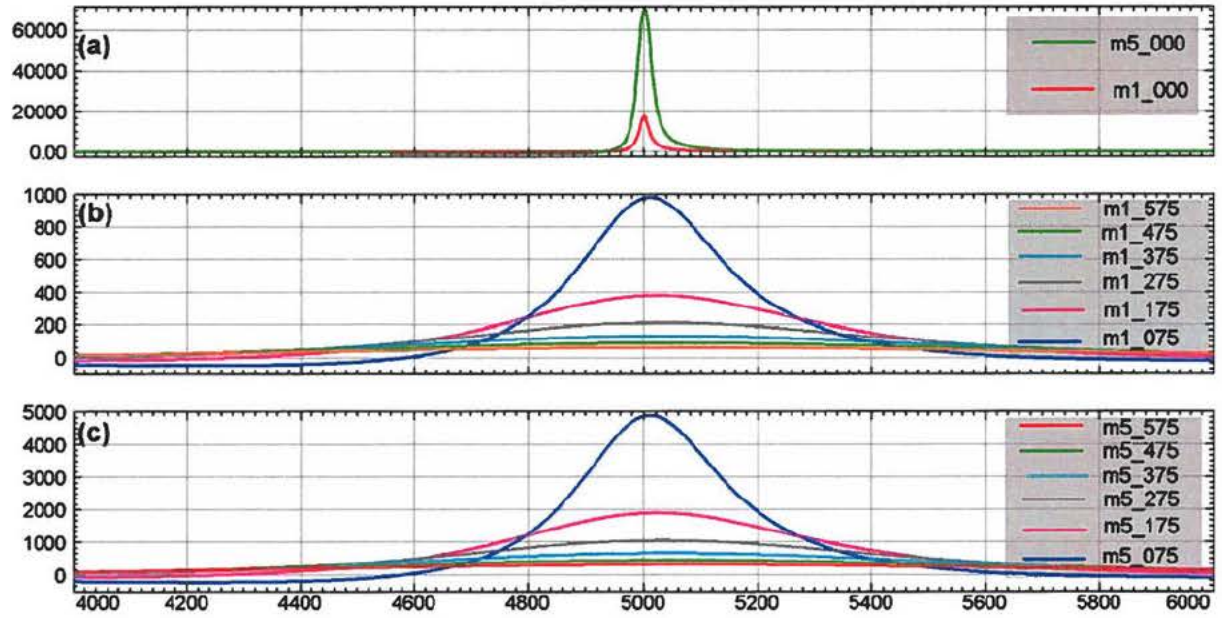

Figure 49. *(a) Magnetic responses at ground level for one dyke with width of 1 m (red curve) and for 5 dykes with a width 1 m and 1 m separation (green curve). (b) Magnetic responses for a dyke with width of 1 m at six different survey altitudes. (c) Magnetic responses for 5 dykes with a width of 1 m and 1 m separation at six different survey altitudes.*

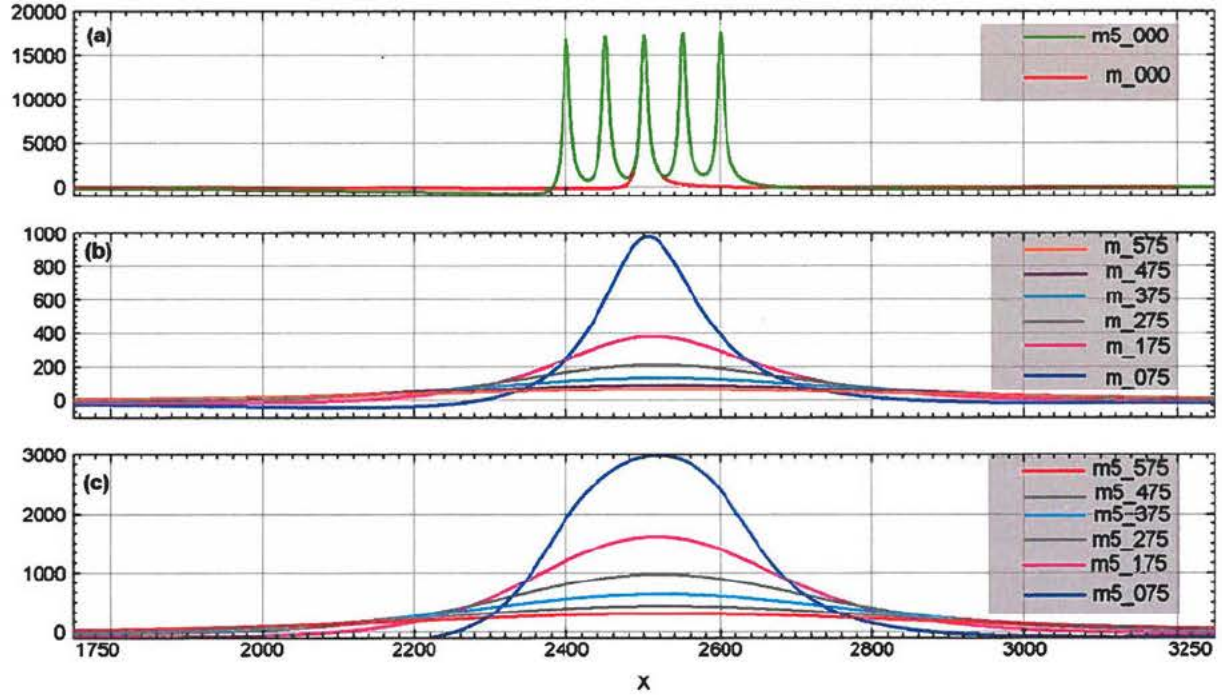

Figure 50. *(a) Magnetic responses at ground level for one dyke with width of 1 m (red curve) and for 5 dykes with a width 1 m and 50 m separation (green curve). (b) Magnetic responses for a dyke with width of 1 m at six different survey altitudes. (c) Magnetic responses for 5 dykes with a width of 1 m and 50 m separation at six different survey altitudes*

5.3 Example 2 – tabular shaped bodies

Gravimetric and magnetic responses are calculated at 75m, 175m, 275m, 275m, 375m 475m and 575m above ground for tabular shaped bodies. In total 13 different models are used by varying the dimension in two directions dx and dz of the bodies (see explanation in Figure 51) and by varying the depth z to the top of the structure. Some of models simulate vertical dykes whereas others represent flat-lying structures. The responses are calculated along profiles crossing the bodies in the plane of vertical symmetry. The density contrast to the background density is +2 g/cm^3 and the susceptibility contrast is 5 SI, i.e. approximately equal to typical average value values for magnetite. Figures with responses are included in Appendix A

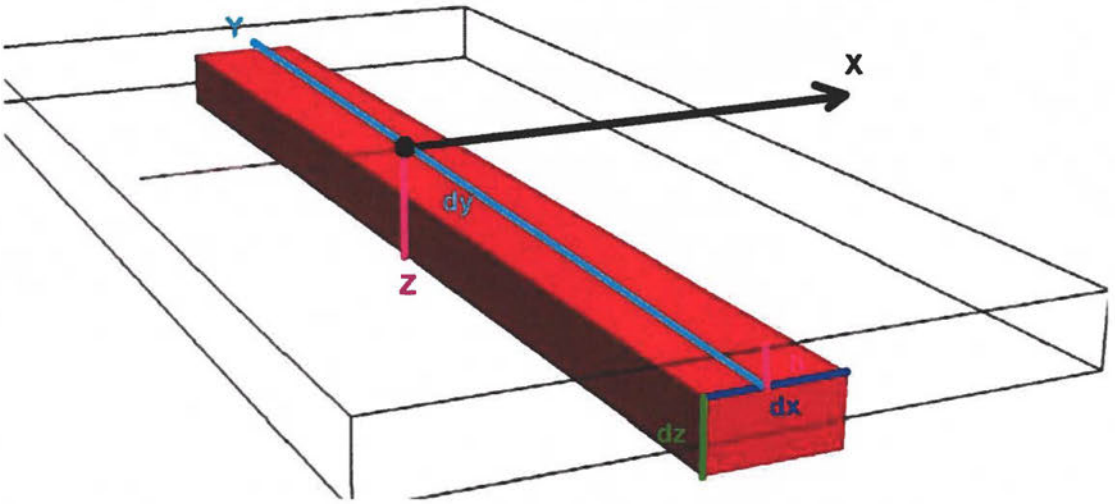

Figure 51. *Perspective view of the principal model consisting of a tabular shaped body with dimension dx along the profile direction x and dimension dz vertically. The body extends 20 km in the direction y orthogonal to the profile direction. The top of the body is at a depth h.*

Inspection of the responses shown in Appendix A reveals the following:

- The magnetic response from vertical dykes where the distance to the bottom is much larger than the distance to the top has one dominating maximum and some long-wavelength side-lopes on each side. This is a typical observation for the survey data.
- The magnetic response from a thin flat lying body has a dominating maximum and an adjacent minimum of approximately the same strength above the edge of the body. Similar maximum and minimum values are not typical for the survey data.
- Bodies with gravity responses in the same range as observed for the survey (5 mGal) have magnetic responses that are much higher than those observed
- Bodies with magnetic responses in the same range as observed for the survey have gravimetric responses that are much smaller than those observed. Basically the gravimetric responses will be below the detection limit or noise level.

5.4 Example 4 – disc shaped bodies

Gravimetric and magnetic responses are calculated at 75m, 175m, 275m, 275m, 375m 475m and 575m above ground for disc shaped bodies. In total 19 different models are used by varying the dimension in thickness d_z and radius r of the bodies (see explanation in Figure 52) and by varying the depth h to the top of the structure. The models represent flat-lying sheet structures. The responses are calculated along profiles crossing the centre of the disc. The density contrast to the background density is +2 g/cm^3 and the susceptibility contrast is 5 SI. Figures with responses are included in Appendix B.

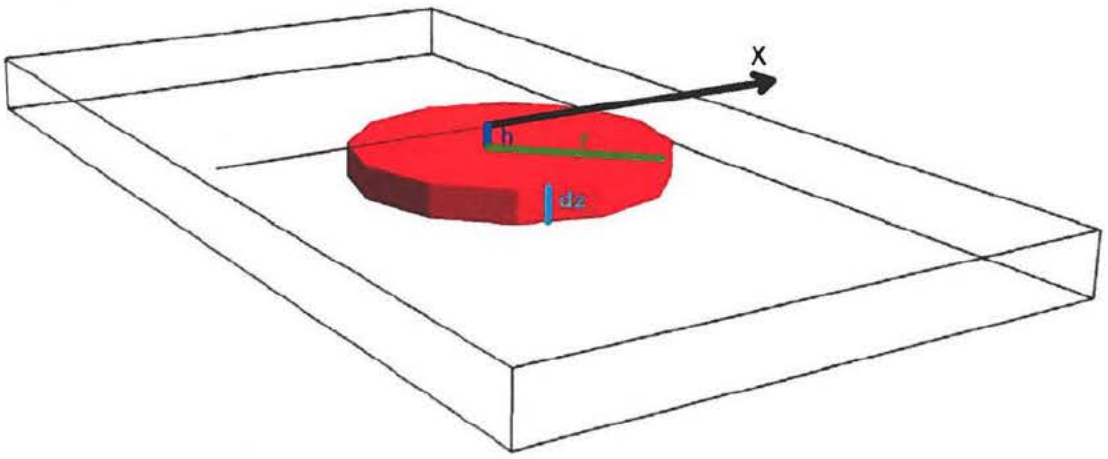

Figure 52. *Perspective view of the principal model consisting of a disc shaped body with radius r and dimension dz vertically. The top of the body is at a depth h.*

Inspection of the responses shown in Appendix B reveals the following:

- The magnetic response from a thin flat lying body has a dominating maximum and an adjacent minimum along edge of the body. In cases with large lateral extent, the response above the centre of the body approach zero (a plate or layer with infinite dimension has zero response). Numerically the minimum is about 50 % of the maximum. A characteristic that is not typical for the survey data.
- The gravity response from a flat lying structure of large lateral extent approaches the value of the Bouguer plate; i.e. approximately $0.042 mGal/m \cdot \rho \cdot d_z$ where ρ is the density contrast in units of g/cm^3 and d_z is the thickness.
- Bodies with gravity responses in the same range as observed for the survey (50 m thickness and 5 mGal maximum) have magnetic responses that are much higher than those observed.
- Bodies with magnetic responses in the same range as observed for the survey have gravimetric responses that are much smaller than those observed. Basically the gravimetric responses will be below the detection limit or noise level.

5.5 Example 5 – adjacent blocks of variable density

The results in section 5.3 and 5.4 indicate that an attempt to produce a gravity response of the same order of magnitude of those observed (5 mGal) using typical densities and susceptibilities for magnetite will produce magnetic responses much higher than those observed. A more realistic model to explain the observed general features can be constructed by using much smaller density variations that are typical for rocks like gneisses; i.e. density contrasts of the order ±0.1-0.4 g/cm^3 from the mean values. The requirement in order to obtain gravity peak values around 5 mGal is then to extend the bodies from the surface to much larger depth (> few km) than those used for the models in appendix A and B. This is illustrated by the model in Figure 53 and the corresponding responses in Figures 53 to 55. The model is constructed as a superposition of two 2-dimensional structures with strikes in orthogonal directions. Basically the final model is a blocky model with blocks ranging in size horizontally from 250 m to 8000 m. The vertical block sizes are 5000 m and 10000 m.

The responses produced are seen to have both peak values and wavelength (anomaly width) in the same range as observed for the gravity survey (Figure 56). The two maps in Figures 55 and 56 are plotted by using the same scale and the colour range is similar for the two maps except for a difference in mean level.

If thin (5m) dykes of magnetite are embedded into the structure shown in Figure 53, the gravity responses will basically remain unchanged as the responses from these dykes are small (<0.2 mGal) as seen in section 5.3 and 5.4. However, the magnetic field strength will change considerably and can be made comparable to those observed.

Responses were calculated for survey altitudes of 75 m, 175 m, 275, 375 m and 475m and shown for one profile in Figure 54. Note that the responses are fairly similar for the various altitudes above ground and that the filtering has little influence on peak values for this type of structures where the dimension of the blocks is 250 m or larger.

A first order interpretation of gravity data can be done using a technique known as terracing (Cordell and McCafferty,1989) if an assumption of vertical block boundaries is reasonable. The terracing technique transforms the map of the smoothly varying gravity field into a map with domains of uniform values separated from each other by zones of large horizontal gradients. The high gradient areas correspond to structural boundaries. The values within the uniform domains will approach the peak values of the gravity field. The technique is illustrated in Figure 57, which shows the results of transforming the synthetic data in Figure 53.

A rough estimate of the density contrast is given by:

$$\Delta\rho = \frac{T_{\max}}{0.042 mGal/m \cdot d_z} \cdot \frac{10000m}{d_h},$$

where $T_{\max}$ is the terraced peak value, d_z is the assumed vertical dimension in units of meter and d_h is the observed horizontal dimension. The first part of the equation corresponds to the standard Bouguer correction (infinite plate with thickness d_z) and the second part corrects for the finite dimension when the horizontal dimension is smaller than the vertical dimension and the data are

for a survey altitude of about 475 m. For the synthetic example, the location with maximum amplitude of 37 mGal and dimension 8000 m, the values of 0.22 g/cm^3 is obtained provided that the assumption of d_z is done correctly. The true value is 0.4 g/cm^3 for this location. If the case of that the horizontal dimension is much larger than the vertical, the first term in the equation above is applicable irrespective of survey altitude. This can be verified from the responses shown in Appendix B for the disc shaped bodies. The validity of performing such an interpretation relies heavily on the correctness to the entered assumptions.

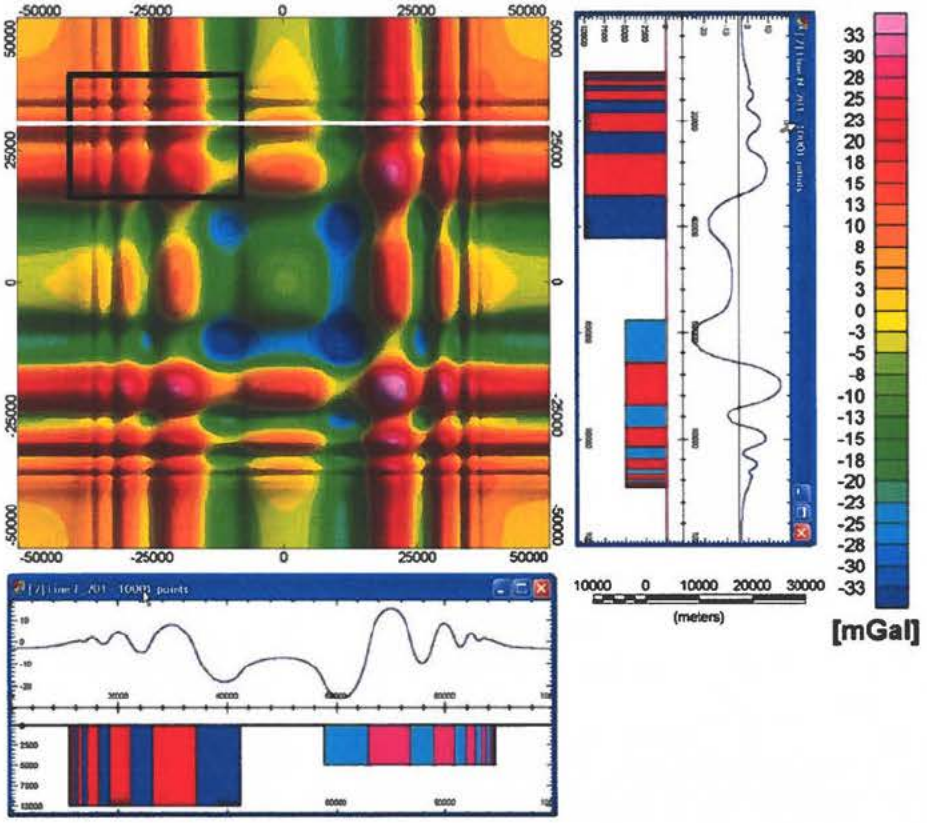

Figure 53. *Synthetic gravity responses (3000 m low-pass filtered) in a 50 km by 50 km grid at an altitude of 475 m from a model constructed as a superposition of two 2-dimensional structures. The two 2-dimensional structures are shown as vertical section along the axis of the map-coordinate frame. Density contrasts are -0.1 g/cm^3 and +0.1 g/cm^3 for the blocks in red and blue colour respectively. Density contrasts are -0.2 g/cm^3 and +0.2 g/cm^3 for the blocks in cyan and light blue colour respectively. Response (for various survey altitudes) along the white lines is shown in Figure 54 and the response within the black rectangle is shown in Figure 55 for easy comparison with data from the SGL 2010 survey.*

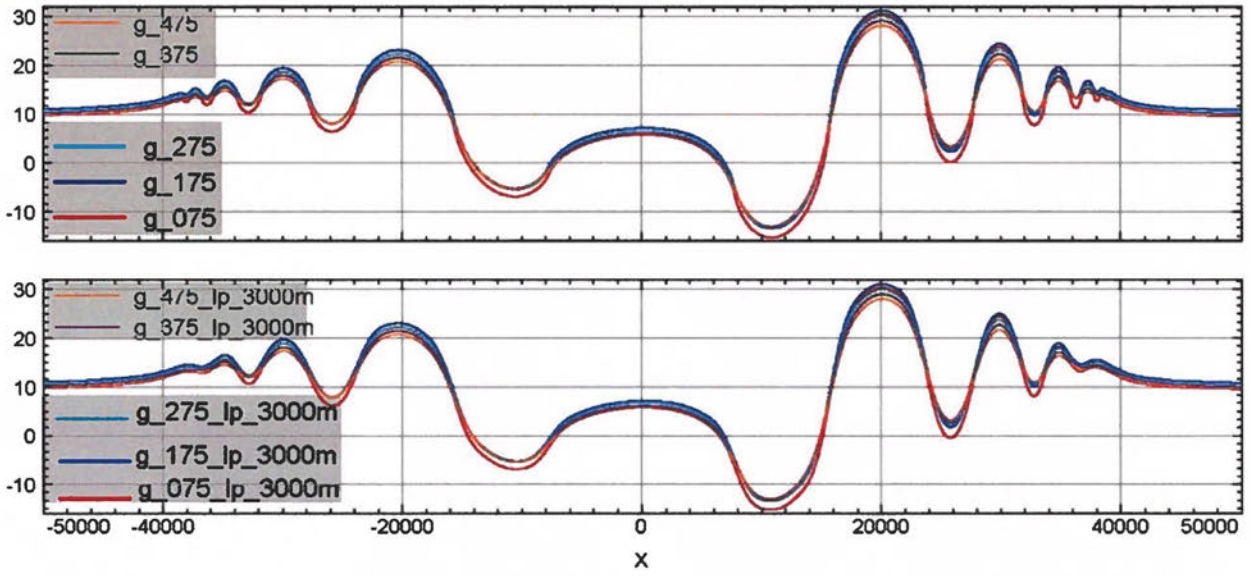

Figure 54. *Upper panel shows the gravity responses at altitudes 75 m, 175 m, 275 m, 375 m, 475 m above ground along the profile marked in Figure 53. The lower panel shows the corresponding 3000 m low-pass filtered data (1500 m half-wavelength cut-off).*

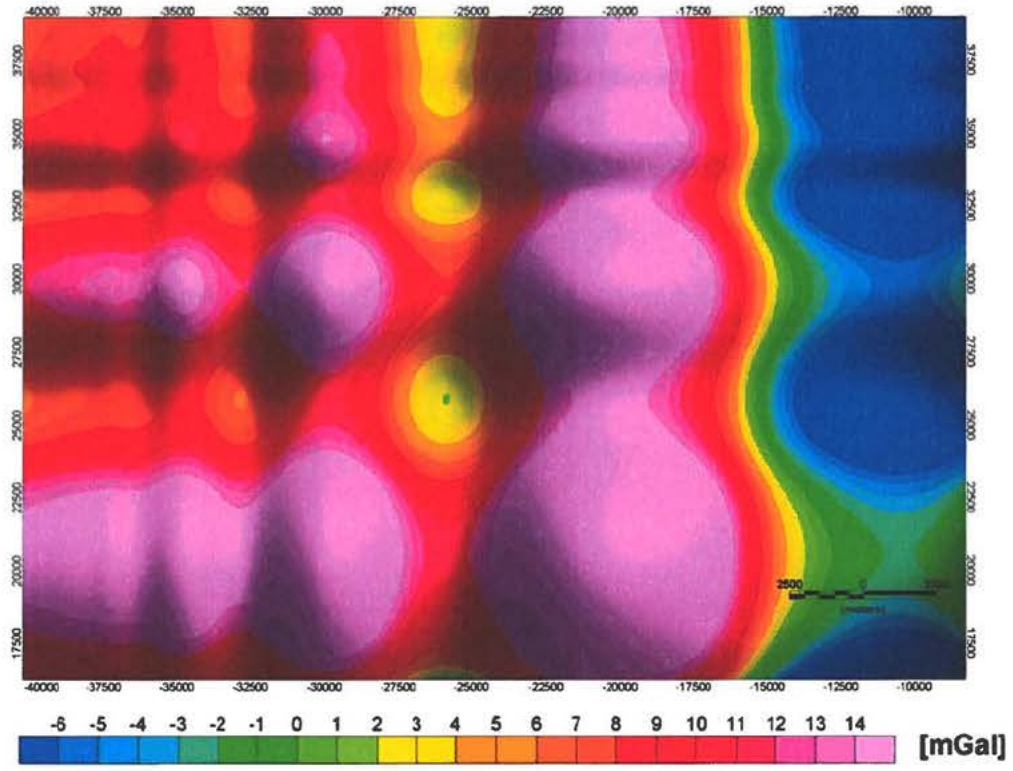

Figure 55. *Subset of the responses from the model shown in Figure 53.*

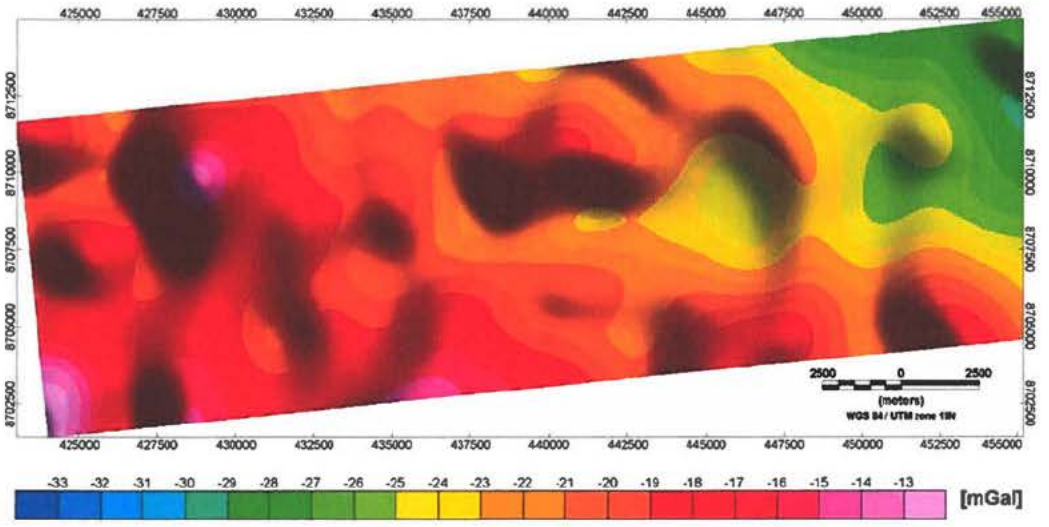

Figure 56. *Subset of the measured gravity responses (BTC1500) from the Inglefield Land survey. The area covered and scale of display is similar to the map in Figure 55.*

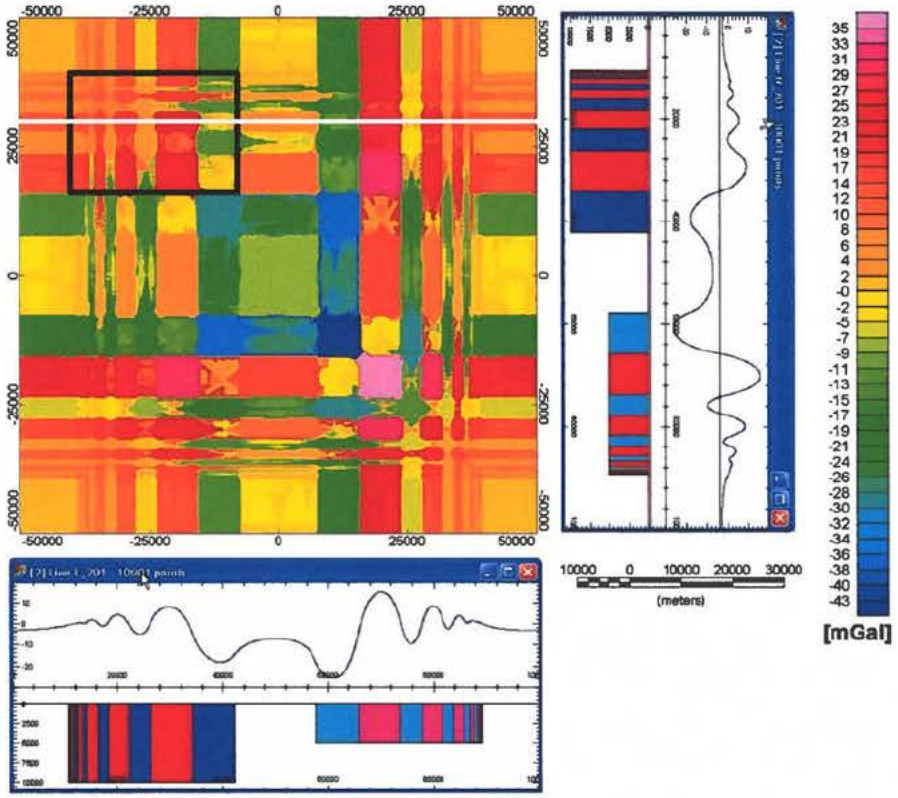

Figure 57. *Terraced version of the gravity response in Figure 53.*

5.6 Conclusion from some simple model response calculations

The attenuation of magnetic field amplitude with survey altitude is illustrated clearly with the examples included. The examples also show the important property that short wavelength features are attenuated much more that the long wavelength. The implication of this is that the ability to discriminate between only one magnetic structure from a composite occurrence of magnetic rocks is not possible when survey altitude is high or when the magnetic rocks are at large depth. This conclusion is also valid for gravimetric data although this is not exemplified here.

Structures with typical magnetite petrophysical properties that can reproduce the observed magnetic data are associated with gravimetric responses that are below the detection limit (or noise level) for the gravity survey data. Equivalently, structures with densities typical for magnetite produce magnetic field responses much higher than those observed.

Structures with typical haematite petrophysical properties could produce gravity anomalies in the same range as observed and still be consistent with the magnetic field recordings. However, similar responses are possible from structures with much lower densities; i.e. densities typical for more common rocks like gneisses.

It was noted that a thin flat lying structure (thin in relation to lateral extent) has a magnetic response that approach zero at the centre of the structure. This implies that the mapped syenite east

of the gravity survey cannot be superficial but must have a fairly large vertical extent in order to be associated with the observed high magnetic field strength.

6. Modelling of data along the 1999 GEUS profile

This section includes result from inversions of all available data along the GEUS 1999 ground profile. The data from the three airborne surveys have been extracted from gridded magnetic data by digitising these along the 1730 m GEUS 1999 profile. Results are presented for inversion based on a joint data set from all four surveys and from four inversions with data from each of the four surveys. The comparison of data along the profile presented above indicated that the original grid provided by Geoterrex Ltd. might have been subjected to heavy low-pass filtering. Therefore data from this survey was re-gridded for the purpose of this modelling. Also a re-gridded version of data from the SkyTEM system is used.

6.1 Result from inversion of magnetic data

The data are modelled by using a single dyke with a strike fixed to an azimuth in the WGS84/UTM19N system of 78 degree and a length along strike of 25 km as principal model. The strike direction is obtained by visual inspection of the grids of the magnetic field variation. The estimated parameters in the inversion is the dip, depth to top, magnetic susceptibility, thickness, position along the profile and finally the depth extent.

The estimated parameters are provided in Table 2 for the five inversions. The measured data and model responses are shown in Figure 58 for the joint data inversion and in Figures 59-62 for inversions based on the individual surveys. The simple dyke model provides a reasonable good fit the measured data in terms of both amplitude and shape of the curves. The purpose of this inversion is not an attempt to obtain a perfect fit to all data. Instead, the purpose is to demonstrate that the data from the four surveys are consistent to a reasonable degree and to evaluate the derived models. Deviations from a perfect fit may be attributed partly to imperfect gridding but certainly also to the use of a very simple principal model.

The estimated depth extent is very large and this parameter is not well determined. This parameter can be made smaller without degrading the data fit to any significant extent. Most of the other parameters are fairly consistent, but some variability is noticed for the depth to the dyke. The estimated value of the susceptibility is close to the values obtained from laboratory measurements of the samples reported in Appel et al. (1995) and consistent with tabulated average values of 6 SI for pure magnetite quoted by Telford et al. (1999). The susceptibility parameter is not well determined from the data since an almost similar fit to the data can be obtained if the thickness times susceptibility product is kept constant. This relation is valid for thickness less that about 80 m, if the ground magnetic data are included in the modelling. Modelling of the data from the SkyTEM survey provides a maximum width of about 100 m. The ability to add constraints on the maximum width decreases with survey ground clearance and values around 200 are found for the AEM Greenland 1994 and SGL 2010 surveys.

Appel et al. (1995) provided an estimate of the mineralised zone of 200-300 m, but pointed out that the data did not allow indentifying individual layers of magnetite within the mineralised zone. Unfortunately they did not provide the actual values for the magnetic properties used in the modelling and the exact location of the data profile used is not shown. The conclusion concerning the ability

to indentify individual layers of magnetite is also valid for the modelling of the other data (1999, 2008 and 2010 surveys); i.e. the model with a single dyke with thickness 4.6 m obtained from the joint inversion can be split into thinner sheets as long as the sum of the thickness and susceptibility product for all sheets equals the value obtained for the model in Table 2.

The conclusion in terms of an estimate of total thickness of sheets with pure magnetite is that this is about 4 to 5 m. This conclusion is only valid if the measured responses have no contributions from disseminated magnetite within the mineralised zone. Note that the data only provides an estimate of the maximum possible width of the mineralised zone and that the ground magnetic profile limits this maximum to about 80 m. A model in which the entire 80 m is uniform requires a susceptibility of 11.6 SI*4.6m/80m = 0.7 SI, a value about 10 times smaller than average values quoted for magnetite (Lowe, 1999).

Table 2. *Model parameter estimates from the four inversions of data along the GEUS 1999 profile with reference to year of measurements and the joint data set*

Input data	1994	1999	2008	2010	Joint data set
Susceptibility [SI]	11.2	11.3	11.1	11.1	11.6
Strike [degree]	78	78	78	78	78
Thickness [m]	6.5	5.0	4.9	5.9	4.6
Depth to top [m]	119	41.9	47	78.2	42.3
Dip [degree]	71	80	76	72	77
Depth extent [m]	6500	7500	6500	5500	6500

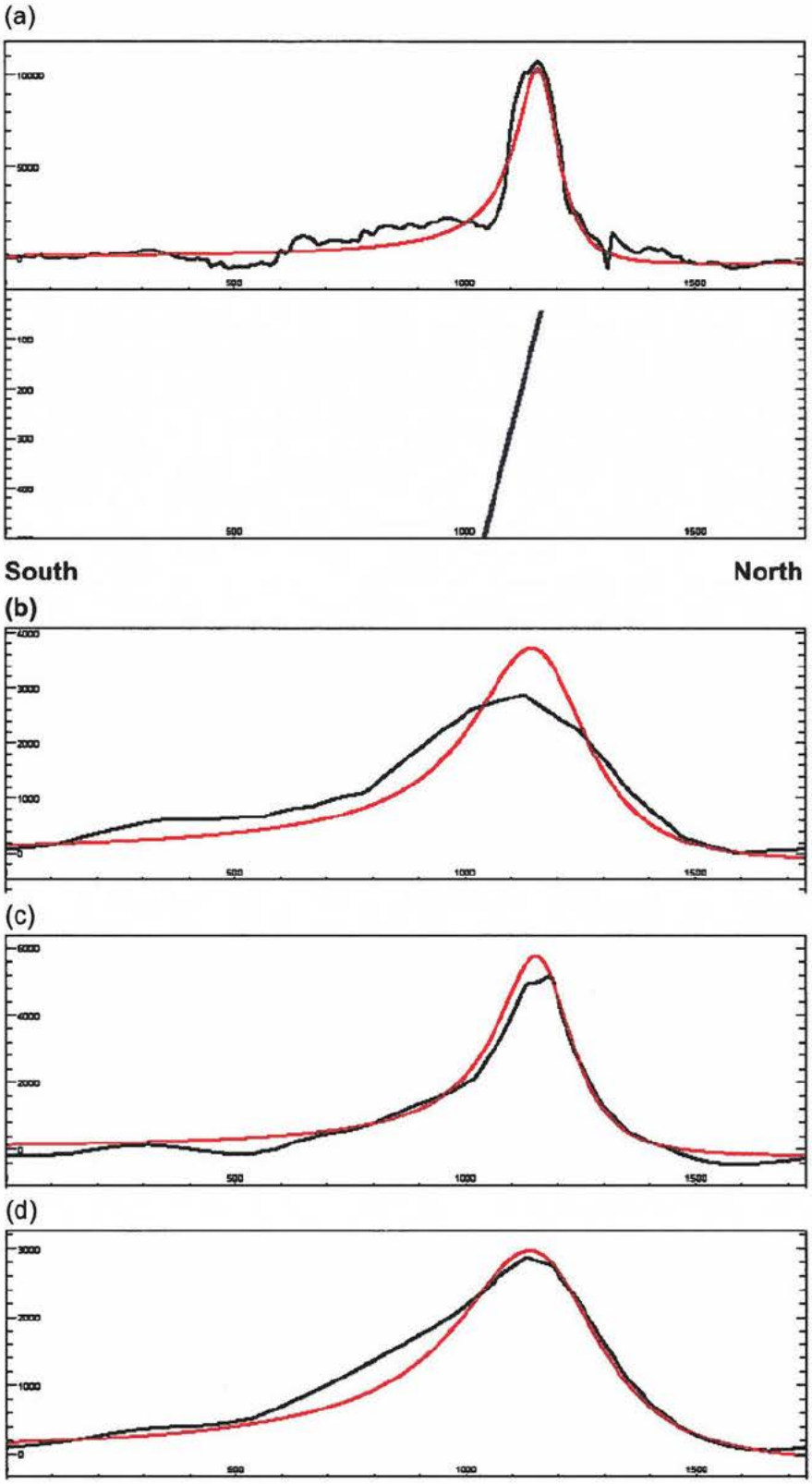

Figure 58. *Measured (black curves) and model (red curves) responses obtained by joint data inversion. The panels are from top to bottom (a) the 1999 ground geophysical data and final model, (b) the AEM Greenland 1994 data; (c) the SkyTEM 2008 data and (d) the SGL 2010 data*

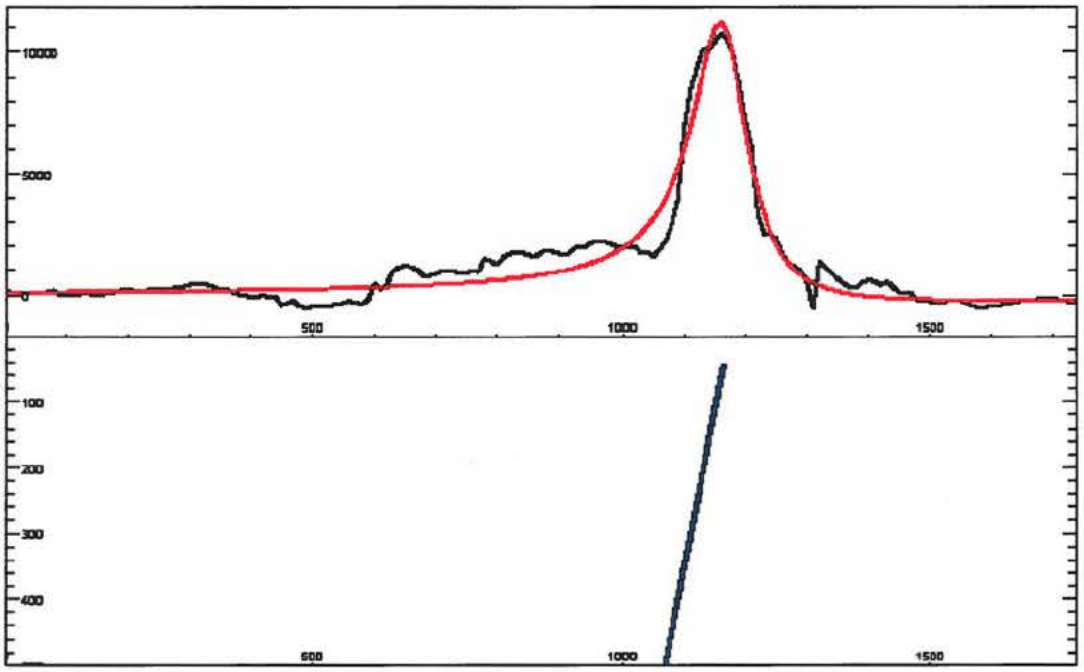

South **North**

Figure 59. *Measured (black curve) and model (red curves) responses obtained by inversion of the 1999 data and the associated model.*

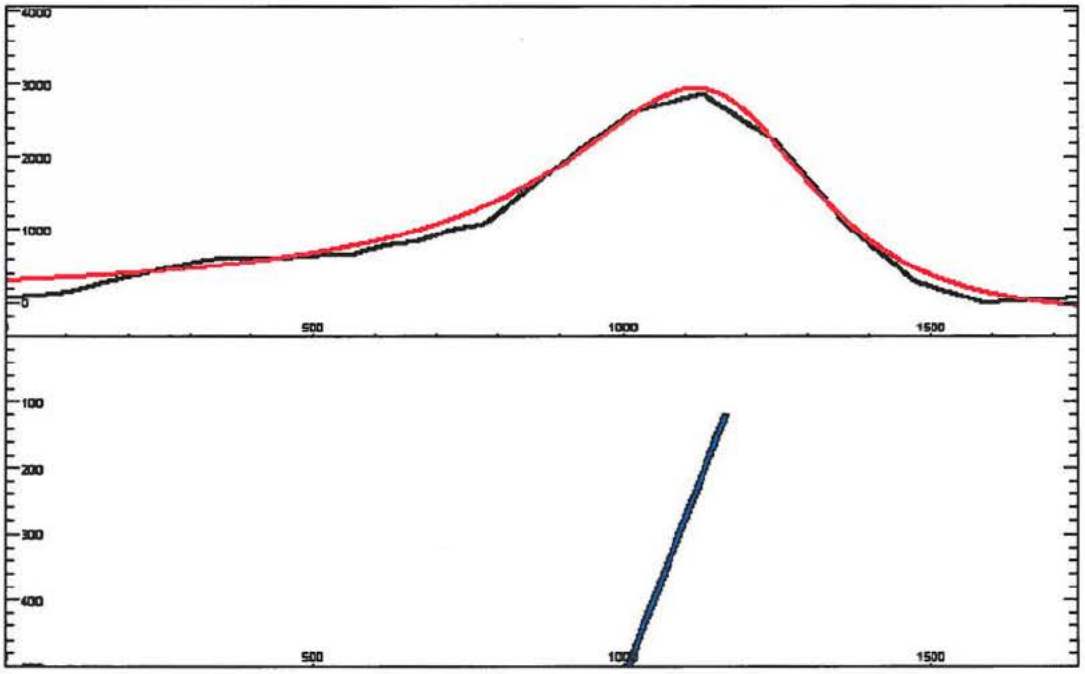

South **North**

Figure 60. *Measured (black curve) and model (red curves) responses obtained by inversion of the AEM Greenland 1994 data and the associated model.*

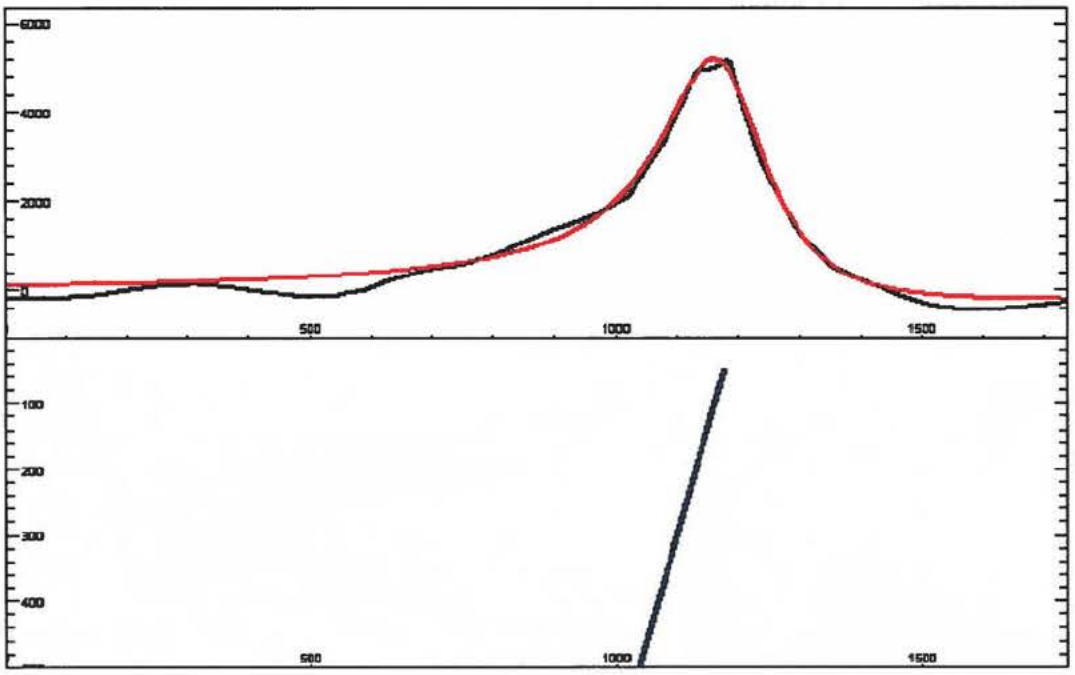

South **North**

Figure 61. *Measured (black curve) and model (red curves) responses obtained by inversion of the SkyTEM 2008 data and the associated model.*

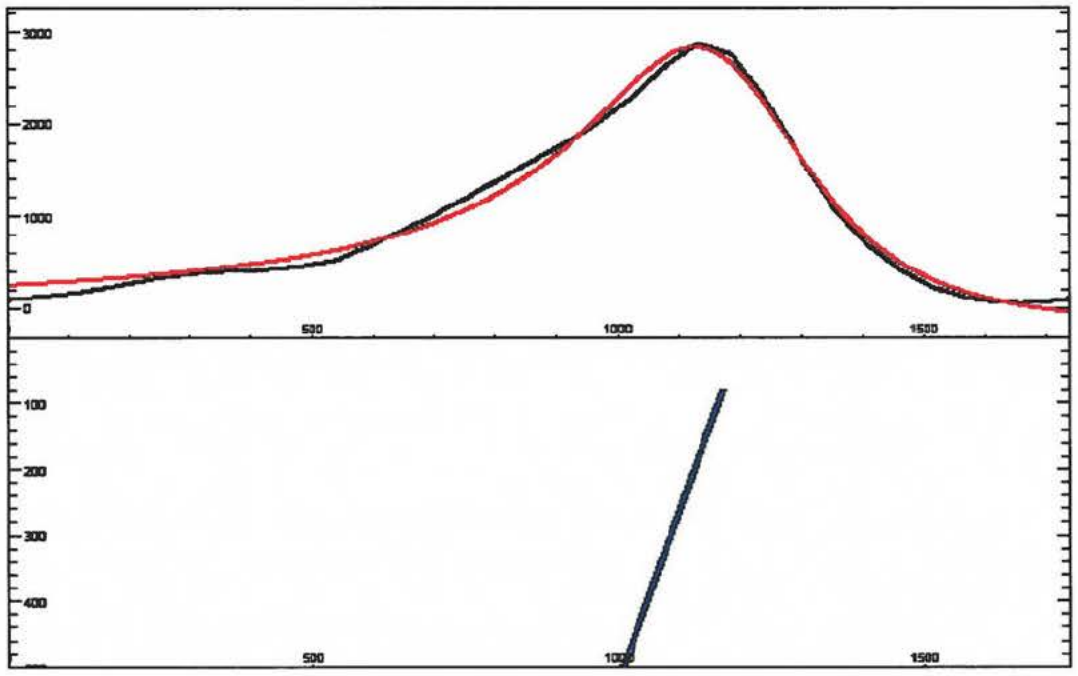

South **North**

Figure 62. *Measured (black curve) and model (red curves) responses obtained by inversion of the SGL 2010 data and the associated model.*

6.2 Comments on gravity responses for the model

The model obtained from the inversion of the magnetic data along the location of the GEUS 1999 ground magnetic profile has a dimension that would not provide a gravimetric response that is detectable from an airborne gravity survey. Inspection of the Bouguer field obtained from the 2010 survey confirms this conclusion. The Bouguer gravity field has a local maximum about 1.5 km south-southwest from the magnetic peak along the GEUS 1999 profile (see Figure 63).

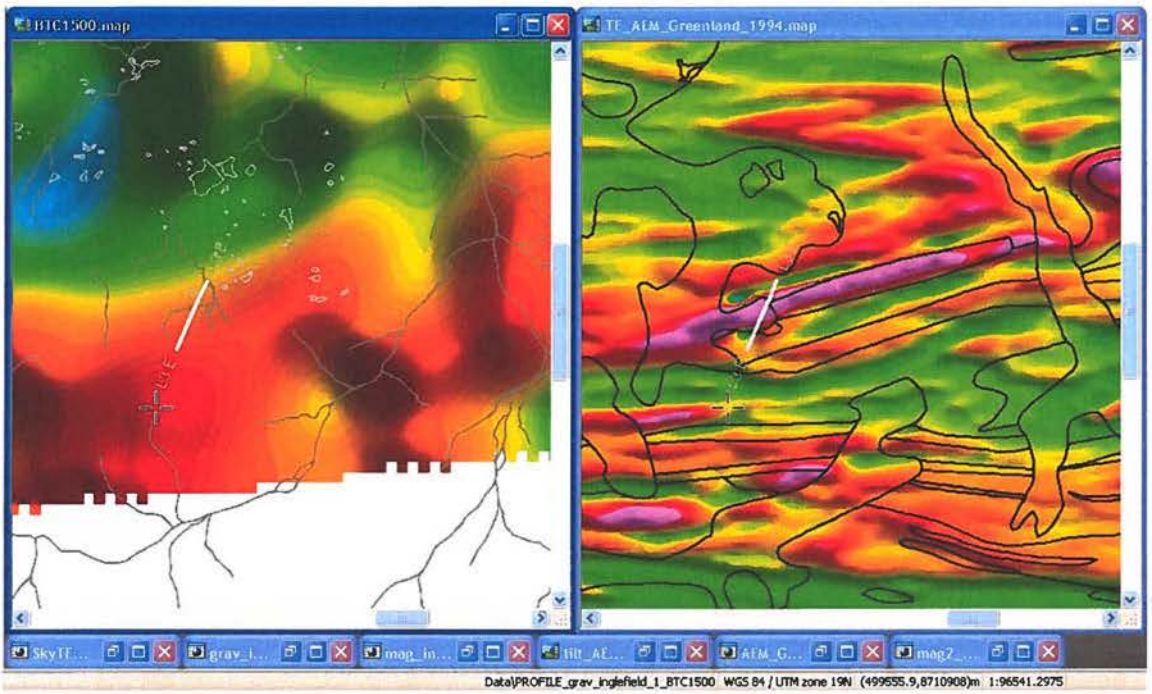

Figure 63. *The left panel shows the Bouguer gravity field and the right panel the magnetic field from AEM Greenland 1994 survey. The two maps cover the same area and the location of the GEUS 1999 profile is shown by the white line. The black lines on the map with magnetic field data are the outline of geological boundaries on the 1:500 000 GEUS geological map.*

7. Modelling of data along lines SGL 333, AEM 19901 and SkyTEM 100590

Line 333 from the combined magnetic and gravity survey cross several peaks of the magnetic field. The location of the profile is shown in Figure 64. Data from this line is chosen for modelling together with a subset of the adjacent line from the AEM Greenland 1994 survey (line 19901) and the SkyTEM 2008 survey (line 100590). The length of line 333 is 11.5 km and the length of line 100590 is 3.3 km.

Tabular bodies/dykes constitute the principal model. As mentioned in the sections above, the thickness and susceptibility parameters are often poorly determined whereas the thickness susceptibility product is better determined. The thickness susceptibility product is therefore tabulated together with the estimated thickness and susceptibility. A normalised thickness corresponding to 10 SI is also provided.

Results obtained from an attempt to make a joint inversion of the 3 data set were not fully satisfactory in terms of data fit, and more work is needed to fully integrate the data into a consistent data set. The problems are related to the regional/residual separation, which is dependent on elimination of the base station level for each survey, and on the line levelling performed by the geophysical contractors.

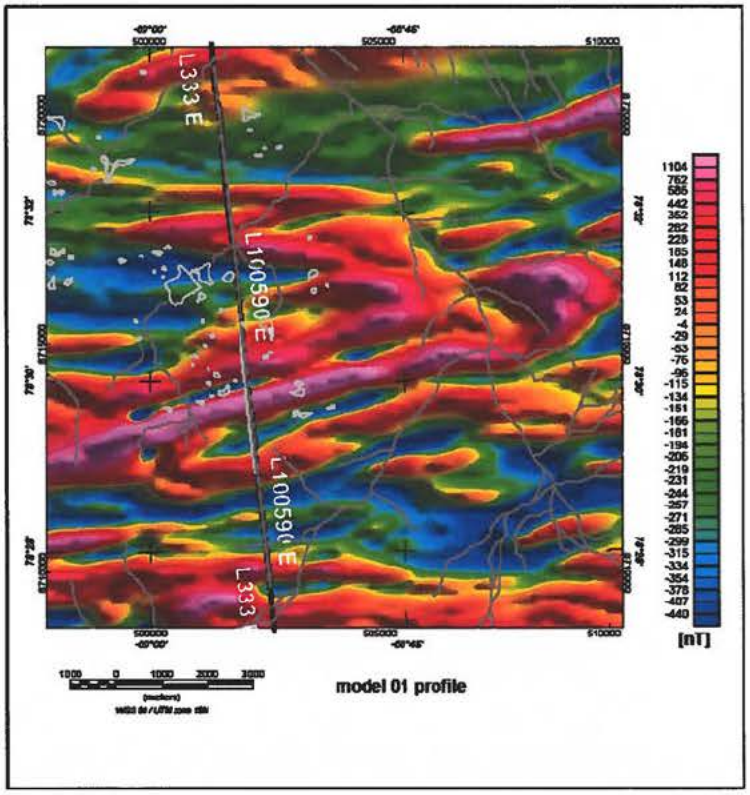

Figure 64. *Image of the magnetic field variation and the location of profiles used in modelling. The thick black line is survey line 19901 from the AEM Greenland 1994 survey. The dark grey line is the location of line 333 from the SGL 2010 survey and the line in light grey colour is survey line 100590 from the SkyTEM 2008 survey.*

7.1 Results from SGL survey Line 333

A total of 11 tabular bodies were used to fit the measured data from line 333, and the results are displayed in Figure 65 and in Table 3. The tabular bodies that are attributed to magnetite occurrences are highlighted in the table with a light blue background colour. The maximum normalised thickness of 6.8 m is found north of the location with magnetic maximum. The dyke associated with the peak anomaly has a normalised thickness of 4 m and an estimated depth of 30 m to the top. The measured profile contains some minor wiggles at distance location 4500 m that are not modelled. These anomalies are likely to be associated with minor near surface occurrences of magnetite.

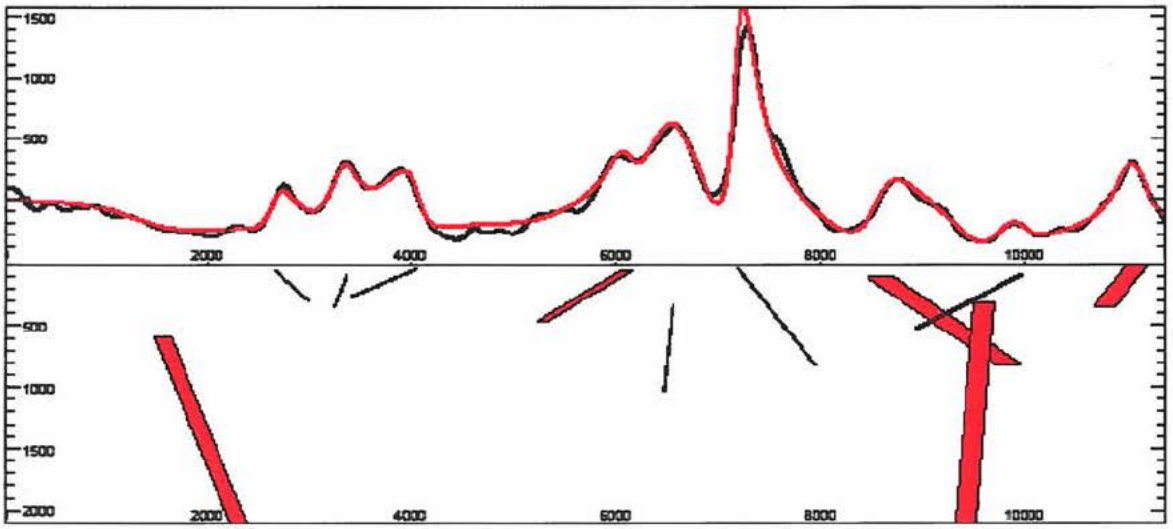

North **South**

Figure 65. *Upper panel shows measured data (black curve) in units of nT and model response (red curve). The lower panel shows the model with parameters as described in Table 3.*

Table 3. *Model parameter estimates from the inversion of data along line 333 from the SGL survey in 2010.*

x	y	z	susc	thick	suscXthick	thick_norm	azimuth	strike_length	depth_extent
502579	8709977	1	0.0589	199.2	11.7388	1.17	90	5000	340.2
502462	8711118	92	0.4504	37.1	16.7081	1.67	90	5000	428.6
502424	8711483	306	-0.1353	192.7	-26.0671	-2.61	74	5000	10000.0
502321	8712488	109	0.1030	244.8	25.2032	2.52	74	5000	704.8
502176	8713895	30	10.0000	4.0	40.0000	4.00	74	15000	793.8
502112	8714514	323	9.2486	7.4	68.4394	6.84	76	6000	710.2
502067	8714952	50	0.1821	95.0	17.3016	1.73	74	6000	412.5
501855	8717007	44	2.0000	12.0	24.0000	2.40	100	5000	214.9
501786	8717676	93	4.0000	4.0	16.0000	1.60	80	5000	259.9
501714	8718380	56	5.0000	2.0	10.0000	1.00	95	6500	243.2
501601	8719470	591	-0.1223	153.4	-18.7548	-1.88	84.1	4000	4426.6

7.2 Results from AEM Greenland 1994 survey Line 19901

A total of 10 tabular bodies were used to fit the measured data from line 19901, and the results are displayed in Figure 66 and in Table 4. The tabular bodies that are attributed to magnetite occurrences, are highlighted in the table with a light blue background colour. The maximum normalised thickness of 6.8 m is found north of the location with magnetic maximum. The dyke associated with the peak anomaly has a normalised thickness of 3.8 m and an estimated depth of 50 m to the top. The measured profile contains some minor wiggles around distance coordinate 4500 m and 10500 m that are not modelled.

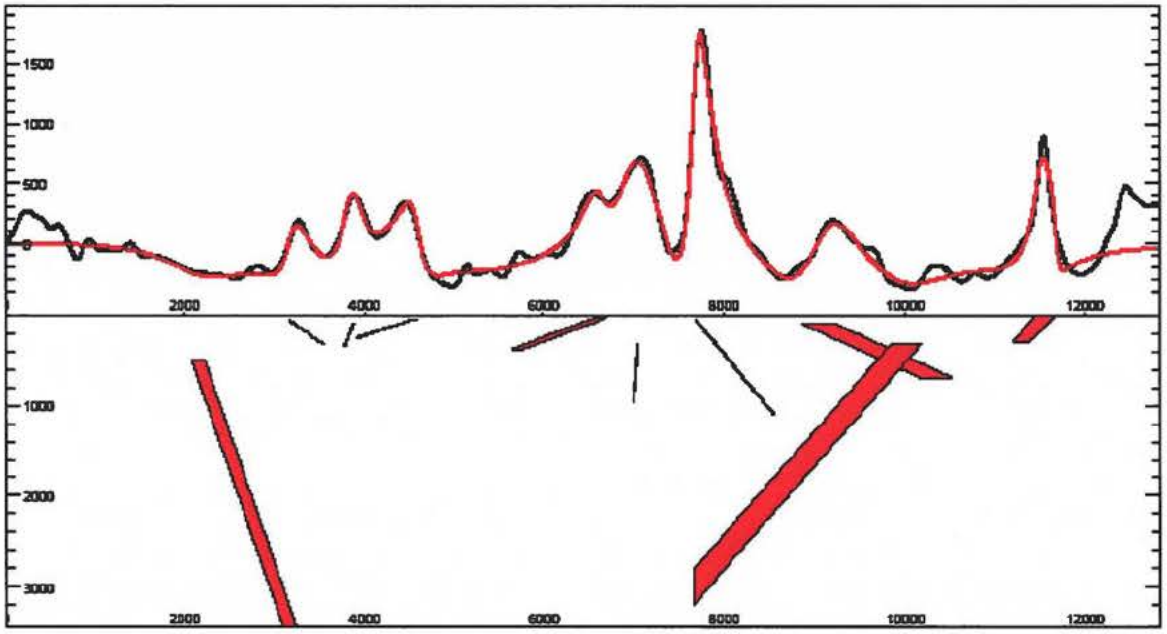

Figure 66. *Upper panel shows measured data (black curve) in units of nT and model response (red curve). The lower panel shows the model with parameters as described in Table 4.*

Table 4. *Model parameter estimates from the inversion of data along line 19901 from the AEM Greenland 1994 survey.*

x	y	z	susc	thick	Susc*thick	thick_norm	azimuth	strike_length	depth_extent
502578	8709988	0	0.066282	191.8	12.712887	1.27	87	4000	310
502416.7	8711554	315	-0.121176	172.3	-20.878624	-2.09	26	4000	9000
502317.3	8712519	99	0.106783	253.6	27.080271	2.71	41	4000	591
502177.5	8713877	50	10.205720	3.7	37.761166	3.78	59	13000	1051
502111.9	8714513	308	9.239714	7.4	68.373878	6.84	90	5347	654
502067.4	8714945	32	0.168333	87.4	14.712287	1.47	41	5760	343
501857.7	8716981	38	1.960501	11.8	23.133915	2.31	52	4985	204
501787.5	8717662	86	4.061704	4.1	16.652985	1.67	69	4818	242
501715.6	8718361	59	5.125663	2.2	11.276460	1.13	64	5500	261
501610.5	8719382	496	-0.112880	141.5	-15.972520	-1.60	-96	5000	3687

7.3 Results from SkyTEM survey Line 100590

A total of 13 tabular bodies were used to fit the measured data from line 100590, and the results are displayed in Figure 67 and in Table 5. The tabular bodies that are attributed to magnetite occurrences are highlighted in the table with a light blue background colour. One body at a depth of about 1000 m were used to eliminate some problems with a level shift of the field variations. This body is not relevant for interpretations and is highlighted in the table with a green background colour. The purpose of this is basically to shift the mean level of the magnetic field. The dyke associated with the peak anomaly has a normalised thickness of 5.3 m and an estimated depth of 68.5 m to the top.

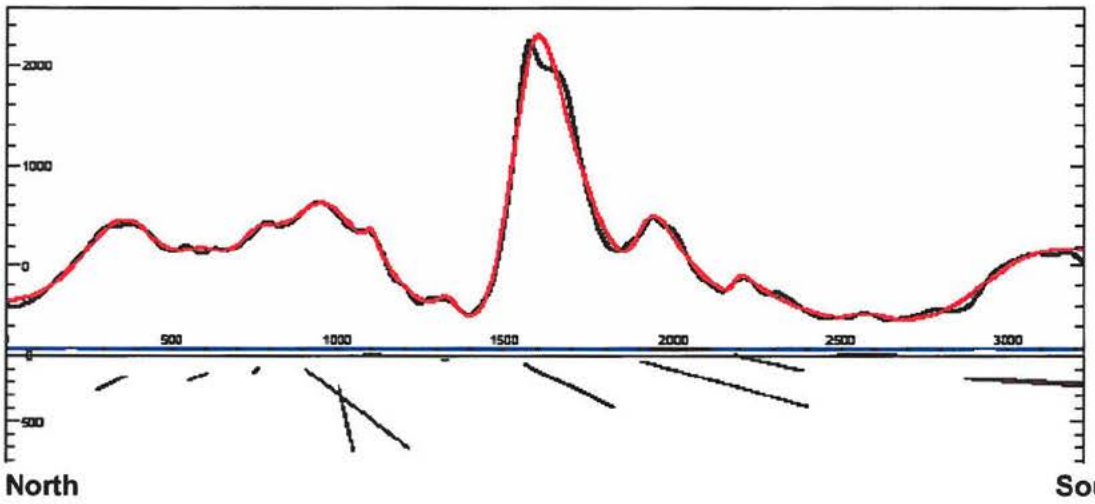

Figure 67. *Upper panel shows measured data (black curve) in units of nT and model response (red curve). The lower panel shows the model with parameters as described in Table 5.*

Table 5. *Model parameter estimates from the inversion of data along line 100590 from the SkyTEM 2008 survey.*

x	y	z	susc	thick	Susc*thick	thick_norm	azimuth	strike_length	depth_extent
502292	8712489	179.9	0.73073	126.7	92.584	9.3	74	11000	2132
502253	8712907	-3.1	0.50000	57.1	28.550	2.9	74	10000	1
502222	8713242	0	0.47940	4.1	1.966	0.2	75	10000	112
502196	8713517	43.8	4.36069	3.3	14.390	1.4	76	9000	337
502172	8713772	1056.7	-0.11566	3140.6	-363.254	-36.3	90	1029.6	122
502164	8713861	68.5	9.69900	5.5	53.344	5.3	75	9000	315
502141	8714105	27.9	3.12482	3.6	11.249	1.1	74	6500	11
502119	8714338	1.0	1.12566	2.2	2.476	0.2	78	5500	11
502112	8714414	230.9	9.63568	2.3	22.162	2.2	74	5500	494
502103	8714512	104.4	9.75670	1.6	15.611	1.6	75	2691.3	604
502089	8714654	93.3	9.80638	3.3	32.361	3.2	75	4500	37
502074	8714812	138	9.88694	4.6	45.480	4.5	75	5500	50
502052	8715051	156.2	9.73092	5.4	52.547	5.3	75	4500	111

7.4 Evaluation of results

The normalised thickness for the dykes associated with interpreted magnetite occurrences has maximum values around 6 m based on a standard susceptibility value of 10 SI. The estimated depth to the top of the dyke associated with the main anomaly is 30 m, 50 m and 68 m based on inversions of the three different dataset. The variation in estimated depth reflects the uncertainties and ambiguities associated with modelling of magnetic data. Similarly, some variability is noticed for other structures. However, the result that the thicknesses of the magnetite sheets are less than about 6 m is consistent among the three different models.

8. Modelling of triangular shaped magnetic anomaly east of Minturn River

A triangular shaped magnetic anomaly is located slightly east of the Minturn anomaly, and this anomaly has been selected for modelling because of its large areal extent. Furthermore, it was noted above in section 4.3 that also the gravity field has a local maximum at this location (see Figure 35). The location is shown in Figure 68 with the AEM Greenland 1994 data as background image. An image of the magnetic field from the SkyTEM 2008 survey is shown in Figure 69 and images of the calculated second vertical gradient of the magnetic field and the pseudo gravity field are shown in Figure 70 and 71 respectively.

The approach used for evaluating this anomaly differs from the methods applied to the profile data. An inspection of the second vertical gradient points to a fairly complex structure and a ribbon-like model is probably needed to give a good geometric description of the structure. Building of such a model is very time-consuming and will have to wait to a later stage. Instead, the anomaly is evaluated in terms of total volume of magnetite occurrence associated with this anomaly. This is done by converting the magnetic field data into pseudo-gravity field values by using values of the magnetic susceptibility of 10 SI and a density of 4.67 g/cm^3 corresponding to magnetite. The pseudo gravity field is shown in Figure 71. A peak value of about 0.07 mGal is obtained. The transformation to pseudo gravity field basically integrates the separate magnetic anomalies into a single gravity anomaly that can be evaluated more easily in terms of volume.

The evaluation of volume is done by comparing the pseudo gravity anomaly with the gravity response from a quadratic plate with horizontal dimension 1500 m x 1500 m and a thickness of 2 m. The magnetic response and gravity response for this model is shown in Figures 72 and 73 respectively. The colour scales for these are similar in range as those used in Figure 69 and Figure 71. We note that the amplitudes for the pseudo gravity field are similar to or slightly smaller than those obtained for the model response. The conclusion is that a total volume associated with the measured anomaly is about 1500 m x 1500 m x 2 m = 4500000 m^3 or 0.0045 km^3.

The peak value of about 0.07 mGal for the pseudo gravity field is much smaller than the actual gravity anomaly co-located at the location of the magnetic anomaly. Figure 74 shows the Bouguer gravity field (1500 m half wavelength, 2.67 g/cm^3 data) after a regional/residual separation performed by removal of a linear trend from the data. Superimposed onto the image are ridge peak locations for the pseudo gravity field. The residual anomaly at the location of the triangular shaped magnetic anomaly is approximately 5 mGal, i.e. about seventy times more than the peak pseudo gravity field. From the display in Figure 74 we note the general lack of correlation between the magnetic peak locations and the peaks for the gravity field. Two other gravity peaks can be observed south and southwest of the triangular shaped magnetic anomaly. These anomalies are also about 5 mGal in amplitude. A guideline for the understanding of the observed responses can be obtained from a map (Figure 75) of terraced Bouguer gravity data with superimposed peaks of the pseudo gravity field. The position of the peak values tends to follow the boundaries obtained from the terraced data. The coincidence between boundaries obtained from application of the terracing technique and peak value favours an interpretation similar to the synthetic example in section 5.5;

i.e. the gravity field observed is mainly determined by block boundaries on a more regional scale and the occurrence of the magnetite is controlled by these boundaries.

A modelling dominated by haematite instead of magnetite results in a volume that is about 70 times larger than the one presented above. It is not possible from the geophysical data to exclude such a model.

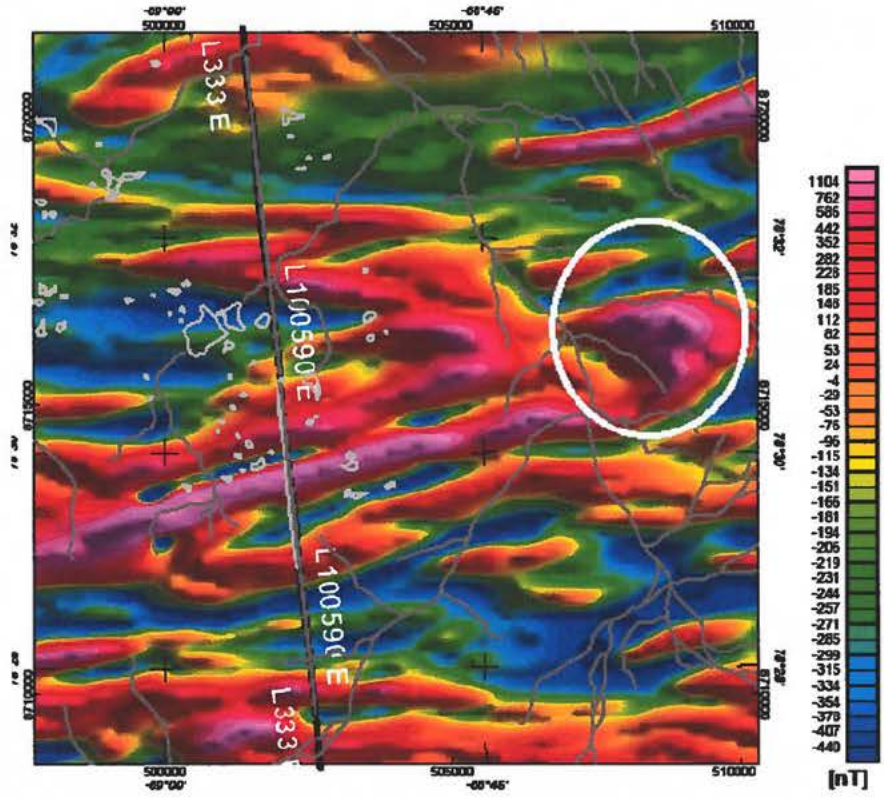

Figure 68. *Location of triangular shaped anomaly selected for modelling. The background image is the AEM Greenland 1994 magnetic anomaly.*

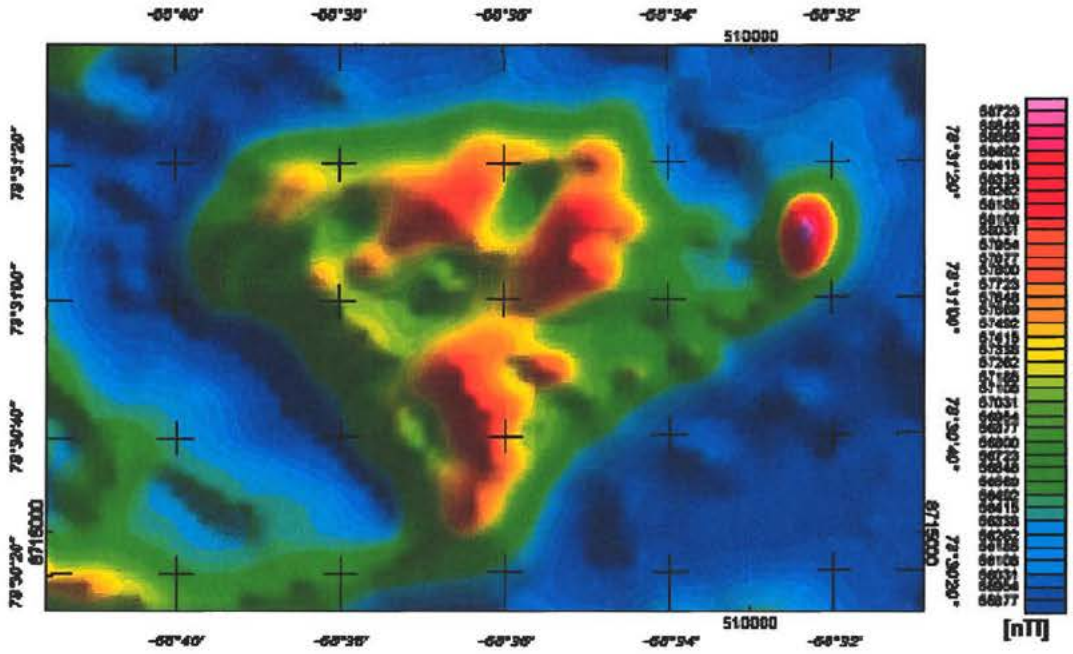

Figure 69. *The triangular shaped anomaly selected for modelling. The background image is SkyTEM magnetic field data.*

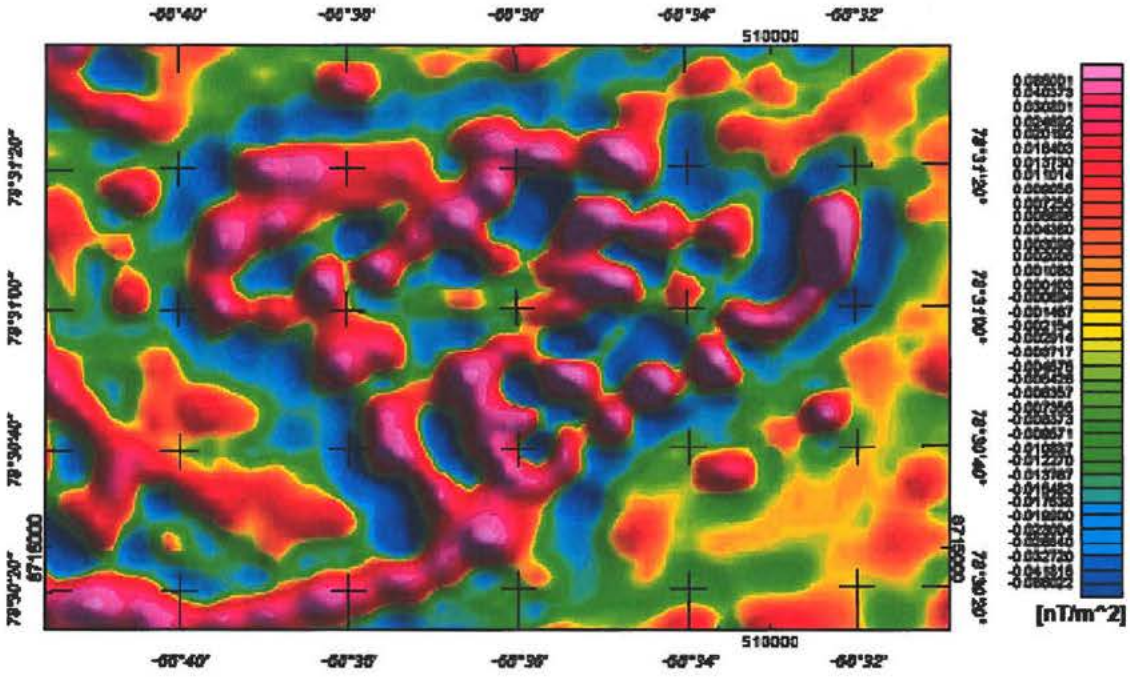

Figure 70. *The triangular shaped anomaly selected for modelling. The background image is the second vertical gradient based on the SkyTEM magnetic field data.*

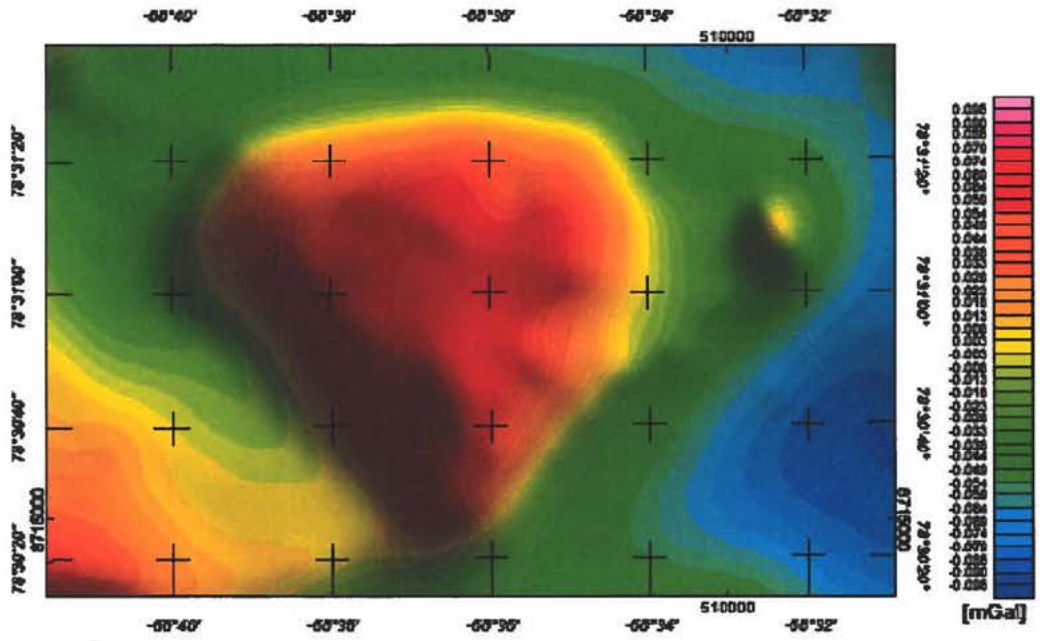

Figure 71. *The triangular shaped anomaly selected for modelling. The background image is the pseudo gravity field based on the SkyTEM magnetic field data.*

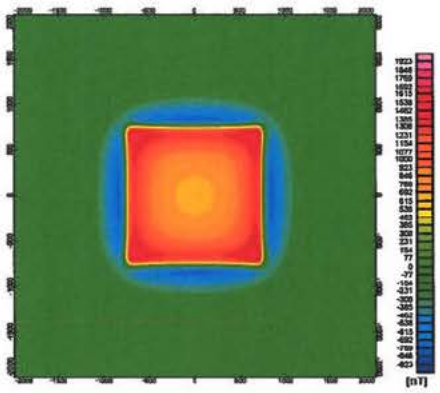

Figure 72. *Magnetic field anomaly for plate model.*

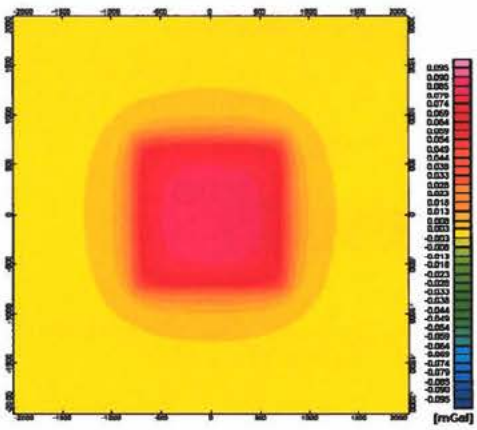

Figure 73. *Gravity field for plate model.*

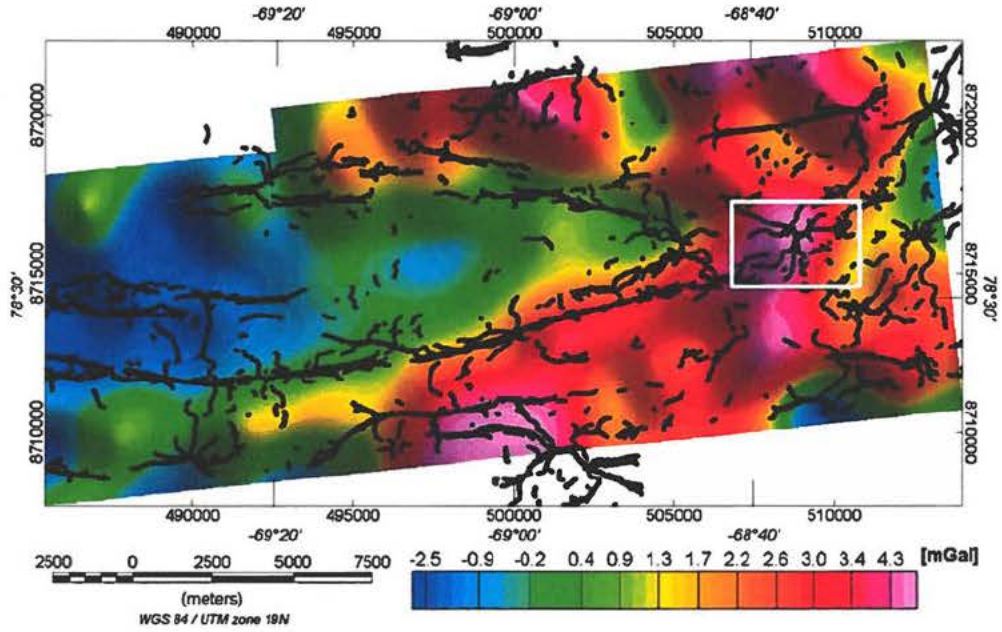

Figure 74. *Detrended Bouguer gravity field with superimposed ridge peaks for the pseudo gravity field marked by filled black circles. The rectangle in white colour outlines the map frame used in Figures 70 and 71.*

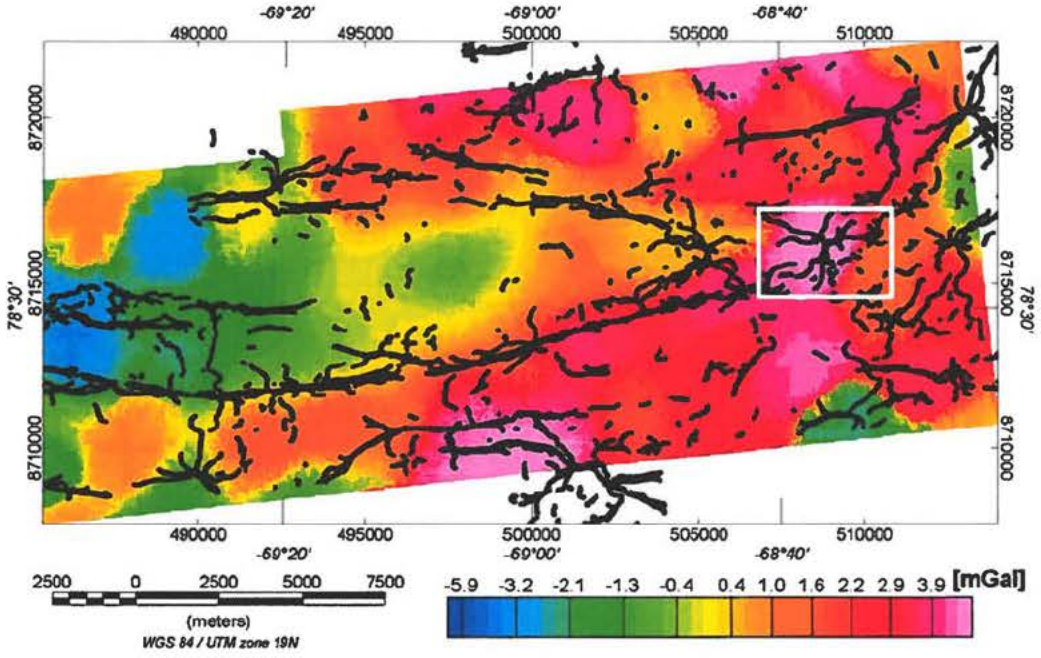

Figure 75. *Terrraced Bouguer gravity field with superimposed ridge peaks for the pseudo gravity field marked by filled black circles. The rectangle in white colour outlines the map frame used in Figures 70 and 71.*

9. Modelling of Line SGL 110

Line SGL 110 is located in the western part of the SGL 2010 survey. A model including four dykes are used to interpret the data. The results are outline in Figure 76 and summarised in Table 6. Two dykes are used to represent the main anomaly. The depth estimates for these are 306 and 738 m respectively.

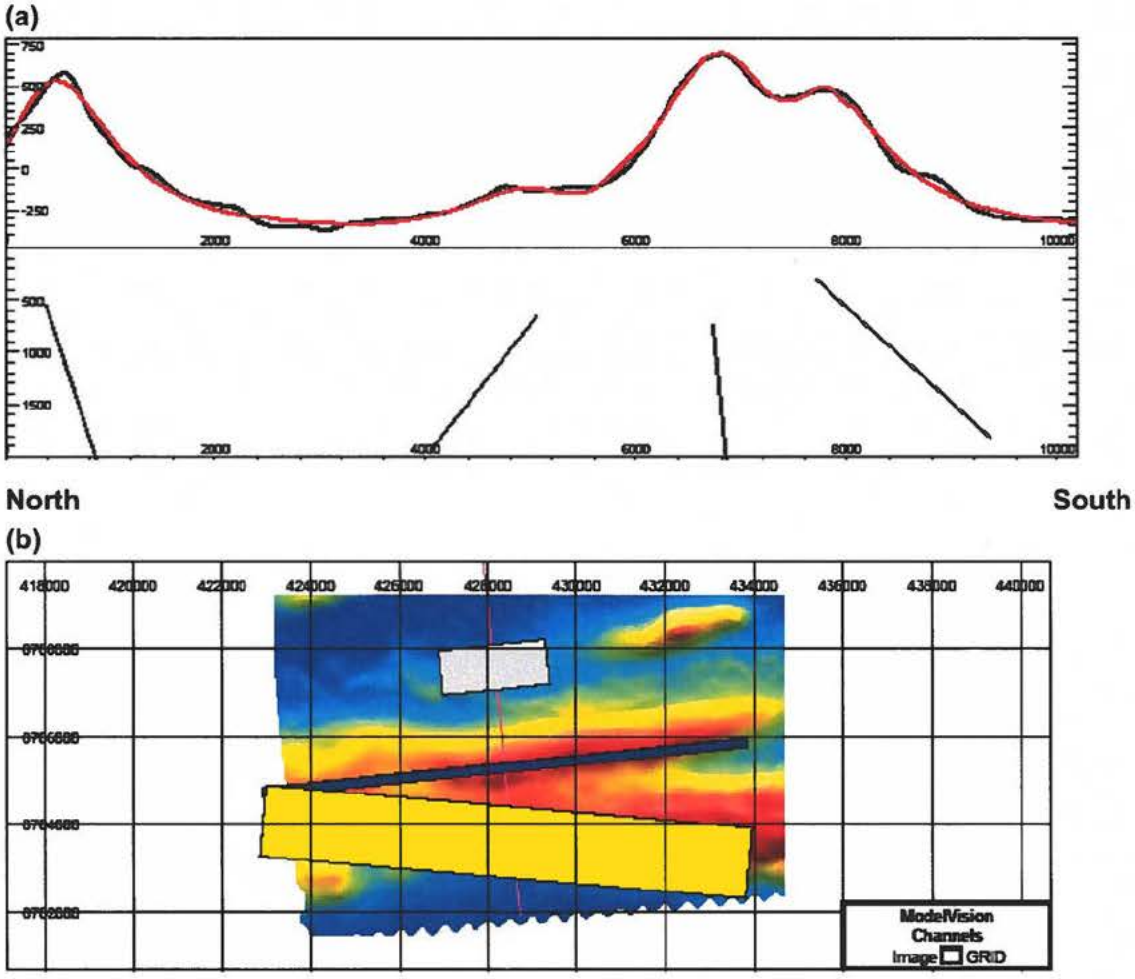

Figure 76. *(a) Upper panel shows measured data (black curve) in units of nT and model response (red curve). The lower panel shows the model with parameters as described in Table 6. (b) image of the magnetic field and outline of model boundaries. Map coordinates are in WGS84/UTM19N.*

Table 6. *Model parameter estimates from the inversion of data along line 110 from the SGL 2010 survey.*

x	y	z	susc	thick	susc*thick	thick_norm	azimuth	strike_length	depth_extent
428461	8704407	306.5	10.12566	4.5	45.56548	4.556548	95	11000	1517
428360.2	8705390	738.9	9.989116	14.1	140.8465	14.08465	84.1	11000	2137.2
428189.2	8707058	660.1	10.12566	3.3	33.41469	3.341469	84.15	2419.4	1279
427713.8	8711694	548.8	9.874336	8.2	80.96956	8.096955	84.15	2105.4	2481.3

10. Modelling of line SGL 186

Line SGL 186 is located in the central part of the SGL 2010 survey. A model including five dykes are used to interpret the data. The results are outlined in Figure 77 and summarised in Table 7. The dyke causing the main anomaly is positioned at a depth of 652 m.

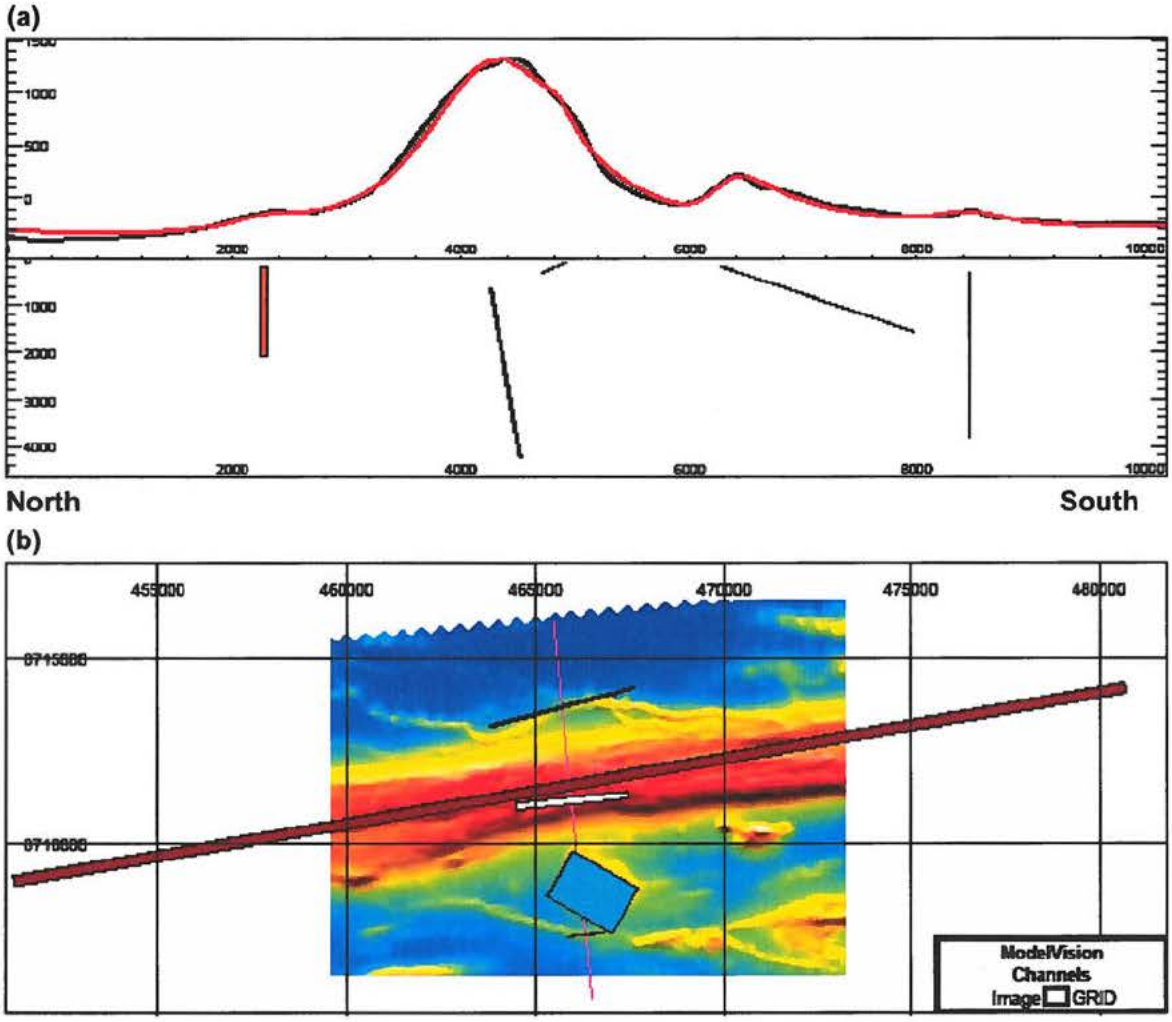

Figure 77. *(a) Upper panel shows measured data (black curve) in units of nT and model response (red curve). The lower panel shows the model with parameters as described in Table 7. (b) image of the magnetic field and outline of model boundaries. Map coordinates are in WGS84/UTM19N.*

Table 7. *Model parameter estimates from the inversion of data along line 186 from the SGL 2010 survey.*

x	y	z	susc	thick	Susc*thick	thick_norm	azimuth	strike_length	depth_extent
466340.8	8707566	300	1.000	7.9	7.9	0.8	84	1000	3488
466857.1	8709313	182.9	10.126	2.5	25.3	2.5	120	2000	1379
465977.5	8711096	103	9.874	1	9.9	1.0	84	3000	200
465910.4	8711747	652.5	10.037	16.6	166.6	16.7	80	30000	3589
465707.5	8713718	427.7	0.100	98.7	9.9	1.0	75	4000	1866

11. Results from Euler deconvolution of magnetic data

The models obtained from inversion of the magnetic along selected profiles indicates an increased depth to the dyke towards west. This conclusion is confirmed by application of the Euler deconvolution technique (Mushayandebvu et al., 2001) to the magnetic field data. The depth estimates are shown in Figure 78.

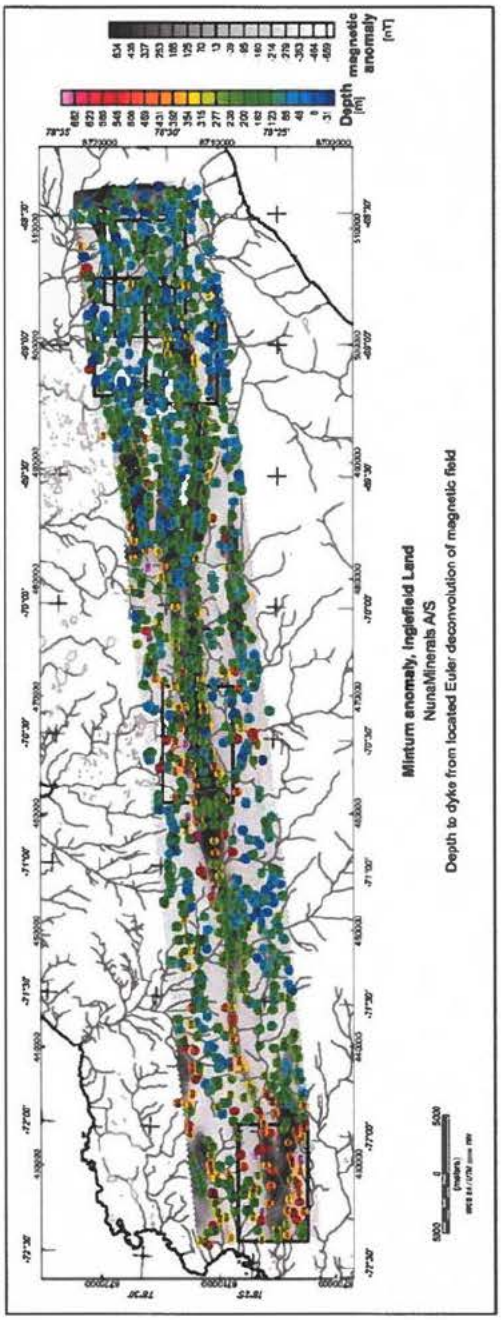

Figure 78. *Depth estimates to top of dykes from Euler deconvolution of the magnetic data from the SGL 2010 survey.*

12. Correlation of magnetic susceptibility data and airborne magnetic responses

An important question with respect to the modelling of the magnetic data is whether the responses are caused by thin sheet like bodies with very high susceptibility (pure magnetite) of whether the responses are caused by thicker geological units with a more moderate susceptibility linked to disseminated magnetite? The answer to this question cannot be determined solely from an investigation of the measured magnetic responses, because of the non-uniqueness inherent in interpretation of potential field data. The susceptibility data obtained during field work by NunaMinerals in September 2010 have maximum values about two orders of magnitude lower than the values usually quoted for pure magnetite and susceptibility values for the magnetite floats collected by GEUS in 1995.

Some positive correlation was noted in section 3.4 between measured susceptibility and measured vertical magnetic gradient. In order to analyse the data further, a model is contructed in this section which is based on the measured susceptibility values shown in Figure 12c. The data in Figure 12c is reproduced here in Figure 79, which also shows the magnetic data along profile 186 from the SGL 2010 survey (see chapter 10). The models consist of 105 sequentially placed vertical sections with a strike along the direction of the anomaly. Each section has a width of 20 m and extends from the surface to a depth of 500 m. The suceptibility for each section is determined in the following way:

1. Interpolation and gridding of the susceptibility data in Figure 12c with a grid cell size of 20m and grid row orietation along strike
2. Find mean and maximum value along strike for each row in the grid
3. The mean and maximum are used to construct two 2-dimensional models

Figure 80 displays (a) the susceptibilies used for the two models and (b) the corresponding magnetic responses at a survey altitude of 120 m. A comparison with the magnetic profile data in Figure 79 shows that the two models have responses in the same order of magnitude as observed and that the width of the anomalies are similar. The conclusion from this comparison is that a model in which the mineralisation mainly is composed of disseminated magnetite and is close to the surface is possible. If this model is valid, the low susceptibilities indicate that the iron concentration cannot be very high. The findings of floats with pure magnetite in the area close to the Minturn River is clearly not in favour of such an interpretation. The larger width of the anomaly (>1 km) in the area outlined in Figure 79 compared to the width of the anomaly closer to the Minturn River (200 m) may be an indication that an interpretation involving both disseminated magnetite occurence and more solid magnetite is likely. The magnetic data are however not conclusive with respect to this statement.

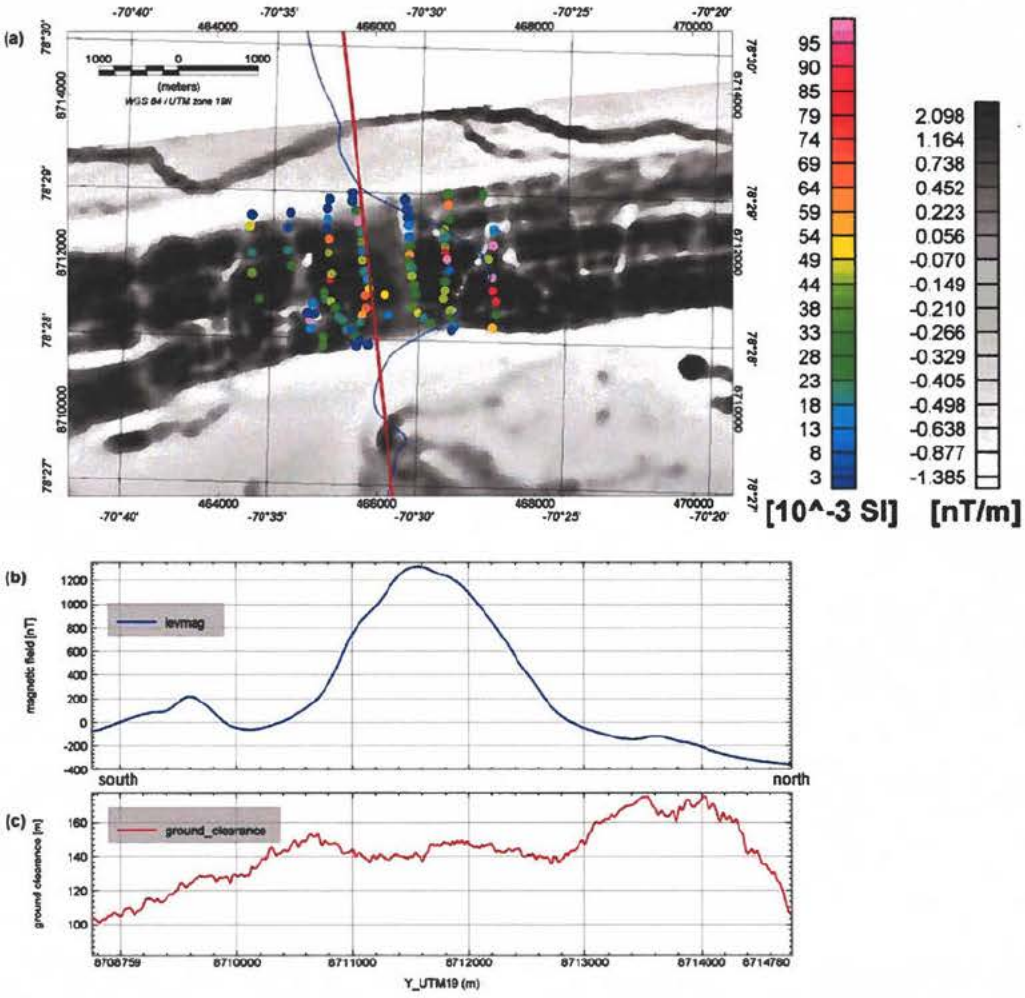

Figure 79. *(a) Susceptibility values plotted as colour filled circles on an image of the vertical gradient of the magnetic field. The straight red line shows flight path for line 186 for the SGL 2010 survey and the blue curve shows the profile of the corresponding magnetic data. (b) Profile of magnetic field for line 186 shown in a frame with UTM coordinate as abscissa and (c) ground clearance.*

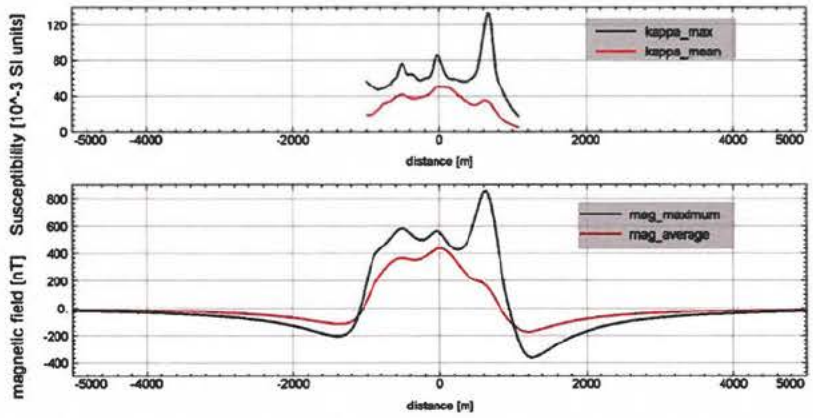

Figure 80. *The upper panel shows the susceptibilities used for the two models. The models consist of 105 vertical 20 m wide sections in a background with zero susceptibility. The lower panel shows the corresponding magnetic field profiles.*

13. Result from terracing of gravity data – entire survey

Terraced data were discussed in section 8 in relation to a triangular shaped magnetic anomaly located east of the Minturn River. Figure 81 shows terraced data for the entire gravity survey. The correlation between peaks of the pseudo gravity field and the derived boundaries are most pronounced for the eastern part of the survey area but some correlation can also be noted for the western part of the survey area.

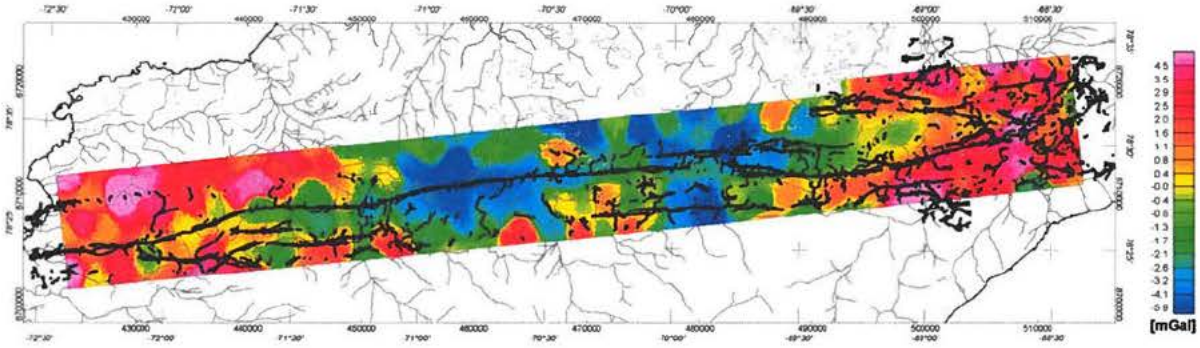

Figure 81. *Terrraced Bouguer gravity field with superimposed ridge peaks for the pseudo gravity field marked by filled black circles.*

14. Target areas for IOCG occurrences

This section contains target areas proposed for further investigation in a search for IOCG occurrences. The target definition is done by inspection of the geophysical data and based on the guidelines listed in the introduction. Gravity data are not available for the entire area of Inglefield Land and the target definition is therefore in some instances based on the GEOTEM and magnetic data only. Some anomalies of high conductivity are included although this is not a typical feature for IOCG occurrences. In total 14 areas are selected, but more areas could be classified to be of interest. The 14 areas are shown in the overview map in Figure 82, which also displays gold concentrations from samples collected by GEUS and others (Thomassen et al. 2000). The target section has not been guided by the results from the previous rock sample analysis, and some of the selected target areas have been sampled previously. An evaluation in which geochemical data are integrated with the geophysical data is proposed for prioritising the targets and for expanding the number of target areas. Figures with data from 14 target areas are included in appendix C.

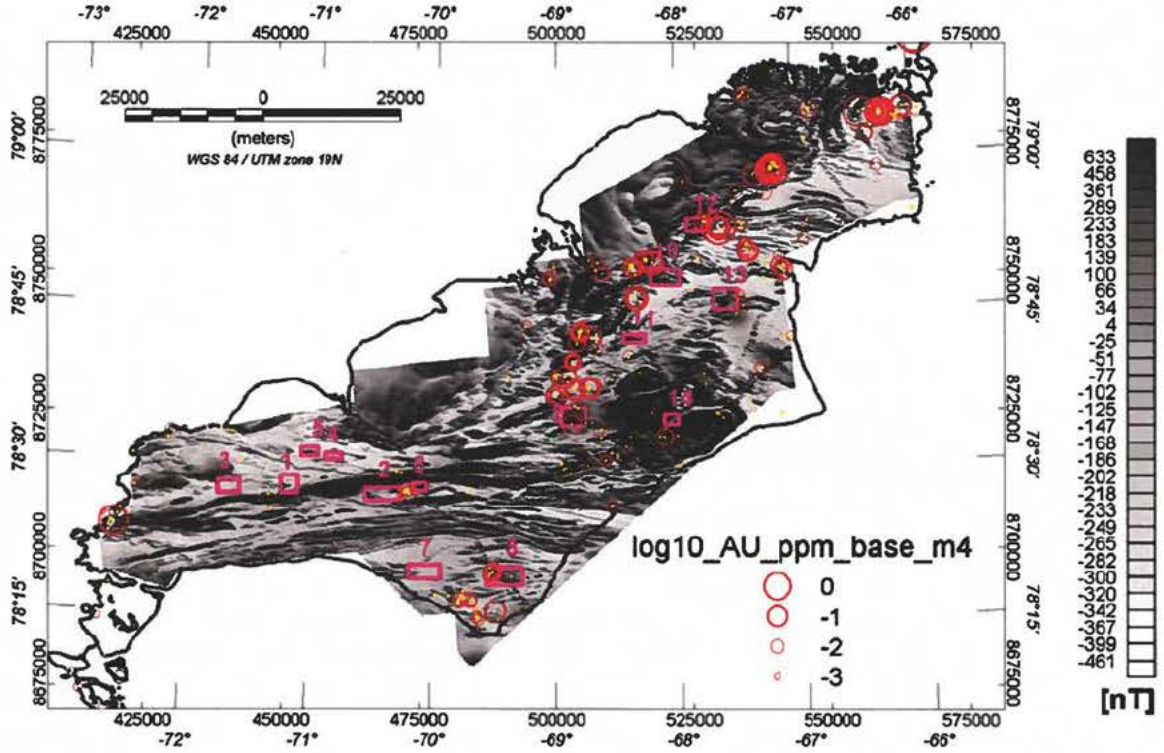

Figure 82. *Image of magnetic total field and target areas marked by rectangles and number in cyan colour. Locations for rock samples are marked by yellow circles and the Au concentration (log_{10} values) in units of ppm is shown by the red circles. The symbol size is proportional to the log_{10} values with -4 used as zero base.*

15. References

Cordell, L. and McCafferty, A.E. 1989. A terracing operator for physical property mapping with potential field data. Geophysics **54**, 621–634.

Corriveau, L., 2007 - Iron oxide copper-gold (±Ag ±Nb ±P ±REE ±U) deposits: a Canadian perspective; in: Goodfellow, W.D., (ed.), Mineral Deposits of Canada: a synthesis of major deposits-types, district metallogeny, the evolution of geological provinces and exploration methods: Geological Association of Canada, Mineral Deposits Division, Special publication no. 5, pp. 309–328.

Dawes, P.R., 2004 - Explanatory notes to the Geological map of Greenland, 1:500 000, Humboldt Gletscher, Sheet 6; Geological Survey of Denmark and Greenland, Map Series, 1, 48p.

Dawes, P.R., Frisch, T., Garde, A.A., Iannelli, T.R., Ineson, J.R., Jensen, S.M., Pirajno, F., Sønderholm, M., Stemmerik, L., Stouge, S., Thomassen, B. and van Gool, J.A.M., 2000 - Kane Basin 1999: mapping, stratigraphic studies and economic assessment of Precambrian and Lower Palaeozoic provinces in north-western Greenland; Geology of Greenland Survey, Bulletin 186, pp. 11–28.

Mushayandebvu, M. F., van Driel, P., Reid, A.B., and Fairhead, J.D., 2001, Magnetic source parameters of two-dimensional structures using extended Euler deconvolution: Geophysics, vol. **66**, no. 3, p 814–823

Sandrin, A. and Elming, S.-Å., 2006. Geophysical and petrophysical study of an iron oxide copper gold deposit in northern Sweden. Ore Geology Reviews, **29**, 1–18.

Sandrin, A., Berggren, R. and Elming, S.-Å., 2007. Geophysical targeting of Fe-oxide Cu–(Au) deposits west of Kiruna, Sweden. Journal of Applied Geophysics, **61**, pp 92–101.

Smith, R.J., 2002. Geophysics of iron oxide copper–gold deposits. In: Porter, T.M. (Ed.), Hydrothermal iron oxide copper–gold and related deposits: a global perspective, vol. 2. Australian Mineral Foundation, Adelaide, Australia, pp. 357–367.

Stemp, R.W. and Thorning, L., 1995 - Airborne electromagnetic and magnetic survey of Inglefield Land, North-West Greenland: Results from project AEM Greenland 1994. Grønlands Geologiske Undersøgelse, Open File Series **95/1**, 45p.

Steenfelt, A. and Dam, E., 1996 - Reconnaissance geochemical mapping of Inglefield Land, North-West Greenland. Danmarks og Grønlands Geologiske Undersøgelse, Rapport, 1996, **12**, 12p.

Telford, W. M., Geldart, .L. P. and Sheriff R. E., 1990. Applied Geophysics. Second edition. Cambridge University Press, pp 792.

Thomassen, B., Pirajno, F., Iannelli, T.R., Dawes, P. and Jensen, S.M., 2000 - Economic geology investigations in Inglefield Land, North-West Greenland: part of the project Kane Basin 1999; Danmarks og Grønlands Geologiske Undersøgelse, Rapport 2000, **100**, 98p.

16. Appendix A - Catalogue of synthetic response from tabular shaped bodies

Gravimetric and magnetic responses are presented for some tabular bodies as outlined schematically in Figure A1 and summarised in Table A1. Responses are calculated for various values of width d_x, thickness d_z.and depth h. The length d_y is kept at a constant value of 20 km. The responses are calculated at altitudes of 75 m, 175 m, 275 m, 375 m, 475 m and 575 m above ground along profile direction X. For symmetry reasons only data for X>0 are shown. The density contrast is 2 g/cm^3 and the magnetic susceptibility is 10 SI.

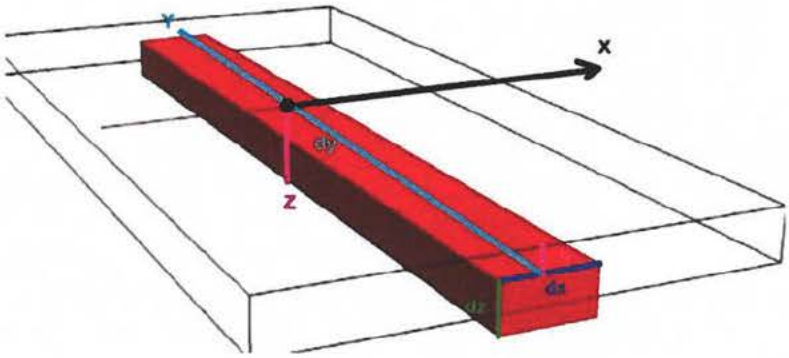

Figure A1. *General outline of shape of tabular body used for model calculations.*

Table 8. *Figure numbers and corresponding parameter values for width dx, thickness dz.and depth h*

Figure no.	Width d_x [m]	Thickness d_z [m]	Depth h [m]
A2	5	50	5
A3	5	250	5
A4	5	500	5
A5	50	50	5
A6	50	250	5
A7	50	500	50
A8	50	50	50
A9	50	250	50
A10	50	500	50
A11	500	50	50
A12	1000	50	50
A13	1000	250	50
A14	1000	500	50
A15	1000	250	250
A16	2000	50	50
A17	2000	250	50
A18	2000	500	250
A19	2000	250	250

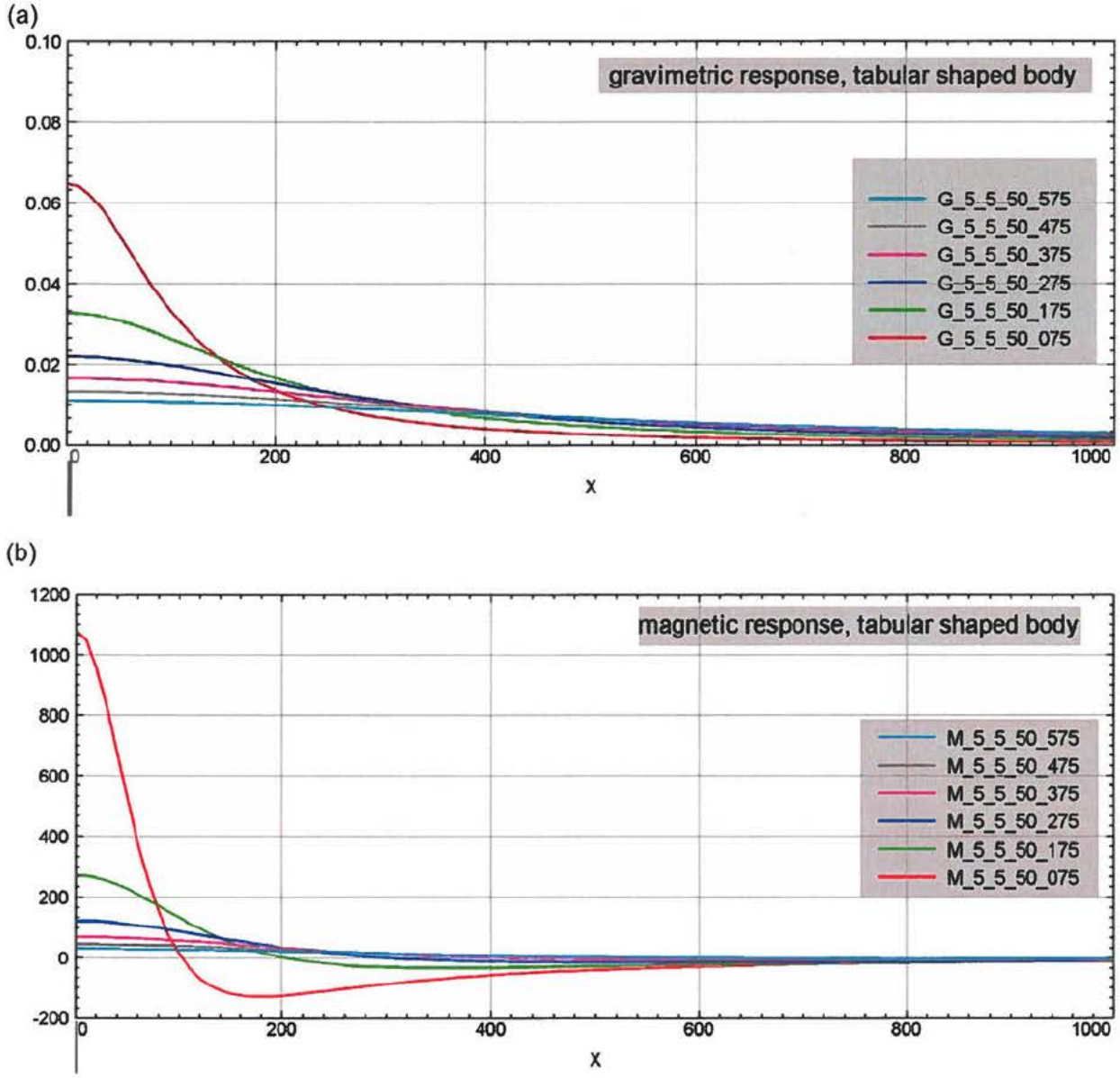

Figure A2. *(a) Gravimetric and (b) magnetic responses from a tabular body with a width of 5 m and thickness of 50 m. The top of the tabular body is 5 m below surface and responses are shown for altitudes of 75 m, 175 m, 275 m, 375 m, 475 m and 575 m.*

(a)

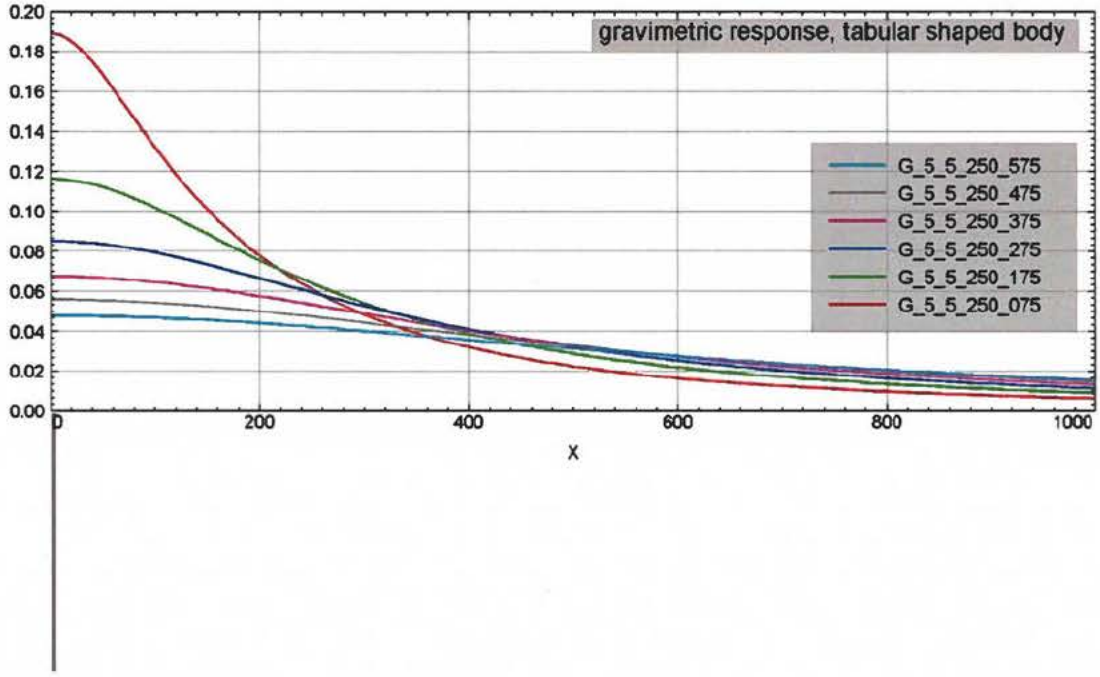

(b)

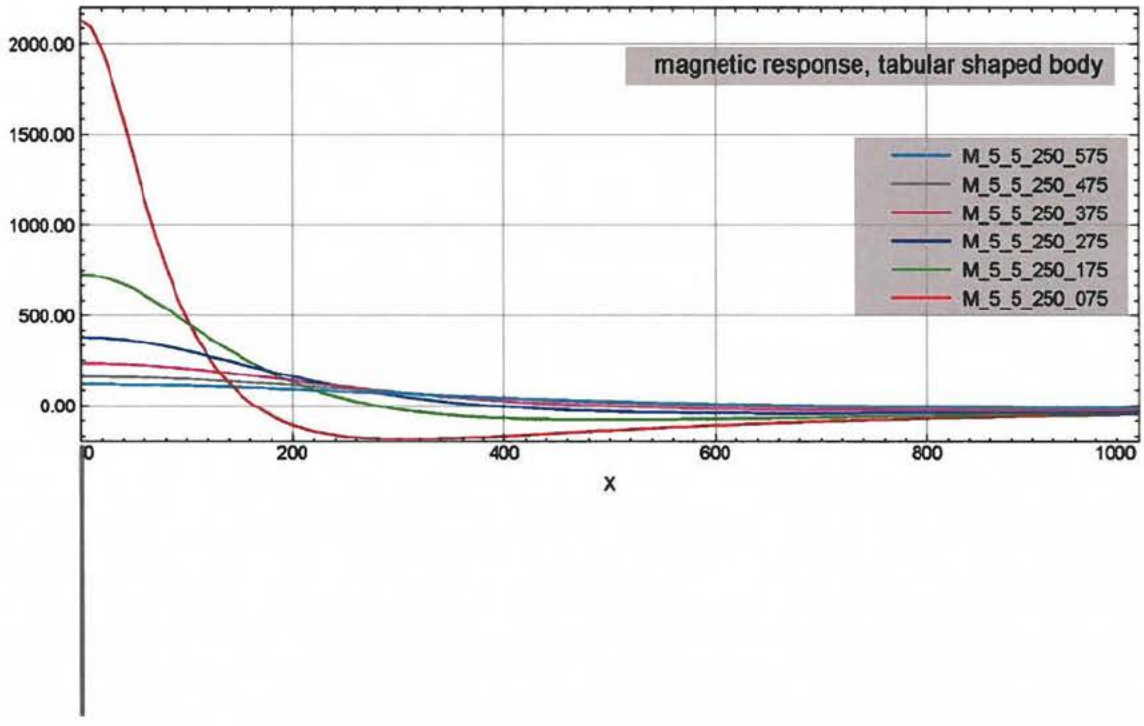

Figure A3. *(a) Gravimetric and (b) magnetic responses from a tabular body with a width of 5 m and thickness of 250 m. The top of the tabular body is 5 m below surface and responses are shown for altitude 75 m, 175 m, 275 m, 375 m, 475 m and 575 m.*

(a)

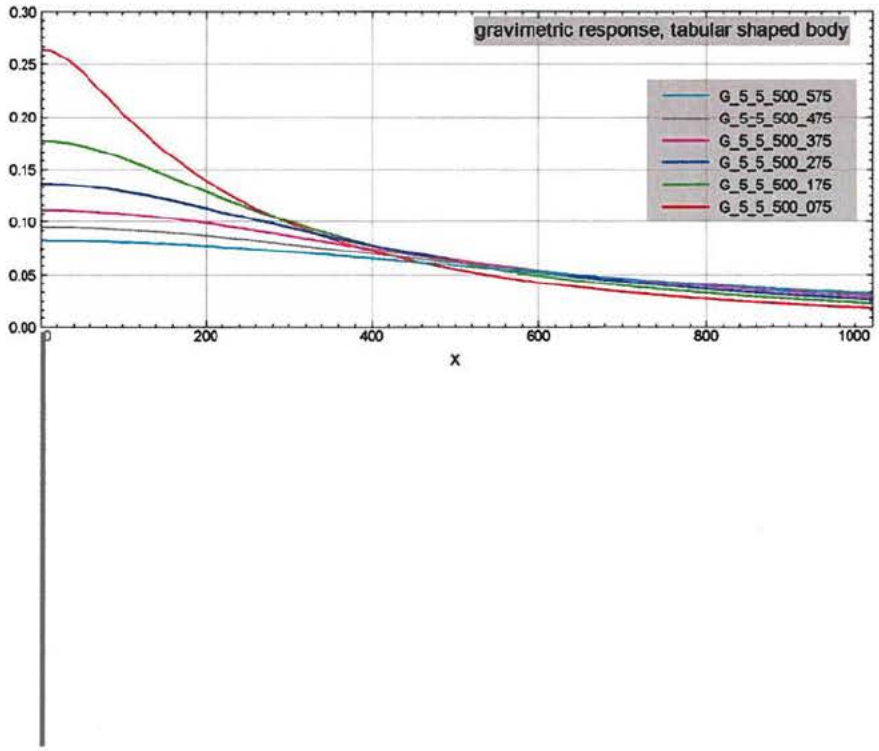

(b)

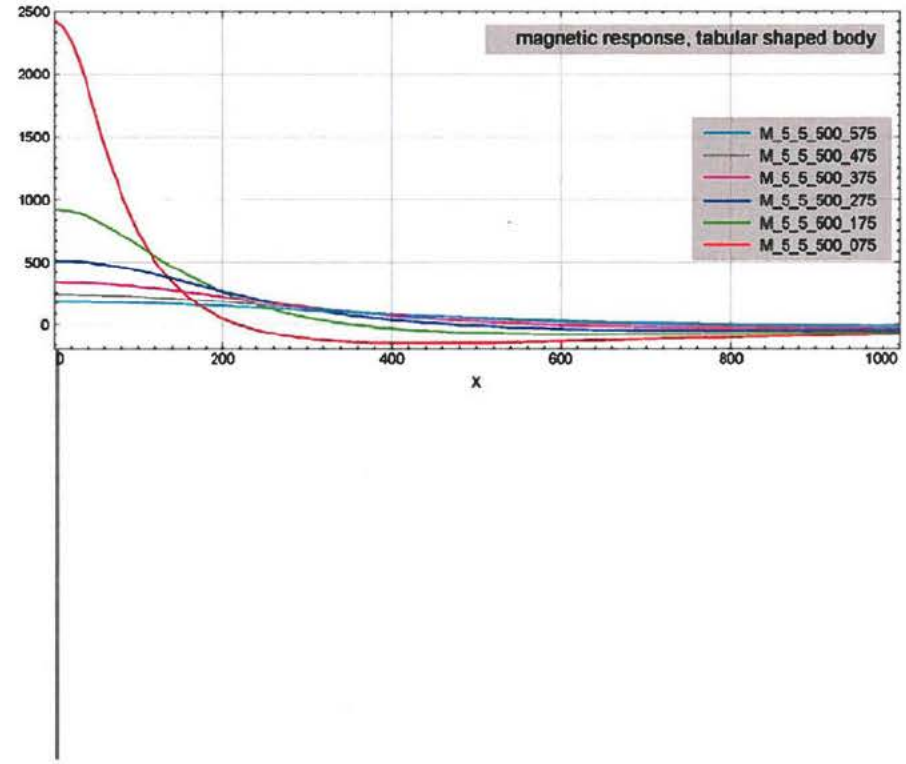

Figure A4. *(a) Gravimetric and (b) magnetic responses from a tabular body with a width of 5 m and thickness of 500 m. The top of the tabular body is 5 m below surface and responses are shown for altitudes of 75 m, 175 m, 275 m, 375 m, 475 m and 575 m.*

(a)

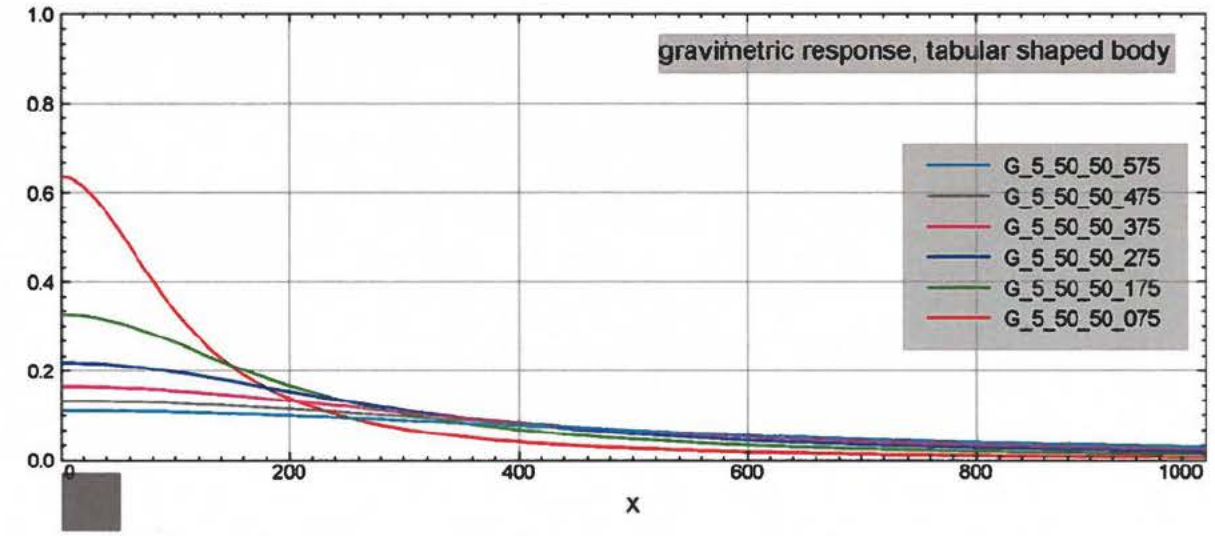

(b)

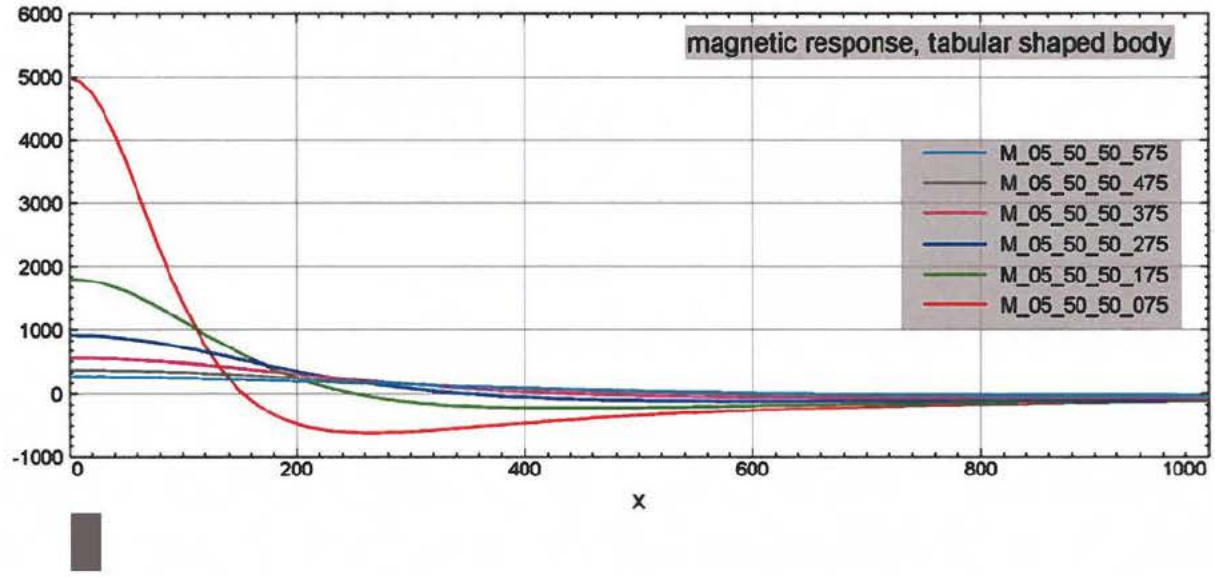

Figure A5. *(a) Gravimetric and (b) magnetic responses from a tabular body with a width of 50 m and thickness of 50 m. The top of the tabular body is 5 m below surface and responses are shown for altitudes of 75 m, 175 m, 275 m, 375 m, 475 m and 575 m.*

(a)

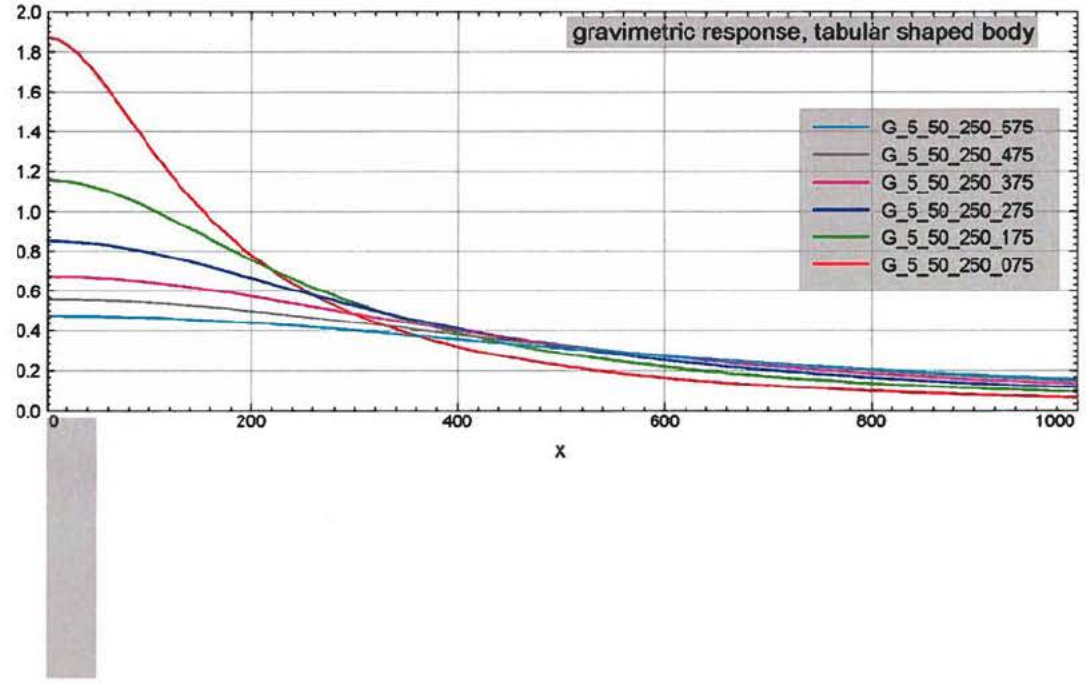

)

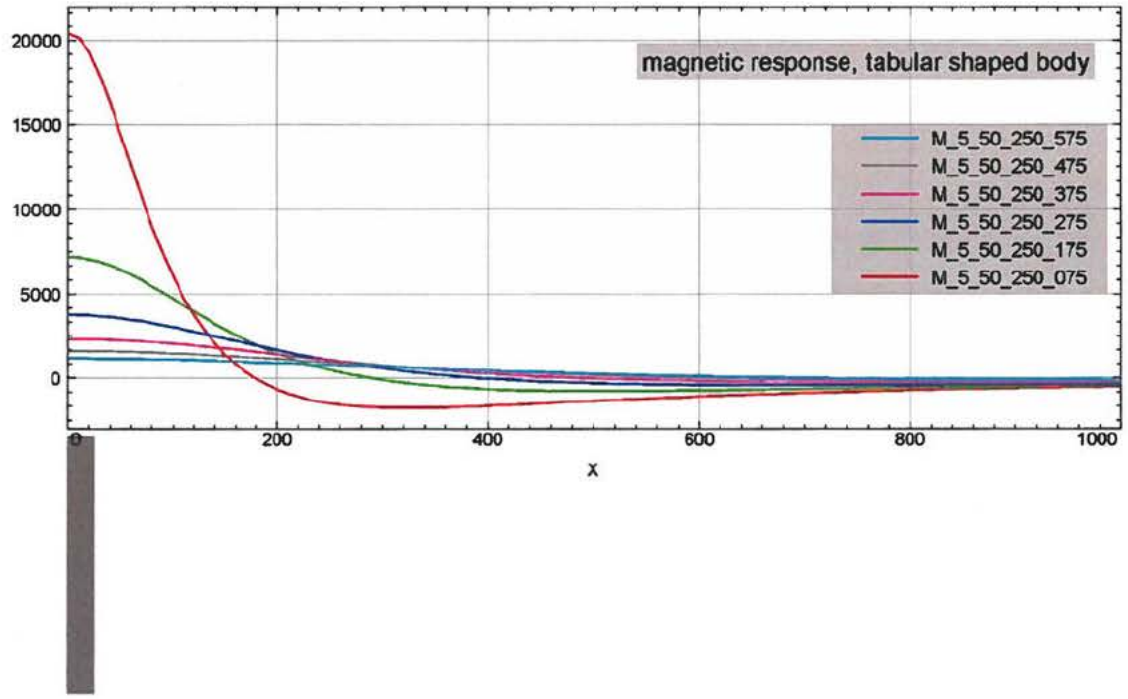

gure A6. *(a) Gravimetric and (b) magnetic responses from a tabular body with a width of 50 m and thickness of 50 m. The top of the tabular body is 5 m below surface and responses are shown for altitudes of 75 m, 175 m, 275 m, 375 m, 475 m and 575 m.*

(a)

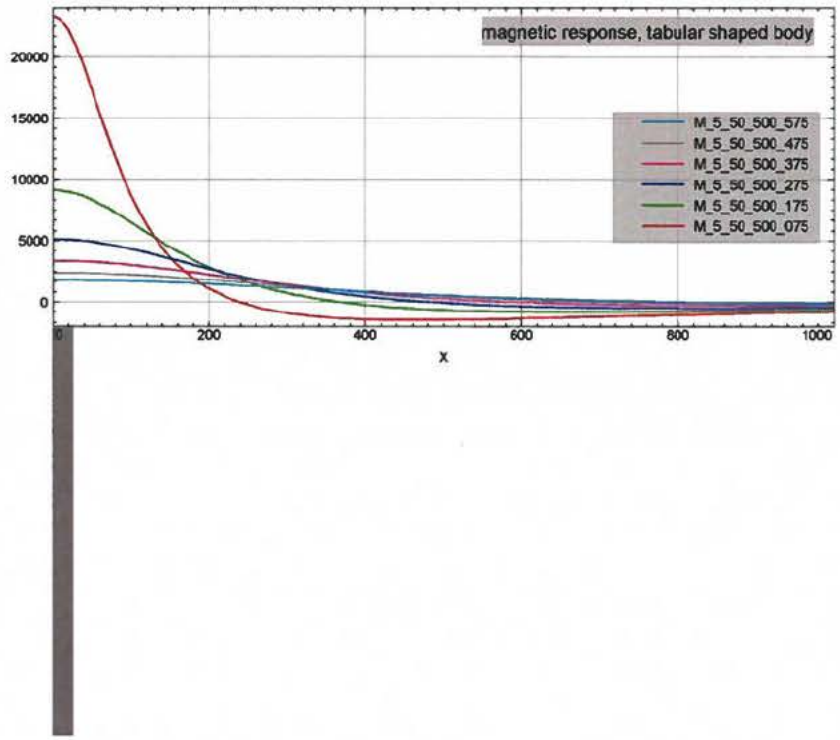

(b)

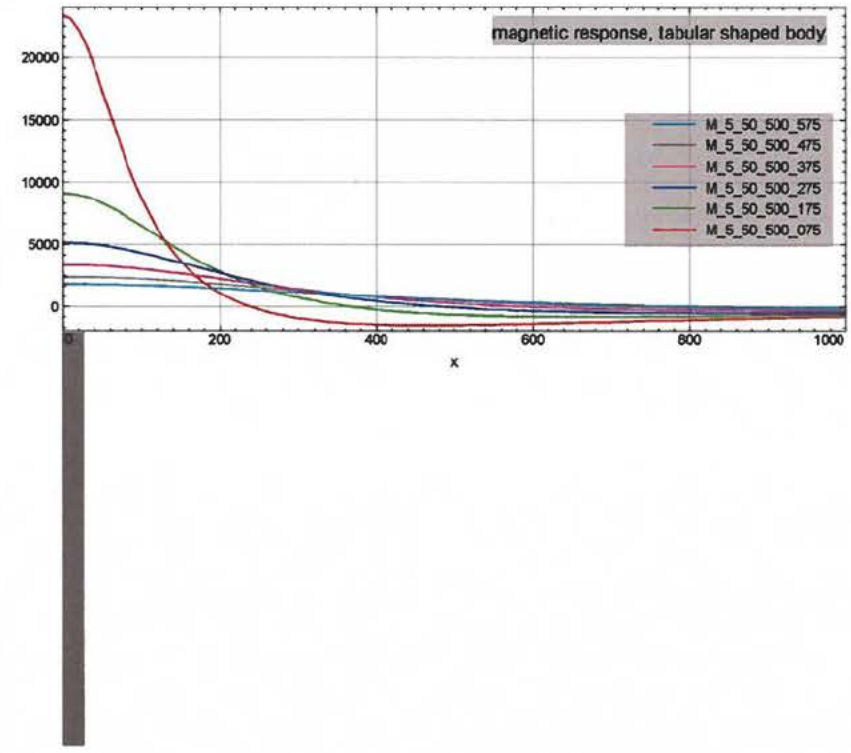

Figure A7. *(a) Gravimetric and (b) magnetic responses from a tabular body with a width of 50 m and thickness of 500 m. The top of the tabular body is 5 m below surface and responses are shown for altitudes of 75 m, 175 m, 275 m, 375 m, 475 m and 575 m.*

(a)

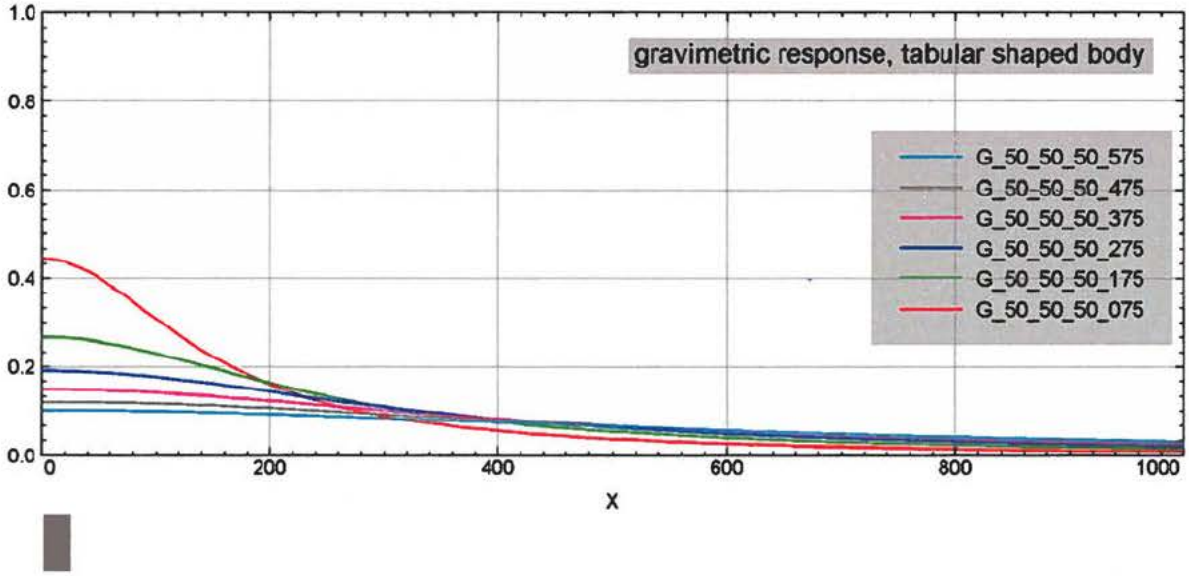

(b)

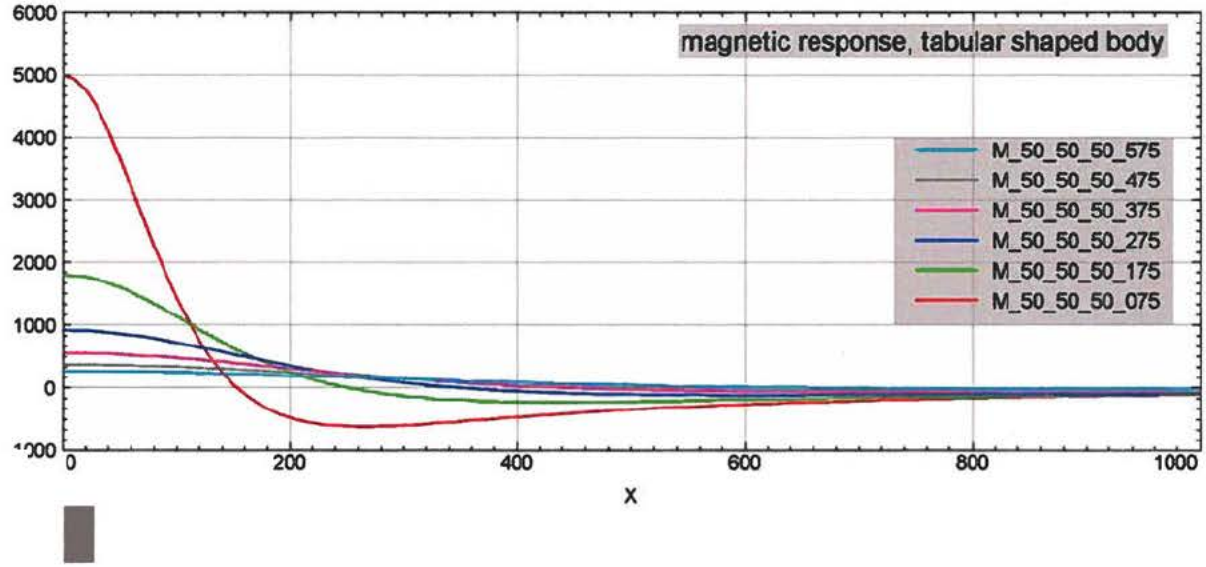

ıre A8. *(a) Gravimetric and (b) magnetic responses from a tabular body with a width of 50 m and thickness of ı. The top of the tabular body is 50 m below surface and responses are shown for altitudes of 75 m, 175 m, m, 375 m, 475 m and 575 m.*

(a)

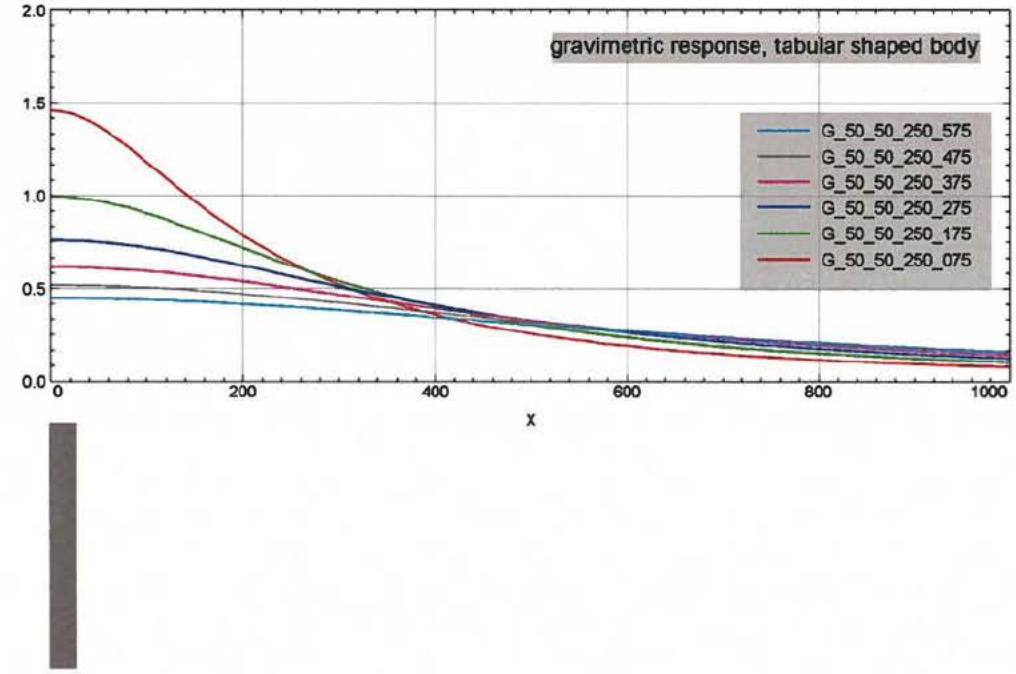

(b)

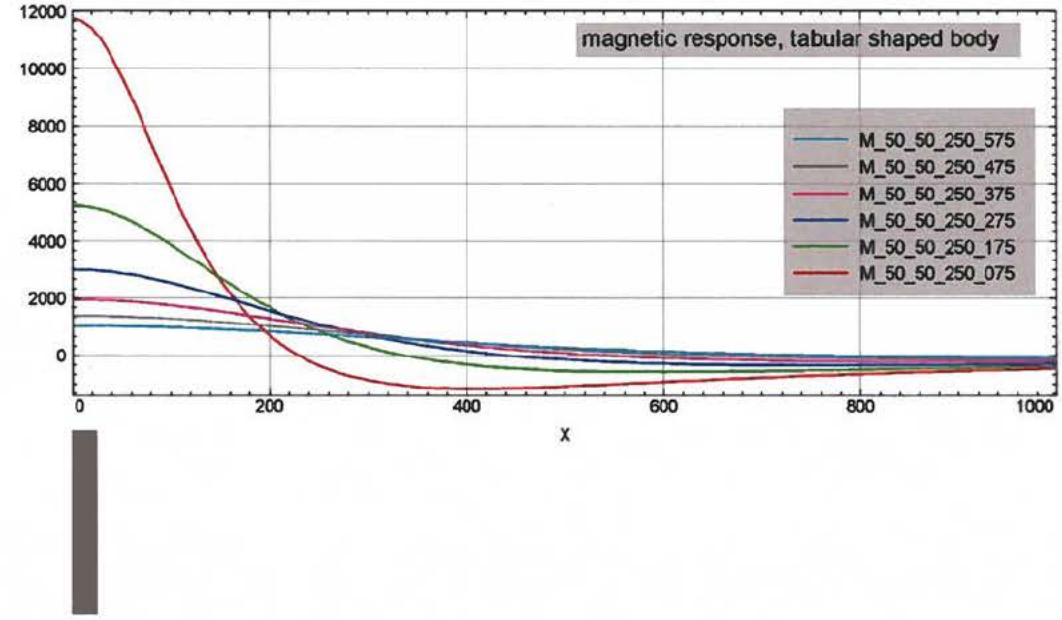

Figure A9. *(a) Gravimetric and (b) magnetic responses from a tabular body with a width of 50 m and thickness of 250 m. The top of the tabular body is 50 m below surface and responses are shown for altitudes of 75 m, 175 m, 275 m, 375 m, 475 m and 575 m.*

(a)

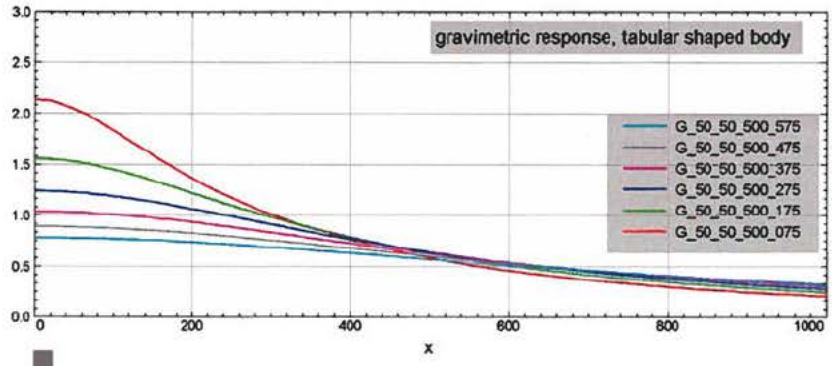

(b)

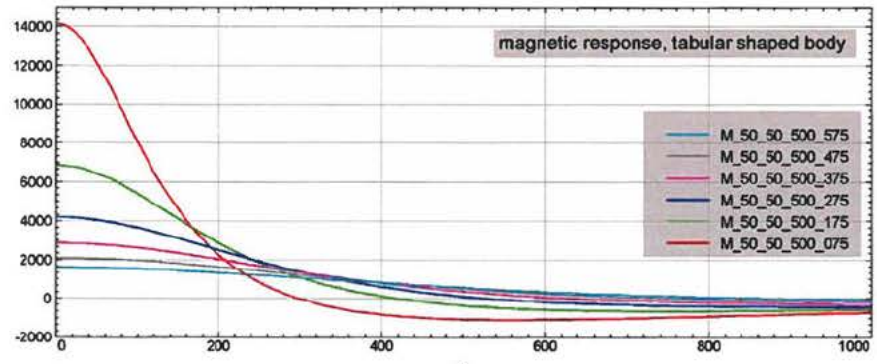

Figure A10. *(a) Gravimetric and (b) magnetic responses from a tabular body with a width of 50 m and thickness of 500 m. The top of the tabular body is 50 m below surface and responses are shown for altitudes of 75 m, 175 m, 275 m, 375 m, 475 m and 575 m.*

(a)

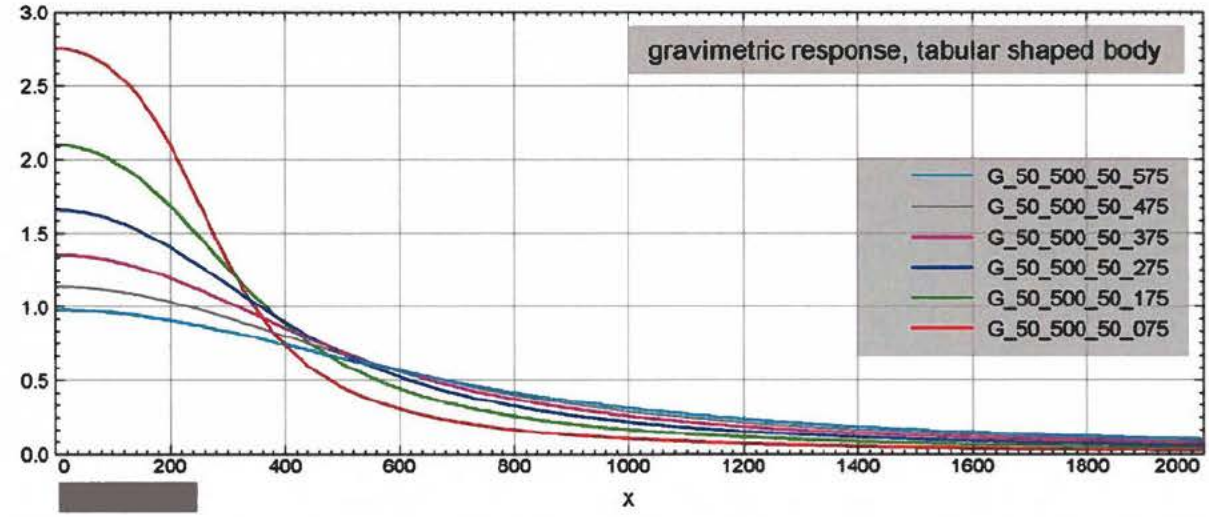

(b)

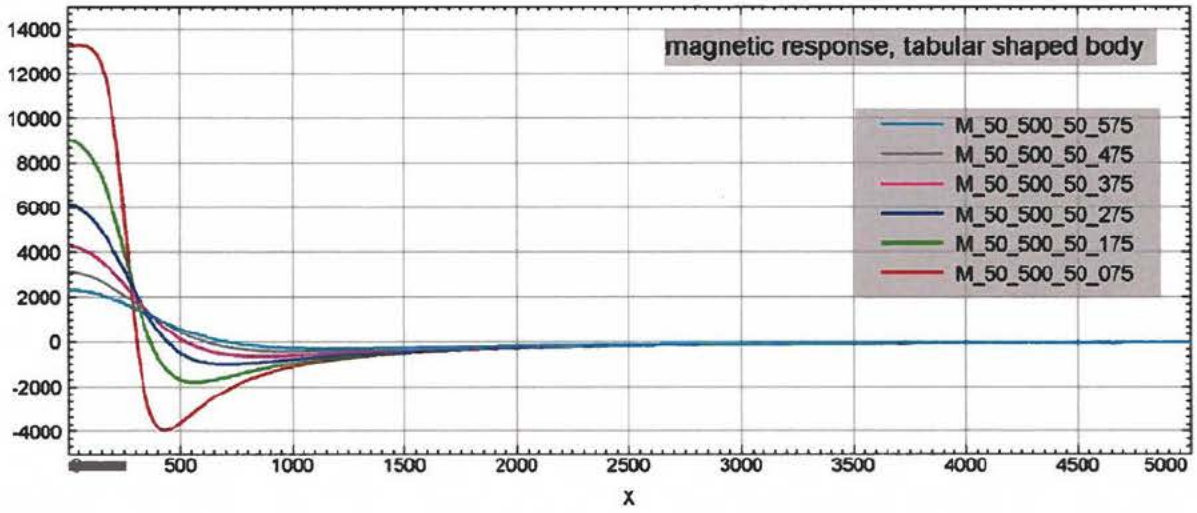

Figure A11. *(a) Gravimetric and (b) magnetic responses from a tabular body with a width of 500 m and thickness of 50 m. The top of the tabular body is 50 m below surface and responses are shown for altitudes of 75 m, 175 m, 275 m, 375 m, 475 m and 575 m.*

(a)

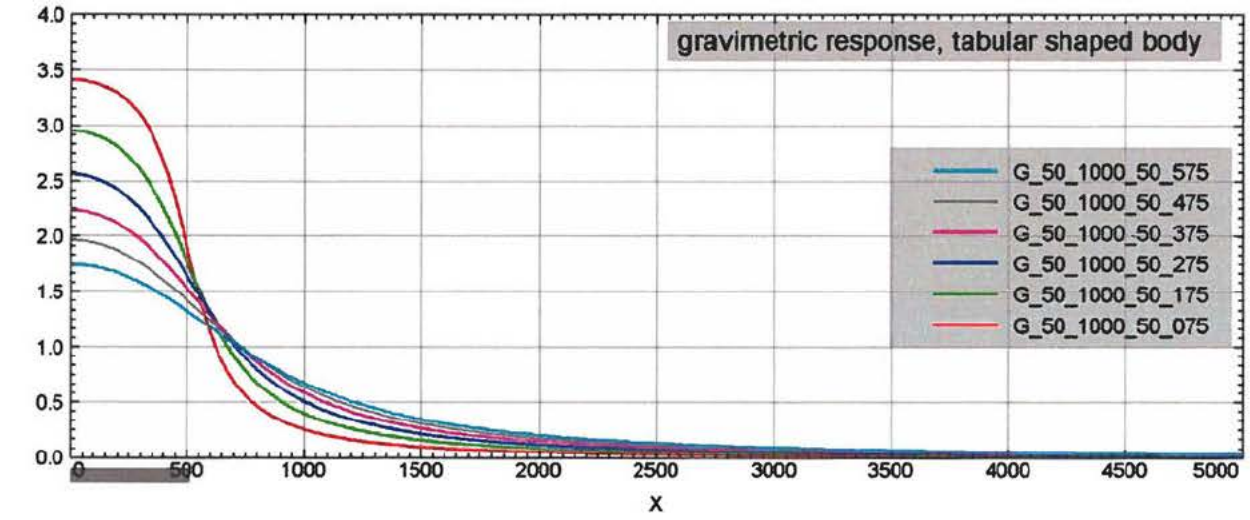

(b)

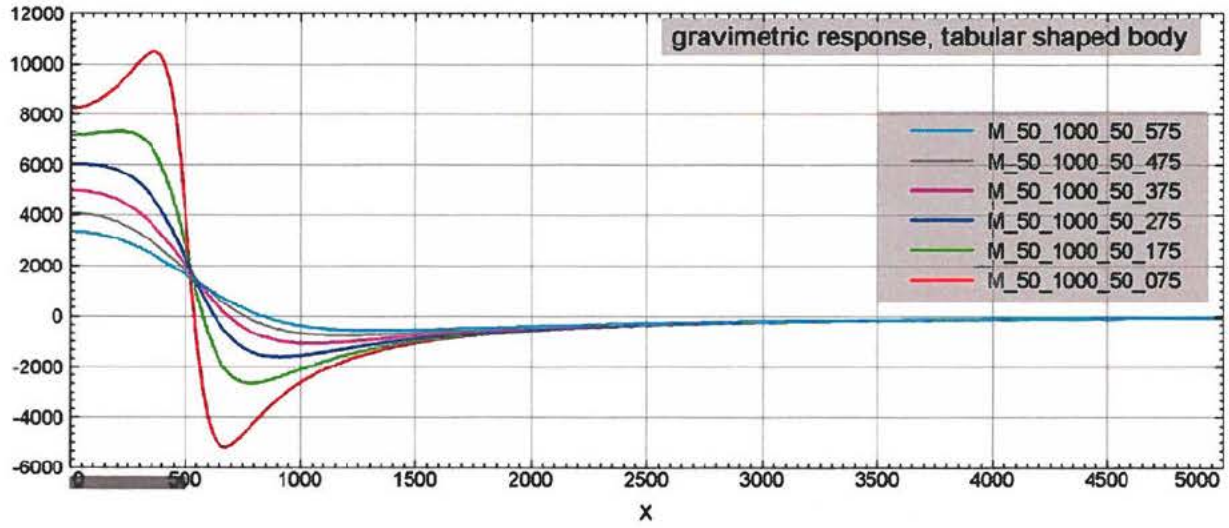

Figure A12. *(a) Gravimetric and (b) magnetic responses from a tabular body with a width of 1000 m and thickness of 50 m. The top of the tabular body is 50 m below surface and responses are shown for altitudes of 75 m, 175 m, 275 m, 375 m, 475 m and 575 m.*

(a)

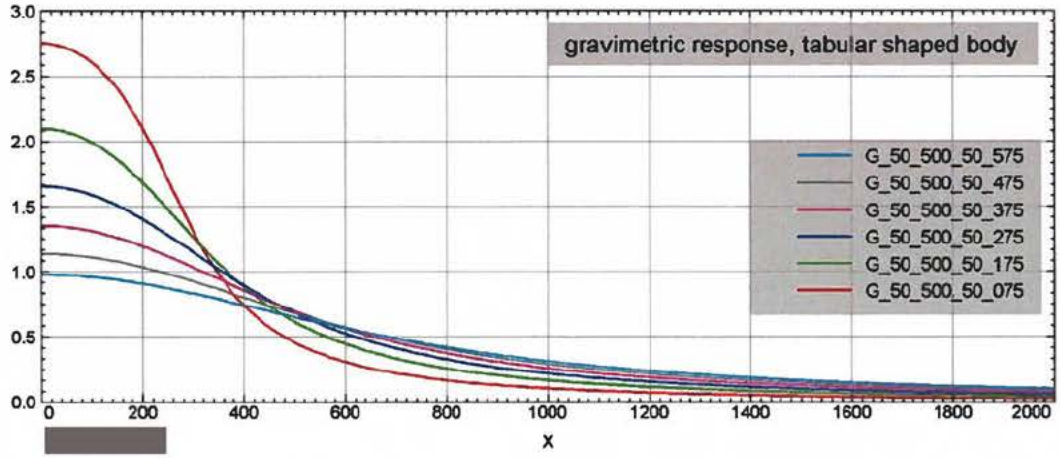

(b)

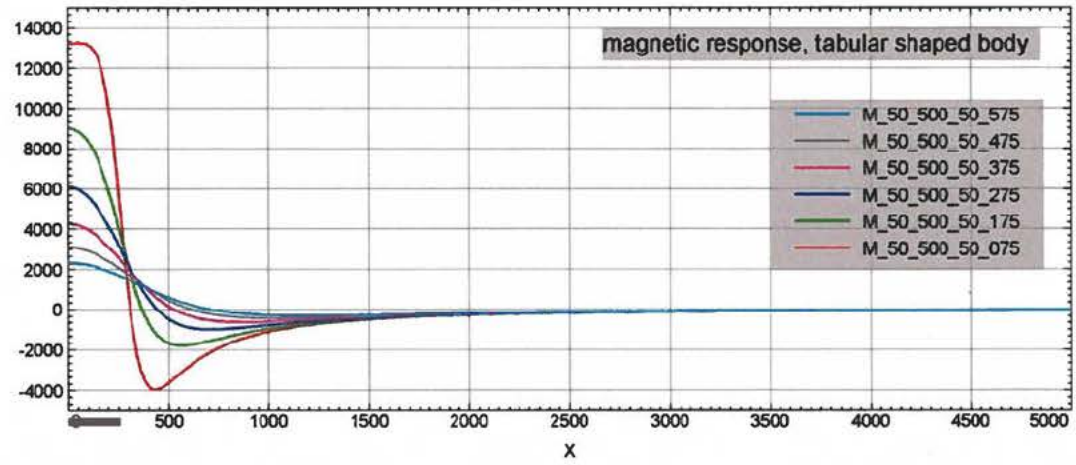

Figure A13. *(a) Gravimetric and (b) magnetic responses from a tabular body with a width of 500 m and thickness of 50 m. The top of the tabular body is 50 m below surface and responses are shown for altitudes of 75 m, 175 m, 275 m, 375 m, 475 m and 575 m.*

(a)

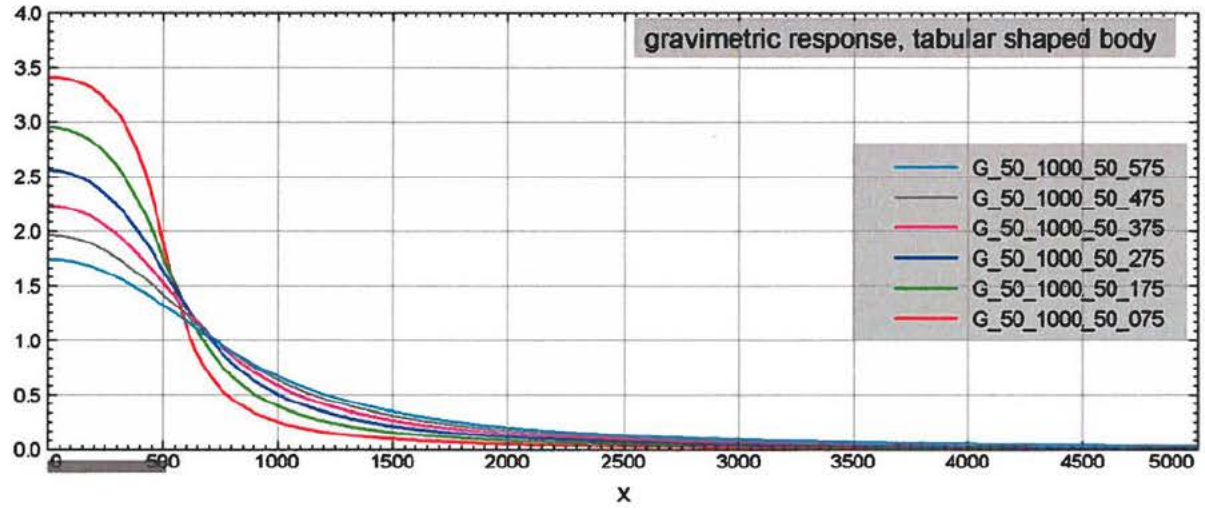

(b)

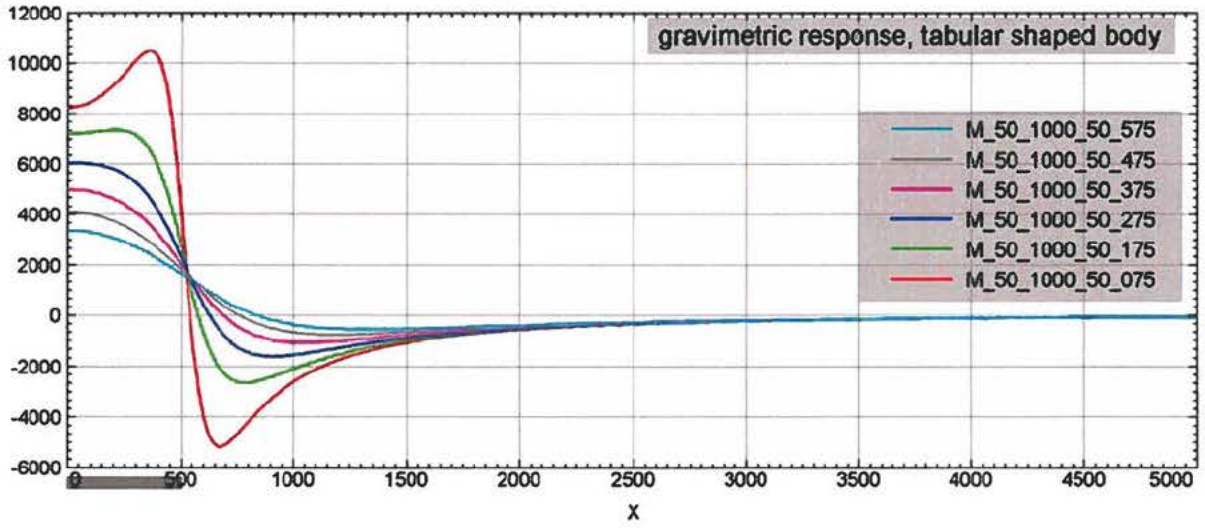

Figure A14. *(a) Gravimetric and (b) magnetic responses from a tabular body with a width of 1000 m and thickness of 50 m. The top of the tabular body is 50 m below surface and responses are shown for altitudes of 75 m, 175 m, 275 m, 375 m, 475 m and 575 m.*

(a)

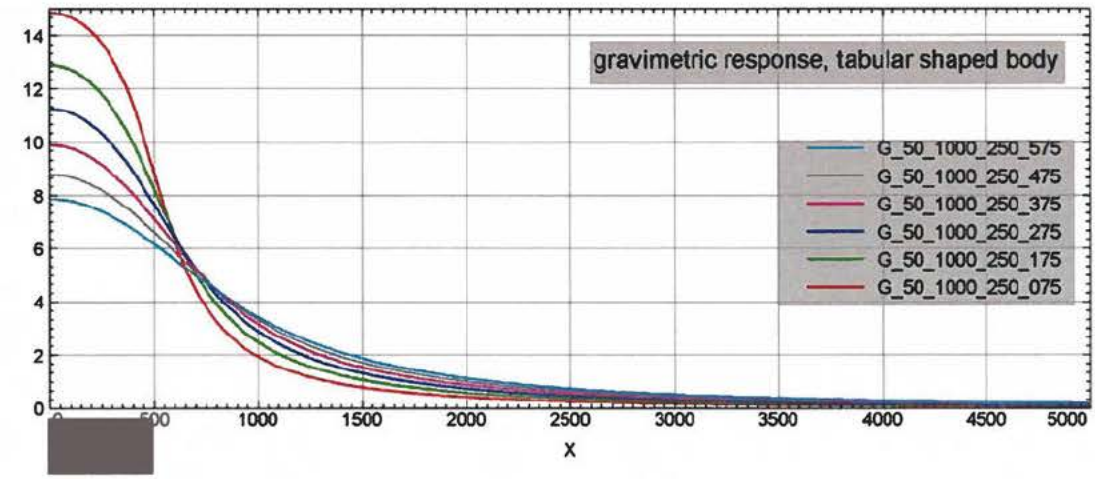

(b)

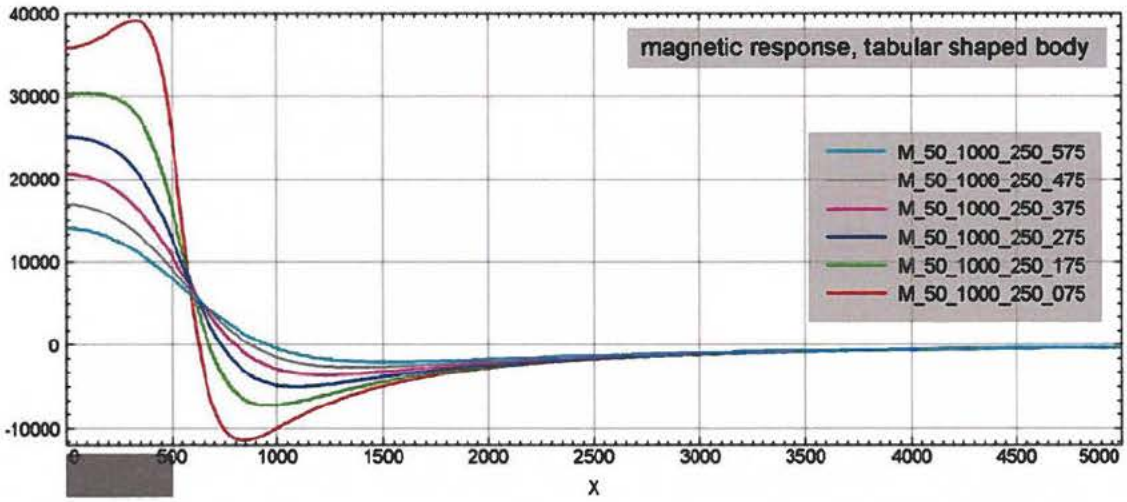

Figure A15. *(a) Gravimetric and (b) magnetic responses from a tabular body with a width of 1000 m and thickness of 250 m. The top of the tabular body is 50 m below surface and responses are shown for altitudes of 75 m, 175 m, 275 m, 375 m, 475 m and 575 m.*

(a)

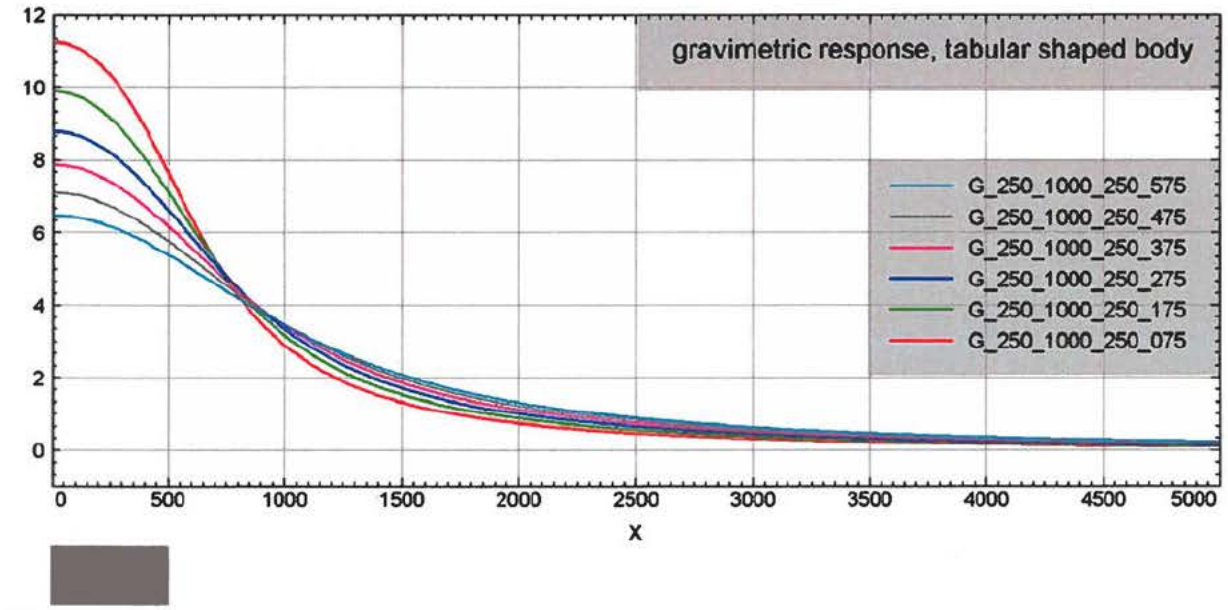

(b)

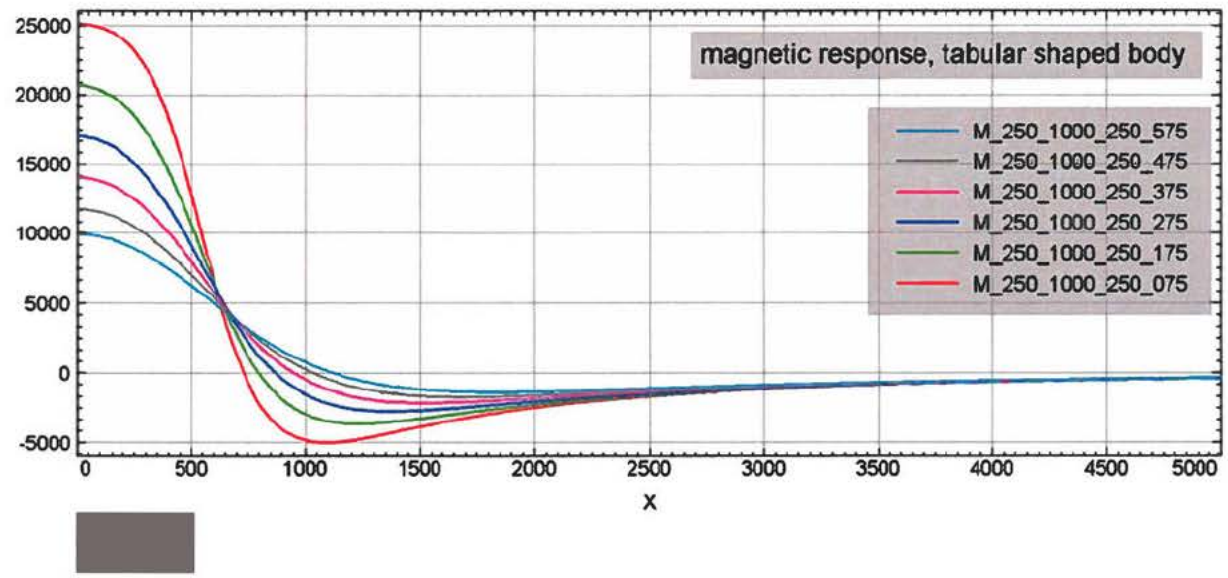

Figure A16. *(a) Gravimetric and (b) magnetic responses from a tabular body with a width of 1000 m and thickness of 250 m. The top of the tabular body is 250 m below surface and responses are shown for altitudes of 75 m, 175 m, 275 m, 375 m, 475 m and 575 m.*

(a)

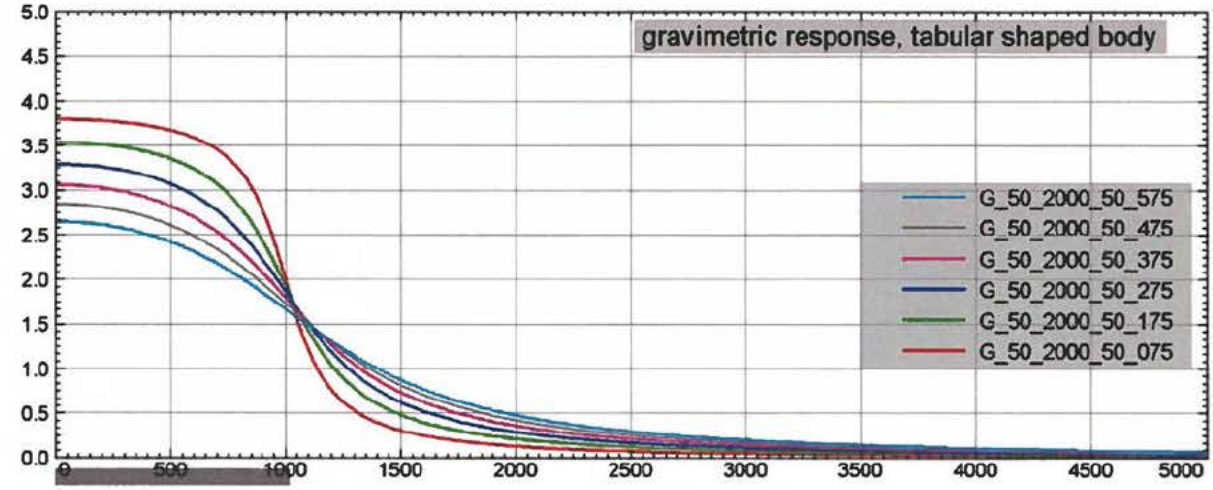

(b)

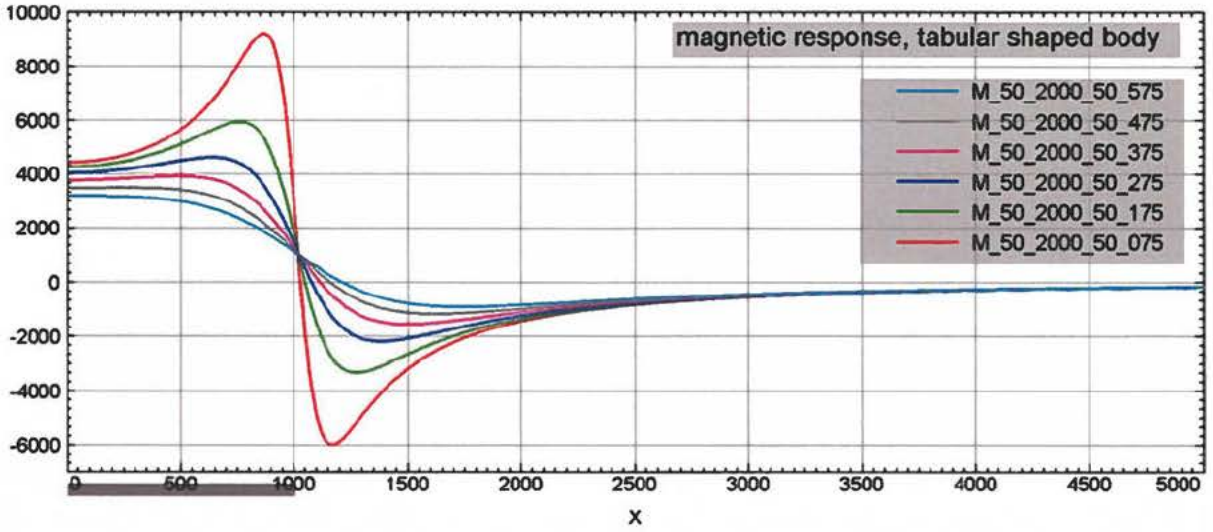

Figure A17. *(a) Gravimetric and (b) magnetic responses from a tabular body with a width of 2000 m and thickness of 50 m. The top of the tabular body is 50 m below surface and responses are shown for altitudes of 75 m, 175 m, 275 m, 375 m, 475 m and 575 m.*

(a)

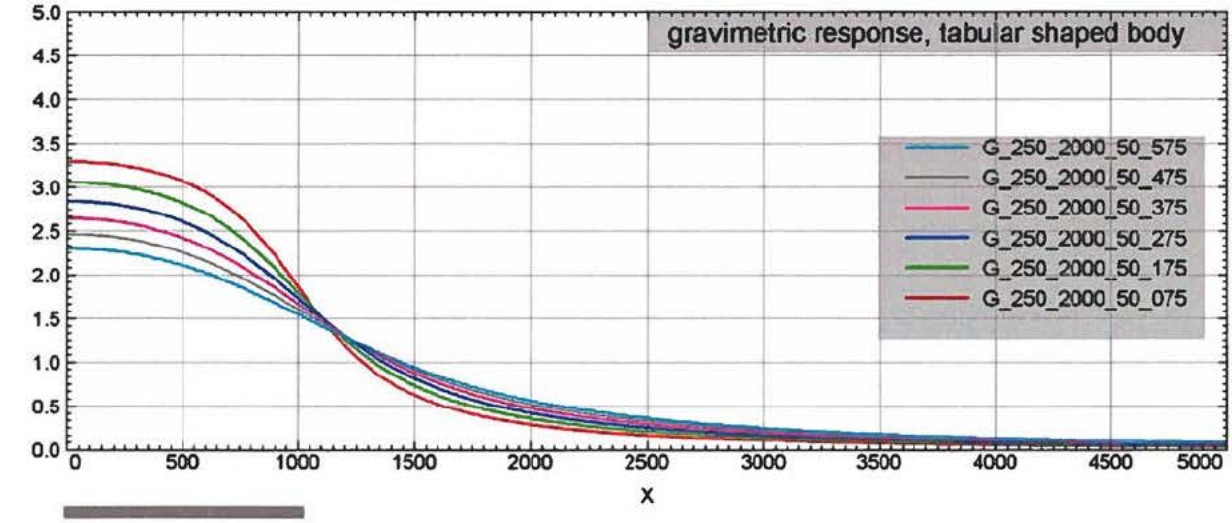

(b)

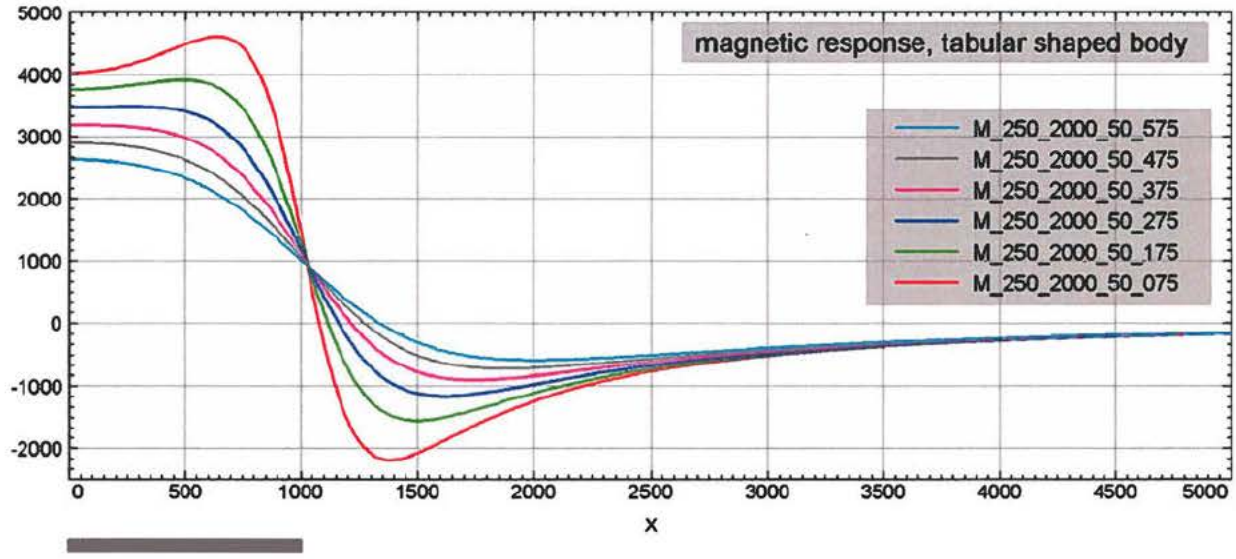

Figure A18. *(a) Gravimetric and (b) magnetic responses from a tabular body with a width of 2000 m and thickness of 50 m. The top of the tabular body is 250 m below surface and responses are shown for altitudes of 75 m, 175 m, 275 m, 375 m, 475 m and 575 m.*

(a)

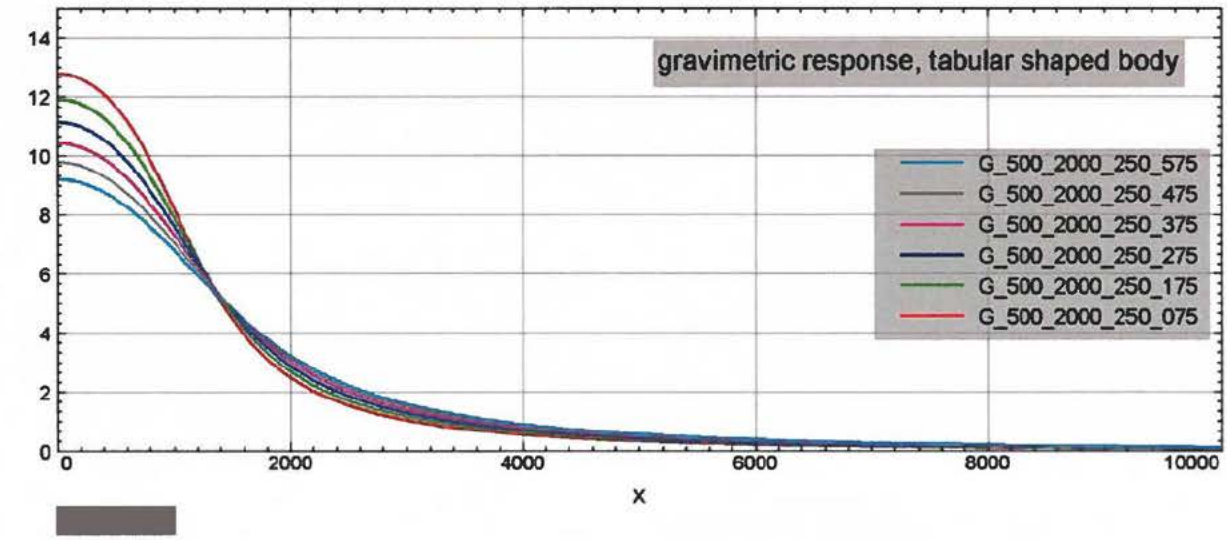

(b)

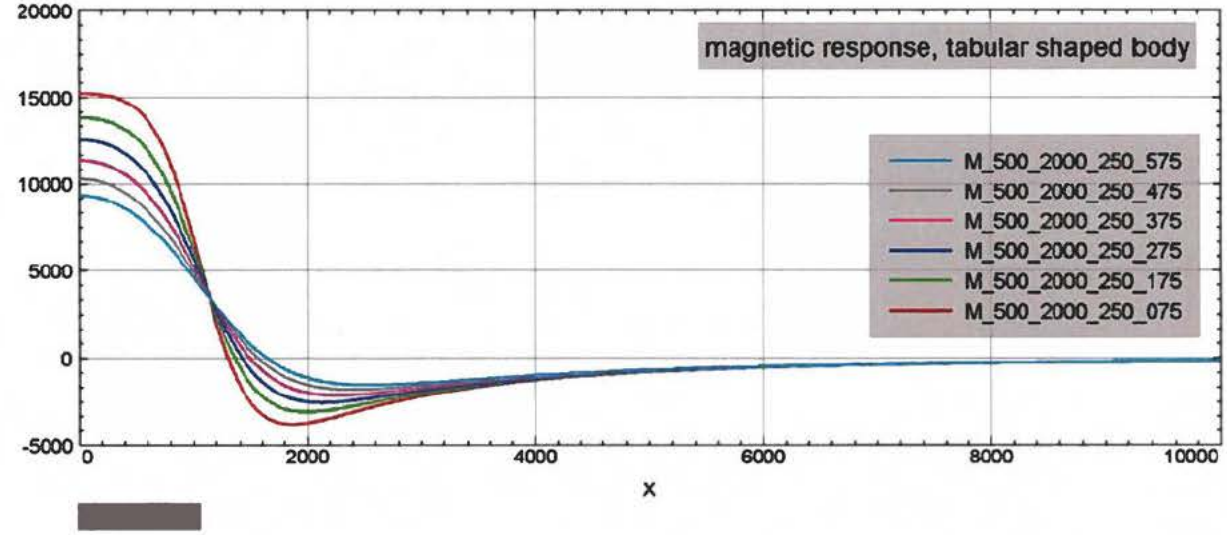

Figure A19. *(a) Gravimetric and (b) magnetic responses from a tabular body with a width of 2000 m and thickness of 250 m. The top of the tabular body is 500 m below surface and responses are shown for altitudes of 75 m, 175 m, 275 m, 375 m, 475 m and 575 m.*

17. Appendix B – Catalogue of synthetic response from disc shaped bodies

Gravimetric and magnetic responses are presented for some disc shaped bodies as outlined schematically in Figure B1 and summarised in Table B1. Responses are calculated for various values of radius r, thickness d_z.and depth h to the top. The responses are calculated at altitudes of 75 m, 175 m, 275 m, 375 m, 475 m and 575 m above ground along profile direction X. For symmetry reasons only data for X>0 are shown. The density contrast is 2 g/cm^3 and the magnetic susceptibility is 10 SI.

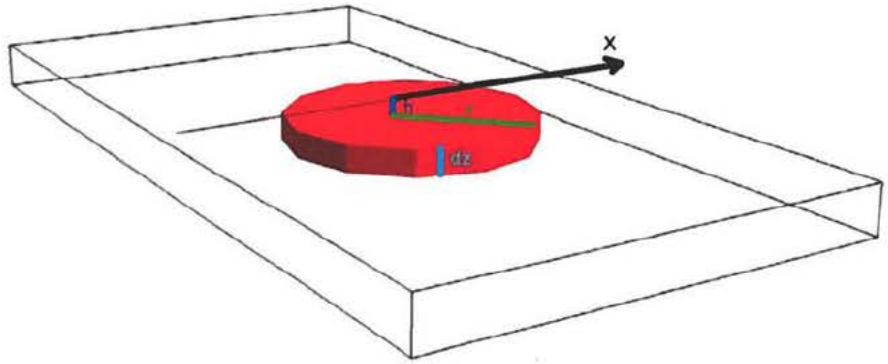

Figure B1. *General outline of shape of disc shaped body used for model calculations.*

Table 9. . *Figure numbers and corresponding parameter values for width dx, thickness dz.and depth h*

Figure no.	Radius r [m]	Thickness d_z [m]	Depth h [m]
B2	500	5	5
B3	500	50	5
B4	500	50	50
B5	1000	5	5
B6	1000	50	5
B7	1000	50	50
B8	2000	5	5
B9	2000	50	5
B10	2000	50	50
B11	4000	5	5
B12	4000	50	5
B13	4000	50	50
B14	8000	5	5
B15	8000	50	5
B16	8000	50	50
B17	16000	5	5
B18	16000	50	5
B19	16000	50	50

(a)

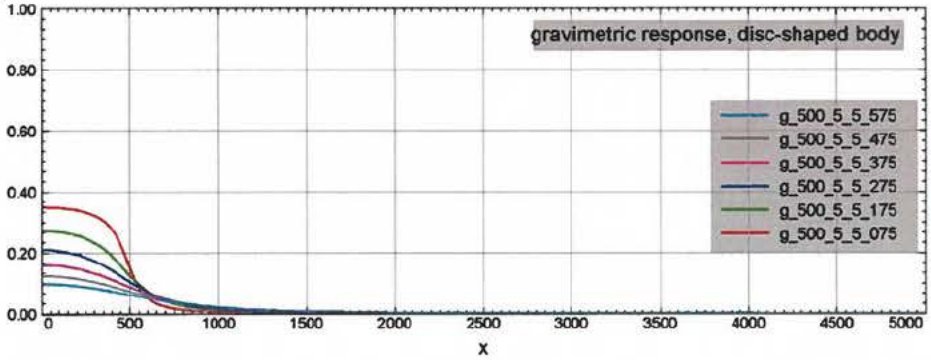

(b)

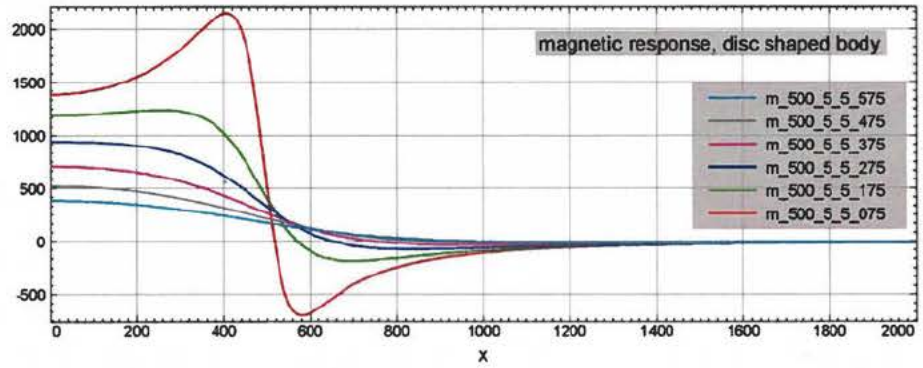

Figure B2. *(a) Gravimetric and (b) magnetic responses from a disc shaped body centred at X=0 m with a radius of 500 m and thickness of 5 m. The top of the disc shaped body is 5 m below surface and responses are shown for altitudes of 75 m, 175 m, 275 m, 375 m, 475 m and 575 m.*

(a)

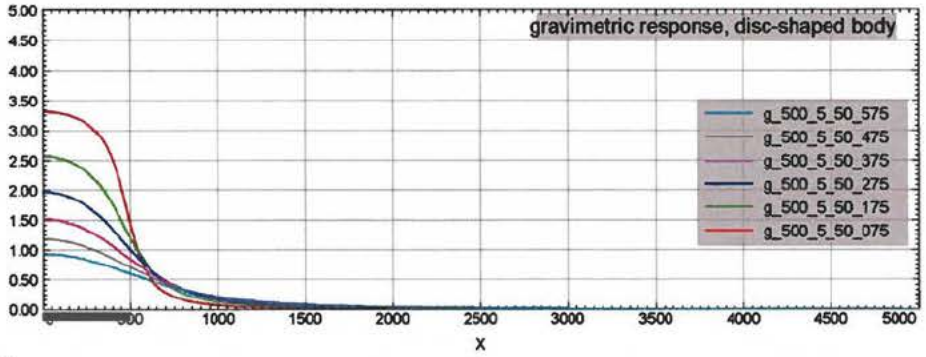

(b)

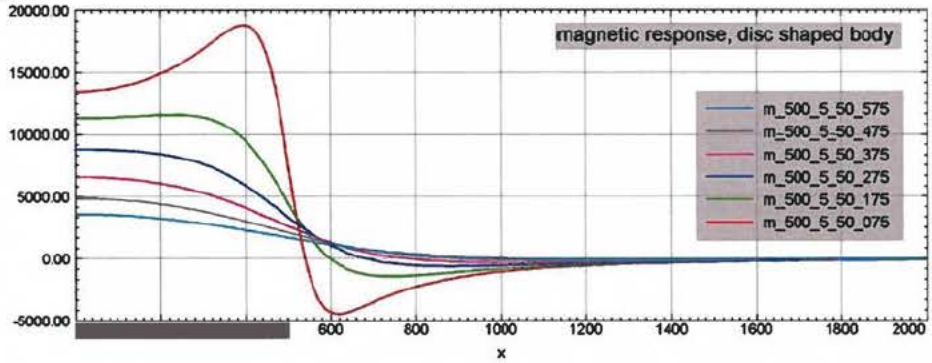

Figure B3. *(a) Gravimetric and (b) magnetic responses from a disc shaped body centred at X=0 m with a radius of 500 m and thickness of 50 m. The top of the disc shaped body is 5 m below surface and responses are shown for altitudes of 75 m, 175 m, 275 m, 375 m, 475 m and 575 m.*

(a)

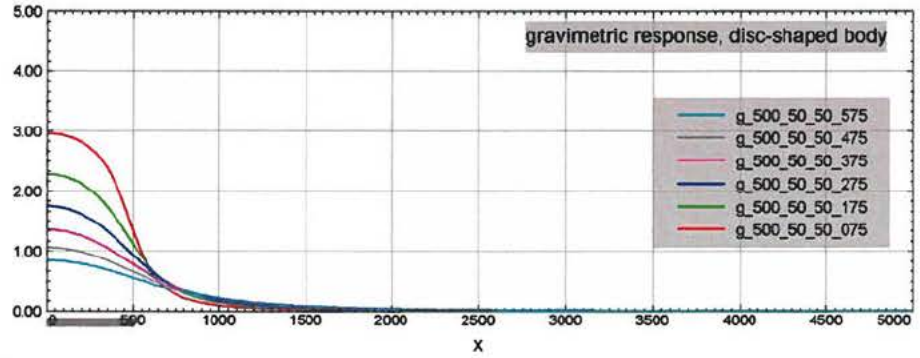

(b)

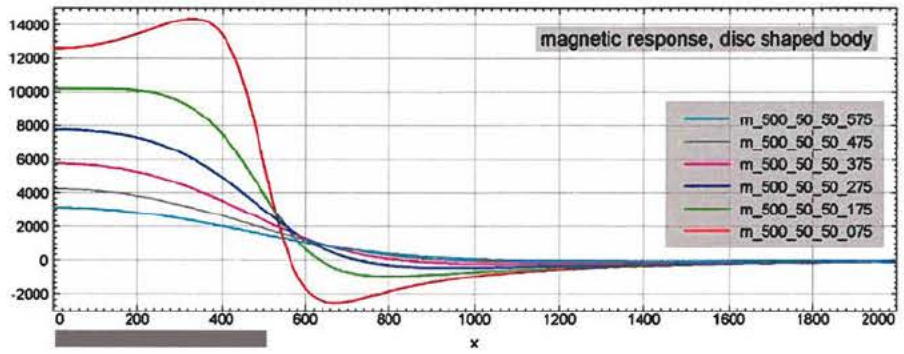

Figure B4. *(a) Gravimetric and (b) magnetic responses from a disc shaped body centred at X=0 m with a radius of 500 m and thickness of 50 m. The top of the disc shaped body is 50 m below surface and responses are shown for altitudes of 75 m, 175 m, 275 m, 375 m, 475 m and 575 m.*

(a)

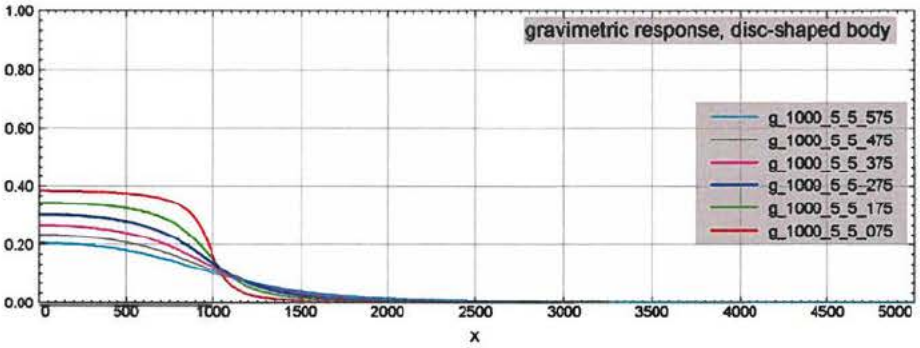

(b)

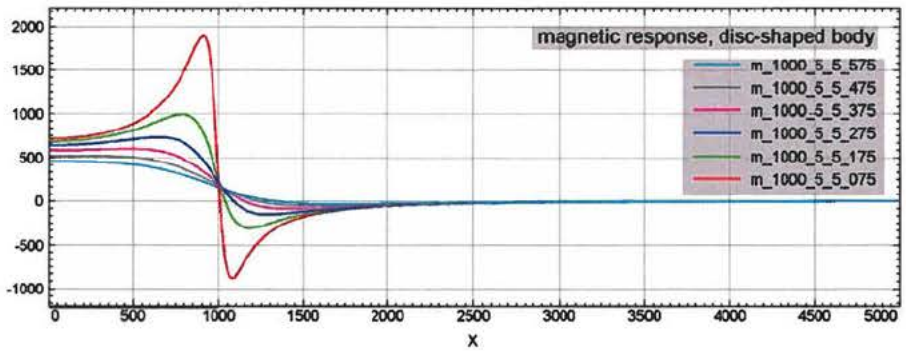

Figure B5. *(a) Gravimetric and (b) magnetic responses from a disc shaped body centred at X=0 m with a radius of 1000 m and thickness of 5 m. The top of the disc shaped body is 5 m below surface and responses are shown for altitudes of 75 m, 175 m, 275 m, 375 m, 475 m and 575 m.*

(a)

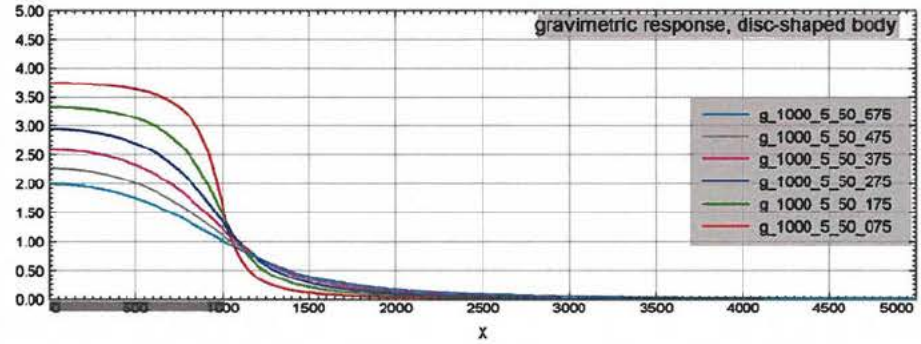

(b)

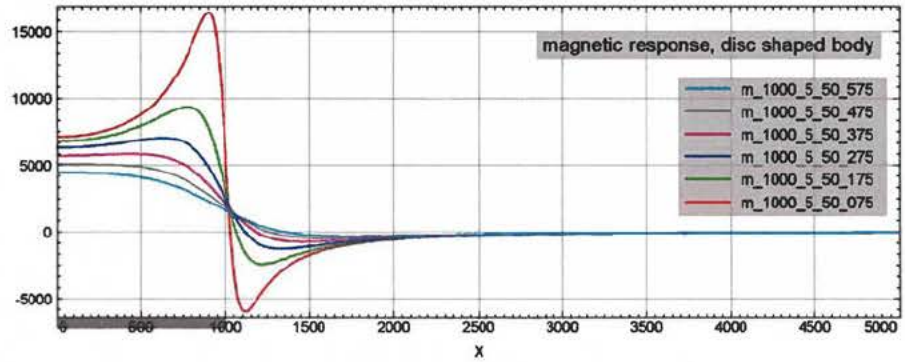

Figure B6. *(a) Gravimetric and (b) magnetic responses from a disc shaped body centred at X=0 m with a radius of 1000 m and thickness of 50 m. The top of the disc shaped body is 5 m below surface and responses are shown for altitudes of 75 m, 175 m, 275 m, 375 m, 475 m and 575 m*

(a)

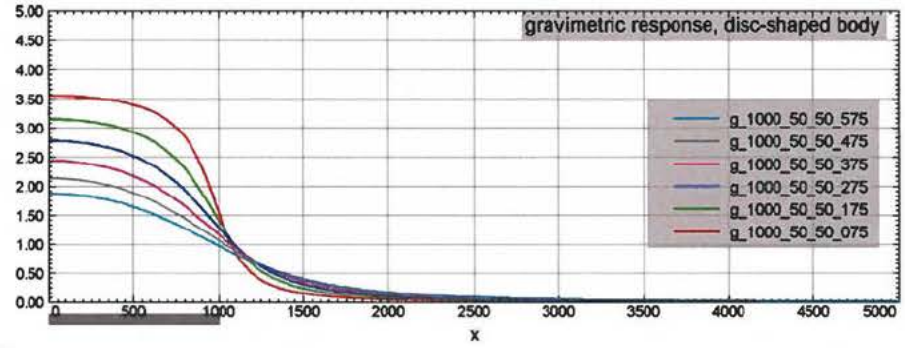

(b)

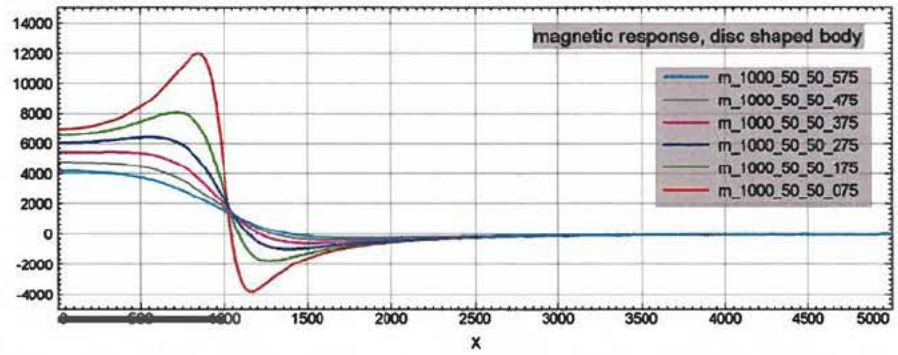

Figure B7. *(a) Gravimetric and (b) magnetic responses from a disc shaped body centred at X=0 m with a radius of 1000 m and thickness of 50 m. The top of the disc shaped body is 50 m below surface and responses are shown for altitudes of 75 m, 175 m, 275 m, 375 m, 475 m and 575 m.*

(a)

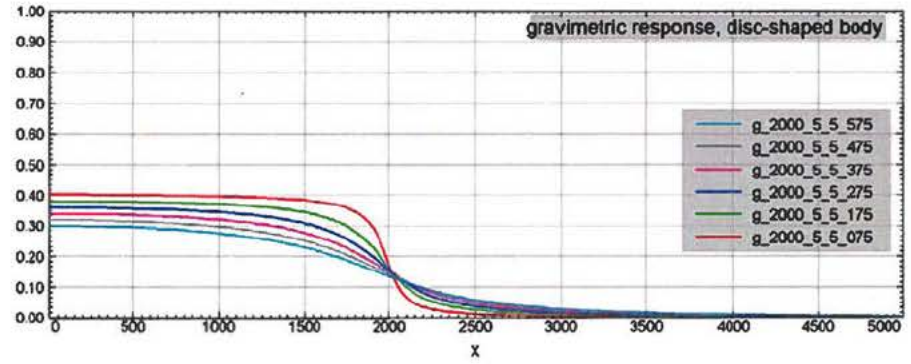

(b)

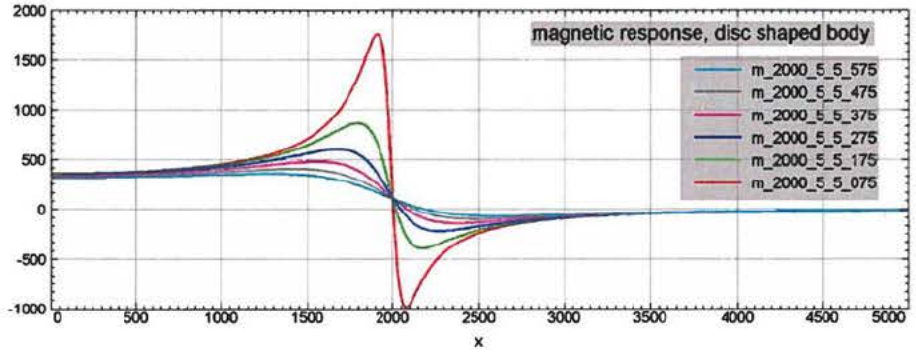

Figure B8. *(a) Gravimetric and (b) magnetic responses from a disc shaped body centred at X=0 m with a radius of 2000 m and thickness of 5 m. The top of the disc shaped body is 5 m below surface and responses are shown for altitudes of 75 m, 175 m, 275 m, 375 m, 475 m and 575 m.*

(a)

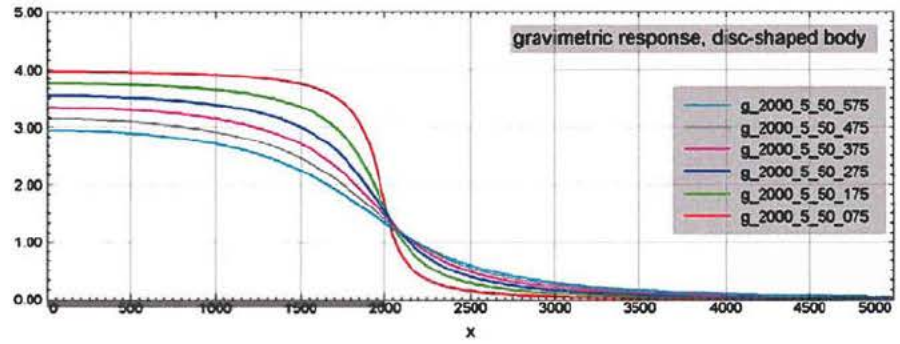

(b)

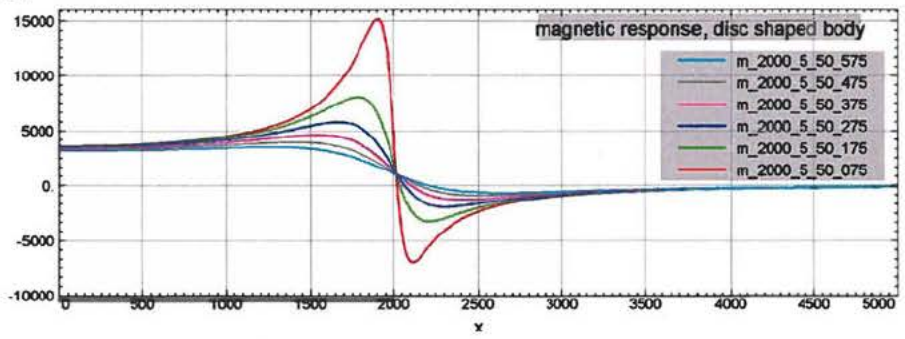

Figure B9. *(a) Gravimetric and (b) magnetic responses from a disc shaped body centred at X=0 m with a radius of 20000 m and thickness of 50 m. The top of the disc shaped body is 5 m below surface and responses are shown for altitudes of 75 m, 175 m, 275 m, 375 m, 475 m and 575 m.*

(a)

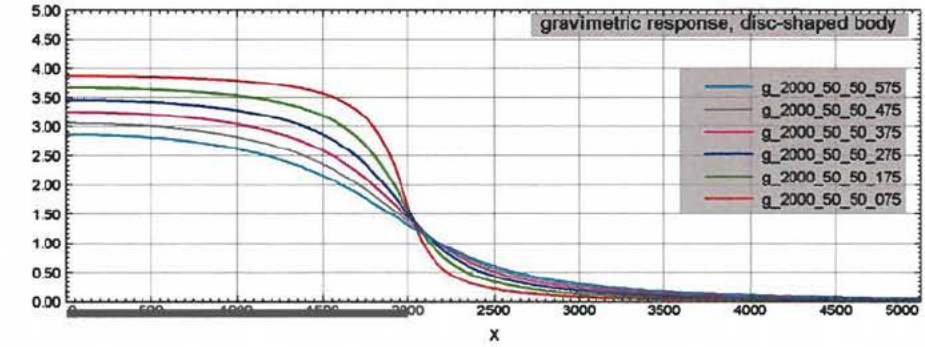

(b)

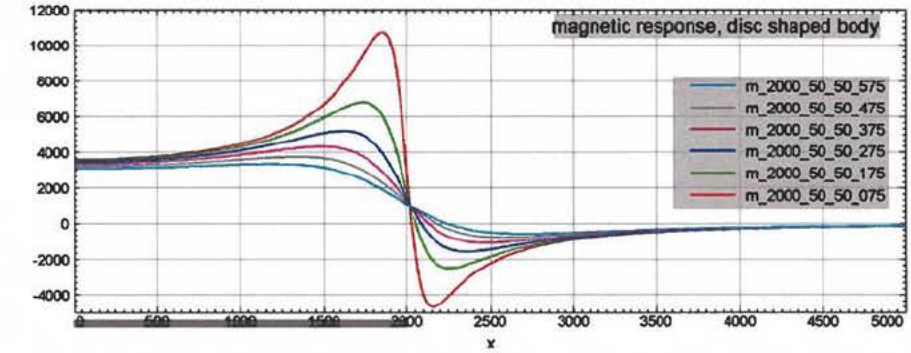

Figure B10. *(a) Gravimetric and (b) magnetic responses from a disc shaped body centred at X=0 m with a radius of 2000 m and thickness of 50 m. The top of the disc shaped body is 50 m below surface and responses are shown for altitudes of 75 m, 175 m, 275 m, 375 m, 475 m and 575 m.*

(a)

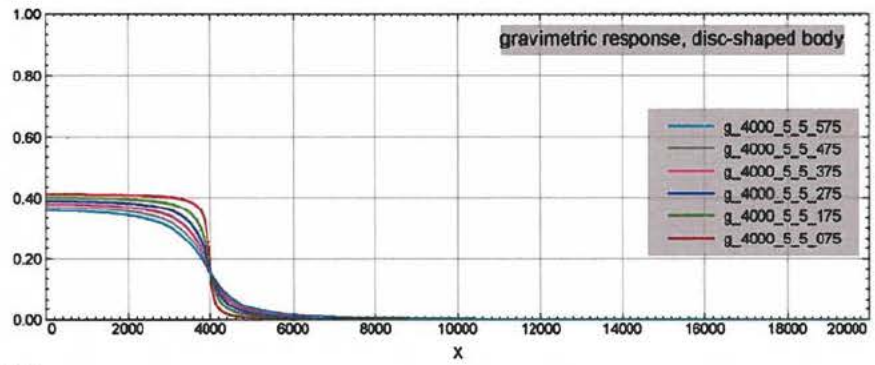

(b)

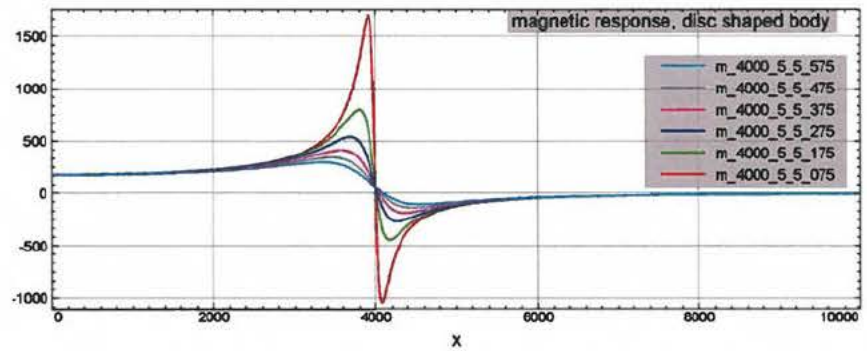

Figure B11. *(a) Gravimetric and (b) magnetic responses from a disc shaped body centred at X=0 m with a radius of 500 m and thickness of 5 m. The top of the disc shaped body is 5 m below surface and responses are shown for altitudes of 75 m, 175 m, 275 m, 375 m, 475 m and 575 m.*

(a)

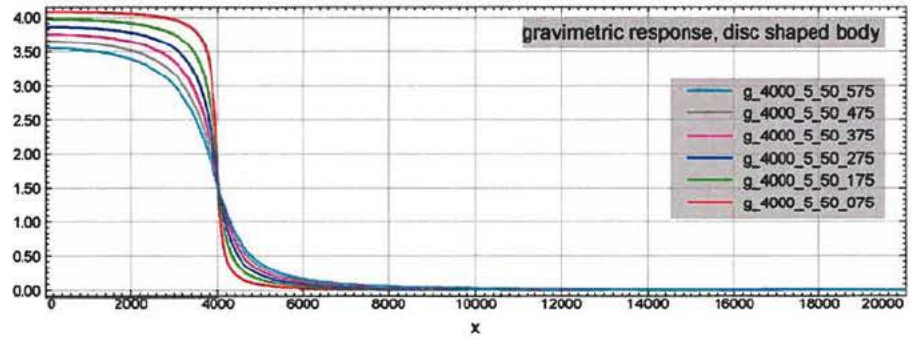

(a)

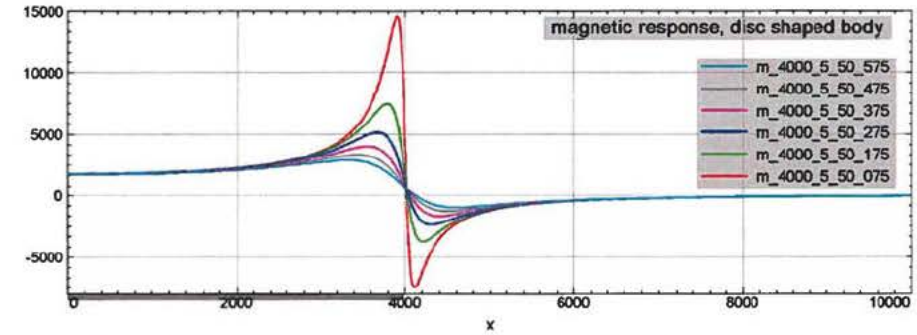

Figure B12. *(a) Gravimetric and (b) magnetic responses from a disc shaped body centred at X=0 m with a radius of 500 m and thickness of 50 m. The top of the disc shaped body is 5 m below surface and responses are shown for altitudes of 75 m, 175 m, 275 m, 375 m, 475 m and 575 m.*

(a)

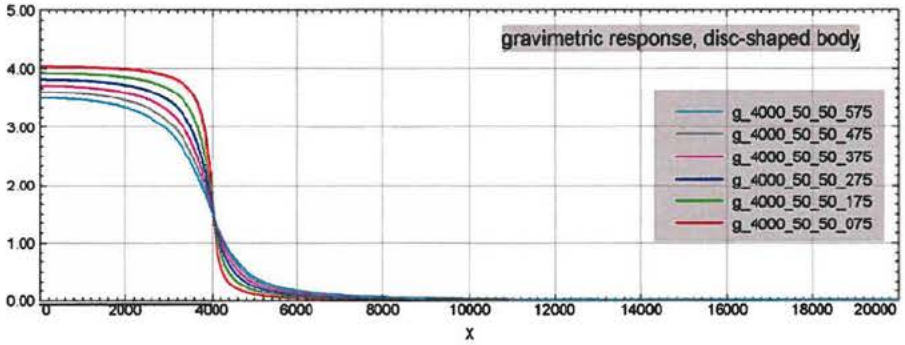

(b)

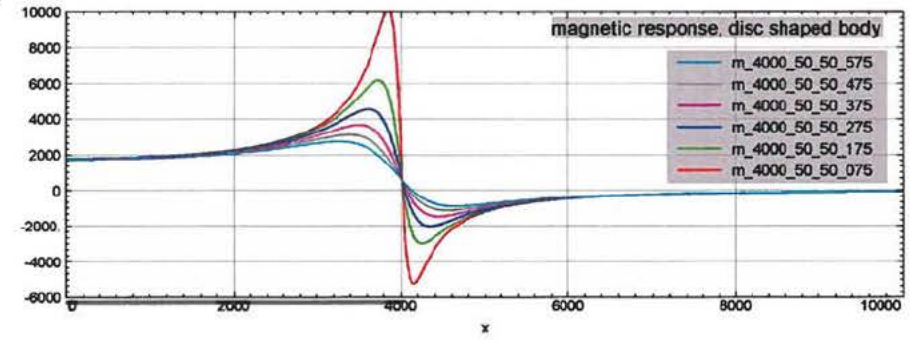

Figure B13. *(a) Gravimetric and (b) magnetic responses from a disc shaped body centred at X=0 m with a radius of 4000 m and thickness of 50 m. The top of the disc shaped body is 50 m below surface and responses are shown for altitudes of 75 m, 175 m, 275 m, 375 m, 475 m and 575 m.*

(a)

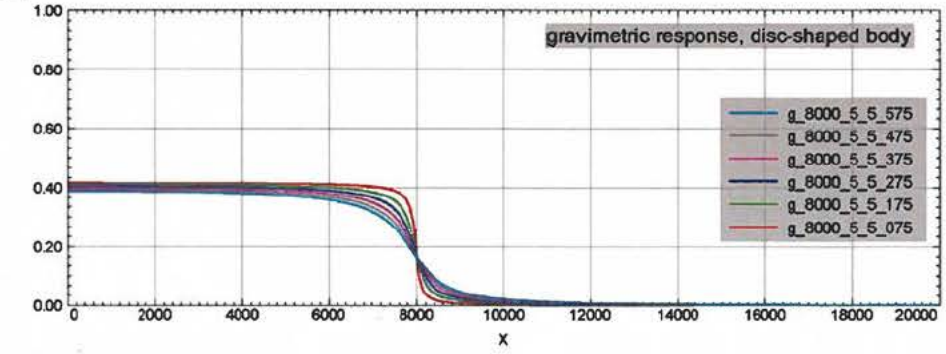

(b)

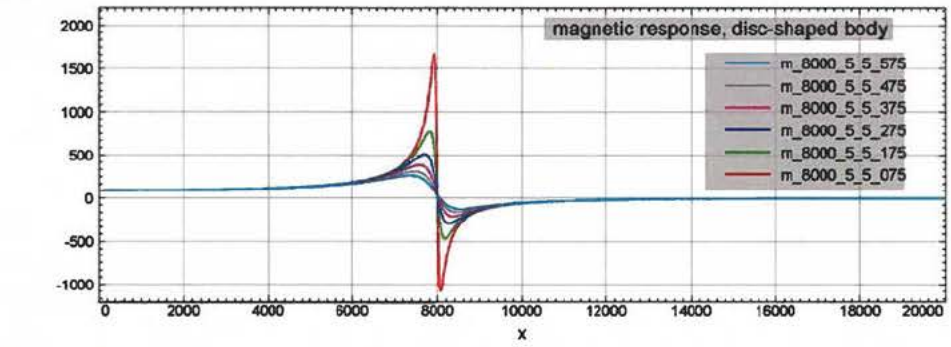

Figure B14. *(a) Gravimetric and (b) magnetic responses from a disc shaped body centred at X=0 m with a radius of 8000 m and thickness of 5 m. The top of the disc shaped body is 5 m below surface and responses are shown for altitudes of 75 m, 175 m, 275 m, 375 m, 475 m and 575 m.*

(a)

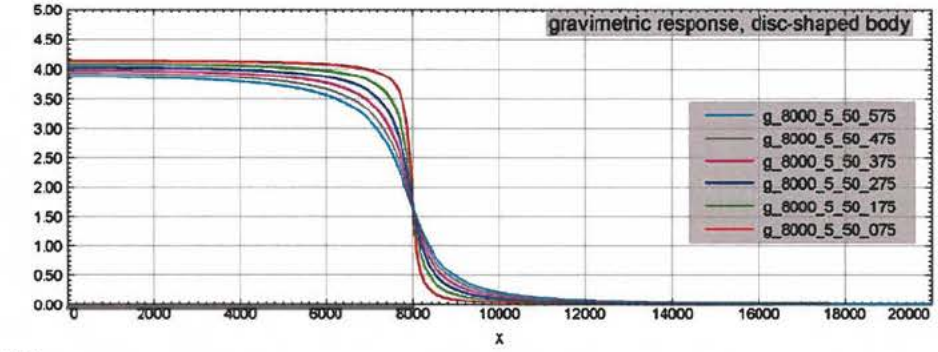

(b)

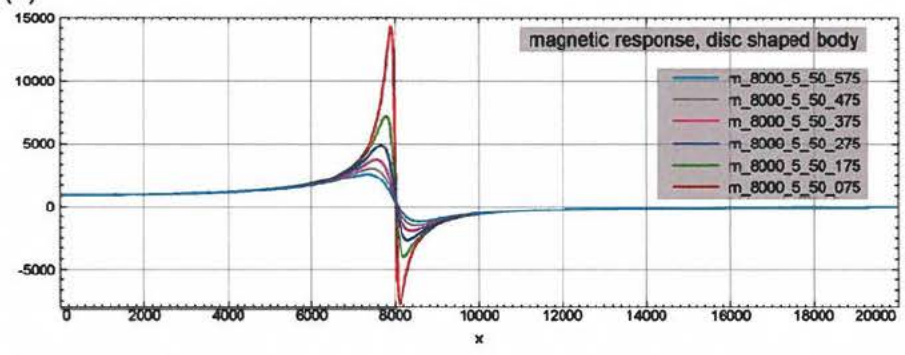

Figure B15. *(a) Gravimetric and (b) magnetic responses from a disc shaped body centred at X=0 m with a radius of 8000 m and thickness of 50 m. The top of the disc shaped body is 5 m below surface and responses are shown for altitudes of 75 m, 175 m, 275 m, 375 m, 475 m and 575 m.*

(a)

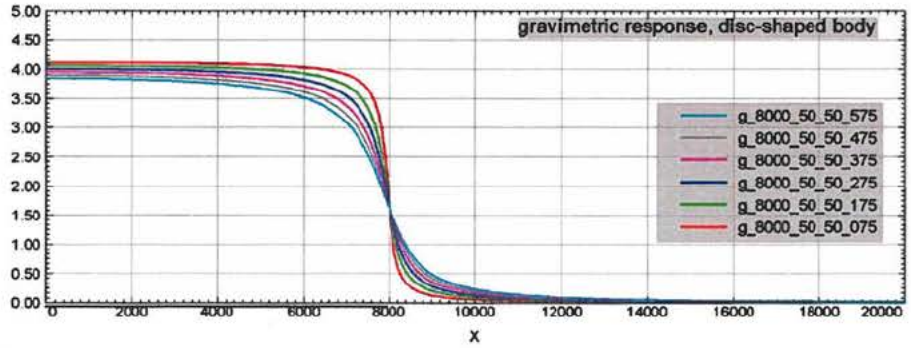

(b)

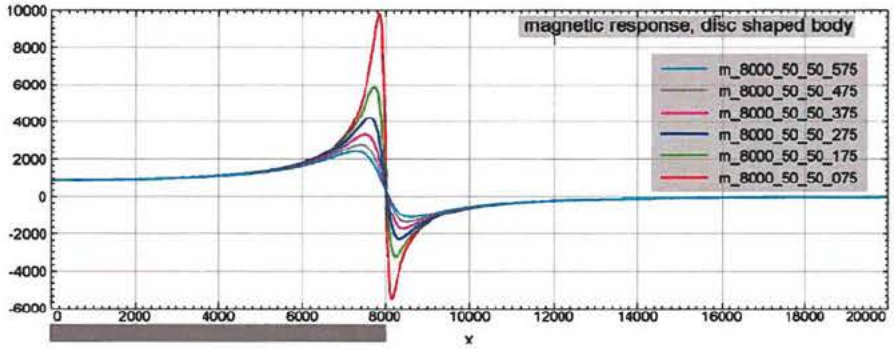

Figure B16. *(a) Gravimetric and (b) magnetic responses from a disc shaped body centred at X=0 m with a radius of 8000 m and thickness of 50 m. The top of the disc shaped body is 50 m below surface and responses are shown for altitudes of 75 m, 175 m, 275 m, 375 m, 475 m and 575 m.*

(a)

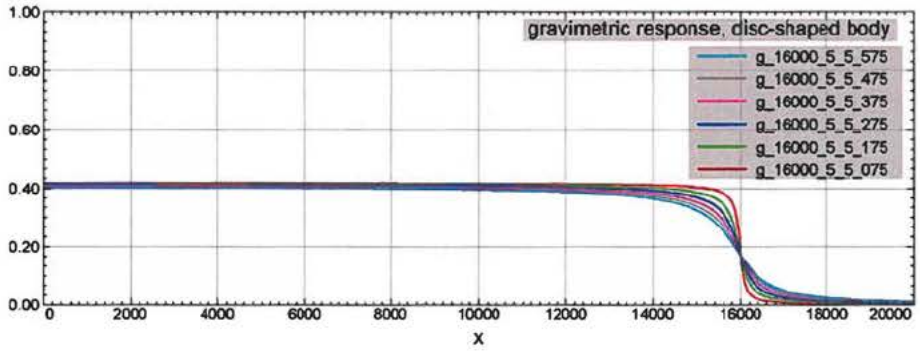

(b)

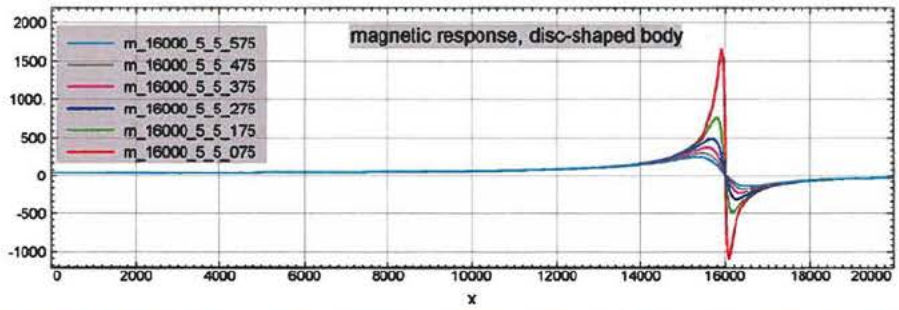

Figure B17. *(a) Gravimetric and (b) magnetic responses from a disc shaped body centred at X=0 m with a radius of 16000 m and thickness of 5 m. The top of the disc shaped body is 5 m below surface and responses are shown for altitudes of 75 m, 175 m, 275 m, 375 m, 475 m and 575 m.*

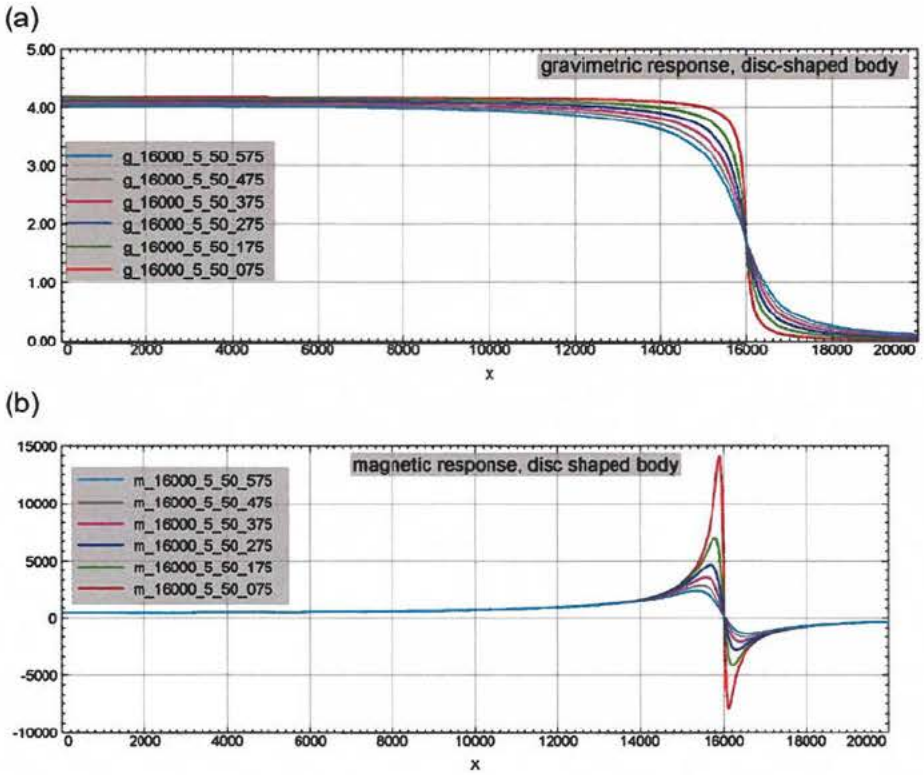

Figure B18. *(a) Gravimetric and (b) magnetic responses from a disc shaped body centred at X=0 m with a radius of 1600 m and thickness of 50 m. The top of the disc shaped body is 5 m below surface and responses are shown for altitudes of 75 m, 175 m, 275 m, 375 m, 475 m and 575 m.*

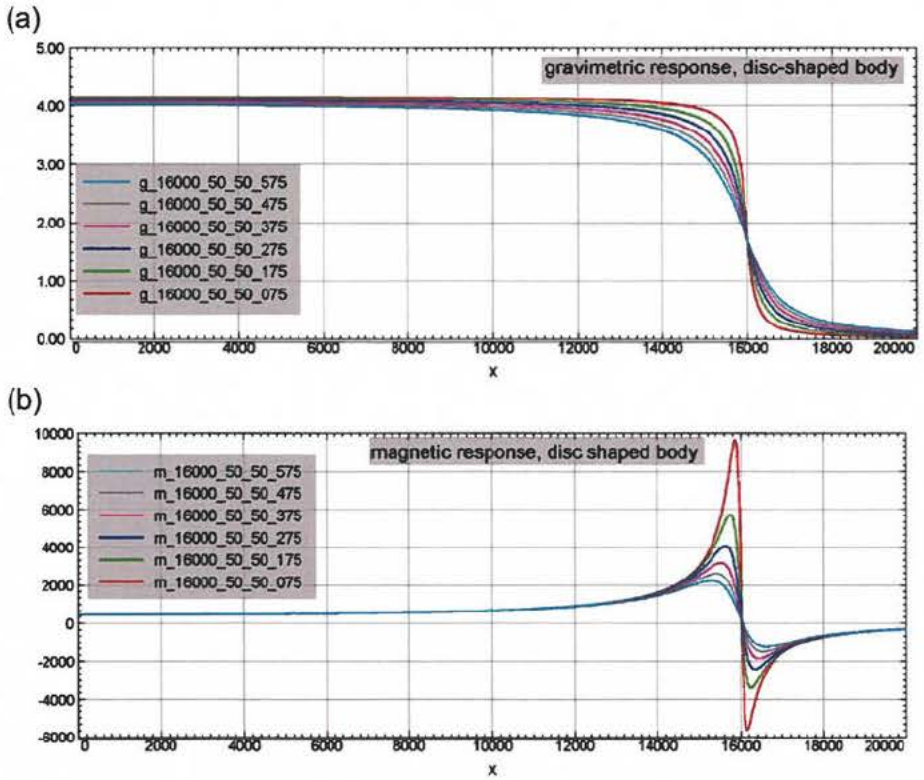

Figure B19. *(a) Gravimetric and (b) magnetic responses from a disc shaped body centred at X=0 m with a radius of 16000 m and thickness of 50 m. The top of the disc shaped body is 50 m below surface and responses are shown for altitudes of 75 m, 175 m, 275 m, 375 m, 475 m and 575 m.*

18. Appendix C – IOCG targets

Screen dumps are provided with four images with identical area coverage and with the target area marked by a black rectangle. The four images are

- total magnetic field (top-left panel),
- GEOTEM decay constant tau in grey scale with superimposed symbol of the vertical gradient of the pseudo gravity field at tau peak locations (top right panel),
- Bouguer gravity after detrending (lower left panel – might be empty)
- vertical gradient of pseudo gravity field with superimposed symbol of GEOTEM decay constant at gradient of pseudo gravity peak locations (lower right panel)

The colour scales used are similar to those used in Chapter 4. Corner locations for each target area displayed are provided in Table C1.

Table C1. Corner locations WGS84/UTM19N for target areas displayed

Target No.	X_UTM19N	Y_UTM19N
target 1		
	449990	8709727
	453136	8709727
	453136	8713010
	449990	8713010
target 2		
	465444	8708332
	471750	8708332
	471750	8710758
	465444	8710758
target 3		
	438551	8709806
	442461	8709806
	442461	8712358
	438551	8712358
target 4		
	457991	8715782
	461132	8715782
	461132	8717016
	457991	8717016
target 5		
	453881	8716516
	456834	8716516
	456834	8717992
	453881	8717992
target 6		
	473877	8710153
	476569	8710153
	476569	8711547
	473877	8711547
target 7		
	473077	8694299
	478832	8694299
	478832	8696792
	473077	8696792

Table C1 - continued. Corner locations WGS84/UTM19N for target areas displayed

Target No.	X_UTM19N	Y_UTM19N
target 8		
	487135	8693127
	493871	8693127
	493871	8696234
	487135	8696234
target 9		
	500745	8721792
	505310	8721792
	505310	8725155
	500745	8725155
target 10		
	517025	8747158
	522328	8747158
	522328	8750111
	517025	8750111
target 11		
	512036	8736825
	516061	8736825
	516061	8738178
	512036	8738178
target 12		
	523491	8757057
	527133	8757057
	527133	8759298
	523491	8759298
target 13		
	528399	8742891
	532628	8742891
	532628	8746327
	528399	8746327
target 14		
	519651	8722016
	522072	8722016
	522072	8723969
	519651	8723969

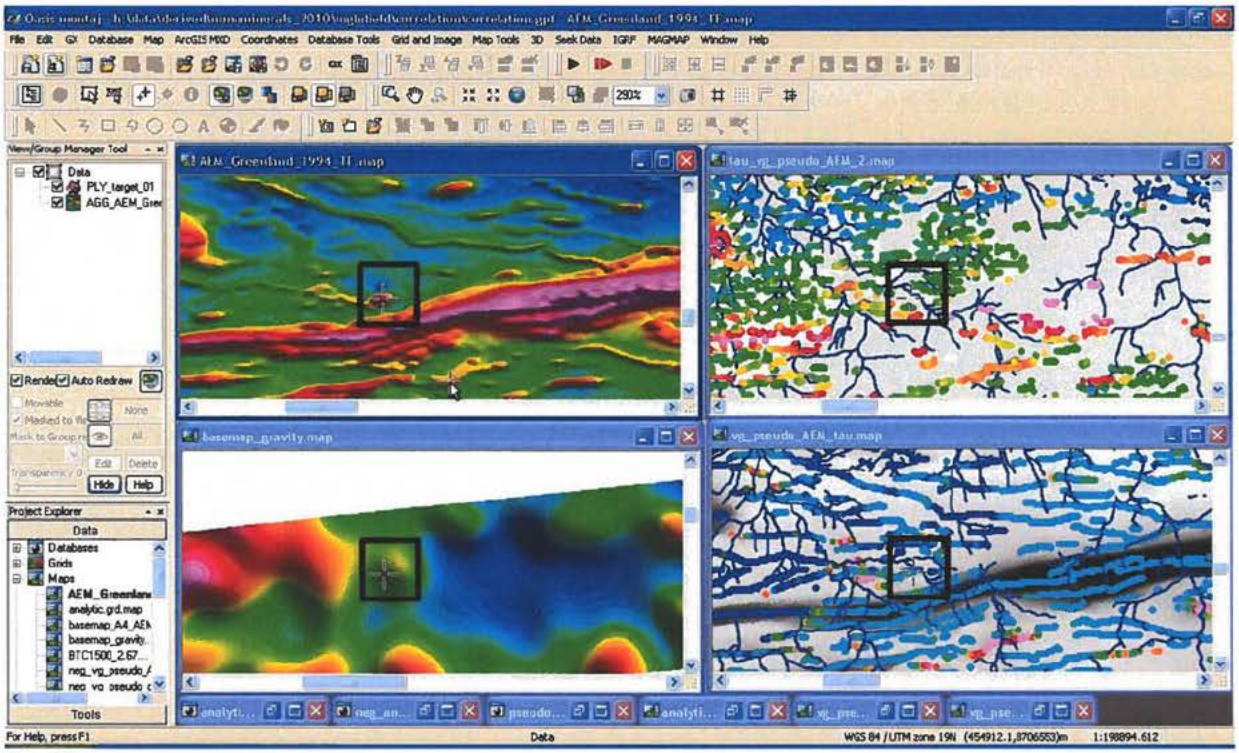

Figure 83. *Target area 1.*

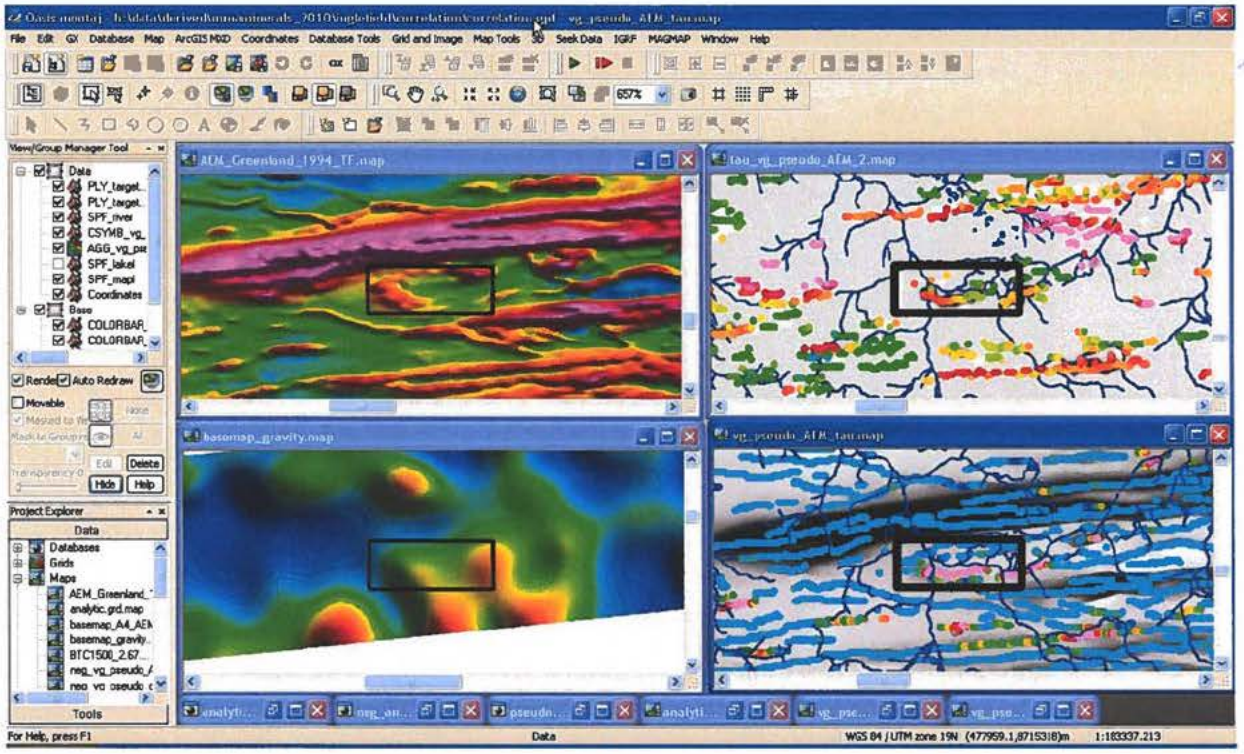

Figure 84. *Target area 2.*

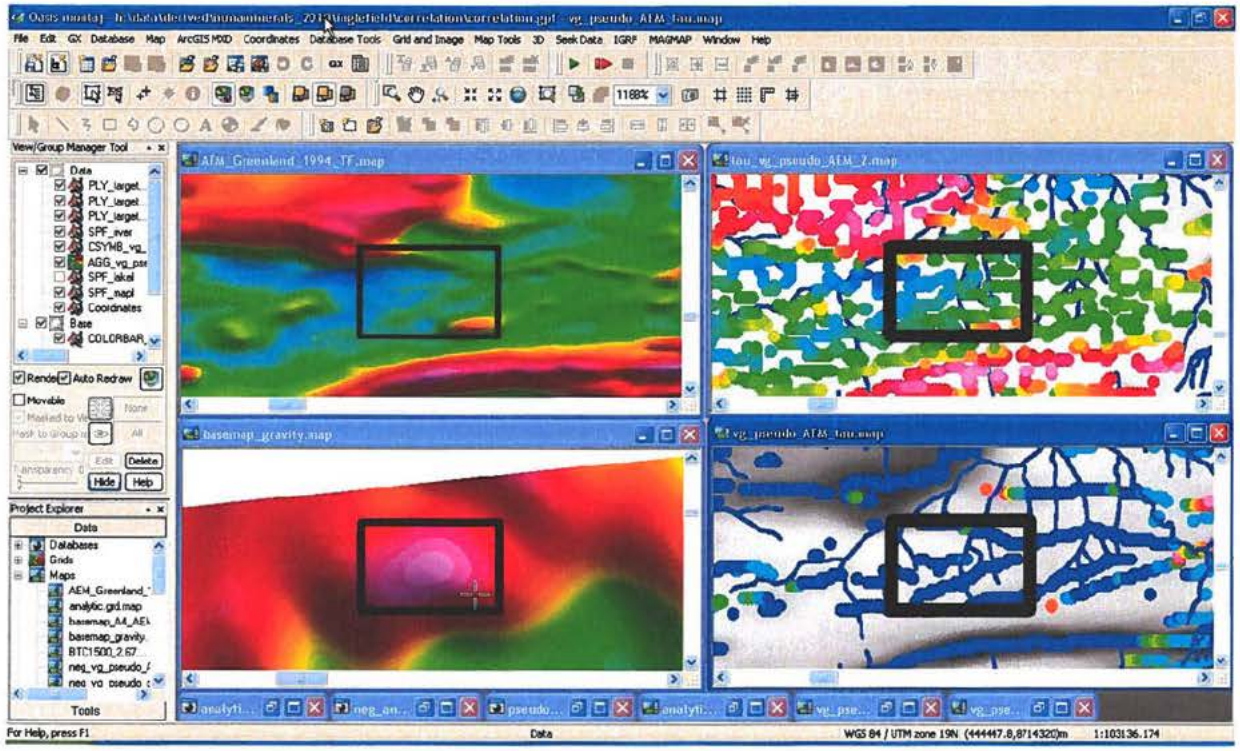

Figure C3. *Target area 3.*

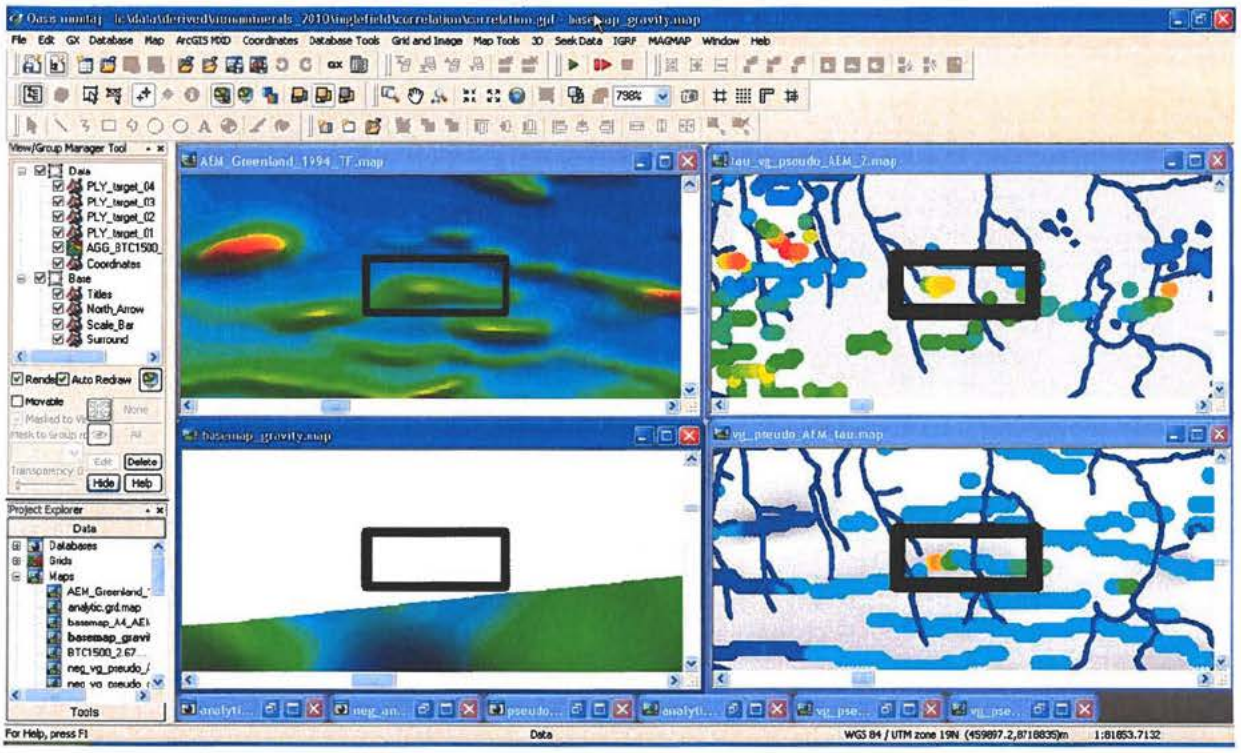

Figure C4. *Target area 4.*

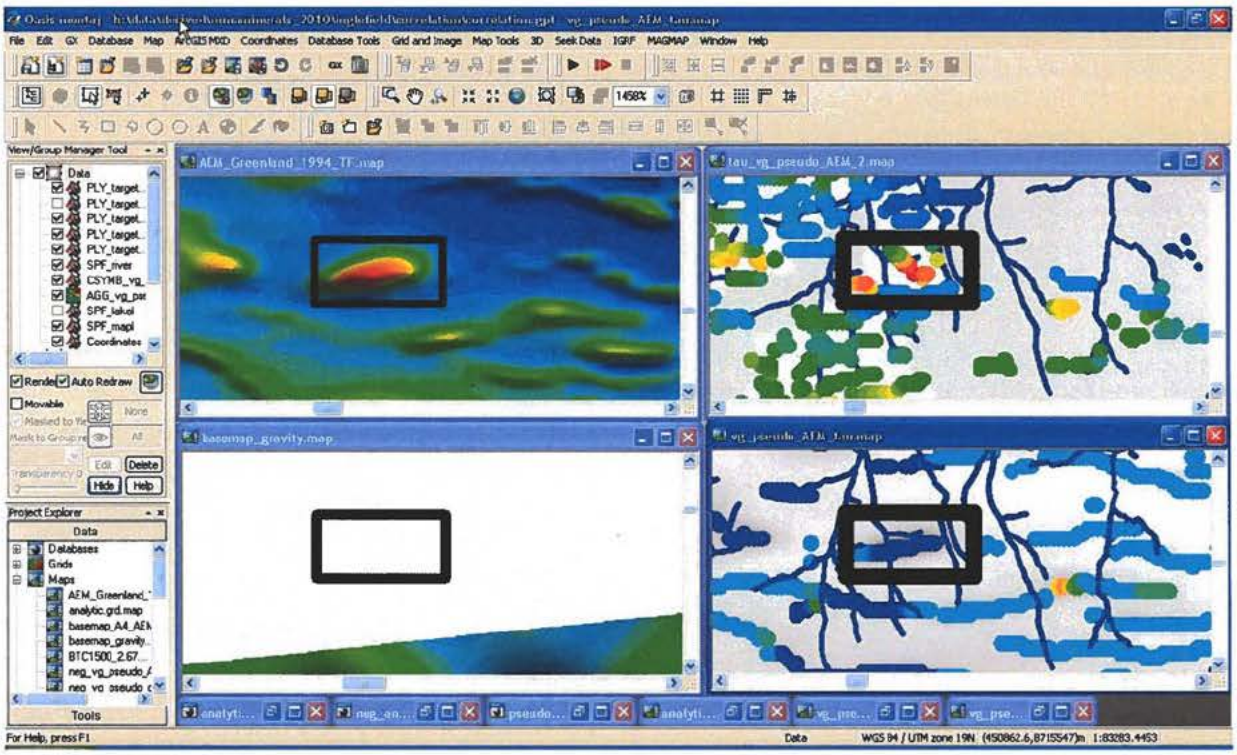

Figure C5. *Target area 5.*

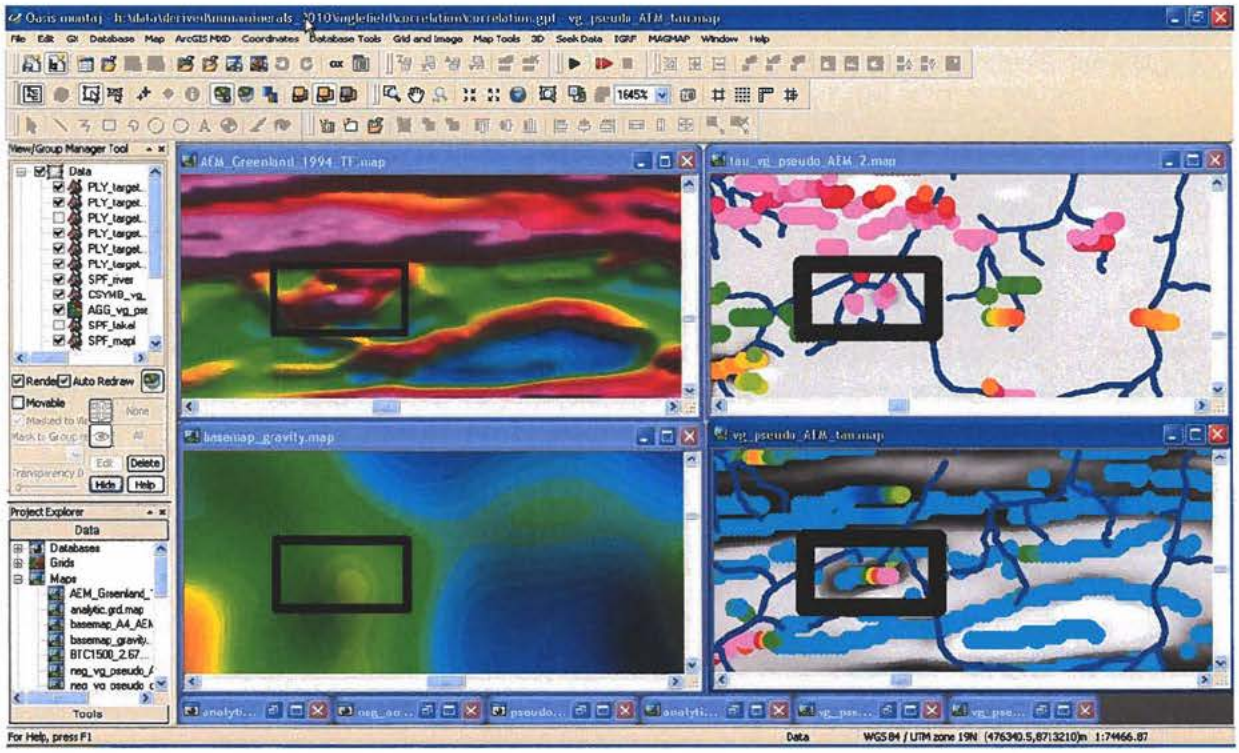

Figure 85. *Target area 6.*

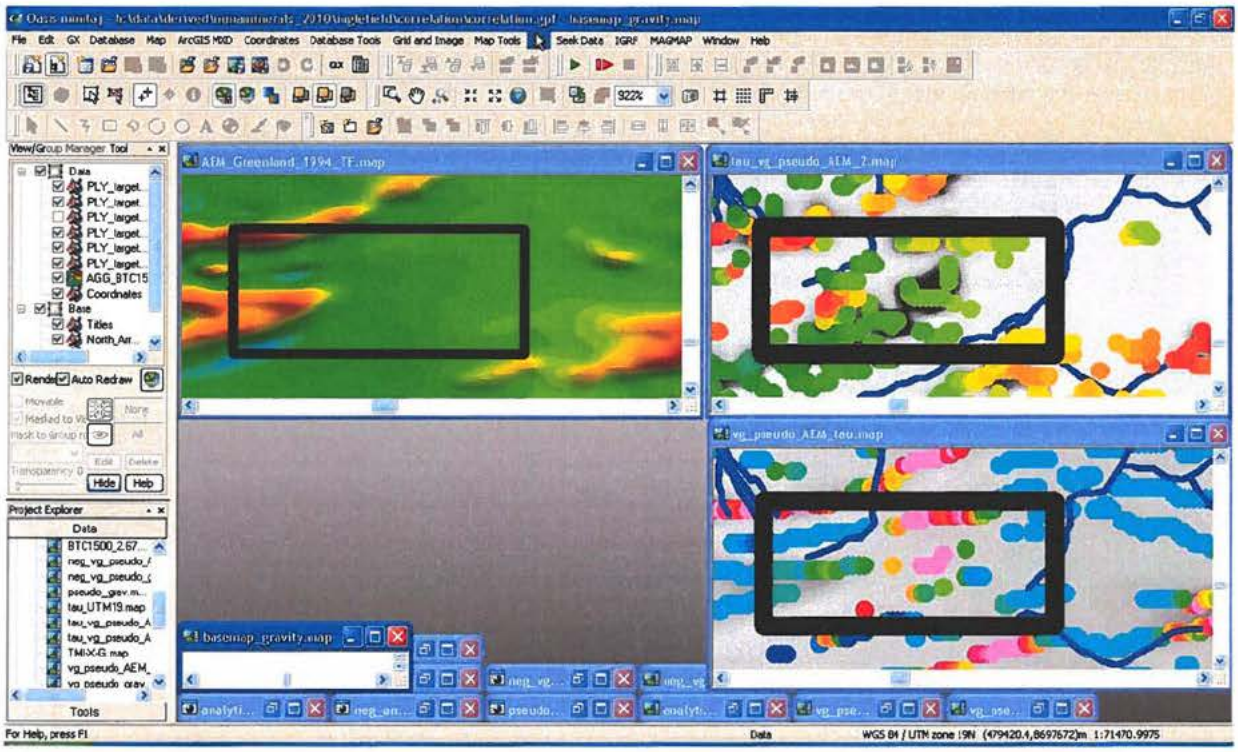

Figure C7. *Target area 7.*

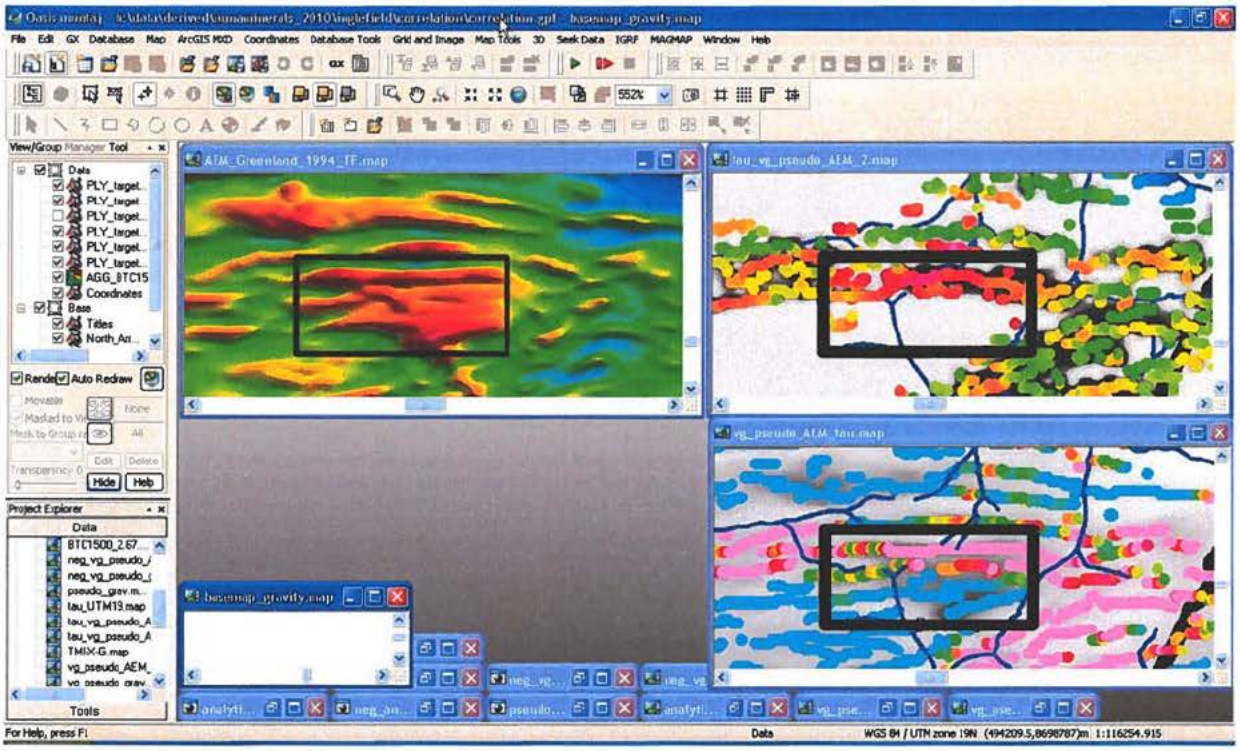

Figure C8. *Target area 8.*

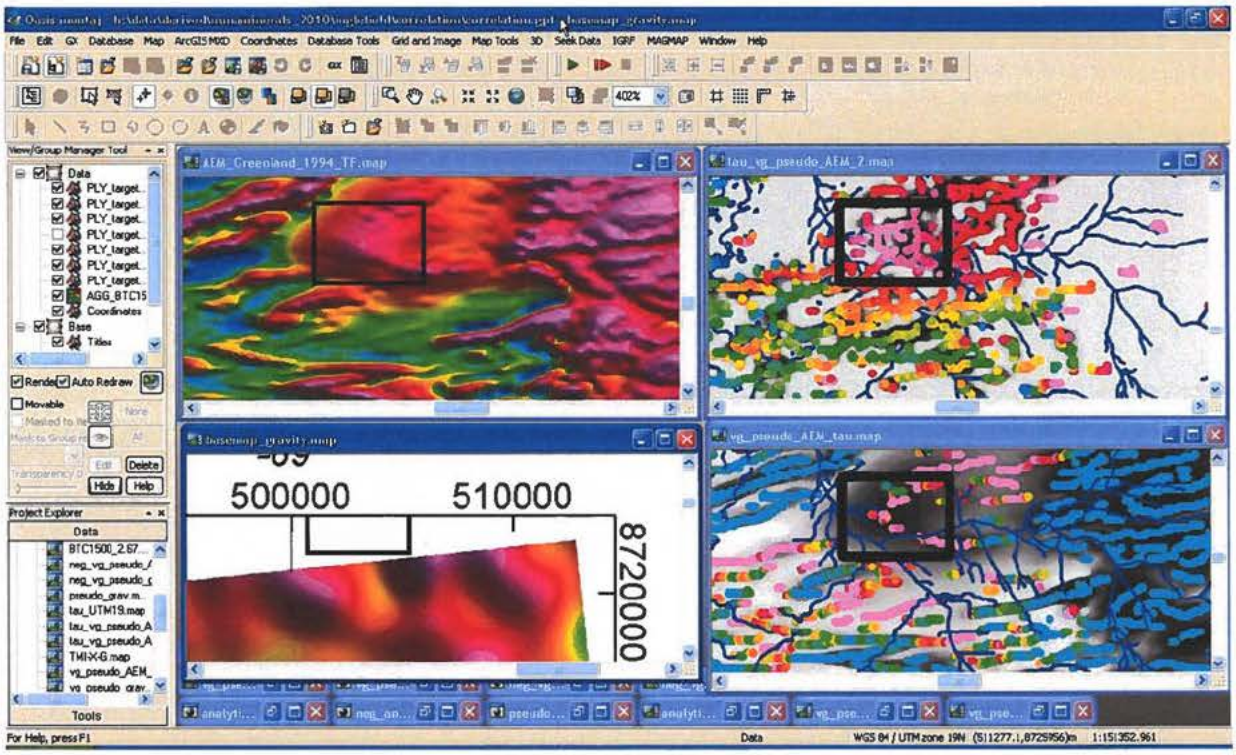

Figure C9. *Target area 9.*

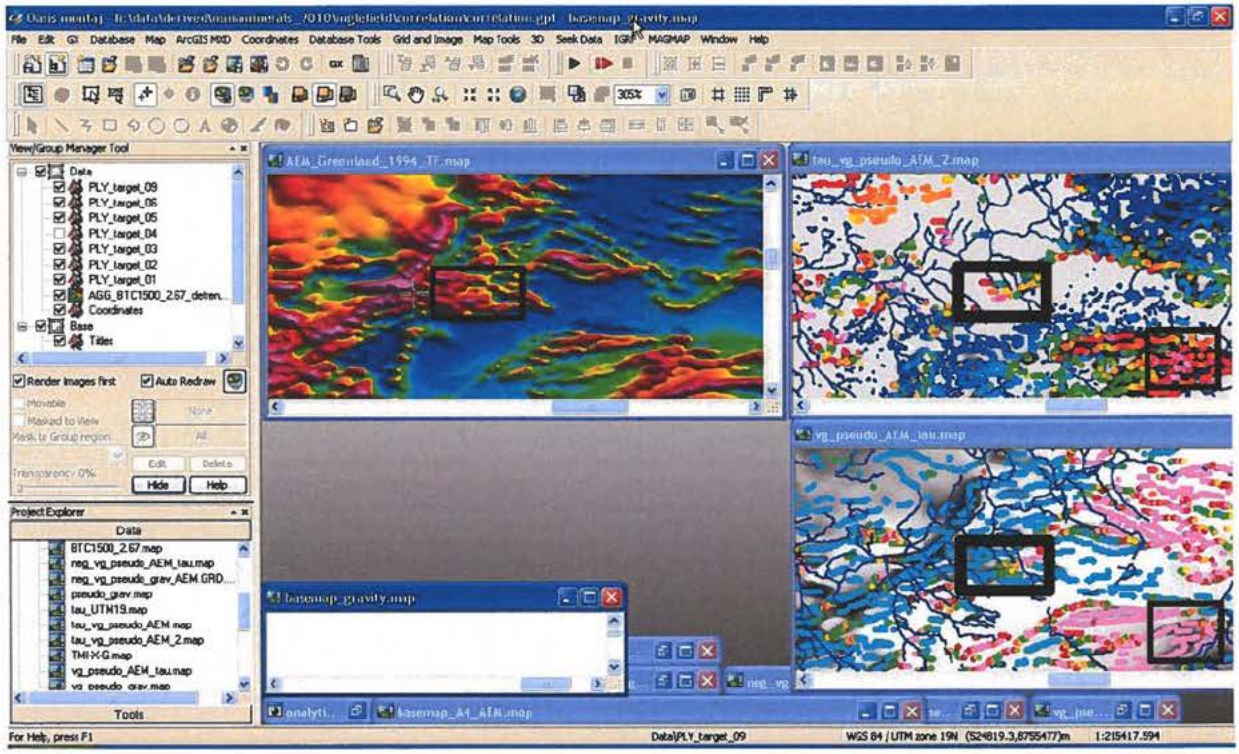

Figure C10. *Target area 10.*

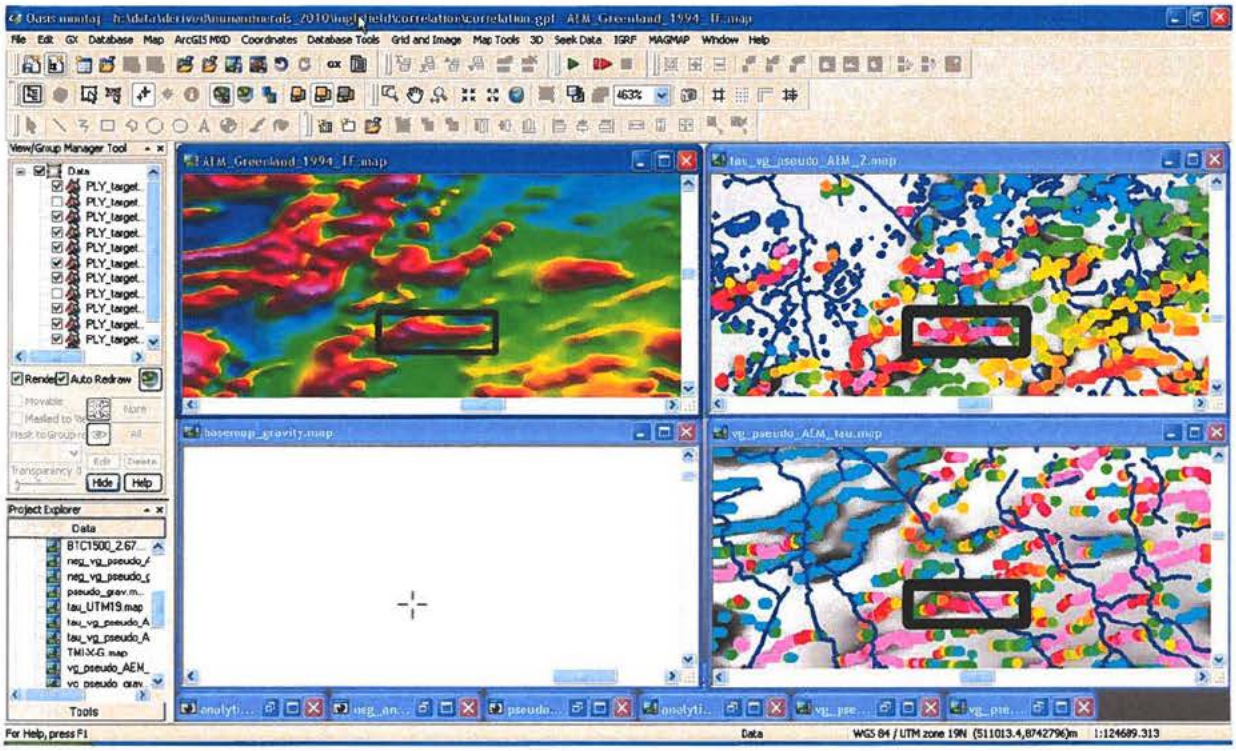

Figure C11. *Target area 11.*

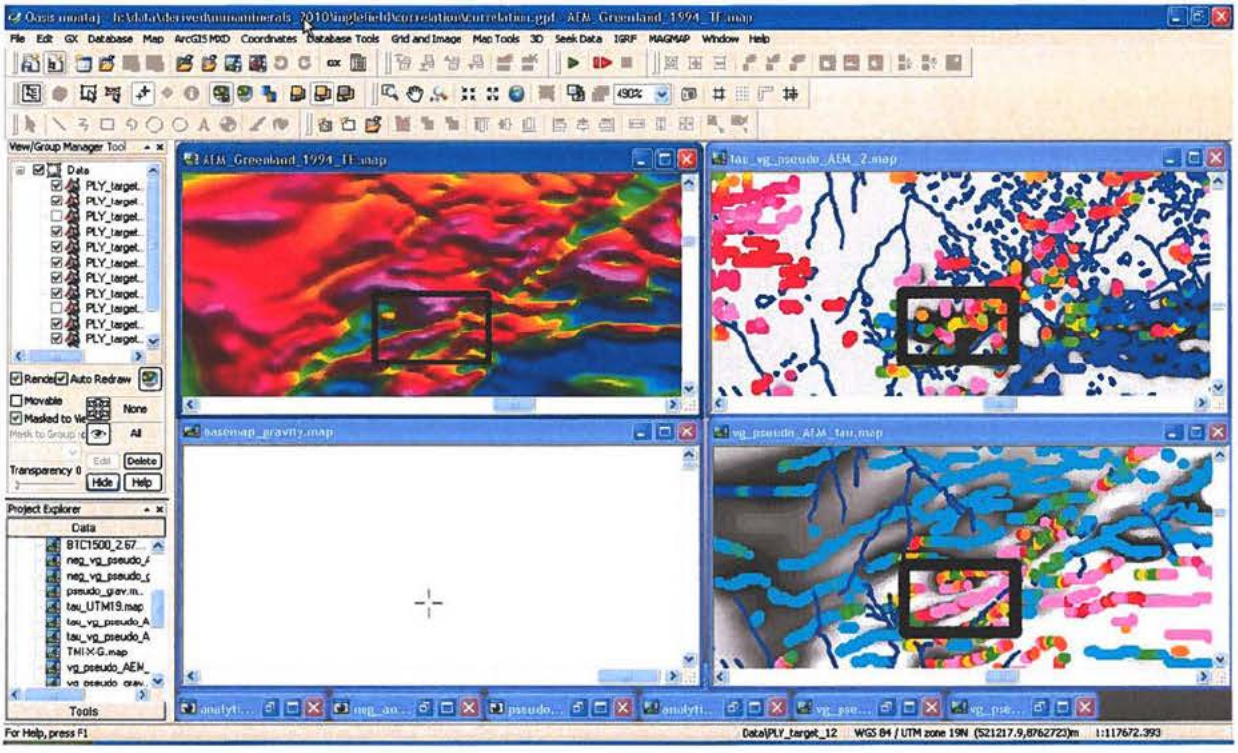

Figure C12. *Target area 12.*

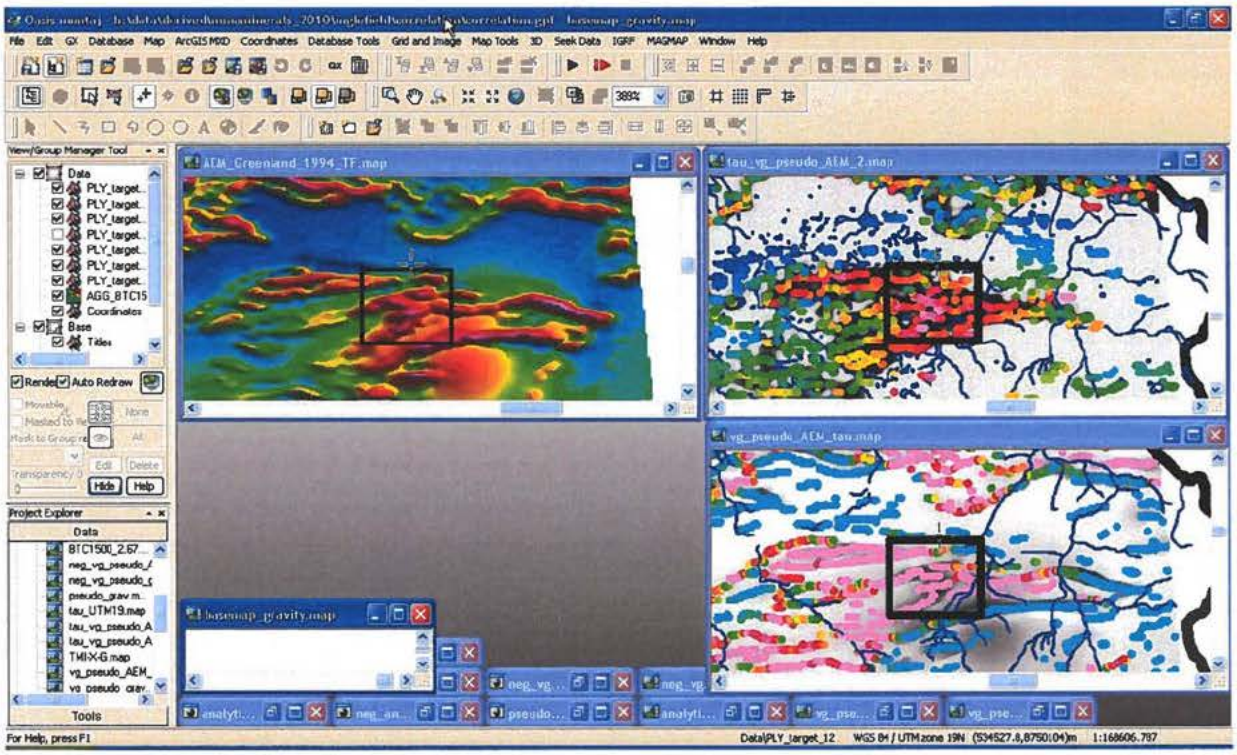

Figure C13. *Target area 13.*

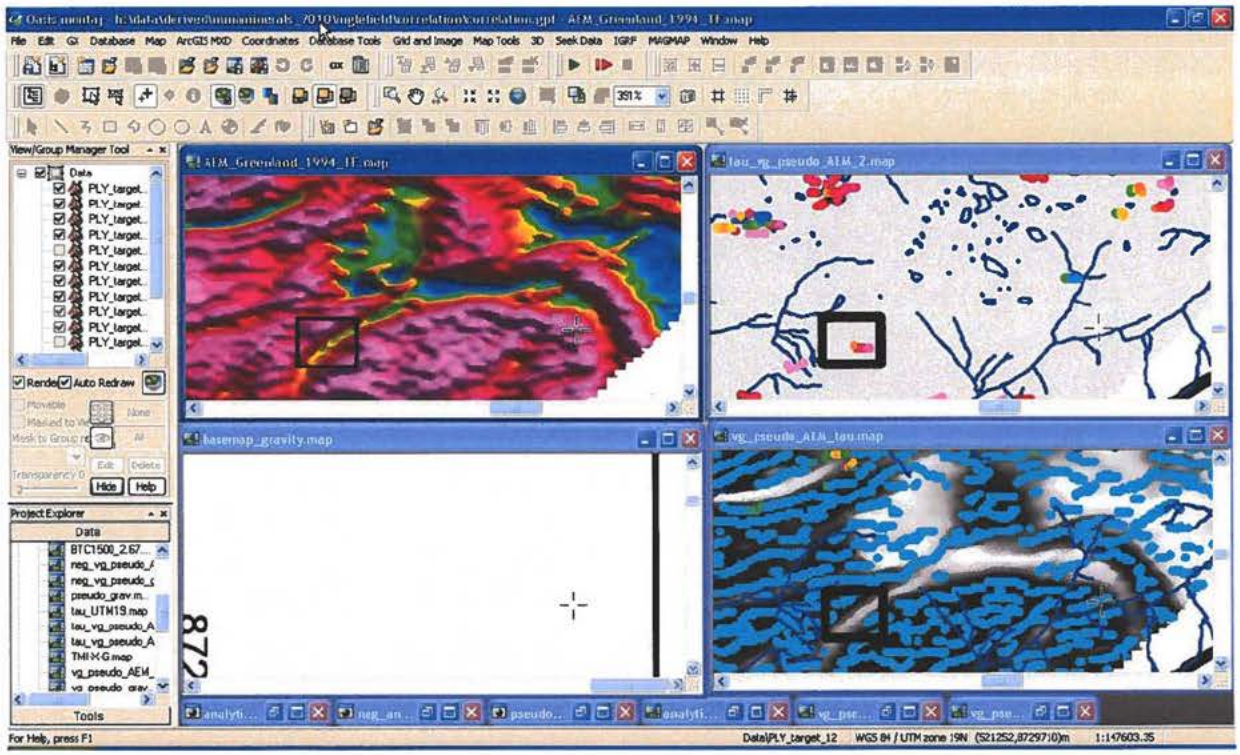

Figure C14. *Target area 4.*